

Northumbria Research Link

Citation: Misti, Siti Nabilah (2016) Development of a precision trimming process for manganin shunt resistors. Doctoral thesis, Northumbria University.

This version was downloaded from Northumbria Research Link:
<http://nrl.northumbria.ac.uk/id/eprint/36271/>

Northumbria University has developed Northumbria Research Link (NRL) to enable users to access the University's research output. Copyright © and moral rights for items on NRL are retained by the individual author(s) and/or other copyright owners. Single copies of full items can be reproduced, displayed or performed, and given to third parties in any format or medium for personal research or study, educational, or not-for-profit purposes without prior permission or charge, provided the authors, title and full bibliographic details are given, as well as a hyperlink and/or URL to the original metadata page. The content must not be changed in any way. Full items must not be sold commercially in any format or medium without formal permission of the copyright holder. The full policy is available online: <http://nrl.northumbria.ac.uk/policies.html>



**Northumbria
University**
NEWCASTLE



UniversityLibrary

**DEVELOPMENT OF A
PRECISION TRIMMING
PROCESS FOR MANGANIN
SHUNT RESISTORS**

SITI NABILAH MISTI

A thesis submitted in partial fulfilment
of the requirements of the
University of Northumbria at Newcastle
for the degree of
Doctor of Philosophy

Research undertaken in the
Faculty of Engineering and Environment

August 2016

Abstract

As electrical energy prices continue to rise, accurate energy consumption monitoring is becoming increasingly important and the introduction of smart energy meters is well-known in this capacity. One of the key components in the smart energy meter is the current sensing shunt resistor and its resistance must be as low as possible, typically in the range $100\ \mu\Omega$ to $10\ \text{m}\Omega$, to minimise energy usage. Although this low resistance requirement reduces power consumption, it is inherently difficult to manufacture shunt resistors in this micro-ohm range to the required precision and at reasonable cost. Typical resistance accuracy of commercially available shunts suitable in this application is $100\ \mu\Omega \pm 5\%$, which can in turn lead to $\pm 5\%$ errors in power measurement within the smart meter.

This research presents a novel automated electro-mechanical trimming process to improve the accuracy and performance of $100\ \mu\Omega$ Manganin shunt resistors for use in smart energy meters. Theoretical and experimental investigations were carried out to determine the optimum technique and design geometry to remove the resistive material from the shunt. More specifically, the work focuses on the development of the precision trimming process to improve the resistance tolerance of the shunt resistors. A novel laboratory prototype of an automated concurrent trimming system is developed which combines the mechanical cutting process and electrical measurement system to remove controlled amounts of material from the Manganin shunt. Design of Experiments (DoE) is then conducted in order to find the optimum feed rate and cutting speed for the trimming process.

The effects of under a varying the trimming geometry on the key performance criteria of the shunt resistors was investigated by simulating the conditions that the shunts will be exposed to when positioned within a high current circuit and encapsulated within a smart energy meter. Tests have examined changes in physical structural conditions as well as electrical properties under a varying environmental conditions. By using concurrent trimming, the tolerance of the Manganin shunt resistors has been reduced from $\pm 5\%$ to less than $\pm 1\%$ within 5 seconds. Trimming does not have a significant effect on the key properties of the shunt resistors and the results obtained can be used to inform production processes for large scale manufacture of precision shunt resistors.

Acknowledgements

Many people have helped me throughout the course of this project, and I would like to take this opportunity to thank some of them. Firstly, many thanks must go to my principle supervisor Dr Martin Birkett for his invaluable knowledge, guidance and encouragement and also his willingness to always make time for me. I would also like to thank my other academic supervisors; Dr Roger Penlington, and Dr David Bell for their continued support and expert advice.

I acknowledge the Department of Mechanical Engineering for the facilities that have been made available to me and in particular, I would like to thank Phil Donnelly, Simon Neville, Sam Hutchinson and David Johnson for their technical advices, help and encouragement along the way.

I also gratefully acknowledge Majlis Amanah Rakyat (MARA), Malaysia for the scholarship award and the financial support it has brought to the project.

Finally, I would like to thank my family, and in particular my husband, Raja Muhamad Hafiz, for his continued support, tolerance and encouragement.

Declaration

I declare that the work contained in this thesis has not been submitted for any other award and that it is all my own work. I also confirm that this work fully acknowledges opinions, ideas and contributions from the work of others.

Name: Siti Nabilah Misti

Signature:

Date: 6 August 2016

Table of Contents

| | |
|------------------------------------------------------------|------------|
| Abstract | ii |
| Acknowledgements | iii |
| Declaration | iv |
| Table of Contents | v |
| List of Tables | ix |
| List of Figures | x |
| Chapter 1 : Introduction | 1 |
| 1.1 Growth and Evolution of the Smart Energy Meter | 3 |
| 1.2 Motivation of the Research | 5 |
| 1.2.1 Problem Statement | 8 |
| 1.3 Aims and Objectives | 9 |
| 1.4 Research Framework | 11 |
| 1.5 Original contributions | 13 |
| 1.6 Research Outcomes | 14 |
| 1.7 Organisation of the Thesis | 15 |
| Chapter 2 : Review of Current Sense Characteristics | 18 |
| 2.1 Current Sensing | 18 |
| 2.1.1 Shunt Resistor | 20 |
| 2.1.2 Induction Sensors | 22 |
| 2.1.3 Hall Effect Sensors | 24 |
| 2.1.4 Comparison of Current Sensing Methods | 26 |
| 2.2 Shunt Resistor Characteristics | 30 |
| 2.2.1 Theory of Operation | 31 |
| 2.2.2 Manganin Resistive Material | 34 |

| | | |
|---------------------------------------------------------|--------------------------------------------------------|-----------|
| 2.2.3 | Manufacturing Method | 37 |
| 2.3 | Key Performance Criteria | 39 |
| 2.3.1 | Resistance | 39 |
| 2.3.2 | Temperature Coefficient of Electrical Resistance (TCR) | 41 |
| 2.3.3 | Thermal Electro Motive Force (EMF) | 42 |
| 2.3.4 | Resistance Stability | 42 |
| 2.4 | Shunt Resistor Selection | 43 |
| 2.5 | Summary | 45 |
| Chapter 3 : Development of Measurement System | | 47 |
| 3.1 | Principles of Resistance Measurement | 48 |
| 3.1.1 | Measurement Techniques | 50 |
| 3.2 | Measurement Uncertainties | 53 |
| 3.2.1 | Accuracy | 54 |
| 3.2.2 | Precision | 56 |
| 3.2.3 | Resolution | 57 |
| 3.3 | Review of Potential Measurement Techniques | 57 |
| 3.4 | Comparison of Available Measurement System | 58 |
| 3.4.1 | Cropico D07 Digital Micro-ohm meter | 60 |
| 3.4.2 | Agilent B2900A/34420A Meters | 62 |
| 3.5 | Summary | 64 |
| Chapter 4 : Material Properties Characterisation | | 65 |
| 4.1 | Material Characterisation | 65 |
| 4.2 | Measurement of Key Properties | 66 |
| 4.2.1 | Material Structure | 66 |
| 4.2.2 | Mechanical Properties of Manganin | 70 |
| 4.2.3 | Electrical Properties of Manganin | 75 |
| 4.2.4 | Thermal Properties of Manganin | 77 |
| 4.3 | Summary | 82 |

| | |
|-------------------------------------------------------------|------------|
| Chapter 5 : Development of Trimming Process | 83 |
| 5.1 Trimming Geometry | 83 |
| 5.1.1 Theoretical Analysis | 84 |
| 5.2 Trimming Techniques | 85 |
| 5.2.1 Anodization | 85 |
| 5.2.2 Laser Trimming | 86 |
| 5.2.3 Sand Blast Trimming | 87 |
| 5.2.4 Milling | 89 |
| 5.2.5 Precision Grinding | 90 |
| 5.3 Trimming Techniques Selection | 91 |
| 5.4 Modelling of Potential Trim Patterns | 93 |
| 5.5 Experimental | 97 |
| 5.5.1 Initial Trials | 98 |
| 5.5.2 Concurrent Trimming | 100 |
| 5.5.3 Results | 103 |
| 5.6 Summary | 104 |
| Chapter 6 : Development of Automated Trimming System | 106 |
| 6.1 Experimental Setup | 107 |
| 6.1.1 Power Supply | 111 |
| 6.1.2 Measurement System | 113 |
| 6.1.3 System Combination | 114 |
| 6.2 Automated System | 116 |
| 6.3 System Optimisation | 122 |
| 6.4 Summary | 124 |
| Chapter 7 : Optimisation of Trimming Process | 125 |
| 7.1 Design of Experiments (DoE) | 126 |
| 7.1.1 Factor Parameters | 127 |
| 7.2 Results and Discussion | 128 |
| 7.2.1 Trimming Time | 131 |
| 7.2.2 Resistance Deviation | 133 |

| | | |
|------------------------------------------------|---------------------------------------------|------------|
| 7.2.3 | Interaction Plot | 135 |
| 7.2.4 | Surface Roughness | 137 |
| 7.3 | Optimisation Process | 139 |
| 7.4 | Summary | 142 |
| Chapter 8 : Reliability Tests | | 143 |
| 8.1 | Characterization | 143 |
| 8.1.1 | Structural Analysis | 144 |
| 8.1.2 | Temperature Coefficient of Resistance (TCR) | 145 |
| 8.1.3 | High Current | 146 |
| 8.1.4 | High Temperature Stability Test | 147 |
| 8.1.5 | Hardness | 147 |
| 8.2 | Results and Discussion | 148 |
| 8.2.1 | Temperature Coefficient of Resistance (TCR) | 150 |
| 8.2.2 | Thermal Modelling | 151 |
| 8.2.3 | High Temperature Stability Test | 155 |
| 8.2.4 | Hardness | 157 |
| 8.3 | Summary | 159 |
| Chapter 9 : Conclusion and Future Works | | 160 |
| 9.1 | Conclusions | 160 |
| 9.2 | Recommendations for Future Work | 163 |
| References | | 165 |
| Appendix | | 173 |

List of Tables

| | | |
|-----------|-----------------------------------------------------------------------------------|-----|
| Table 2.1 | Comparison between different types of current sensing [47]. | 26 |
| Table 2.2 | Typical properties of Manganin resistance alloys [67]. | 34 |
| Table 2.3 | Comparison of different Manganin properties. | 35 |
| Table 2.4 | Comparison on different resistors from different manufacturers. | 43 |
| Table 3.1 | Summary of system accuracy of potential resistance measurement equipment. | 59 |
| Table 3.2 | Resistance measurement readings using the Cropico D07 digital micro ohm meter. | 61 |
| Table 3.3 | Reading for resistance measurement using combination of Agilent meters. | 63 |
| Table 4.1 | Total weight percentage (wt. %) for Manganin samples. | 68 |
| Table 4.2 | Summarised of results for Manganin density. | 72 |
| Table 4.3 | Summarised of results for Manganin hardness. | 75 |
| Table 4.4 | Resistivity measurements for 20 samples of shunt resistors. | 76 |
| Table 4.5 | Calculated results for thermal conductivity of Manganin at different temperature. | 80 |
| Table 4.6 | Summary of the measured properties values. | 82 |
| Table 6.1 | Operating characteristics for Agilent 34420A [133]. | 119 |
| Table 7.1 | Factor parameters and their corresponding levels for the experiment. | 128 |
| Table 7.2 | Experimental results for trimming time and resistance deviation. | 130 |
| Table 7.3 | ANOVA results for Trimming Time (s). | 131 |
| Table 7.4 | ANOVA results for resistance deviation (%). | 133 |
| Table 7.5 | ANOVA results for resistance deviation (%). | 139 |

List of Figures

| | | |
|------------|-------------------------------------------------------------------------------------------------------------|----|
| Figure 1.1 | Past and projected world energy consumption [5]. | 1 |
| Figure 1.2 | Block diagram of the key components in the smart energy meter [17]. | 4 |
| Figure 1.3 | The proposed research framework. | 11 |
| Figure 2.1 | (a) Typical shunt resistor and (b) the principle of operation [50]. | 20 |
| Figure 2.2 | (a) Current transformer and (b) the principle of operation [52]. | 22 |
| Figure 2.3 | Principle of operation of Rogowski coil [56]. | 23 |
| Figure 2.4 | (a) Hall effect sensor and (b) the principle of operation [6]. | 24 |
| Figure 2.5 | Ohm's Law Wheel [65]. | 33 |
| Figure 2.6 | Qualitative Resistance-Temperature Curve for Manganin [73]. | 36 |
| Figure 2.7 | Shunt resistor construction. | 37 |
| Figure 2.8 | Electron beam welding process [80]. | 38 |
| Figure 2.9 | 100 $\mu\Omega$ Manganin shunt resistor specifications. | 45 |
| Figure 3.1 | Connecting a Shunt Resistor. | 49 |
| Figure 3.2 | Four wire resistance measurement. | 50 |
| Figure 3.3 | Selection of Optimum Measuring Technique [73]. | 51 |
| Figure 3.4 | 4 wire Kelvin connection [92]. | 52 |
| Figure 3.5 | (a) Series of measurements and (b) Values plotted in a histogram [95]. | 53 |
| Figure 3.6 | Uncertainty of 5 % reading and a read value of 70 V [97]. | 55 |
| Figure 3.7 | The uncertainty increment of the usage of a shunt resistor [97]. | 55 |
| Figure 3.8 | Connection of a shunt resistor to Cropico D07. | 60 |
| Figure 3.9 | Connection of a shunt resistor to Agilent meters. | 62 |
| Figure 4.1 | Chemical spectra for (a) Manganin sample 1 and (b) Manganin sample 2. | 67 |
| Figure 4.2 | XRD patterns for both sample of Manganin. | 69 |
| Figure 4.3 | XRD diagrams of as-deposited and annealed Manganin films on Al ₂ O ₃ substrate [109]. | 70 |

| | | |
|-------------|-----------------------------------------------------------------------------------------------------------------------------------------------------------------------------------------------------------------------------------------------------------------------------------------------------------|-----|
| Figure 4.4 | Block diagram for density measurement. | 71 |
| Figure 4.5 | Principle of Vickers hardness measurement [112]. | 73 |
| Figure 4.6 | Impression of Vickers hardness test made on Manganin sample. | 74 |
| Figure 4.7 | Block diagram for thermal conductivity experiment setup. | 78 |
| Figure 4.8 | Heat capacity experiment setup. | 81 |
| | | |
| Figure 5.1 | Block diagram of laser trimming process [119]. | 87 |
| Figure 5.2 | Schematic illustration of sand-blast trimming [127]. | 88 |
| Figure 5.3 | Schematic illustration of end milling process [129]. | 89 |
| Figure 5.4 | Schematic of surface grinding [131]. | 90 |
| Figure 5.5 | Various initial trimming designs and patterns. | 93 |
| Figure 5.6 | Total current density results using ANSYS 14.5 for Manganin strip with different trimming patterns, using: (a) untrimmed, (b) Design A – hole cut, (c) Design B – square cut, (d) Design C – semi-circular cut, (e) Design D – double semi-circular ended cut and (f) Design E – double square ended cut. | 95 |
| Figure 5.7 | Shunt resistor element dimensions and trim geometry. | 97 |
| Figure 5.8 | Graph for initial trimming process on different design. | 99 |
| Figure 5.9 | Block diagram of concurrent trimming test using a milling machine. | 102 |
| Figure 5.10 | Results of resistance versus depth of cut for 5 samples using the initial concurrent trimming process. | 104 |
| | | |
| Figure 6.1 | Schematic of concurrent trimming system using linear a precision saw. | 107 |
| Figure 6.2 | Different views of concurrent trimming system. | 108 |
| Figure 6.3 | Flow diagram of the proposed trimming control. | 109 |
| Figure 6.4 | Front panel of the LabVIEW system. | 110 |
| Figure 6.5 | Block diagram for initializing the current source. | 111 |
| Figure 6.6 | Block diagram to set current and output protection status. | 112 |
| Figure 6.7 | Block diagram for the measurement system. | 113 |
| Figure 6.8 | Block diagram of concurrent trimming system and divided into different sections. | 115 |
| Figure 6.9 | External circuit used to control relay. | 117 |
| Figure 6.10 | Block diagram of concurrent trimming process using multipoint measurement. | 118 |
| Figure 6.11 | Block diagram for final configurations for trimming system. | 121 |
| Figure 6.12 | Block diagram for precision trimming process. | 123 |

| | | |
|-------------|-----------------------------------------------------------------------------------------------------|-----|
| Figure 7.1 | Main effects plot for Trimming Time (s). | 132 |
| Figure 7.2 | Main effects plot for Resistance Deviation (%). | 134 |
| Figure 7.3 | Interaction Plot for Resistance Deviation (%). | 135 |
| Figure 7.4 | Interaction Plot for Trimming Time (s). | 136 |
| Figure 7.5 | Surface images at different cutting speeds. | 137 |
| Figure 7.6 | Surface roughness (Ra) versus cutting speed. | 138 |
| Figure 7.7 | Interval plot of resistance deviation vs cutting speeds, error bars for 5 samples at each speed. | 140 |
| Figure 7.8 | Approximate values of the cutting speed. [157] | 141 |
| | | |
| Figure 8.1 | Connection of a Manganin shunt resistor to LPC 6-220 models power supply. | 146 |
| Figure 8.2 | (a) Top and (b) side views of a shunt resistor trimmed with a square cut. | 148 |
| Figure 8.3 | Resistance values of the shunt resistors before (untrimmed) and after trimming with the square cut. | 149 |
| Figure 8.4 | Resistance versus temperature for untrimmed and square cut shunt resistor samples. | 150 |
| Figure 8.5 | Temperature-Resistance graph for untrimmed shunt resistor. | 152 |
| Figure 8.6 | Temperature-Resistance graph for shunt resistor trimmed using square cut. | 152 |
| Figure 8.7 | Thermal images of 100 $\mu\Omega$ shunt resistors (a) untrimmed and (b) trimmed with square cut. | 153 |
| Figure 8.8 | Change in Resistance for the shunt resistor over a period of 1 week. | 154 |
| Figure 8.9 | Chemical spectrum for Manganin shunt resistor. | 155 |
| Figure 8.10 | (a) Shunt resistor and (b) SEM images of the shunt resistor after stability test. | 156 |
| Figure 8.11 | Hardness measurement using Alicona microscope. | 156 |
| Figure 8.12 | Hardness values for the shunt resistor, error bar for 8 different areas on the surface. | 157 |

Chapter 1

Introduction

The basic need for light and heat, as well as the recent advancements in technology has made the production and distribution of energy an essential part of everyday life. Around 605×10^{18} Joules (J) of energy is currently required to meet the world's total energy demand [1]. In the past 25 years (from 1990 to 2015) the energy necessary to satisfy this demand increased steadily by around 10×10^{18} J per year and this trend is predicted to continue until the year 2035, see Figure 1.1. This trend is also supported by a statement from the International Energy Agency (IEA), who estimate in 2010 that there will be a 56% increase in the world's energy requirement by 2040 [2-4].

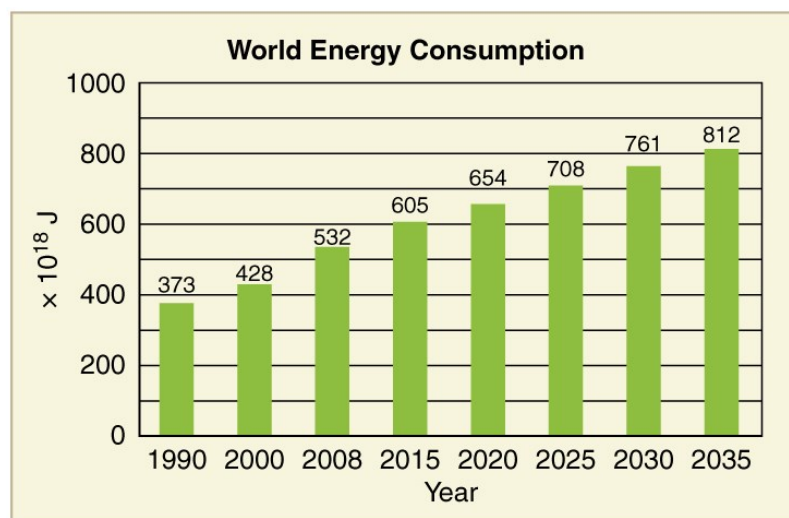


Figure 1.1: Past and projected world energy consumption [5].

The increase in energy requirements has made a huge impact on the energy price and this can be seen in the rising cost of energy. Not only does this affect the average household consumer, the industrial sector also needs to seriously consider energy consumption as an important factor in addition to their traditional ways of operation, which usually put raw material costs, labour costs, and productivity as their main concerns [6]. They believe that by utilising and reducing energy wastage, the energy cost will be reduced and it will benefit them in both planning and operations. Customers nowadays will also be looking for “green” suppliers.

Therefore, to make the consumer aware of the energy usage in their household, hence maximising the utilisation of energy, data regarding its usage is extremely valuable and it will motivate the user to modify their behaviour in consuming energy [7]. In order to effectively manage energy consumption, the accurate quantification of energy usage needs to be carried out to determine its degrees of freedom for improvement [6].

The introduction of the smart energy meter has provided the consumer with such a way of supervising their energy usage. The traditional electric meter is not user friendly as it is hard for the consumer to determine their usage, although it has been serving a purpose since the beginning of the 20th century. With the use of information gained through the smart energy meter, the user can make smarter decisions and manage their energy usage economically. This smarter approach for energy consumption was supported by the United Kingdom (UK) Secretary of the Department of Energy and Climate Change (DECC), Ed Miliband, who described that changes in electrical measurement are imperative in order to reduce the energy usage and received benefits from using the smart energy meter [8]:

“The meters most of us have in our homes were designed for a different age, before the climate change. Now we need to get smarter with our energy ... so it’s important we design a system that brings the best value to everyone involved.”

Ed Miliband, DECC’s Secretary, 11 May 2009.

1.1 Growth and Evolution of the Smart Energy Meter

The new generation of energy measurement applications will surpass its predecessor in many ways. This application can be used by the user through smart appliances, power supplies, and smart plugs, in order to accurately manage their energy usage. Utility companies nowadays are pushing to replace old mechanical meters with smart energy meters with up to 500 million units being produced worldwide over the next 5 years [9, 10]. In the UK itself, the intention to have all 26 million homes equipped with smart meters by 2020 was announced by the DECC in 2009 [8, 11-14]. These smart energy meters have the potential to save in the region of £14 billion per year in energy usage and would save on average the sum of £65 per UK household bill.

The function of a smart meter is very similar to a traditional electricity meter located in a residence or business but the smart meter will identify and present the energy consumption in more detail than its predecessor presents. This new kind of energy meter can automatically send meter readings directly to the energy supplier, eliminating the need to take the meter reading at the consumers' premises. This will allow the supplier to always have an accurate meter reading; which means no more estimated bills.

However, the smart meter is not an intrinsic energy saving device and it cannot directly reduce the energy bill. The device comes with add-ons such as a meter display, which will allow the consumer to monitor and plan their usage and serves as a catalyst in changing their behaviour and habit in using energy in their premises. The use of the smart meter will also help energy companies to map the energy usage in the UK more accurately, making them more efficient in supplying energy to the consumer. Furthermore, the smart energy meter will help the government to meet the greenhouse gas reduction target of at least 34% by 2020 [15]. This can be achieved by reducing the peak demand, where all the information generated from the meters will allow suppliers to offer cheaper electricity when demand is low and increase the price at times of high demand, thereby cutting carbon emissions when only a few power stations are operating on standby.

Figure 1.2 shows a block diagram of the key internal components of a smart energy meter. The three main sectors involved in the smart energy meter design include the power system, communications and energy measurement. A switched mode power supply provides power to the electronics in the meter, converting the main line alternating current (AC) voltage to the direct current (DC) low voltages required to power the meter. A backup battery is also included in the power system to ensure the metering electronics remain powered even when the mains supply is disabled [16].

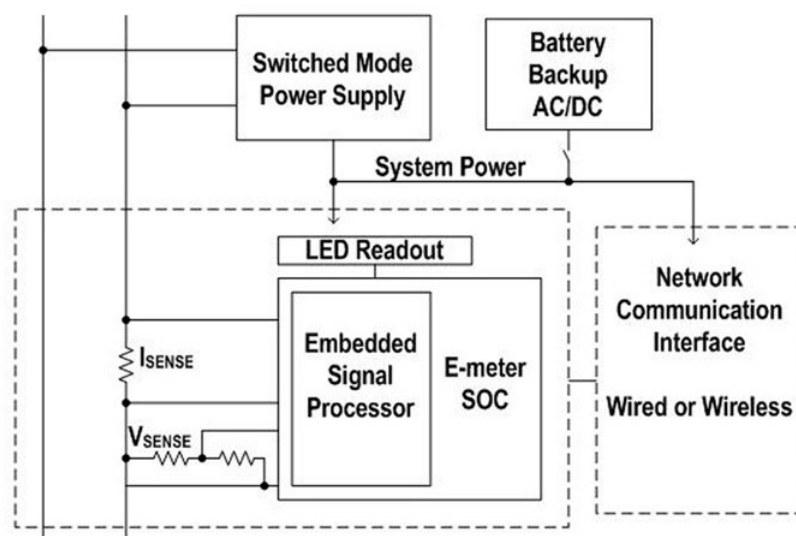


Figure 1.2: Block diagram of the key components in the smart energy meter [17].

There are a vast number of solutions available for communication interface between the smart energy meter and the utility or end user. Communication properties vary widely depending on various factors such as the location of an individual meter, the utility service provider in the specific area, geographical regions and the longevity and maturity of those supported technologies. It works in a variety of different ways; for example First Utility's meters use an in-built subscriber identification module (SIM) card similar to the ones used in mobile phones to send the reading; while most other suppliers are looking at using long range radio [18, 19].

There are several methods of current sensing in energy meters including shunt resistors, current transformers, hall sensors and also Rogowski Coils [20, 21]. The choice of current transducer depends on several economic and technical factors. Shunt resistors offer advantages of low power loss, high stability and precision of electric resistance and low temperature coefficient when compared to other current sensing methods [22]. Shunt resistors remain as the best option for residential smart energy meters as these precise low-value resistors with maximum current below 100 amps (A) are considerably lower cost compared to other options.

Furthermore, by using a shunt resistor, the current flow can be measured through a circuit with high precision. A shunt resistor requires less work to assemble and this can be carried out by connecting the shunt in a series connection to the high current electric bus bar. After the connection, the current flowing through the shunt can be measured and calculated. Typically, the calculation is based on the common proportional relation between the voltage across and the current that flows through a predefined resistor in terms of its resistance value. These advantages have led to a growing demand for high precision, low value shunt resistors in the range of $100\mu\Omega$ to $1m\Omega$ to measure the flow of electrical current in smart energy meters and other important growing applications such as electric vehicle charging stations.

1.2 Motivation of the Research

Electricity usage is usually measured in kilowatt-hours (kWh). Equation (1.1) shows the power usage, P , in kilowatts (kW) is calculated by measuring the line voltage, V , and current, I , passing through the meter and multiplying them together. This is then multiplied by the time, t , which is typically measured by a timer within the meter using the mains frequency, to give energy usage, E , in kWh. The calculation is defined using Ohm's Law [22-24] to determine the amount of electricity used:

$$V(V) = I \times R \quad (1.1)$$

$$I(A) = \frac{V}{R}$$

$$P(kW) = I \times V$$

$$E(kWh) = P \times t$$

Within the smart meter, the mains voltage is typically measured using a voltage divider circuit consisting of several low powers, high precision resistors, whilst the level of current flow is determined by measuring the voltage drop across a high current shunt resistor and then dividing it by the resistance value of the shunt itself.

The precision to which the resistance value of this high current shunt can be manufactured is therefore critical to the measurement of current in the smart meter and ultimately to the calculation of energy used by the consumer. Moreover, in order to handle the high levels of current flowing through the meter and in turn minimise joule heating (I^2R) effects, the resistance value of the shunt must also be as low as possible, typically less than $200\mu\Omega$. Unfortunately, this desired combination of low and precise resistance is not commercially achievable and the most accurate shunt available in the market to-date has a standard manufacturing tolerance of $\pm 5\%$. This value of tolerance is provided by the manufacturer of the electrical component in percentage to comply with standards for value differences [25, 26].

For example, the measured resistance value of a shunt resistor with a nominal value of $100\mu\Omega$ and a tolerance of $\pm 5\%$, could be anywhere in the range of $95\mu\Omega$ to $105\mu\Omega$. Within the smart meter, this wide tolerance of resistance of the current sensing shunt can in turn result in corresponding errors in the determination of current flow and thus the measurement of electricity usage and will ultimately cost the consumer more or less for the energy they have actually used.

For example; using Equation (1.1), if 20A of current at 240V is being measured by a shunt resistor with an assumed nominal value of $100\mu\Omega$ ($100 \times 10^{-6}\Omega$) and a $\pm 5\%$ tolerance, the energy usage and thus cost to the consumer can in turn be either over or under calculated from its nominal value by up to 5% as follows:-

Variation in measured voltage drop across the shunt:

$$V_{\max} = I \times R_{\max} = 20 \times (105 \times 10^{-6}) = 2.1mV$$

$$V_{\text{nom}} = I \times R_{\text{nom}} = 20 \times (100 \times 10^{-6}) = 2.0mV$$

$$V_{\min} = I \times R_{\min} = 20 \times (95 \times 10^{-6}) = 1.9mV$$

Variation in calculated current flowing:

$$I_{\max} = \frac{V_{\max}}{R_{\text{nom}}} = \frac{2.1 \times 10^{-3}}{100 \times 10^{-6}} = 21A$$

$$I_{\text{nom}} = \frac{V_{\text{nom}}}{R_{\text{nom}}} = \frac{2.0 \times 10^{-3}}{100 \times 10^{-6}} = 20A$$

$$I_{\min} = \frac{V_{\min}}{R_{\text{nom}}} = \frac{1.9 \times 10^{-3}}{100 \times 10^{-6}} = 19A$$

Variation in calculated energy used in 1 hour:

$$E_{\max} = I_{\max} \times V \times t = 21 \times 240 \times 1 = 5.04kWh$$

$$E_{\text{nom}} = I_{\text{nom}} \times V \times t = 20 \times 240 \times 1 = 4.8kWh$$

$$E_{\min} = I_{\min} \times V \times t = 19 \times 240 \times 1 = 4.56kWh$$

Variation in cost of electricity to the consumer for 24 hours with unit price (Up) taken as $\pounds 0.169/kWh$ [27].

$$Cost_{\max} = E_{\max} \times t \times Up = 5.04 \times 24 \times 0.169 = \pounds 20.44$$

$$Cost_{\text{nom}} = E_{\text{nom}} \times t \times Up = 4.8 \times 24 \times 0.169 = \pounds 19.47$$

$$Cost_{\min} = E_{\min} \times t \times Up = 4.56 \times 24 \times 0.169 = \pounds 18.50$$

If the tolerance of the shunt can be reduced to $\pm 1\%$, the difference in cost the consumer will be facing is only ± 19 pence compared to ± 97 pence per day. The above scenario is only based on one energy supplier's unit price and for 24 hours usage but shows how the error in cost to the consumer could soon mount up over the space of a few months and years. In average, if energy usage within a normal household is estimated to be 5000 kWh per year, it will cost around £845 but this figure can be easily reduce or increase with more accurate measurements using a shunt resistor within the smart energy meter.

Moreover, if the shunt has a high positive tolerance and thus a higher resistance value, it will dissipate more heat for a fixed current passing through it (I^2R) which can lead to additional temporary increases in resistance due to the positive temperature co-efficient of resistance of the device, as discussed in Chapter 2. This will in turn result in further increases in cost.

1.2.1 Problem Statement

Shunt resistors used to measure the flow of current in smart energy meters suffer from poor resistance tolerance due to the inherent difficulties in manufacturing accurate devices below $200\mu\Omega$. The current method used to overcome this resistance tolerance inaccuracy is to calibrate it out during the overall performance testing of the assembled meter. However, this method is not always accurate across the full operating conditions of the meter and involves the addition of compensation software, which increases the overall cost of the meter. A more efficient way to improve the accuracy of the smart energy meter would be to reduce the resistance tolerance of the shunt resistor to less than $\pm 5\%$, ideally $\pm 1\%$ and mitigate the requirement for this additional software and calibration process.

One potential method of controlling the resistance tolerance of the shunt is through a process known as trimming, where small sections of material are removed from the resistive metal alloy element of the shunt to increase its resistance value in a controlled manner from an initial low value to its target value [28, 29]. Theoretically, by trimming the resistive material into a tolerable and symmetrical shape, the standard manufacturing tolerance of the shunt

resistor can be precisely controlled [30, 31]. This, of course, only works if the shunt resistor is deliberately pre-manufactured with a resistance that is lower than the target trim value. There are a number of trimming techniques currently available including anodization, heat trimming, laser trimming, sand blast trimming, and precision grinding [32].

However these techniques are typically employed to trim other resistive technologies such as thin film, thick film and wire wound resistors and their use to trim low resistance shunts has received very little attention [33]. The focus of this research is to explore the possibility of using these or alternative trimming techniques to precisely control the resistance tolerance of high current shunt resistors to improve the accuracy of smart energy meters and other high current measuring devices. The most suitable trimming techniques will be chosen in terms of versatility, cost, time, and labour skill requirements.

1.3 Aims and Objectives

Taking into account the numerous design and performance related issues and gaps in the previous research efforts pertaining to the precision measurement of shunt resistors, the main aims of this research are defined as follows:

1. Develop a measurement system based on 4-wire Kelvin connection capable of measuring $50\mu\Omega$ - $10m\Omega$ shunts with high accuracy and repeatability.
2. Perform theoretical analysis and simulation studies on potential trimming techniques to develop a practical trimming process for the shunt resistors capable of reducing the standard manufacturer's tolerance to less than 5%.
3. Generate a set of optimum trimming process conditions to minimise shunt resistor tolerance from $\pm 5\%$ to $\pm 1\%$ and reduce the trim time.

4. Validate the feasibility of the proposed trimming process through a series of further tests to establish if trimming causes any significant changes to the structural and electrical properties and performance of the components.

The objectives of this research are:

1. Carry out a thorough literature survey and preliminary studies, in order to acquire in-depth knowledge and understanding pertaining to the key areas of electrical performance of existing shunt resistors and the technical advantages and challenges of trimming techniques available under study.
2. Develop an accurate measurement system based on the potential measurement techniques and equipment that is suitable to measure low resistance values in the range of $50\mu\Omega$ to $10m\Omega$.
3. Design alternative trim geometries, which are suitable for shunt resistors by performing theoretical analysis and simulation studies on the shunts. In particular investigating the effect of varying trim geometry on the high current performance of the shunt.
4. Investigate different types of trimming techniques available and conduct an initial trimming process. Perform modifications to the design to reach the optimum solution while making sure it does not change the properties and behaviour of the shunt resistors.
5. Determine the preferred operating parameters and conditions for trimming the shunt resistor to achieve targeted resistance value in minimum time.
6. Validate the feasibility of the proposed trimming process by conducting a series of reliability tests on mechanical and electrical properties of the trimmed shunt resistors.

1.4 Research Framework

The research will carry out an investigation to reduce the value of standard manufacturing tolerance of $\pm 5\%$ for $100\mu\Omega$ Manganin shunt resistors. The following Figure 1.3 shows the process flow of how this project is carried out in order to achieve the aims and objectives defined in section 1.3. The project is broken up into three main phases:

- Phase 1: Development of Research Understanding
 - (1) Conduct a theoretical analysis study on a way to improve the resistance tolerance of the shunt resistors related to heat transfer and current density.
 - (2) Research different types measurement systems available and choose the most precise and economic system. The selected measurement system will be improved to make sure the accuracy of readings obtain throughout the experiments are repeatable and reliable.

- Phase 2: Modelling of Shunt Resistors
 - (1) Investigate the trimming techniques available and the most accurate and suitable ways to trim the shunt resistors. It is then proposed to trim the resistance value of the shunt resistors to target value by removing controlled amounts of material from the resistive elements.
 - (2) The parts are then modelled in SolidWorks CAD software and then analysed using Thermal Electric functions in ANSYS software to find out the optimum trimming designs.
 - (3) Determine if different types of trimming geometry used cause any detrimental effects to the shunt resistors properties.

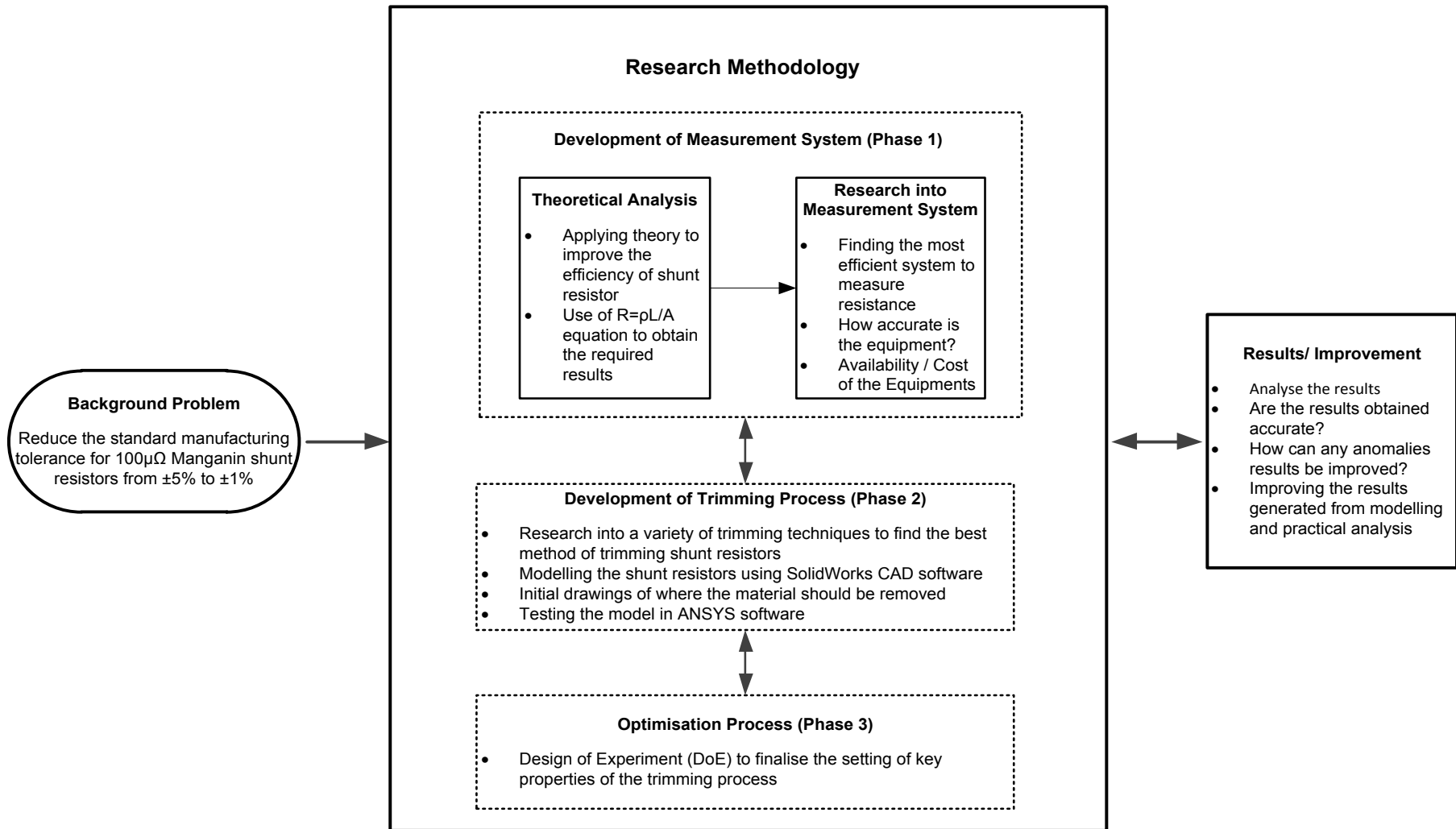


Figure 1.3: The proposed research framework.

- Phase 3: Optimisation Process
 - (1) Simulation software (LabVIEW) is used for this means to capture better measurement readings while conducting concurrent resistance trimming. The advantages of using this method are the increase in accuracy and confidence and also the increased efficiency.
 - (2) Design of Experiments (DoE) for the variables in the shunt trimming process will be used in this research. Variables or factors that will affect the outcome of the experiment will be determined and all of these factors will be used to generate the optimum process settings.
 - (3) Validate the results from the trimming process and check the reliability of the shunt resistors after trimming.

1.5 Original contributions

During the course of this research, original contributions pertaining to the design, analysis and optimization of the precision trimming process for 100 $\mu\Omega$ Manganin shunt resistors have been achieved. The research carried out has resulted in the following contributions to knowledge:

1. The development of measurement system to measure low resistance shunts which is capable of measuring 50 $\mu\Omega$ -10m Ω shunts with high accuracy and repeatability.
2. The development and optimisation of a precision trimming process to adjust the tolerance of a Manganin shunt resistor from $\pm 5\%$ to $< \pm 1\%$ for use in the manufacturing of smart energy meters, which delivered the high linearity required for accurate power measurement and the isolation necessary to meet industry standards regulating power and communications for smart energy meters.

3. The development of an automated precision trimming process prototype, which can be modified to use in the full scale manufacturing of shunt resistors.
4. Validation of the trimming effect on the structural and electrical properties of Manganin shunts resistors.

The potential future benefits that can be achieved from this research include reducing the production cost of smart energy meters by removing the need to calibrate out the errors introduced by the shunt in the meter. It will give energy manufacturers a huge benefit in using the more accurate measurement. Successful testing of the trimmed shunt resistors that meets the highest requirements laid out in ASTM standards. The end users of the meters will also benefit from more accurate energy measurement and only pay for how much energy they actually used. These contributions are supported by a number of publications as detailed in the next section.

1.6 Research Outcomes

1. S. N. Misti, M. Birkett, D. Bell, and R. Penlington, (2014). "A new trimming approach for shunt resistors used in metering applications," in *Electronic Design (ICED)*, 2014 2nd International Conference on, pp. 94-99.
2. S. N. Misti, M. Birkett, D. Bell, and R. Penlington, (2015). "Practical Implementation of a Concurrent Trimming Approach for Manganin Shunt Resistors," *Int'l Journal of Computing, Communications & Instrumentation Engg. (IJCCIE)*, vol. 2, pp. 81-85.
3. S. N. Misti, M. Birkett, D. Bell, and R. Penlington, (2016). "Experimental Investigation into Concurrent Trimming for

Manganin Shunt Resistor," Journal of Thermal Engineering.
(accepted for publication)

4. S. N. Misti, M. Birkett, D. Bell, and R. Penlington, (2016). "Investigation into Cutting Speed and Feed Rate Effects When Trimming Manganin Shunt Resistor," 5th International Conference on Engineering Optimization - Iguassu Falls, Brazil, 19-23 June 2016.
5. S. N. Misti, M. Birkett, D. Bell, and R. Penlington, (2016) "Effect of abrasive machining on the electrical properties $\text{Cu}_{86}\text{Mn}_{12}\text{Ni}_2$ alloy shunts," MDPI Materials Journal. (under review)
6. S. N. Misti, M. Birkett, and R. Penlington, (2016) "High-temperature XRD Investigations on Phase Transformations of Manganin," CrystEngComm. (to be submitted)

1.7 Organisation of the Thesis

This thesis mainly focuses on the development and optimization of a precision trimming process for Manganin shunt resistors used in energy applications; in which the relevant background information, key contributions and results, and in-depth discussions on the notable findings derived from the proposed work are presented and organized as follows:

The present chapter introduces the smart energy meter as a viable technology option, particularly in reducing energy consumption; in which the key components of smart energy meter are highlighted accordingly here. Taking into account the main challenges and open research issues pertaining to the system under study addressed in Section 1.2, the aims and objectives of the proposed research study are outlined in Section 1.3. Correspondingly, the research framework and original contributions of this research project are presented in Section 1.4 and Section 1.5, respectively.

Chapter 2 explains the growing demand for high precision, low value shunt resistors to measure the flow of electrical current. Different types of current sensing methods are discussed in detail and the reasons why the shunt resistor is chosen to be used in smart energy meters. The characteristics of the shunt resistor used in this project are studied, including how it is constructed and the properties of the materials used to manufacture its resistive element. Properties of existing shunt resistors are then described in an accurate manner. In addition, the principles and properties of different types of shunt resistors produced by different manufacturers are compared.

Next, Chapter 3 reviews the principles of resistance measurement, which include the Kelvin method of 4 terminal connections and any possible measurement errors. Different equipment is tested to see which one is more accurate and will be used throughout the experiment. A number of initial measurements are taken to validate the repeatability. Furthermore, the development of the measurement system to measure the Manganin shunt resistors is also discussed.

Chapter 4 explores the properties of Manganin, as the material has been used worldwide in the industry but very limited information could be found about its properties. Confirmation on each property is required in order to perform simulation on alternative geometry in the next chapters. Various different tests on structural, thermal and electrical properties of Manganin are conducted and these properties were used to find the rate of heat transfer and current density in the element. In addition, two different types of Manganin are compared to find if the materials have different compositions, which affect its properties.

In Chapter 5, the development of trimming techniques are investigated, taking into account the design geometry and the theoretical analysis. Trimming shunt resistors is a practical option for decreasing their tolerance, in which the technical advantages and major limitations of the different trimming techniques are addressed accordingly here. Modelling of heat transfer for alternative trim geometries and electrical current using Finite Element Analysis in ANSYS software are carried out in order to determine the best design. A thorough review of the relevant literatures pertaining to trimming techniques is presented

here, and the main contributions of the study are addressed subsequently. Initial trimming is then conducted to finalise the trimming geometry thereby resulting in the proposal of a new trimming process, which is discussed in detail in the next chapter.

Chapter 6 presents the new prototype trimming system, which was produced by the proposed electro-mechanical trimming process. Software known as LabVIEW was used to make an automated process ready for scale up for volume manufacturing of the precision shunt in the future. The literatures that are related to the system design were also included in this chapter and respectively mentioned. Slight modification was made to the process of trimming the shunt in order to comply with the need of controlling the cutting ability and establishing a reliable resistance measurement system.

Next, the main focus in Chapter 7 is to design a prototype trimming system for the experiments that will be carried out on the shunt resistor. A full factorial Design of Experiment (DOE) was used in order to get the optimum process settings for the newly designed trimming system. Parameters such as cutting speed and feed rate were considered in the DOE process and it was repeated three times to make sure that the results are reliable, and consistent. After the experiments, the data gained was analysed, especially on the time taken for the trimming process of the shunt and the resulting resistance deviation measurements.

Chapter 8 investigates the effect of trimming conducted using design geometries developed in the previous chapter on key electrical and structural properties of 100 $\mu\Omega$ Manganin shunt resistors. The focus is concerned on how the performance of the shunts will be affected after trimming when used in the smart energy meter. The trimmed samples were subjected to a series of experiments and environmental tests in accordance with various control standards and test procedures.

Finally, Chapter 9 presents the key concluding remarks and recommendations and directions for future research in this area.

Chapter 2

Review of Current Sense Characteristics

Almost all electrical products use resistors, from microprocessors which hold millions of resistors per square inch to a single use of resistor as a heating element in household items such as a stove, toaster, or a fan heater. A resistor is an electrical component that is capable of using electrical resistance as a circuit element to determine the current flow in the circuit or sense any changes that occur in a circuit [21, 34-36]. In the microelectronic industry, low and stable values of resistance over a wide temperature range are very desirable and resistors satisfy both criteria by possessing low resistivity and a small Temperature Coefficient of Resistance (TCR). Furthermore, resistances are commonly used in industry where demands are high for devices which measure the flow of current in electronic systems.

2.1 Current Sensing

Even though current sensors have been reviewed many times over the years, they still receive a lot of attention and are becoming really important in several applications such as hybrid electric vehicle and metering applications [6, 37-40]. In order for a smart energy meter to produce more complex power

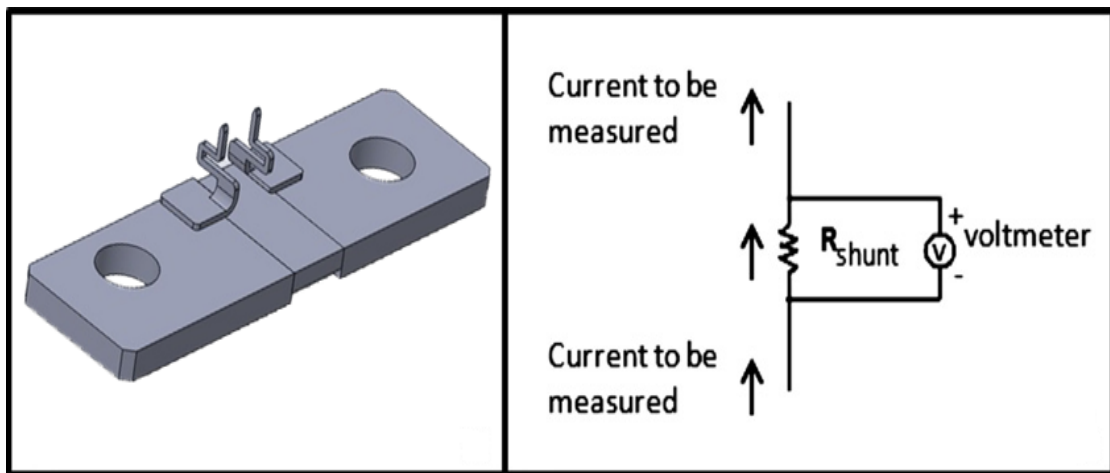
quality statistics, it requires precise voltage and current measurements. The accuracy of energy metering is very much associated with the voltage and current sensing equipment used in the system [41, 42]. Between those two criteria, current sensing is more difficult to measure as it has a wider measurement range and it also needs to be handled in a broader frequency range because of its current waveform which has a rich harmonic content [43]. There are three common types of current sensors technologies used in energy metering; the shunt resistor, the inductive sensor and the Hall effect sensor. The technology chosen largely depends on whether the power distribution is multiphase or single-phase. All of these technologies have their unique design requirements of accuracy, common-mode voltage, and directionality.

Current sensing can be split into two types which are direct and indirect. Indirect current sensing is derived from Ampere's and Faraday's laws [44, 45] and can be carried out by placing a coil around a conductor. By doing this, a voltage is induced across the coil that is proportional to the current. This method does not tamper with the circuit directly as there is no intrusion to the system for the current sensing purpose. Therefore, the system is inherently isolated. Indirect current sensing is usually used to measure large load currents in the range of 100A to 1000A. However, indirect sensing requires expensive sensors and it is not practical to be carried out on a PCB due to the requirement to place the sensing coil around the current carrying conductor [46].

On the other hand, direct sensing is basically taken from Ohm's law. A shunt resistor is placed in series with the circuit's load and a voltage is sensed across the shunt resistor which is proportional to the circuit's load current. Different amplifiers can be used to measure the voltage across the shunt and these includes current shunt monitors, operational amplifiers, difference amplifiers, and instrumentation amplifiers [47]. In contrast to the indirect sensing, direct sensing is an invasive method to the monitored system as the sensing circuitry needs to be connected electrically. Usually, this method is used when galvanic isolation is not required and is commonly carried out for load currents of less than 100A [48].

2.1.1 Shunt Resistor

Shunt resistors are popular in current sensing due to their relative ease of implementation. They are a low cost, small in size and a simple solution with reasonable accuracy, making them a favourite in many power electronic applications. Figure 2.1 illustrates a typical shunt resistor and its principle of operation, which is based on the voltage drop across the designated shunt resistance, which is used as a proportional measure of the current flow [49]. The current runs through a resistive element and the voltage drop is measured at this instant. This method can be used equally well in either alternating currents (AC) or direct currents (DC).



(a)

(b)

Figure 2.1: (a) Typical shunt resistor and (b) the principle of operation [50].

The shunt resistor may also generate a considerable amount of power loss at high currents and this can be calculated by using Ohm's law. Power loss in the shunt resistor will increase with the square of a current (I^2R), and this will restrict the implementation of the shunt resistor in high current applications. However, the use of shunt resistors is very desirable in measuring transient current pulses with fast rise-times and high amplitudes. In this application, the shunt resistors high frequency behaviour is very important.

The simplest way to measure current in an electrical circuit is by using the Ohm's law of resistance. However, there is still a notable drawback to the

direct sensing method in measuring the current. The connection between the mains circuit and the current sensing circuit can alter the real value of the current that flows in the system [51]. Although this problem can be solved with an electrical isolation, which is achieved by employing an isolation amplifier, this solution is proven to be very expensive. This solution will usually give a better current sensing performance but every parameter needs to be considered and it is not usually worth the financial sacrifice for a better performance.

A low resistance current shunt can give good accuracy and simple current measurement at a lower cost. The parasitic inductance of a shunt also has to be considered when performing a high precision current measurement. Even though the typical inductance will only measure a few nH, it will affect the impedance magnitude of the shunt at high frequencies. Therefore, this effect will be significant enough to cause noticeable error at low power factors.

Even though the shunt resistor is a favourite in electrical applications, the disadvantages of it are obvious where the measured current has to be interrupted to introduce the sensor, shunts for large currents are bulky, dissipate heat and the output is galvanically connected with the measured circuit. It is therefore often avoided for use in high current applications as they can generate significant power loss [38]. Apart from that, shunt resistors are also associated with a small voltage drop across the resistor. The voltage drop needs amplification that will alter the bandwidth, hence increasing the cost and size of the sensors [37].

2.1.2 Induction Sensors

Faraday's law is used by induction based current sensors in order to measure current. The most common types of induction based current sensors that are used in energy metering are the current transformer and Rogowski coil. Figure 2.2 shows an example of current transformer and its operation principle.

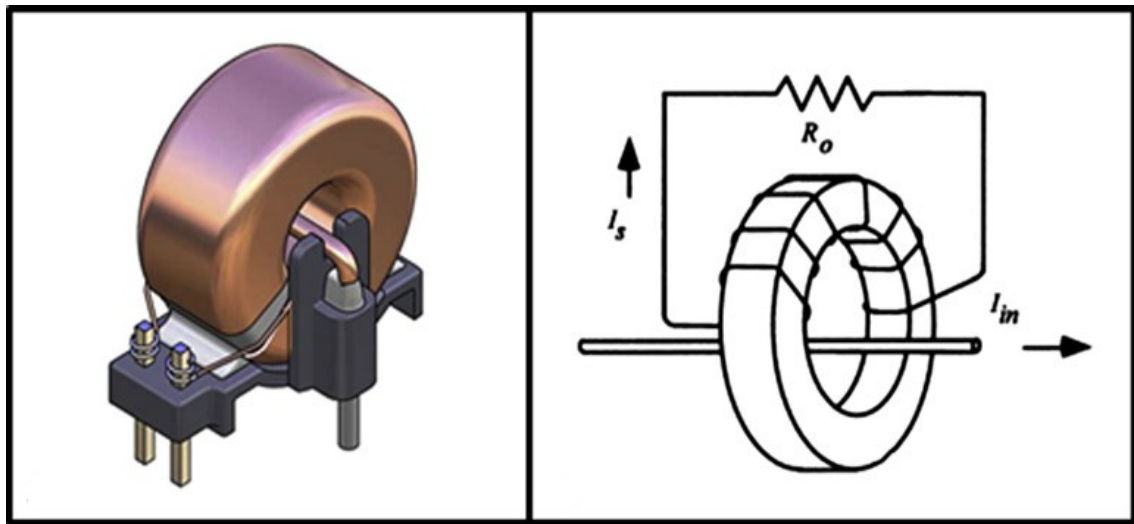


Figure 2.2: (a) Current transformer and (b) the principle of operation [52].

The current transformer has one significant advantage over the Rogowski coil, which is the output voltage is directly proportional to the primary current and this occurs without the existence of an integrator [53]. The current transformer operates by the conversion of the primary current into a relatively smaller secondary current. Current transformers can be split into two main types which are the solid core and split core. In terms of accuracy, the solid core is more accurate than the split core. However, the installation of a solid core transformer is more difficult [43]. Most of the current transformers used in industry use iron as their core and in some cases when the current transformer is exposed to a current that is beyond its rating, the core will probably become magnetically saturated. As a result of that, the core has to be demagnetized in order to retain its optimum accuracy levels. Therefore, a higher accuracy of current transformer can be achieved by exposing the core to a lower magnetizing current [52]. On the other hand, split core current transformers can be easily installed without causing interruption to the power system. Thus, they

are an ideal solution for remote power metering application in industrial facilities.

Rogowski coils use a similar approach to current transformers. In order to prevent hysteresis, saturation and non-linearity, theoretically, a Rogowski coil is commonly made from an air-core coil. Typically, the setup of a Rogowski coil consists of a coiled wire around a power line with an air core, as seen in Figure 2.3. The air core differs from an iron core as it does not saturate, even in a large permanent magnetic field [54]. Even though it has this advantage, it is also possible for other interference to affect the air core. For instance, a large inductive field might affect the ac current and this will change the value of the current sensed by the coil [55].

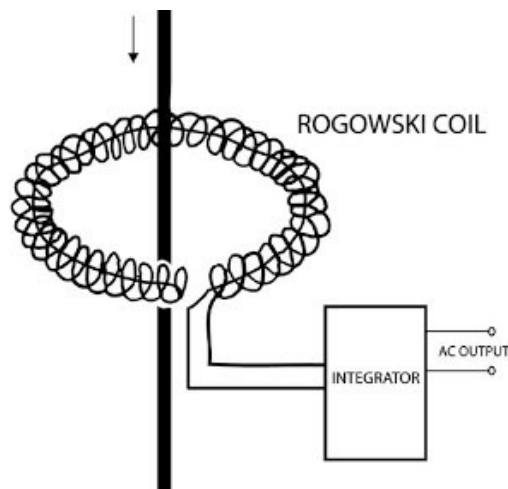


Figure 2.3: Principle of operation of Rogowski coil [56].

The basic operating principle of the Rogowski coil is to measure the primary current with the use of mutual inductance. The Rogowski coil cannot be used in direct current components as the EMF is only produced if there is a change in the magnetic field. However, this type of current sensor can be used to measure alternating current easily up to thousands of amps. Therefore, it is very useful in high current measuring applications. Without an iron core, the Rogowski coil will have non-linearity over a wide measurement range, from a hundred amps down to milliamps [57]. Rogowski coils are usually used in network quality analysis, energy efficiency, network deflection and network drops.

2.1.3 Hall Effect Sensors

One of the most common sensors that uses the magnetic field is the Hall-effect sensor. This type of sensor is best suited to direct currents, where it can take an open or closed loop form. The three main components in a Hall-effect sensor are the core, Hall-effect device, and a signal conditioner. Figure 2.4 displays an example of hall effect sensor and its operation principle.

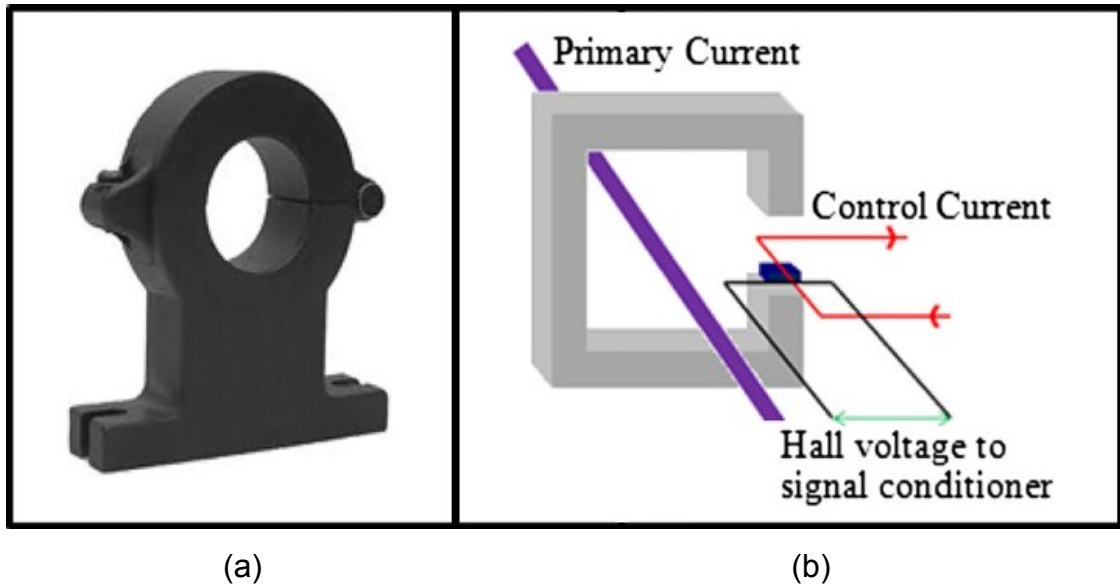


Figure 2.4: (a) Hall effect sensor and (b) the principle of operation [6].

Voltage will be produced perpendicular to both the field and current when a current-carrying conductor is placed into a magnetic field. This phenomenon is known as the Hall-effect. The basic principle of Hall-effect is shown in Figure 2.4(b). The figure shows that the current passes through a thin sheet of Hall element (semiconducting material) when the output connections are connected perpendicular to the direction of the current. If the magnetic field is not present, a uniform current distribution with no potential difference will be seen at the output. If there is a perpendicular magnetic field, a Lorentz force will be exerted on the current. As the force will disrupt the current distributions, a potential difference of voltage will be shown across the output.

The resulting voltage in this is the Hall voltage (VH). This interaction of magnetic field and current can be shown in the Equation (2.1) as follows:

$$VH = RH \left(\frac{I}{t} \times B \right) \quad (2.1)$$

where VH is the Hall Voltage in volts, RH is the Hall Effect co-efficient, I is the current flow through the sensor in amps, t is the thickness of the sensor in mm and B is the Magnetic Flux density in Teslas.

A measurable potential difference will be produced when a constant current flows through the device and the activated sensor is exposed to a magnetic field. The main advantage of a magnetic field sensor compared to a resistive or induction sensor is the ability to sense currents that produce both static and dynamic magnetic fields. While resistive or induction sensors only sense the dynamic magnetic fields [37]. However, the Hall-effect sensor is very sensitive to the external magnetic field; hence it is not suitable to an electrically noisy environment. Moreover, their readings can vary with temperature and are not always linear over a wide range of current, and they are also sensitive to the location of the measured conductor [38].

Many types of sensing device can use the Hall-effect as their current sensors. The Hall voltage is proportional to the vector cross product of the current and the magnetic field. The Hall element is the basic magnetic field sensor and it requires signal conditioning to make the output usable for most applications. The signal conditioning electronics needed are the amplifier stage and temperature compensation [58]. Voltage regulation is needed when operating from an unregulated supply. Although Hall Effect sensors are not as accurate as current transformers, they are cheaper. A Hall sensor can be pushed against the power line with no physical interconnection where with a current transformer; the power line and the sensing coil must be manually assembled.

2.1.4 Comparison of Current Sensing Methods

The performance of the different current sensing techniques is compared in Table 2.1. After all the current measuring methods have been discussed, the advantages and common application areas can be classified.

Table 2.1: Comparison between different types of current sensing [47].

| Resistor Type/ Specification | Shunt Resistor | Current Transformer | Hall Effect Sensor |
|---------------------------------------|-------------------|------------------------|-----------------------|
| Cost | Very Low | Medium | High |
| Linearity Over Measurement Range | Very Good | Fair | Poor |
| High Current Measuring Capability | Very Poor | Good | Good |
| Power Consumption | High | Low | Medium |
| DC-High Current Saturation Problem | No | Yes | Yes |
| Output Variation with Temperature | Medium | Low | High |
| DC Offset Problem | Yes | No | Yes |
| Weight | Medium | Heavy | Medium |

According to Jiang et. al [59], measured current and voltage is essential in energy metering as it will be used in the power and energy calculations. In order to get the value of current and voltage, a sensor is imperative in the circuit and there are several common options to the sensor which will include shunt resistors, current transformers, and Hall sensors [6, 20]. Of all the mentioned current sensing solutions, the shunt resistor is probably the most versatile and cost effective among them. Therefore, it is quite understandable that it is the preferred option in the household smart energy meter.

The use of other current sensing methods is not suitable for a low current flow. For example, a Rogowski coil can only measure alternating current and would not be suitable for low current flow. In a shunt measuring method, it is said to have high accuracy and suitable is for both direct current and alternating

current. However, in alternating current applications, a current transformer is said to be better than a shunt because there will be fewer losses in the circuit, assuming that the single-turn primary is of sufficient size.

The shunt application area covers the integration into control and regulation systems, and is widely used in process and energy technology. There are also shunts that work with current transformers and this measurement method is suitable for a higher alternating currents. It is also a potential-free type of measurement and the application area covers the installations and system technology, and network monitoring and analysis. Hall-effect is used for higher currents, either direct or alternating currents and it is commonly used in control processing of several individual systems, PV systems and general energy technology.

According to Klaiber and Turpin [60], current sensors can be judged according to six key qualities:

1. Accuracy - The accuracy of a power calculation obviously depends on the accuracy of the current sensors. Based on IEC and ANSI standards, Class 1 power meter will need current sensors with accuracy better than $\pm 1\%$ from nominal full scale reading, which would generally involve sophisticated manufacturing and expensive materials. An alternative is to calibrate the power meter for each single sensor it uses. Accounting for the specific qualities of each sensor lets a power meter operate in its most precise operating mode.
2. Drift - The drift of a sensor relates to how a reading varies over time independent of the initial system calibration. Changes in the ambient humidity and temperature, component aging, and so forth, all affect drift. A low drift level - meaning that the sensor is highly immune to such constraints - is important when building high-performance, stable and reliable power meters.

3. Phase shift - The accuracy of the true active power or energy calculation relates not only to how accurately and linearly the ac current and voltage sensors record amplitude; the phase shift that may arise between the measurements of these correlated values also plays a role. The phase shift should of course be as low as possible.
4. Linearity - The linearity of the sensor refers to the stability of its qualities within the full operating mode. A high linearity is essential for accurately measuring primary currents that span a wide range, especially those at low levels. Several technologies only work well over a limited measuring range, generally limiting their use to rather high or low currents.
5. Integration - Being passive devices, current transformers need no wiring other than a two-wire output connection to the main power monitoring unit. High-accuracy power meters require specific calibration for each sensor. They may have low-current outputs that are safer than traditional 1 or 5 A signals which can be accessed while the system operates. Current outputs are also almost insensitive to interference and should be preferred to voltage outputs when long cables connect the sensors to the power meter.
6. Price – Sensor price is important, of course, especially when the task calls for three accurate current sensors measuring three-phase power. However, the price of the current sensor is not the only consideration. Installation and maintenance costs can be significant, particularly when wiring must be powered down and unhooked while technicians add solid-core sensors. This is why split-core sensors can reduce costs as a whole.

A current sensing resistor is designed for low resistance as to minimize power consumption. As a result, the calibrated resistance senses the current flowing through it in the form of a voltage drop which is detected and monitored by control circuitry. Information about the current flow in electrical and electronic applications is important in order to make critical choices in minimizing the supply of the source while optimizing the output of the load. There are many of differences between the systems that needed to be considered and this will include the cost, isolation, bandwidth, size, precision, or measurement ranges. Nowadays, the information is needed to be used for monitoring purposes and the importance of having a specialist sensing technique has to be discovered in order to get a precise and easy to control system.

Applications that used large magnitudes of currents are suitable to be measured by combining a voltmeter and shunt resistor [61]. In these applications, normally the resistance will be measured in the order of milliohms or micro ohms. Therefore, even at full current, the voltage that will be dropped is considerably low. The low resistance of this current sensing circuit is very much similar to the resistance in a wire connection and therefore it has to be connected correctly to prevent huge measurement errors. In order to only measure the voltage drop in the shunt, without including any unwanted voltage from the system's circuit; the shunts are normally connected with the presence of four connection terminals. These four connection terminals will be discussed in detail in Chapter 3.

Another main problem in achieving precise readings or measurements is power losses. A precise reading is very important because analogue control loops are widely known to be replaced by digital control loops. The small voltage drop in the shunt also needs to be amplified and this will alter the bandwidth but its addition will sacrifice the advantages of the shunt resistor in terms of its size and cost. Therefore, power electronics engineers are seeking an alternative to the shunt resistor with a similar accuracy but with lower power losses.

However, the use of shunt resistor remains the most suitable device to measure the current in today's applications. This statement was supported by Cathal Sheehan and Mark Strzegowski, product-marketing managers for Bourns' and Analog Device who characterize shunts as simple, inexpensive, and unaffected by the magnetic and inductive fields that befuddle magnetic and inductive sensors [20]. The market nowadays has moved towards a wider dynamic range and they intend to include the application of current measurement for the user to freely manage their own energy usage. Therefore, the need for a device that can manage to measure the current accurately from 100 mA to 100 A with the similar level of accuracy as a current transformer which stands at 0.1% but at a lower cost, has never been so high.

2.2 Shunt Resistor Characteristics

The most suitable solution for the current sensor is the shunt resistor as they are low in cost, small in size, and simple to implement, while giving a reasonable accuracy. Almost all of the power meters that are being used worldwide are single-phase and they typically use a simple shunt resistor as the current-sensing element. Although shunts have inherent problems with heating, their voltage response is equally linear. However, they cannot cope with large loads because of their self-heating effect. On the other hand, current transformers have a small phase distortion that requires compensation, especially when the applications need to be equipped with a sophisticated measurement system, such as for reactive and harmonic energy measurements. Overall, generally, single-phase power-distribution meters use shunt resistors for current sensing, while three-phase meters use current transformers.

A deeper understanding of shunt resistor characteristics is analysed in detail in this section since they will be used in smart energy meters and are the focus of this research.

2.2.1 Theory of Operation

In order to learn more about shunt resistors, we need to have a thorough understanding of the theory behind their operation. Ohm's Law is widely used in the study of electricity and it was named after its discoverer, a Bavarian mathematician and physicist, Georg Ohm and states that the current flowing between two points in a conductor is directly proportional to the voltage or voltage drop and it is also inversely proportional to the resistance between those two points. The equation for Ohm's Law is expressed as:

$$V = I R \quad (2.2)$$

This expression is known as the Ohm's Law of resistance [62] and the relationship in this equation can be used to calculate the currents, I , resistance, R , and voltage, V . The relationship of current sensing techniques is based on the basic physical principal of Ohm's law of resistance and Faraday's law of induction. Originally, Ohm's law of resistance is the simplification of the Lorentz Law, which is expressed as:

$$J = \sigma (E + v \times B) \quad (2.3)$$

where J is the current density, E is the electric field, v is the charge velocity, B is the magnetic flux density acting on the charge and σ is the material's conductivity [63, 64]. The velocity of the charges in the second term can usually be neglected, as the velocity value is significantly small. Thus, the experiment reduces to the following:

$$J = \sigma E \quad (2.4)$$

The expression of $J = \sigma E$ in Equation (2.4) above, is visibly different from $V=IR$, since they do not use the same terms. However, both of these equations are related. Ohm's law comes in two forms. The expression of $J = \sigma E$ can be known as the microscopic version where it is used to define the relation

of the electric field and current density in some materials. On the other hand, the second version $V = IR$ focuses on the current flow on the macroscopic level in bulk materials that are considered to be perfectly homogenous. The length, L , and cross-section area, A , will be used further on in the equation in order to connect the microscopic to the macroscopic version.

The potential difference or voltage between the two ends of a material is expressed as $V = EL$. The material in the expression is typically set up in a uniform electric field, E , and the field is then oriented parallel to the material's long axis. The Ohm's law of $J = \sigma E$ is effective in every point of the material's bulk interior. The value of J is consistent throughout the material and this is because of the material's homogenous characteristics and the constant state of E . In any point of the material, the total current that will flow through must follow the expression of $I = JA$, and this relationship of the current, I , and voltage, V , can be shown below.

$$\begin{aligned}
 J &= \sigma E \\
 \frac{I}{A} &= \sigma \frac{V}{L} \\
 V &= I \left(\frac{L}{\sigma A} \right) \\
 &\equiv IR
 \end{aligned}$$

The macroscopic or global form of Ohm's law is shown in the expression of $V = IR$, and this equation is equivalent to the microscopic or local form of $J = \sigma E$. The global form involves quantities which are integrated over the macroscopic extent of the conducting material. The quantity in parentheses is defined as the resistance, R of the piece of material, where ρ is the resistivity of the material in ohm metres, Ωm :

$$R \equiv \frac{L}{\sigma A} \equiv \frac{\rho L}{A} \tag{2.5}$$

Figure 2.5 shows all the mathematical relationships between P , I , V and R . When two of the four variables are known, 12 formulas can be derived from the combination of Ohm's Law and Joule's Law. The wheel is very helpful and effective because it is easy to remember and apply. All the user has to do is choose a quadrant of the variable that they want to calculate, and select a corresponding segment of the known variables in order to get the final value of the unknown variable.

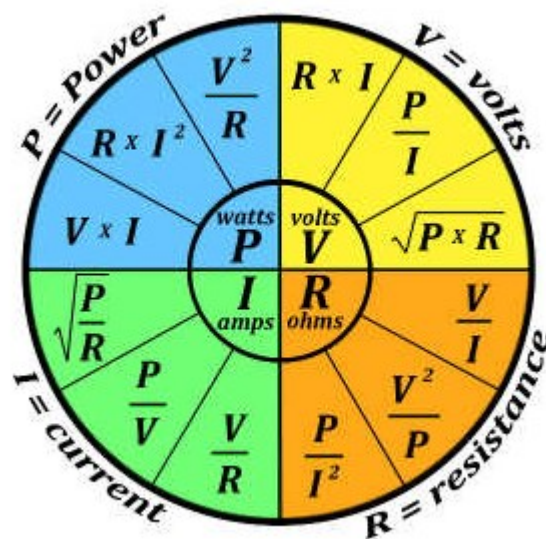


Figure 2.5: Ohm's Law Wheel [65].

From the wheel, V is the electrical potential or voltage (measured in volts, V), I is the current (measured in amperes, Amps, A), and R is the resistance (measured in ohms, Ω). P is the electrical power that is absorbed or produced in a circuit. As an example, voltage will be supplied to a circuit and produce power which will be absorbed by a load such as a light bulb or heater. The absorbed power will then be converted into light and heat for the user. The symbol for power is P and it is measured in Watt (W). The higher value of watts in an electrical appliance means that more power will be consumed by it.

2.2.2 Manganin Resistive Material

Edward Weston discovered the alloy Manganin which consist of copper, nickel, and manganese that was prepared through a complicated series of heat treatments in 1892. In the following year, he received the basic patent regarding to the manufacturing process, composition of the alloy, and the usage of the alloy for electric resistors. The production of the Manganin alloy, took place in Germany and it has now been universally accepted into the application for precision resistors and many other resistive components [66]. Originally, Manganin was the name of a specific alloy, but the term is now generic and covers several different compositions as stated in Table 2.2.

Table 2.2: Typical properties of Manganin resistance alloys [67].

| Basic composition (wt. %) | Resistivity (nΩm) | Temperature Coefficient of Resistance (ppm/°C) | Coefficient of thermal expansion (μm/m°C) | Tensile strength (MPa) | Density (g/cm³) |
|----------------------------------|--------------------------|-------------------------------------------------------|--------------------------------------------------|-------------------------------|-----------------------------------|
| 87Cu-13Mn | 480 | ±15 (15-35°C) | 18.7 | 275-620 | 8.2 |
| 83Cu-13Mn-4Ni | 480 | ±15 (15-35°C) | 18.7 | 275-620 | 8.4 |
| 86Cu-10Mn-4Ni | 380 | ±10 (40-60°C) | 18.7 | 345-690 | 8.4 |

The chemical elements mentioned are as follows; Cu (Copper), Ni (Nickel) and Mn (Manganese). There are also different types of Manganin manufactured by different companies such as Sandvik (with the element of Cu85Mn11Ni4), Kanthal (Cu85Mn11Ni4), Isabellenhütte (Cu86Mn12Ni2), and Goodfellow (Cu86Mn12Ni2). Table 2.3 shows the comparison of these Manganin properties.

Table 2.3: Comparison of different Manganin properties.

| Sources / Properties | Sandvik [68] | Kanthal [69] | Isabellenhütte [70] | Goodfellow [71] |
|--------------------------------------------------------|---------------------|---------------------|----------------------------|------------------------|
| Element (wt. %) | Cu85Mn11Ni4 | Cu85Mn11Ni4 | Cu86Mn12Ni2 | Cu86Mn12Ni2 |
| Density (g/cm ³) | 8.4 | 8.4 | 8.4 | 8.4 |
| Hardness (Gpa) | 110 | 110 | - | 124-159 |
| Tensile Strength (MPa) | 390 | 390 | 390 | 300 |
| Elongation at Break (%) | 30 | 30 | >25 | <50 |
| Electrical Resistivity (μΩcm) | 43 | 43 | 43 | 43-48 |
| Specific Heat Capacity (J/gK) | 0.41 | 0.41 | 0.41 | - |
| Thermal Conductivity (W/mK) | 22 | 22 | 22 | 22 |
| Melting Point (°C) | 1020 | 1020 | 960 | 960 |
| Maximum Service Temperature, Air (°C) | 20 | Room temperature | 140 | 300 |
| Coefficient of Thermal Expansion (10 ⁻⁶ /K) | 18 | 18 | 18 | 14-19 |

All Manganin alloy types have moderate resistivity at 20°C from 38 to 48 μΩm and low TCR (less than ±15 ppm/°C). The TCR of commercial Manganin is usually less than ±10 ppm/°C for an interval of 10°C on either side of the peak resistance, see Figure 2.6. The electrical stability of these alloys, verified by several decades of experience, is such that their resistance values change no more than 1 ppm per year when the material is properly heat treated and protected [72].

Manganin alloys are characterized by rather sharp, parabolic relations between temperature and resistance. The curves of temperature versus resistance for Manganin in wire and shunt form are shown in Figure 2.6. The shunt curve shifts from 20°C and 50°C because this material will normally operate at a higher temperature while the Manganin alloy in wire coil is designed for use in stable measuring conditions at 20°C ambient room conditions. Therefore, the difference between those two curves can be seen clearly at the peak resistance and temperature. However, they share the same resistance at 350°C which is the lowest resistance in the curves [73].

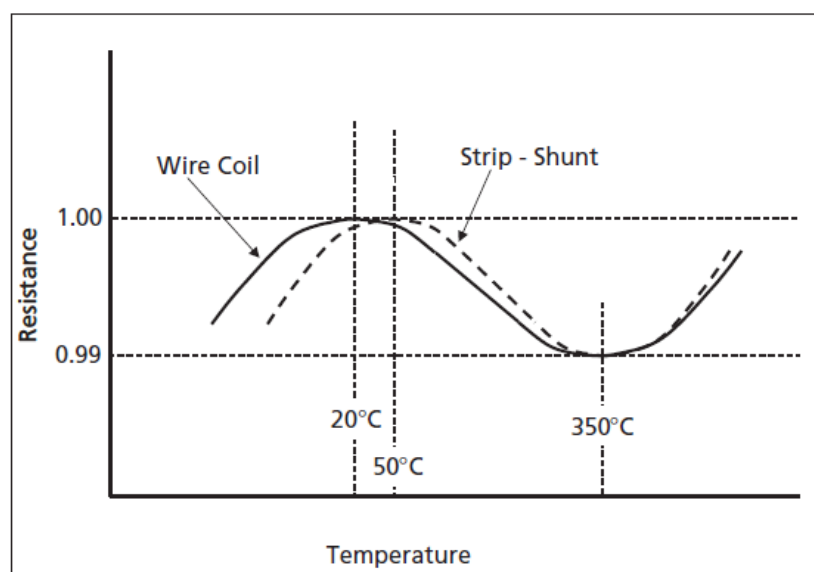


Figure 2.6: Qualitative Resistance-Temperature Curve for Manganin [73].

This property severely restricts the range of temperature over which resistance is stable, thus limiting the use of Manganin to devices for which operating temperatures are both stable and predictable. For some applications, the maximum of the peak temperature is kept near room temperature by controlling composition and minimizing the effects of small changes in ambient temperature. When instruments are designed for operation above ambient temperature, the chemical composition of Manganin is chosen so that the peak will occur in the operating temperature range. The so-called Manganin shunt, which carries high currents and consequently gets hot in use, usually has a peak temperature from 45 to 65°C [74].

Manganin is also susceptible to selective oxidation or preferential corrosive attack [75]. This may occur during manufacture, heat treatment or fabrication. Selective oxidation results in the formation of a copper-rich (manganese-depleted) zone on the surface of the material. This copper-rich sheath has the effect of greatly increasing the TCR and raising the peak temperature well beyond the range at which any precision resistor would ordinarily be used [76].

The resistivity of Manganin is approximately 500 nΩm at 25°C and is adequate for most instrumentation purposes. The thermoelectric potential versus copper is very low, usually less than -2 μV/°C from 0 to 100°C [77]. Manganin has a tensile strength that is noticeably higher than brass and cast iron. It also has electrical conductivity lower than silver, the ability to carry high current densities better than copper, thermal conductivity better than constantan and a density lower than nickel.

2.2.3 Manufacturing Method

Shunt resistors for use in smart energy meters require specific construction using a Copper-Manganin resistive material which has to be electron-beam welded to two copper terminations, see Figure 2.7.

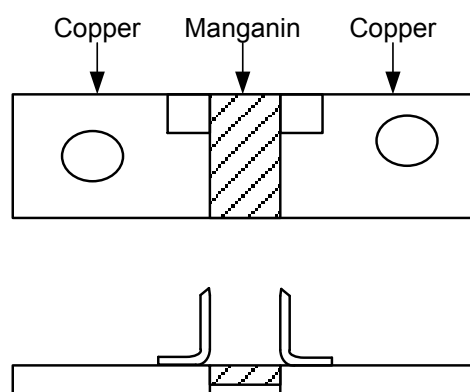


Figure 2.7: Shunt resistor construction.

Electron beam welding is a welding process which utilizes the heat generated from a beam of high energy electrons. The electrons strike the work piece and the kinetic energy that was generated by the electrons is converted into thermal energy as it hits the metal. As a result of that, the work pieces will be joined together, forming a weld after solidification. The process, shown in Figure 2.8, has to be conducted in a vacuum chamber at a pressure of about 2×10^{-7} to 2×10^{-6} psi, and both of the joined materials must be good electrical conductor [78, 79].

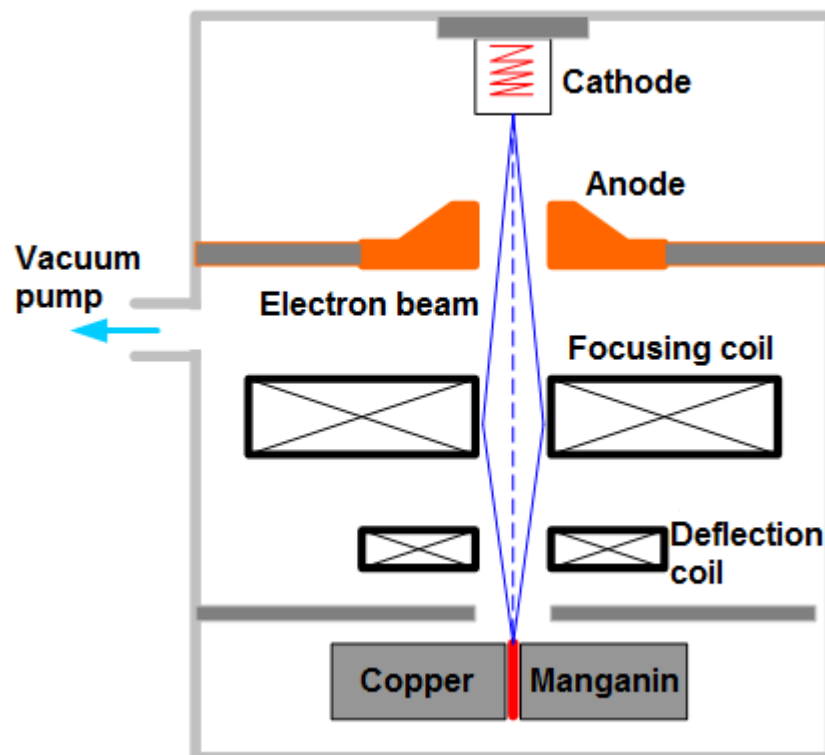


Figure 2.8: Electron beam welding process [80].

An electron gun (cathode) emits the electrons and due to the high voltage supplied between the cathode and anode, which is about 150 kV, the electrons are then accelerated up to 30% to 60% of the speed of light. Therefore, the kinetic energy of the accelerated electrons will increase and become high enough in order to melt the targeted weld area. Some of the electrons energy turns into X-ray irradiation. The accelerated electrons are then focused into a fine beam in the focusing coil which is then moved by the deflection coil along the weld.

Work pieces with thickness from 0.01 mm to 150 mm for steel and up to 500mm for aluminium are suitable to be welded with the electron beam process. It can be used in joining metals, especially if it involves metals that are difficult to weld by using other methods such as refractory metals (tungsten, molybdenum, niobium), and chemically active metals (titanium, zirconium, beryllium). Dissimilar metals also can be joined by using electron beam welding.

There are two known advantages in using the electron beam welding which will benefit the experiments in this research. Firstly, the small weld bead size of electron beam welding minimizes the mixing of dissimilar metals. As this process uses no other material to join the two pieces of metal, it limits any additional joint resistance. Therefore, when calculating the resistance of the Manganin, no additional series resistances need to be incorporated.

2.3 Key Performance Criteria

There are a number of criteria that can be used to compare existing shunt resistors and this comparison is beneficial in determining the most important parameters for the selection of shunts for this research. The criteria that will be discussed include the resistance, temperature coefficient of electrical resistance (TCR), thermal electromotive force (EMF), and resistance stability.

2.3.1 Resistance

Theoretically as defined in Section 2.2.1, resistance is the relationship between voltage which is the amount of electrical pressure (V), and ampere (A), amount of electrical current (I). It can be seen as the ratio of voltage with the electric current that flows in the circuit. This relationship will show the property of the conductor which is resisting the current flow in it. The standard unit for electrical resistance is ohms (Ω). According to Ohm's law, if the resistance is constant, the behaviour of the material can be predicted by using $I = V/R$.

Resistance can also be seen in terms of the bulk resistivity. Either terms of resistivity and resistance are both temperature dependent. The higher the temperature is, the higher the resistivity will be. The reasons for these changes in resistivity can be explained by considering the flow of current through the material. The flow of current is the movement of electrons from one atom to another under the influence of an electric field. Electrons are very small negatively charged particles and will be repelled by a negative electric charge and attracted by a positive electric charge. Therefore if an electric potential is applied across a conductor (positive at one end, negative at the other) electrons will transfer from atom to atom towards the positive terminal [81].

The effect of heat on the atomic structure of a material is to make the atoms vibrate, and the higher the temperature the more violently the atoms vibrate. In a conductor such as a copper wire, which already has a large number of free electrons flowing through it, the vibration of the atoms causes many collisions between the free electrons and the captive electrons. Each collision uses up some energy from the free electron and is the basic cause of resistance [82]. The more the atoms jostle around in the material, the more collisions are caused and hence the greater the resistance to current flow. In a material where the resistance increases with an increase in temperature, the material is said to have a positive temperature coefficient.

Materials chosen for the construction of resistors used in electronic circuits are carefully selected conductors that have a very low positive temperature coefficient. In use, resistors made from such materials will have only very slight increases in resistivity, and therefore their resistance. Using such materials for the manufacture of resistors creates components whose value changes only slightly over a given range of temperature.

2.3.2 Temperature Coefficient of Electrical Resistance (TCR)

The temperature dependence of a materials resistance can be predicted by using the TCR. TCR is the relative change of resistance when the temperature is changed by one degree Celsius (°C). A resistor's TCR tells how much its value changes as its temperature changes. It is usually expressed in ppm/°C (parts per million per degree Celsius) units. The higher the coefficient, the greater an increase in electrical resistance for a given temperature increase [83].

$$TCR = \frac{R2 - R1}{R1(T2 - T1)} 10^{-6} \quad (2.6)$$

TCR is calculated using Equation (2.6). From the equation, $R1$ is the initial resistance at temperature $T1$ and $R2$ is the end resistance at temperature $T2$. Typical values of $T1$ and $T2$ are 20°C and 70°C respectively.

The resistors' temperature dependence is normally determined by the precision of the resistance alloy itself. However, in most cases, low-ohmic resistors are also affected by the terminations, which results from the measurement of the sense voltage carried out by two additional contacts located directly on the resistive material. For example, major inaccuracies in TCR and the resistance value may occur as a result of poor layout or construction. The poor layout is also said to be able to distort the resistance value and TCR by more than 100%. By calibration, the additional resistance on the leads may be avoided but, the effect on TCR will still remain the same. Therefore, the common practice that is used on many data sheets of specifying the TCR of the resistive material is somewhat incorrect [84].

The lead resistance is very low in resistors that are made from electron welded composites such as Cu-Manganin-Cu. This is because of the low resistivity copper substrates that are used in this product. It is also possible to implement the optimum four-terminal configuration that will satisfy the criteria in

application in terms of rated resistance and TCR, all with the right combination of layout, soldering and resistor.

2.3.3 Thermal Electro Motive Force (EMF)

Thermal EMF is the small voltage that will be generated when two different materials or metals that were joined are subject to a change in temperature. This property will be used to determine the best material for the new shunt resistor. The thermal EMF is dependent on the temperature of the junction and the composition of the Mn and Cu metals joined. The unit for the thermal EMF of the junctions is specific in $\mu\text{V}/^\circ\text{C}$. The effect of thermal EMF in the shunt is undesirable as it can affect the resistance measurement value. This problem can be overcome by using an offset compensation which is a measuring technique that reduces or eliminates thermal EMFs in low level resistance measurements [85].

2.3.4 Resistance Stability

One of the important characteristics for a current sensor is its long-term stability. The reliability of the sensor is essential for the user, so minimum supervision and calibration time is required. Therefore, it is important for the resistance material to be stable against corrosion or the vulnerability to any metallurgical changes [86]. Manganin alloy is the ideal material for the sensor application as it is known to have a homogenous mixed crystal structure. This alloy is carefully annealed and stabilised in order to attain its thermodynamic ground state, hence resulting in a resistance stability in the range of parts per million (ppm) per annum.

2.4 Shunt Resistor Selection

There are several types of shunt resistors available in the market, manufactured by different companies. Basically, all of these products use the same base element, copper, but with a little difference in the percentage of the other elements added and as a result of that, there are some differences in the properties of these companies' products. Table 2.4 is shown in order to compare the existing shunt resistors available from different manufacturers and this table was produced based on the criteria that were discussed in the previous sections. Although there are many suppliers offering a vast range of current sensing solutions; a selection of shunt resistors from three major electronic component manufacturers will be considered in this research: TT Electronics, Isabellenhütte and Vishay Dale.

Within Table 2.4, there are some fields with no values in them as there was no data acquired from the company regarding those specific criteria. However, the point of showing the table is to broadly discuss the pros and cons between the three available shunt resistors and select the most suitable type for this research. Even though different companies produce a shunt that is dissimilar on many aspects, they share the same resistance tolerance which is at 5%. This is because this is the best tolerance they can currently achieve. If the tolerance can be lowered by even by 1%, the accuracy of the sensors will improve and this will give an improved accuracy in determining the value of the current flow.

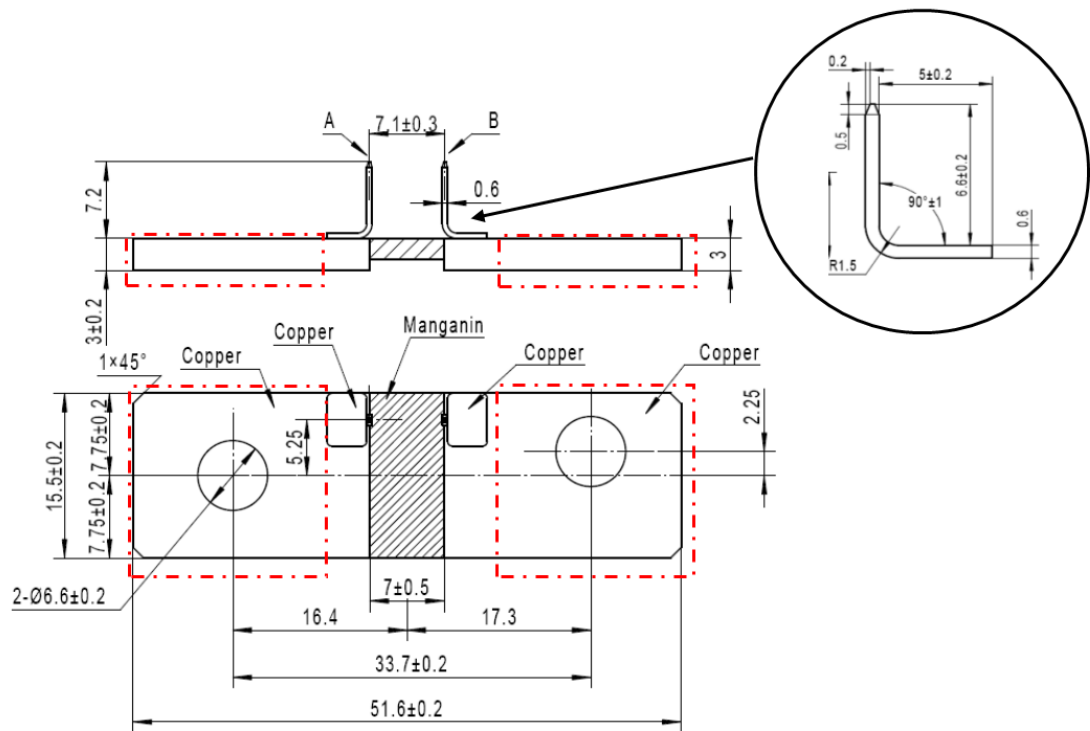
Table 2.4: Comparison on different resistors from different manufacturers.

| Properties | TT Electronics [21] | Isabellenhütte [87] | Vishay Dale [88] |
|----------------------------------|----------------------------|----------------------------|-------------------------|
| Resistance Value ($\mu\Omega$) | 100 | 100 | 100 |
| Power dissipation | 1 to 3 W | | 3 W |
| Ohmic values ($\mu\Omega$) | 25 to 500 | 100 to 1000 | 50 to 1000 |

| | | | |
|-----------------------------------------------|------------|------------|------------|
| Temperature Coefficient of Resistance (ppm/K) | 100 to 200 | 30 | 225 |
| Resistance Tolerance (%) | 5 | 5 | 5 |
| Operating temperature range (°C) | -55 to 170 | -55 to 170 | -65 to 170 |
| Inductance (nH) | < 1 | < 1 | < 5 |
| Thermal EMF (μV/K) | 3 | 0.3 | < 3 |

Since this research will only focus on lowering the resistance tolerance, which all three companies share the same value of the main aspect of the shunt selection lies in their availability and accessibility. The location of TT Electronics is very near to where the research is based; therefore, the exchange of data and samples can be carried out smoothly. This research used a 100μΩ Manganin shunt resistor manufacture by TT Electronics to explore the possibility to trim the shunt resistors by removing a controlled amount of resistive material in order to reduce the standard tolerance of ±5%.

The construction of the 100μΩ Manganin shunt resistor is shown in Figure 2.9. All samples were constructed from a 15 × 7 × 3 mm thick Manganin (86 wt.% Cu, 12 wt.% Mn, 2 wt.% Ni) resistive element which was electron beam welded to two 22.5 × 15 × 3 mm copper plates with two tin plated copper voltage terminations, which permits more accurate measurement of the resistance value of the shunt, producing a 100 μΩ ±5%, 3W rated, shunt resistor.



- Notes:
1. General dimensional tolerance = $\pm 0.1\text{mm}$
 2. A-B of resistance = $100\mu\Omega \pm 5\%$
 3. Spot welded pins must withstand 100% pull test at 25kg
 4. Pins to be plated with 4 μm min of tin
 5. - · - · - = post-tinned areas to be plated with 6 μm min of tin including holes

Figure 2.9: 100 $\mu\Omega$ Manganin shunt resistor specifications.

2.5 Summary

In summary, there are a number of important characteristics of the shunt resistor that are desirable in order to get the best result in this research. The key characteristics were listed and analysed in this chapter before making the final shunt selection. The favourable characteristics for this research are that the selected shunt has to be stable and repeatable in a wide range of current which stands from 0 to 100 A at the operating temperature of -25 to +55 °C with air humidity from 30 to 100%.

The shunt resistor also uses the most suitable resistive material, which is Manganin, and the simplicity of it really stands out from all other current sensing choices. The shunt resistor construction also proves to be low cost, and its implementation can be carried out by a simple connection to the measurement circuitry. Therefore, the most balanced and suitable current sensing device to be used in this research is the shunt resistor that uses Manganin as its resistive material.

The next chapter will focus on the resistance measuring system that will be used to accurately determine the resistance value of the shunt resistor samples during the trimming process.

Chapter 3

Development of Measurement System

The previous chapter looked at the physical properties of Manganin shunt resistors. This current chapter deals with establishing a precision measurement system to accurately measure the resistance value of the shunt resistors with high repeatability. It is relatively easy to measure the resistance of mid-range 1Ω - $100k\Omega$ components by using a digital multimeter. However, measuring $100\mu\Omega$, particular to less than 1% accuracy is very hard and many errors can occur, which can be contributed by many factors such as lead resistance, device heating and non-ohmic contacts.

In order to trim $100\mu\Omega$ shunt resistors to $\pm 1\%$, an accurate method of resistance measurement must be established first. Repeatable measurements of accuracy of $\leq 10\%$ of the 1% tolerance 0.1% are required because that will determine the accuracy, precision, and/or resolution for the measurement. Normally, the resistance of a conductor can be determine by forcing the current to pass through the work piece by using one pair of leads and measuring the voltage drop with another pair of leads. There are also specific methods that can be used in order to measure the resistance and it will depend to the shape and size of the work piece. Furthermore, this research focuses on lowering the tolerance and this will mean that the need for sensitive instruments is

paramount in order to note even the slightest change in resistivity while conducting the experiments or tests.

This chapter will firstly review potential techniques to measure $\mu\Omega$ resistance before comparing the performance of two potential measurement systems to accurately measure the resistance of a sample of Manganin shunt resistors.

3.1 Principles of Resistance Measurement

A committee was formed in the United States in 1861 in order to develop a resistance standard. Many familiar names such as James Clerk Maxwell, James Prescott Joule, Lord William Thomson Kelvin, and Sir Charles Wheatstone are among the member of the committee. In the early days, in 1864, the standard of resistance used in an electrical application was a coil of platinum-silver alloy wire which was sealed in a container filled with paraffin. This standard setup was used for 20 years and the studies on creating a more reliable standard were made by the old National Bureau of Standards (NBS) which is known today as the National Institute of Standards and Technology (NIST) and they are the ones who control the standard usage of "OHM" [89].

Measuring the low resistance will helps identify the value of resistance elements that have increased over the acceptable values. This measurement can be carried out by controlling the flow of current in the equipment with specific design parameters. According to Ohm's Law, by controlling the V_{ac} and V_{DC} of a specific energy source, the drawn amount of current is dependent on the resistance of the circuit.

Nowadays, with the increase of electrical and electronic device usage in every household and industry, demand for electrical circuits with high quality, precision, and reliability is increasing. This situation differs from years ago where the ability of an electronic device to measure up to 10 mili-ohms was acceptable. However, in the present, there is demand especially in the industrial

electrical environments, where the engineer is required to be able to take measurement which will show the repeatability of a few micro-ohms or less.

The low resistance measurement range is usually taken to be below 1Ω . Therefore, it is imperative to have high end test equipment that will minimize the errors by the test lead resistance, and/or the contact resistance in between the tested materials and the probe tip. In this stage, the standing voltage across the materials that are measured, for instance; the thermal EMF in the joints of different metals, need to be discovered and identified as they may cause errors in the system [61]. In order to solve this error, a four terminal measurement method can be carried out with a reversible test current and a Kelvin Bridge meter. Many low resistance ohmmeters are able to detect the lower range down to 0.1 micro-ohms and this level of measurement will be useful in order to perform a number of low range resistance tests.

The resistance of material measurement is very useful in a wide range of industries. For instance, low resistances ohmmeters can help in identifying a number of problems that could have led the apparatus to failure or breakdown. Therefore, low resistance testing is highly recommended for a wide range of industrial practices such as manufacturing, motor windings, circuit breaker, ground bonds, weld joints, small transformers, switches, and resistive components [90].

The common schematic of a current measurement in a shunt resistor is shown in Figure 3.1.

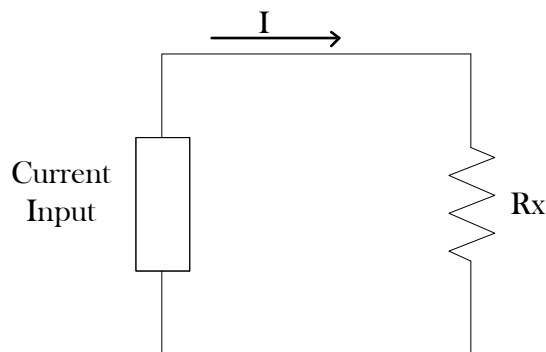


Figure 3.1: Connecting a Shunt Resistor.

In this method, the current is directed through an external shunt resistor rather than into the ammeter or data acquisition board. Theoretically, there is no limit to the amount of current in this measurement method, provided the voltage drop across the shunt does not go over the voltage range of the meter.

Typically, in order to measure the true DC current, 4 wire measurements will be taken by the resistance ohmmeter, see Figure 3.2. The DC current will flow through the component (R_x) and the ohmmeter's internal standard. Then, the voltage between those two points will be recorded and the ratio of these readings will be used to calculate the resistance. By using this method, the current only needs to be steady for a few milliseconds in order for the reading to be taken. However, this method requires two measurement circuits and since the measured voltage value will be very small, μV measurement sensitivity is required.

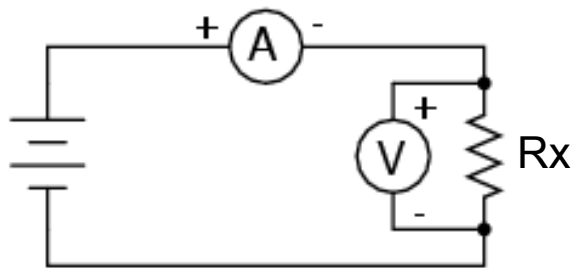


Figure 3.2: Four wire resistance measurement.

3.1.1 Measurement Techniques

The selection of measurement technique depends on the degree of information required from the measurement, and the magnitude of the resistance being measured. Resistance readings cover a wide range of values from micro-ohms into the thousands of meg-ohms region. Figure 3.3 shows the measurement range in which each type of measurement technique performs best.

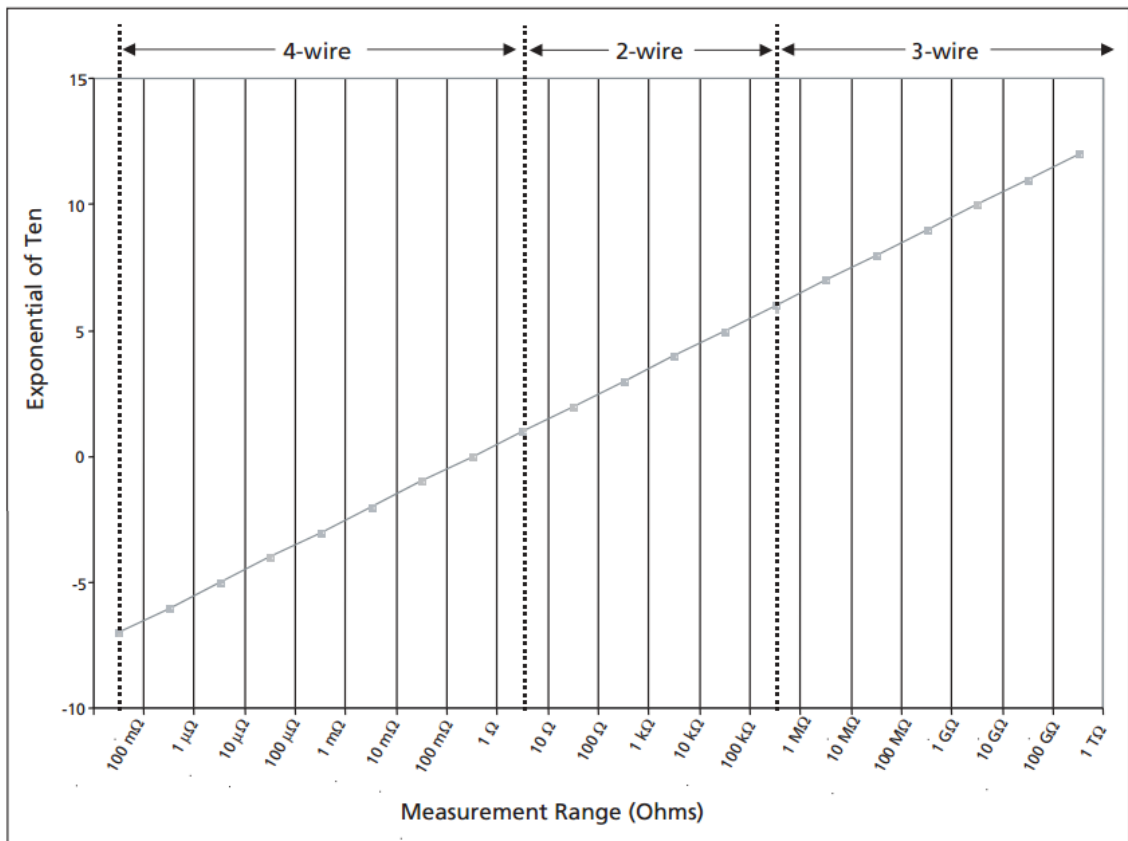


Figure 3.3: Selection of Optimum Measuring Technique [73].

Two wire testing is the simplest method and it is used to make a general assessment of a circuit element, conductor or the routing of a conductor in a circuit. It is generally used when the probe's contact resistance, series lead resistance or parallel leakage resistances do not degrade the quality of the measurement beyond a point acceptable to the operator. Three wire testing is reserved for very high resistance and is typically used for measurements above 10 MΩ. Normally, this type of testing is associated with diagnostic insulation resistance. The test method uses a third test lead as a guard, and allows for resistances in parallel with the test circuit to be eliminated from the measurement [73].

Four wire testing is the most accurate method when measuring circuits below 10 Ω as this method eliminates errors due to lead and contact resistances. This is the test method associated with low resistance ohmmeters. The four wire measurement negates the errors due to the probe lead wire and any contact resistance values in the final reading, ensuring more accurate

measurements. Four wire testing is also known as the Kelvin configuration and features four wire connections; two wires known as the current or source leads carry the current passing through the shunt, while the other two wires, which are known as the potential or sense leads, sense and measure the voltage drop across the shunt resistor. Even though there are still some small current flows in the potential leads, this current is negligible and can be ignored. The voltage drop in the sense terminals of the meter is more or less the same as the voltage drop across the shunt resistor. This method of measurement will result in an accurate and consistent reading when measuring resistance is below 10Ω .

This is probably the most suitable way to measure the $100\mu\Omega$ shunts which is by the connection of four separate wires, which are two wires for the current (C and C1), and two wires for the potential or sense (P and P1), as seen in Figure 3.4. Even though the placement of the current wires is not critical to the setup, the current wires are very much preferable to be placed outside the potential. However, the potential wires must be connected exactly to the desired measured points. Therefore, the measured value is exactly between these potential wire points [91].

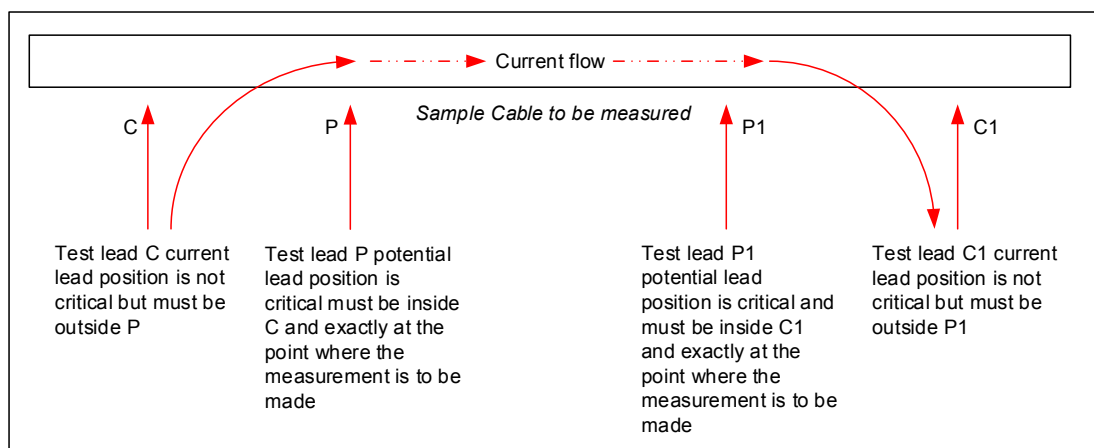


Figure 3.4: 4 wire Kelvin connection [92].

3.2 Measurement Uncertainties

It is quite impossible to have an absolute certainty of the quantity in a measurement. Tolerance and disturbance will surely play its part in contributing to the degree of uncertainty in a measurement scenario. Furthermore, the equipment will also have its own distinctive limiting factor. Terminologies of measurement uncertainties are often used as follows [93]:

- **Accuracy:** The error of the measured value with the real measurement.
- **Precision:** The repeatability of a measured value which is spread around the average values.
- **Resolution:** The smallest detected change to be distinguished in the magnitude of the measured value.

The concept of accuracy and precision are often used interchangeably as they are synonymous. However, these two words bear different meanings. The accuracy is the closeness or deviation of the measured value to the actual value. Precision is the random spread of the measured values. The measured values will be shown in a certain variation after a number of measurements were taken under a stable voltage or any other parameter. This is because of the thermal noise in making the measurement, either in the measuring equipment or the measurement set up [94]. These variations are shown in Figure 3.5(a). These measured values can also be plotted in a histogram which is shown in Figure 3.5(b).

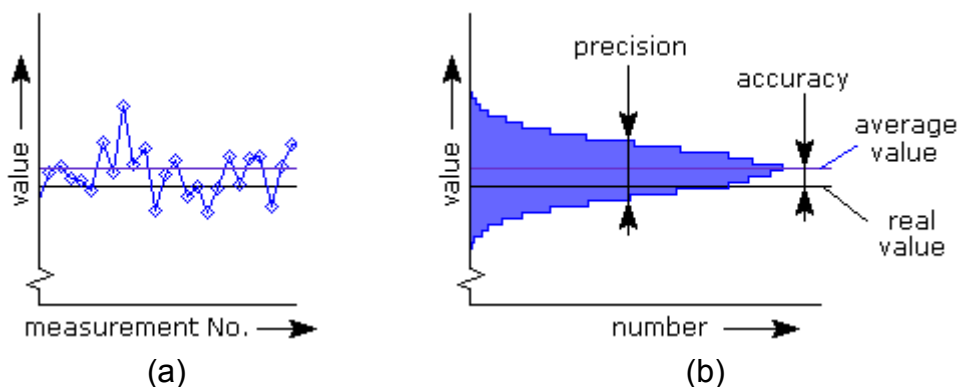


Figure 3.5: (a) Series of measurements and (b) Values plotted in a histogram [95].

The histogram shows how often a measured value occurs. The mode measured value is the most frequently measured value, which is located at the highest point in the histogram and it is indicated as the blue line in both of the graphs in Figure 3.5. The real value of the parameter is represented by the black line. What separates the mean measured value and the real value is the accuracy. The width of the histogram depicts the spread of the individual measurements and this distribution of measurements is called precision.

3.2.1 Accuracy

The indication of the closeness to the actual value of measurement is the accuracy. A series of measurements will need to be taken and the average of the measurements will be used rather than taking a single measurement which depends a lot on precision that can affect the accuracy.

There are two values of the uncertainty of measuring instruments, which are the uncertainty of reading and over the full scale. The total measurement of uncertainty will be determined by both of these specifications. The value of these measurement uncertainties is written down in percentage (%) or in parts per million (ppm) whichever is more relative to the current national standard. 1% is equivalent to 10,000 ppm.

After the calibration of an instrument, the specified uncertainty will be suitable for certain temperature ranges and for a specified period of time. However, different ranges on other uncertainties may also apply to this. The reading of a measurement could be read with the indication of the percentage deviation without further specification. The reason for this inaccuracy is caused by the tolerances of the voltage dividers, digitization, and the absolute deviation of the readout [96].

For example, in Figure 3.6, a voltmeter with a reading of 70V which has a $\pm 5\%$ reading specification, will experience an uncertainty of 3.5V (5% of 70V), either in the upper and lower region. Therefore, the range of the actual voltage will be between 66.5V and 73.5V.

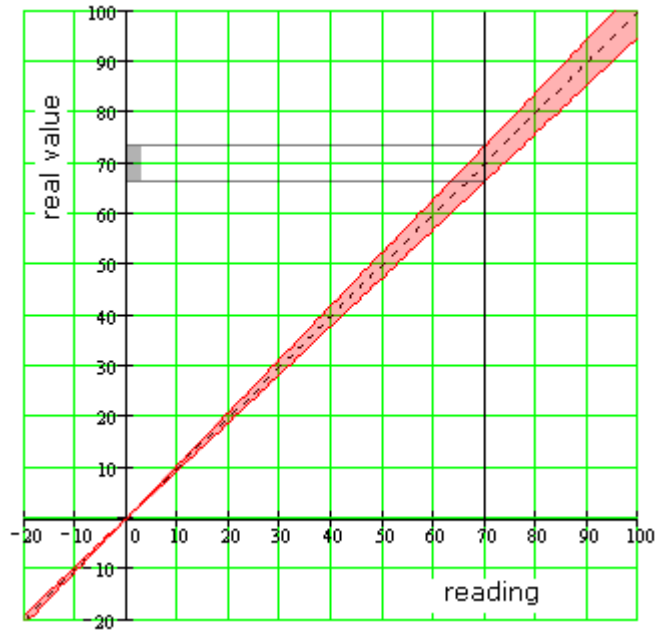


Figure 3.6: Uncertainty of 5 % reading and a read value of 70 V [97].

As a shunt resistor is commonly used to measure currents, the measurement in the shunt has to consider all of the tolerances that may contribute to the total uncertainty. The total uncertainty can be calculated by multiplying the tolerance of the shunt with the reading uncertainty of the measuring instrument. By using the values in Figure 3.7, the total uncertainty can be measured by using the equation given in Equation (3.1). Replacing the % reading and % shunt values in the equation with 1.5% and 2.0% respectively will result in a total reading uncertainty of 3.53%.

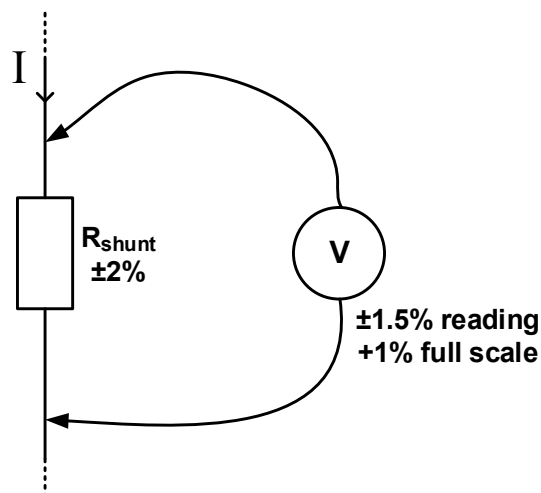


Figure 3.7: The uncertainty increment of the usage of a shunt resistor [97].

$$\begin{aligned} \% \text{ total} &= \left[1 - \left(1 + \frac{\% \text{ shunt}}{100 \%} \right) \times \left(1 + \frac{\% \text{ shunt}}{100 \%} \right) \right] \times 100\% \\ \% \text{ total} &= \left[\left(1 + \frac{1.5\%}{100\%} \right) \times \left(1 + \frac{2\%}{100\%} \right) - 1 \right] \times 100\% = 3.53\% \end{aligned} \quad (3.1)$$

The resistance of a shunt is temperature dependent; therefore, the value of resistance is specified for a given temperature. This temperature dependence is written in the expression of ppm/°C.

For example, a calculation of the resistance value in an ambient temperature (T_{amb}) of 30°C, with a shunt specification: $R=100\Omega$ and 22°C (R_{nom} and T_{nom} respectively), and lastly with the temperature dependence of 20 ppm/°C is shown in Equation (3.2):

$$\begin{aligned} R &= \left[1 + (T_{amb} - T_{nom}) \times \frac{ppm}{1000000} \right] R_{nom} \\ R &= \left[1 + (30^\circ C - 22^\circ C) \times \frac{20}{1000000} \right] 100\Omega = 100.016\Omega \end{aligned} \quad (3.2)$$

There is another effect to the resistance value when current flows through a circuit. The flowing current through the shunt will cause the energy to dissipate as heat and the temperature will rise, hence altering the value of resistance. However, the change depends on a number of factors. Therefore, in order to get an accurate measurement, the shunt has to be calibrated with a specified flow of current and environmental conditions in which it will operate.

3.2.2 Precision

The random measurement error can be defined by using the term precision. The random nature of deviation in the measurements is probably rooted from thermal origins. However, it is not possible to define the absolute error because of the arbitrary nature of this kind of noise. Precision will only provide the probability of a measurement value between given limits [98].

Over-sampling or filtering can be carried out in order to improve the precision of a measurement. The average of all the individual measurements is calculated to minimise the noise quantity. This step also reduces the bandwidth and the spread of the measured values, hence increasing the precision of the measurement reading [99].

3.2.3 Resolution

Resolution usually has the smallest effect on values but still can be distinguished in a measurement system. However, the specified resolution of an instrument is not related to the accuracy of measurement. An analogue signal is converted into a digital equivalent with the AD converter. The resolution, which is the difference between two values, is always equal to one bit, or 1 digit in the case of a digital multimeter [100].

The resolution can also be expressed in different units other than bit. As an example, consider a digital oscilloscope with an 8-bit AD converter. When the vertical sensitivity is set up to 100 mV/div with the number of divisions equal to 8, the total range of the values will be up to 800 mV. The 8 bits show $2^8 = 256$ different values. Therefore, the resolution in volts is $800 \text{ mV} / 256 = 3.125 \text{ } \mu\text{V}$.

3.3 Review of Potential Measurement Techniques

Resistance, DC current and DC voltage are measured most often with digital multi meters (DMMs). Generally, these instruments are adequate for measurements at signal levels greater than 1 μV or 1 μA or less than 1 G Ω . However, a number of error sources can have serious impacts on the low current measurement accuracy of DMMs [101]. For example, the ammeter may cause measurement errors if it is not connected properly and the source resistance of the device under test will affect the noise performance of a feedback ammeter and also the measurement accuracy.

There are different types of instruments available to make DC measurements including micro-ohmmeters, electrometers, DMMs, Source Meter instruments, source-measure units (SMUs), Pico meters, Nano-volt meters and also low current preamps. The important characteristics of micro-ohmmeters will be discussed in detail as the instrument is used throughout the project. A micro-ohmmeter is a special type of ohmmeter designed especially for making low level resistance measurements [102]. While techniques used for making resistance measurements are similar to those used in a DMM, micro-ohmmeter circuits are optimized for making low level measurements. The typical micro-ohmmeter can resolve resistance as low as $10\ \mu\Omega$.

For the purpose of this research, two micro-ohmmeters were tested to identify the resistance values of the shunt resistor. These values have a tolerance range between $100\ \mu\Omega \pm 5\%$. Potential measurement techniques were investigated to develop a precise and accurate measurement system for the shunt resistors. In order to achieve the objective of reducing the tolerance of the shunt resistors, a system to accurately measure the resistance value is required. Measuring the value of a $100\ \mu\Omega$ resistor is not trivial and a system accuracy of $\pm 0.1\%$ (i.e., 10% of the initial 1% tolerance target) was strived for.

3.4 Comparison of Available Measurement System

The main selection criteria was minimum total system error when measuring $100\ \mu\Omega$ at 1 A. The total system error should be as low as possible and ideally be less than 10% of the tolerance being measured; in this case 0.1% (10% of 1%). An overview of the potential micro-ohmmeters is presented in Table 3.1. There are three meters available for this research, which are the Cropico D07 Micro-Ohm Meter, Agilent B2900A Precision Source/Measure Unit and Agilent 34420A Nano-Volt/Micro-Ohm Meter. All these meters were tested in order to establish the best measurement system in terms of measuring low resistance values suitable for $100\ \mu\Omega$ Manganin shunt resistors.

Table 3.1: Summary of system accuracy of potential resistance measurement equipment.

| Model | Resistance, Current or Voltage | Total error | Total % Error | Total System % Error |
|----------------------------------------------|--------------------------------|-------------|---------------|----------------------|
| Cropico D07 Micro-Ohm Meter | Resistance | 0.0000014 | 1.4 | 1.4 |
| Agilent B2900A Precision Source/Measure Unit | Current | 0.0018 | 0.18 | 225.195 |
| | Voltage | 0.00022502 | 225.015 | |
| Agilent 34420A Nano-Volt/Micro-Ohm Meter | Resistance | 2.007E-06 | 2.007 | 2.007 |
| Agilent B2900A Precision Source/Measure Unit | Current | 0.0018 | 0.18 | 0.187 |
| | Voltage | 7E-09 | 0.007 | |

The first measurement system shown in Table 3.1 is the Cropico D07 Micro-Ohm Meter. The total error for this system is 1.4% and is well outside the target of 0.1%. Both the Agilent B2900A and 34420A models can source the required current of 1 A, but their overall system errors are too large at 225.195% and 2.007% respectively. It appeared that the most suitable method to measure at 1 A with reasonable accuracy was to combine separate current source and voltage sense meters. The combination of the Agilent B2900A source meter and 34420A Nano-volt meter has a lower combined system error of 0.187% and was expected to be the most suitable measuring system available for this research. However, to confirm this, resistance measurement trials were undertaken with both of the available systems.

3.4.1 Cropico D07 Digital Micro-ohm meter

In this experiment a digital micro-ohmmeter, type Cropico D07, was used to measure the resistance value of the shunts. The four-wire Kelvin method of measurement was used as it is preferred for resistance values below $100\ \Omega$ as it reduces the effect of test lead resistance giving more accurate and consistent results.

As shown in Figure 3.8, the four-wire Kelvin method involves feeding a constant known current (I) through the shunt resistor whilst accurately measuring the voltage potential (v_e) dropped across the Manganin strip. Although some small current will flow in the potential leads, it is insignificant and can be disregarded. In order to produce a realistically measurable voltage drop, a source current of $10\ \text{A}$ is used with the input range set to $600\ \mu\Omega$. This produces a voltage of nominally $1\ \text{mV}$ across the $100\ \mu\Omega$ Manganin strip. However, since this substantially large current of $10\ \text{A}$ can cause unwanted heating effects within the resistor element, a pulsed current of $10\ \text{ms}$ frequency was used to enable more accurate resistance measurements to be taken.

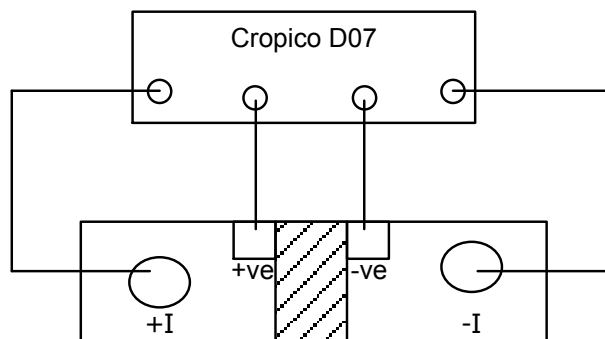


Figure 3.8: Connection of a shunt resistor to Cropico D07.

In this experiment, the resistance value of 20 shunt resistors was measured 5 times to observe if the digital micro-ohm meter could give accurate and repeatable readings. Measurements were taken at 15 second intervals to ensure consistency in the experiment and reduce fluctuation of the readings. The results collected in Table 3.2 from the micro-ohmmeter readings indicated that each resistor used in the experiment was within a $100 \mu\Omega \pm 5\%$ tolerance which was claimed by the manufacturer. The distribution of resistance measurements using Cropico micro-ohm meter is low with average range of 0.705 and standard deviation of 0.2778.

Table 3.2: Resistance measurement readings using the Cropico D07 digital micro ohm meter.

| Sample No. | Measurement No. ($\mu\Omega$) | | | | | Average ($\mu\Omega$) | Range ($\mu\Omega$) | Standard Deviation ($\mu\Omega$) |
|------------|---------------------------------|------|------|------|------|-------------------------|-----------------------|------------------------------------|
| | 1 | 2 | 3 | 4 | 5 | | | |
| 1 | 95.6 | 96.3 | 95.3 | 95.7 | 95.5 | 95.68 | 1 | 0.3768 |
| 2 | 96.3 | 96.1 | 96.5 | 96.3 | 96.6 | 96.36 | 0.5 | 0.1949 |
| 3 | 96.2 | 95.8 | 96 | 95.9 | 96.5 | 96.08 | 0.7 | 0.2775 |
| 4 | 97.5 | 97.3 | 97.6 | 97.8 | 97.1 | 97.46 | 0.7 | 0.2702 |
| 5 | 96.1 | 97.1 | 96.9 | 96.6 | 97 | 96.74 | 1 | 0.4037 |
| 6 | 95.8 | 96.2 | 96.1 | 96.5 | 95.9 | 96.1 | 0.7 | 0.2739 |
| 7 | 94.5 | 94.1 | 93.9 | 94.6 | 94.3 | 94.28 | 0.7 | 0.2864 |
| 8 | 97.2 | 97.3 | 97.6 | 97.3 | 96.9 | 97.26 | 0.7 | 0.2510 |
| 9 | 96 | 96.5 | 96.2 | 96.3 | 96.8 | 96.36 | 0.8 | 0.3050 |
| 10 | 96.3 | 96.5 | 97 | 96.3 | 96.9 | 96.6 | 0.7 | 0.3317 |
| 11 | 95.8 | 96 | 95.7 | 96.3 | 95.4 | 95.84 | 0.9 | 0.3362 |
| 12 | 97.5 | 97.7 | 98.1 | 97.9 | 97.4 | 97.72 | 0.7 | 0.2864 |
| 13 | 95.3 | 95.7 | 96 | 95.1 | 95.5 | 95.52 | 0.9 | 0.3493 |
| 14 | 96.9 | 97.2 | 96.4 | 96.8 | 96.3 | 96.72 | 0.9 | 0.3701 |
| 15 | 94.6 | 94.9 | 94.8 | 95.1 | 94.9 | 94.86 | 0.5 | 0.1817 |
| 16 | 98.3 | 98.4 | 98.6 | 99 | 98.5 | 98.56 | 0.7 | 0.2702 |
| 17 | 97.7 | 97.6 | 97.8 | 97.4 | 98 | 97.7 | 0.6 | 0.2236 |
| 18 | 96.8 | 96.6 | 97 | 97.1 | 96.7 | 96.84 | 0.5 | 0.2074 |
| 19 | 96 | 95.8 | 96.1 | 96.3 | 95.9 | 96.02 | 0.5 | 0.1924 |
| 20 | 95.8 | 95.7 | 96.1 | 95.9 | 95.7 | 95.84 | 0.4 | 0.1673 |
| Average | | | | | | 96.43 | 0.705 | 0.27778 |

3.4.2 Agilent B2900A/34420A Meters

Next, the combination of Agilent B2900A power supply and Agilent 34420A Nano-volt meter was used to measure the resistance. All resistance measurements were performed using the 4-wire Kelvin method as shown in Figure 3.9. A fixed current of 1 A was supplied to the shunt via the current (I) terminals from an Agilent B2900A source meter, whilst the voltage drop across the pre-soldered voltage (V) terminals was continuously monitored using an Agilent 34420A Nano-volt meter.

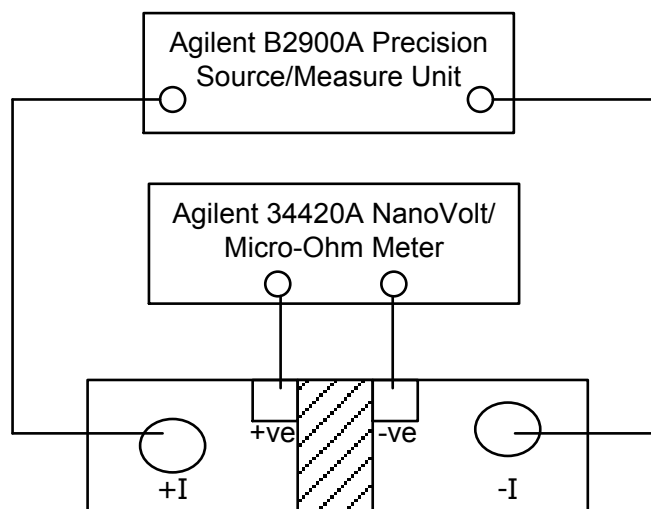


Figure 3.9: Connection of a shunt resistor to Agilent meters.

Similar with the previous experiment, the resistance value of 20 shunt resistors was measured 5 times to observe if the combination of the meters could give more accurate and repeatable readings. Measurements were taken using IntuiLink software that was attached to Microsoft Excel and connected to PC using a GPIB cable. The results collected in Table 3.3 from measurement readings using both Agilent meters indicated that each resistor used in this experiment was also within a $100 \mu\Omega \pm 5\%$ tolerance which was claimed by the manufacturer.

Table 3.3: Reading for resistance measurement using combination of Agilent meters.

| Sample No. | Measurement No. ($\mu\Omega$) | | | | | Average ($\mu\Omega$) | Range ($\mu\Omega$) | Standard Deviation ($\mu\Omega$) |
|------------|---------------------------------|------------|------------|------------|------------|-------------------------|-----------------------|------------------------------------|
| | 1 | 2 | 3 | 4 | 5 | | | |
| 1 | 97.1 96 | 97.1 92 | 97.1 97 | 97.1 99 | 97.2 04 | 97.1976 | 0.012 | 0.0044 |
| 2 | 99.9 8 | 99.9 66 | 99.9 57 | 99.9 34 | 99.9 5 | 99.9574 | 0.046 | 0.0172 |
| 3 | 99.9 44 | 99.9 22 | 99.9 03 | 99.9 17 | 99.9 28 | 99.9228 | 0.041 | 0.0150 |
| 4 | 99.0 7 | 99.0 67 | 99.0 58 | 99.0 42 | 99.0 14 | 99.0502 | 0.056 | 0.0230 |
| 5 | 99.0 09 | 99.0 88 | 99.1 69 | 99.0 2 | 99.0 98 | 99.0768 | 0.16 | 0.0650 |
| 6 | 97.2 02 | 97.1 98 | 97.1 95 | 97.2 05 | 97.1 55 | 97.191 | 0.05 | 0.0205 |
| 7 | 99.6 65 | 99.5 87 | 99.6 57 | 99.6 3 | 99.6 88 | 99.6454 | 0.101 | 0.0387 |
| 8 | 97.8 86 | 97.8 22 | 97.8 52 | 97.9 05 | 97.9 71 | 97.8872 | 0.149 | 0.0566 |
| 9 | 97.4 03 | 97.4 11 | 97.4 09 | 97.4 03 | 97.3 93 | 97.4038 | 0.018 | 0.0070 |
| 10 | 97.2 8 | 97.2 47 | 97.2 34 | 97.1 89 | 97.2 98 | 97.2496 | 0.109 | 0.0424 |
| 11 | 95.6 56 | 95.6 98 | 95.6 55 | 95.6 73 | 95.6 59 | 95.6682 | 0.043 | 0.0182 |
| 12 | 96.3 22 | 96.3 45 | 96.3 87 | 96.3 32 | 96.3 66 | 96.3504 | 0.065 | 0.0263 |
| 13 | 97.7 39 | 97.7 56 | 97.7 93 | 97.7 75 | 97.7 49 | 97.7624 | 0.054 | 0.0216 |
| 14 | 96.7 64 | 96.7 35 | 96.7 76 | 96.7 24 | 96.7 66 | 96.753 | 0.052 | 0.0223 |
| 15 | 96.4 22 | 96.4 19 | 96.4 05 | 96.4 24 | 96.4 26 | 96.4192 | 0.021 | 0.0083 |
| 16 | 97.8 81 | 97.7 64 | 97.7 55 | 97.7 6 | 97.7 8 | 97.788 | 0.126 | 0.0528 |
| 17 | 96.9 89 | 96.9 7 | 97.0 56 | 96.9 91 | 97.0 26 | 97.0064 | 0.086 | 0.0343 |
| 18 | 96.4 24 | 96.4 17 | 96.3 96 | 96.4 15 | 96.4 13 | 96.413 | 0.028 | 0.0104 |
| 19 | 99.0 73 | 99.0 59 | 99.1 04 | 99.0 11 | 99.0 76 | 99.0646 | 0.093 | 0.0341 |
| 20 | 97.0 83 | 97.0 81 | 97.1 09 | 97.1 2 | 97.0 63 | 97.0912 | 0.057 | 0.0230 |
| Average | | | | | | 97.7449 | 0.0685 | 0.02705 |

Measurement results using the Agilent meters were found to be more accurate with higher resolution. The average resistance measurement for the 20 shunt resistors is 97.7449 $\mu\Omega$. Average measurement range and standard deviation using the combination of Agilent meters were 0.0685 and 0.02705 respectively highlighting that this system gave more repeatable results, making the measurement system more reliable to be used throughout the experiments.

3.5 Summary

Acquiring the right measurement system is crucial in this research as it will determine the credibility of the results in the trimming experiments. After all the measurement techniques, systems and uncertainties have been discussed in this chapter, the most suitable measurement system for this research is achieved by combining the Agilent B2900A source meter with 34420A Nano-volt meter. This system has the lowest total system error at 0.187% and will be used for all resistance measurements in this research (unless otherwise stated).

Both resistance measurements conducted using Cropico and Agilent meters in Table 3.2 and Table 3.3 were compared to support the decision. The Agilent meters gave a better measurement range of 0.0685 $\mu\Omega$ compared to 0.705 $\mu\Omega$ for the Cropico micro-ohm meter. Repeatable resistance measurements are essential to achieve accurate readings throughout the research and the higher resolution of the Agilent meters is deemed the best option to measure resistance in the $\mu\Omega$ range.

Chapter 4

Material Properties Characterisation

The next stage of the research is to investigate and accurately determine a number of key characteristics and properties of the shunt resistors that will be used during subsequent experimental stages of the research. As the performance characteristics are a combination of physical properties and their response to electrical and thermal factors, this chapter will discuss these properties.

4.1 Material Characterisation

As discussed earlier, Manganin is used as the resistive material in the shunt resistors because it's low temperature coefficient of resistance. This means that as the current passing through the Manganin increases, the resultant temperature rise through Joule heating will not change the resistance significantly [103, 104]. For operation within a smart energy meter, the meter readings must remain valid regardless of the current flowing. Therefore, the resistance of the shunt will still reflect the actual energy usage when Manganin is used. When alloys with a high temperature coefficient get hot, this results in

an increase in resistance and so producing an increase in voltage drop, thus giving an inconsistent reading of current flow and power used.

Since there are different Manganin compositions available in the market, a thorough investigation of the material was carried out in order to verify the properties of the specific type of Manganin that is used to produce the shunt resistor samples. This is to make sure that any experiments conducted and simulations carried out on the shunt resistor sample have accurate properties.

4.2 Measurement of Key Properties

Sequences of experiments were carried out in order to determine the properties of the Manganin that will be used in the simulation experiments in Chapter 5. This is important as the properties given in resources such as books or data sheets differ from the Manganin to be used during this research. The important properties that needed to be determined are the chemical structure and composition, density, thermal conductivity, and the specific heat.

4.2.1 Material Structure

The morphology and composition of the Manganin samples were investigated using scanning electron microscope (SEM). The measurements of the samples were taken using a FEI Quanta 200 secondary electron microscope at an accelerating voltage of 20 kV. Chemical composition was acquired using an Oxford Instruments INCA X-ray detector at 8000x magnification for 60 seconds. Energy dispersive spectroscopy (EDS) analysis measurements were made using a lithium-drifted silicon detector attached to the SEM.

Two different samples were used for the experiment to confirm the properties of different Manganin compositions. Sample 1 is the Manganin, which was cut off from the shunt resistor provided by TT Electronics, and sample 2 is a Manganin rod which is acquired from an Isabellenhütte shunt

sample. The chemical spectrum in Figure 4.1 shows that the peaks are of Cu, Ni, and Mn, with the presence of lower peaks of C and O. The results of the chemical analysis for both samples are all within ± 5 wt. % of the proposed nominal values.

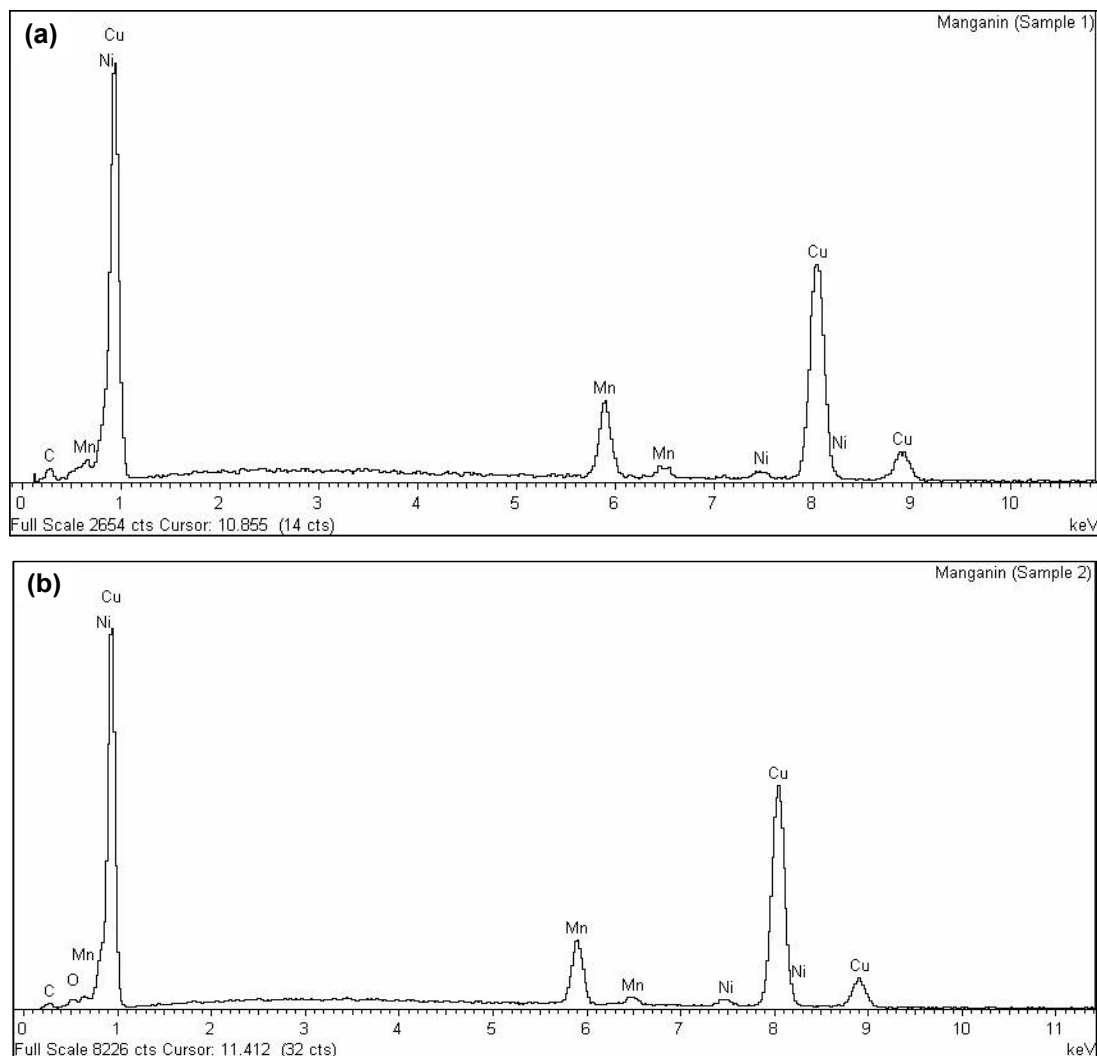


Figure 4.1: Chemical spectra for (a) Manganin sample 1 and (b) Manganin sample 2.

The XPS spectrum of the two Manganin samples is shown in Table 4.1. The results are normalised to only Cu, Mn and Ni as these three components are the composition of Manganin. Total weight percentage (wt. %) for both samples are slightly different from the data sheet value published by the two companies which is $86\text{Cu}12\text{Mn}2\text{Ni}$ for both samples. It can be seen that Sample 2 has higher percentage of Cu compared to Sample 1 which were 87.57 wt. % and 84.3 wt. % respectively.

Table 4.1: Total weight percentage (wt. %) for Manganin samples.

| Manganin Type | Mn | Ni | Cu | Total (wt. %) |
|----------------------|-----------|-----------|-----------|----------------------|
| Published value | 12.0 | 2.0 | 86.0 | 100 |
| Sample 1 | 12.4 | 3.3 | 84.3 | 100 |
| Sample 2 | 10.5 | 1.9 | 87.6 | 100 |

Both samples were then tested using X-ray Diffraction (XRD) to see if the structure changes with change in temperature. X-ray diffraction is a family of non-destructive techniques used in many scientific fields to investigate the crystallographic structure of materials. This technique is based on the diffraction of an X-ray beam caused by the interaction with crystalline solids [105, 106]. X-ray diffraction takes place because the atomic spacing in a crystal (with an order of magnitude of an Å) is in the same range as the wavelength of X-rays. By analysing the intensity and the orientation of the diffracted pattern from an irradiated Manganin sample it is possible to determine its crystal structure.

The arrangement of atoms in a given type of crystal structure can be described in terms of a unit cell and the entire crystal structure can be formed by the repetition of it [107]. A unit cell is defined by the lattice parameters which are the length of the edges of the cell and the angles between them. The Bragg's model can be used to determine the unit cell parameters. In this model, the atoms of the crystal (which are the scattering centres) are represented by sets of parallel planes in which the atoms are located. Each plane acts as a mirror and reflects the incident X-ray. The orientation of a specific set of planes spaced by a distance d , is identified by three numbers (h, k, l) named Miller's indices [108]. In the case of a simple cubic structure the distance, d , is derived from the following relationship:

$$d = \frac{a}{\sqrt{h^2 + k^2 + l^2}} \quad (4.1)$$

XRD scan results from both samples are shown in Figure 4.2 where two peaks are found at 111 and 200. Sample 2 is found to be different at the 200 peak where it can be suggested that the grain size is smaller compared to Sample 1 due to the composition and how it is made.

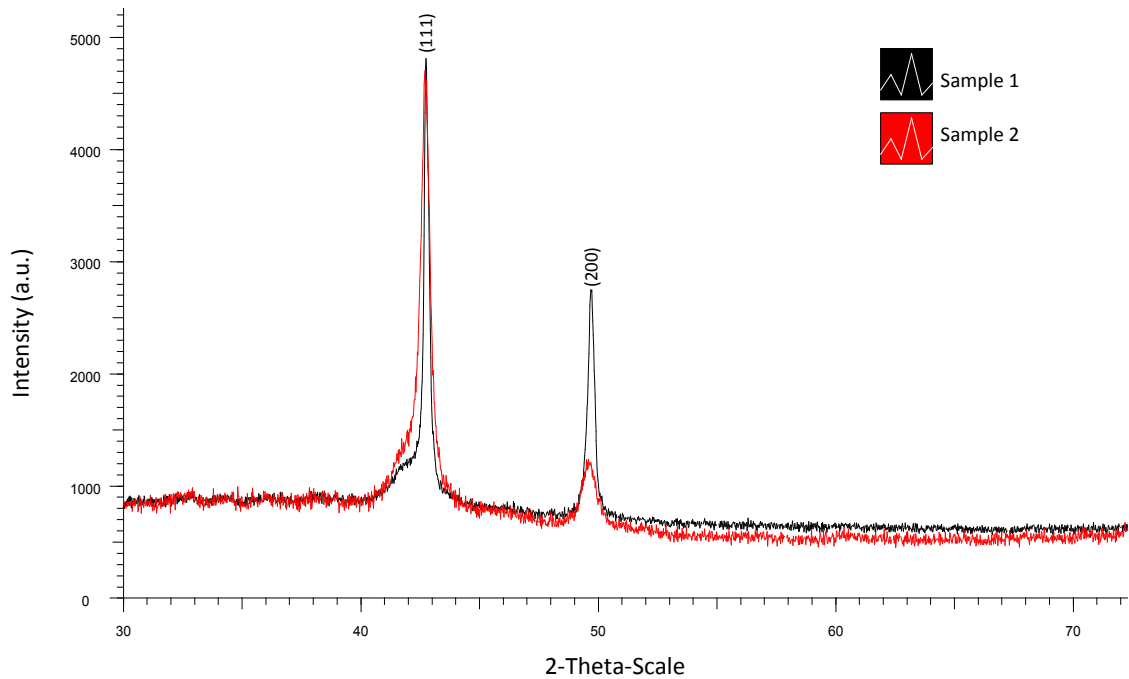


Figure 4.2: XRD patterns for both sample of Manganin.

Even though Manganin is a quite well known material, the crystallography database available did not have any information on Manganin or the CuMnNi alloy. The results obtained from the XRD test are compared to previous research conducted by Lin [109] where a Manganin film is deposited on an Al_2O_3 substrate as seen in Figure 4.3 and used as a reference. Miller indices from the reference are used to identify the peaks obtained throughout the experiment.

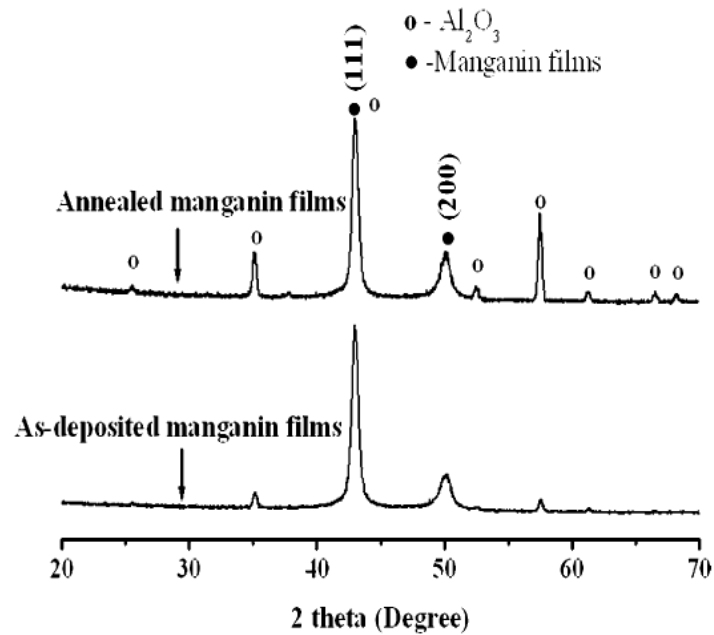


Figure 4.3: XRD diagrams of as-deposited and annealed Manganin films on Al_2O_3 substrate [109].

4.2.2 Mechanical Properties of Manganin

Density

Mass and volume are the physical properties of matter and may vary with different objects. The amount of matter contained in an object is called mass. Its measure is usually given in grams (g) or kilograms (kg). Volume is the amount of space occupied by an object. The units for volume include litres (l), meters cubed (m^3), and gallons (gal). An object's density is defined as its mass per unit of volume.

The bulk density of the Manganin sample was measured by the water buoyancy method. Since the samples are cut straight from the shunt resistor, their different shapes and weights make it hard to calculate the volume accurately. A simple experiment is conducted in order to determine the Manganin density. The experiment set up can be referred to in Figure 4.4. There are some precautions in this experiment, where the Manganin needed to be carefully lowered down into the fully filled beaker in order to minimize the splash effect. The splash effect might affect the result of the experiment and

even though the effect might be minimal, precise density is desirable. The large beaker also had to be filled carefully to its brim as it will allow the water to overflow out of the beaker as soon as the Manganin was dropped in it. The experiment was repeated 3 times to make sure the results obtained were accurate.

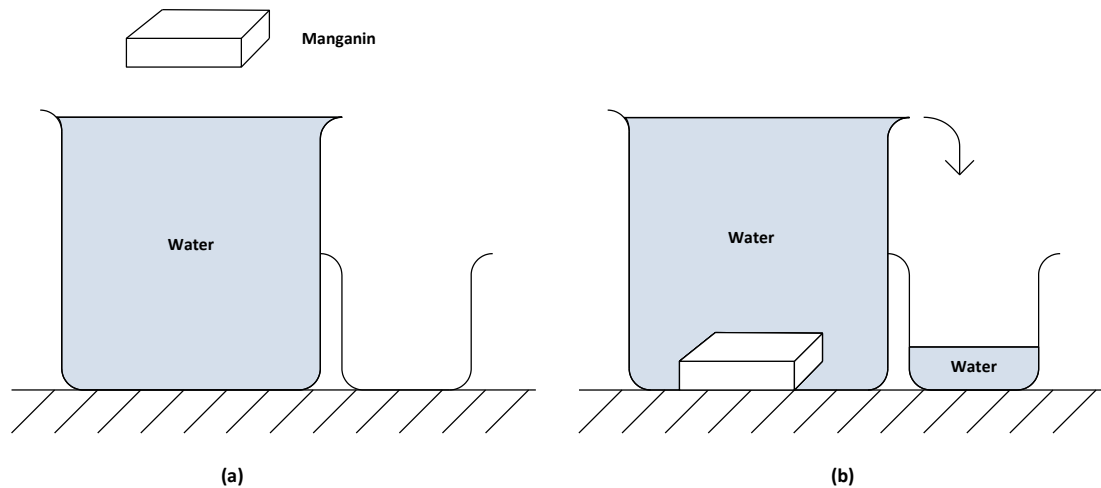


Figure 4.4: Block diagram for density measurement.

Water displacement was used where the large beaker was filled up to the brim, and the Manganin was carefully dropped in it. The mass of water displaced in the small beaker was measured and used to calculate the volume of the Manganin. Since water's density is $\approx 1 \text{ g/cm}^3$, the volume of the Manganin sample can be calculated using:

$$\begin{aligned} \text{Volume of Manganin } (V_m) &= \text{Volume of water } (V_w) \\ &= \frac{\text{Mass of water } (M_w)}{\text{Density of water } (\rho_w)} \end{aligned} \quad (4.2)$$

Where v is the volume of Manganin samples and weight is the mass of displaced water. The density of the Manganin sample can then be calculated using:

$$\text{Density } (\rho) = \frac{\text{Mass of sample } (M)}{\text{Volume of sample } (V)} \quad (4.3)$$

The experiment was also repeated using a Manganin rod sample. The reason for this is to check if different Manganin samples will have same properties and to validate the results calculated earlier since the volume of Manganin is not the same shape. It is easier to calculate the density of a Manganin rod since the volume of the sample can easily be calculated. All calculated results for Manganin density is presented in Table 4.2 and was compared to published data sheet value. The average density of both Manganin samples was calculated at 8.42 g/cm³.

Table 4.2: Summarised of results for Manganin density.

| Published Value | Manganin Shunt | | | Manganin Rod |
|-----------------|----------------|-----|------|--------------|
| | 1 | 2 | 3 | |
| 8.4 | 8.36 | 8.4 | 8.44 | 8.47 |

Hardness

Due to its simplicity and the fact that minimal machining is required to prepare the sample, the use of the Vickers indentation method to quantify hardness has become quite popular [110]. The Vickers micro-hardness test was undertaken to study the fine scale hardness of the Manganin resistive alloy in 8 different areas using a micro-hardness tester model HV-1000A. A diamond indenter was applied to the surface of the specimens. Upon removal, the impression of the indent was used for the quantification of hardness as seen in Figure 4.5. A load of 500 gf was used for a duration of 10 seconds. Vickers micro-hardness was evaluated in accordance with ASTM E384 [111].

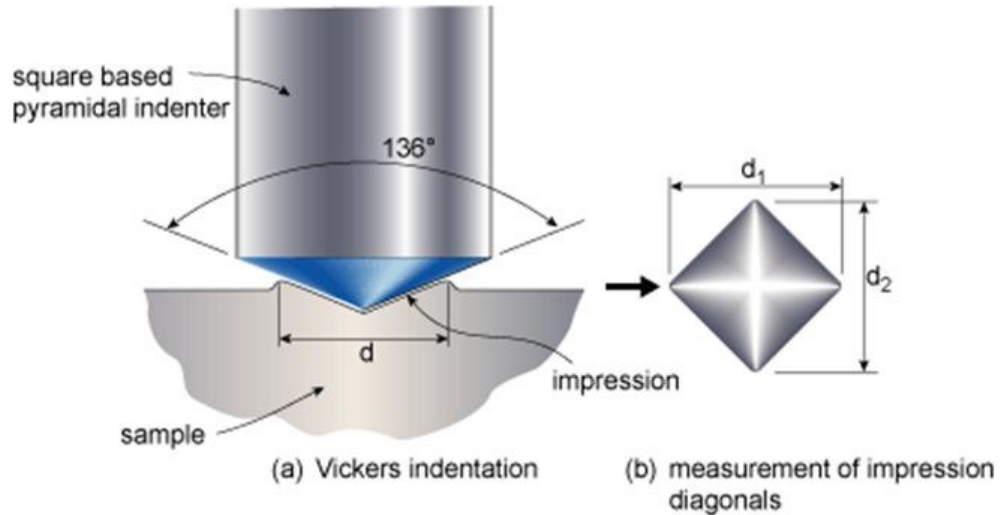


Figure 4.5: Principle of Vickers hardness measurement [112].

After the load was removed, the two impression diagonals (d_1 and d_2) were measured using an Alicona Infinite Focus G4 optical scanner to the nearest $0.1 \mu\text{m}$, and then averaged to give d . The Vickers hardness value (HV) was then determined by the ratio L/A , where L is the load applied to the diamond and A is the surface area of the resulting indentation in square millimetres, as determined by:

$$A = \frac{d^2}{2\sin(136^\circ/2)} \quad (4.4)$$

$$A \approx \frac{d^2}{1854.4}$$

Hence HV is calculated by:

$$HV = \frac{L}{A} \quad (4.5)$$

$$HV = \frac{1854.4L}{d^2}$$

The load, L , is in grams-force and the average diagonal, d , is in μm (although the hardness number units are expressed in units of kgf/mm^2 rather than the equivalent $\text{gf}/\mu\text{m}^2$).

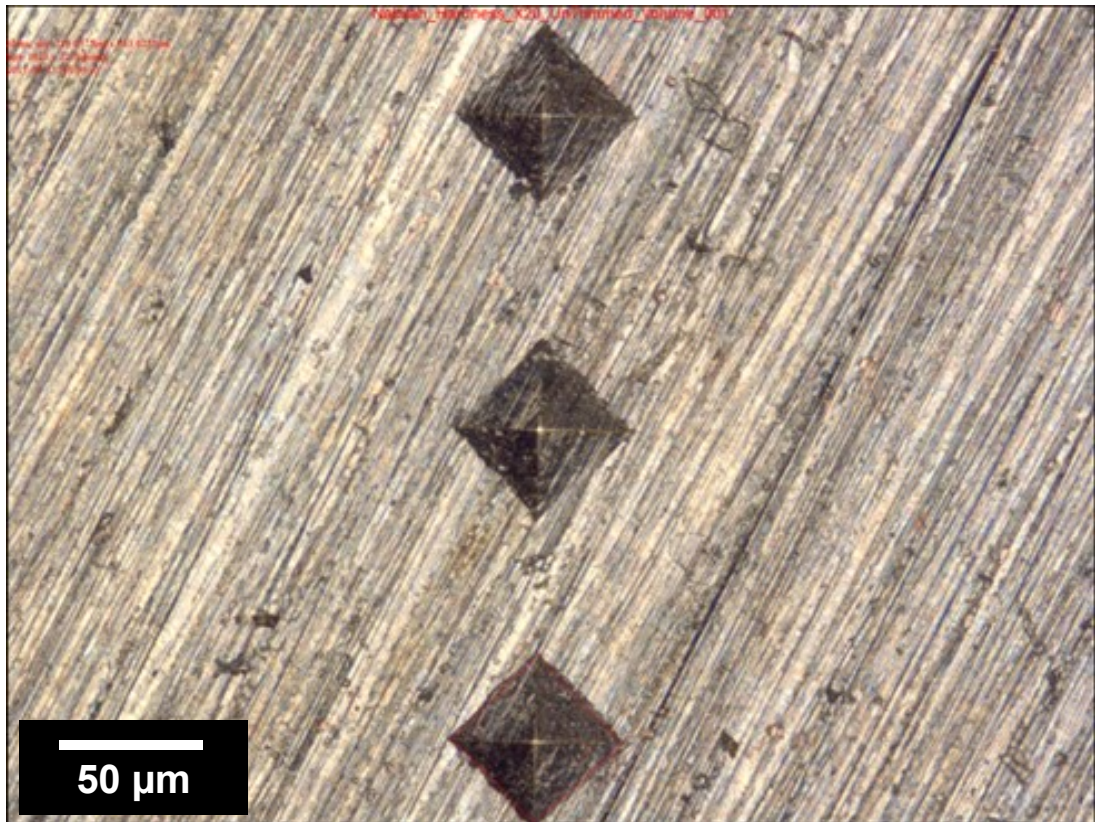


Figure 4.6: Impression of Vickers hardness test made on Manganin sample.

Table 4.3: Summarised of results for Manganin hardness.

| Measurements | <i>d1</i> | <i>d2</i> | Average, <i>d</i> | <i>HV</i> |
|--------------|-----------|-----------|-------------------|-----------|
| 1 | 109.8859 | 112.3737 | 111.1298 | 150.1559 |
| 2 | 115.3427 | 108.2066 | 111.7747 | 148.4283 |
| 3 | 112.1102 | 112.1102 | 112.1102 | 147.5411 |
| 4 | 115.0763 | 111.5163 | 113.2963 | 144.4681 |
| 5 | 114.5104 | 112.0535 | 113.2820 | 144.5047 |
| 6 | 115.0521 | 114.5536 | 114.8029 | 140.7013 |
| 7 | 116.7001 | 116.1732 | 116.4367 | 136.7805 |
| 8 | 114.8105 | 117.0336 | 115.9221 | 137.9975 |
| Average | | | | 143.8221 |

From the calculation in Table 4.3, the hardness values for the Manganin are ranging from 137 to 150 *HV*, and the average for these values is 144 *HV*. Therefore, it was confirmed that the value for the Manganin alloy is noticeably higher compared to the material database which is 110 *HV* with 1mm thickness [68, 69]. This is perhaps because the Manganin sample that was used in this experiment has thickness of 3mm, hence causing the difference in the results obtained.

4.2.3 Electrical Properties of Manganin

Resistivity

The resistivity, ρ represents the resistance across two opposite faces of a cubic metre of material. Resistivity tells how resistive a material is and its units are ohm metres. Experimentally, the dependence upon these properties is a straightforward one for a wide range of conditions, and the resistance of a wire can be expressed as Equation (4.6) where R is the resistance, L is the length and A is the cross sectional area:

$$R = \frac{\rho L}{A} \quad (4.6)$$

In order to get the value of ρ , the value of resistance R should be known and this value is obtained from the digital micro-ohmmeter readings. The measurement for the length (L), width (W) and thickness (T) are received from the Keyence microscope model VHX-700F. 20 samples was measured in order to get the average resistivity of the Manganin shunt resistance. Table 4.4 presented the results for the measurements with the average resistivity calculated at 37.6885 Ωm .

Table 4.4: Resistivity measurements for 20 samples of shunt resistors.

| Resistance, R ($\mu\Omega$) | Length, L (mm) | Width, W (mm) | Thickness, T (mm) | Resistivity, ρ (Ωm) |
|----------------------------------------------------------------|----------------------------------------|---------------------------------------|-------------------------------------------|-------------------------------------------------------------------------|
| 95.68 | 6.93 | 14.23 | 1.75 | 34.32 |
| 96.36 | 7.02 | 14.41 | 1.85 | 36.66 |
| 96.08 | 7.06 | 15.31 | 1.73 | 36.11 |
| 97.46 | 7.00 | 15.28 | 1.82 | 38.79 |
| 96.74 | 6.71 | 15.3 | 1.72 | 37.83 |
| 96.1 | 6.80 | 15.33 | 1.83 | 39.57 |
| 94.28 | 7.28 | 15.35 | 1.76 | 34.89 |
| 97.26 | 7.08 | 15.3 | 1.71 | 35.87 |
| 96.36 | 6.84 | 15.31 | 1.76 | 37.89 |
| 96.6 | 6.56 | 15.37 | 1.88 | 42.55 |
| 95.84 | 6.84 | 15.35 | 1.78 | 38.21 |
| 97.72 | 7.04 | 15.27 | 1.72 | 36.53 |
| 95.52 | 6.71 | 15.3 | 1.79 | 38.91 |
| 96.72 | 6.99 | 15.3 | 1.80 | 38.11 |
| 94.86 | 7.15 | 15.3 | 1.80 | 36.54 |
| 98.56 | 7.21 | 15.29 | 1.75 | 36.65 |
| 97.7 | 6.74 | 15.27 | 1.74 | 38.44 |
| 96.84 | 7.12 | 15.36 | 1.83 | 38.23 |
| 96.02 | 6.69 | 15.28 | 1.84 | 40.28 |
| 95.84 | 7.12 | 15.32 | 1.81 | 37.39 |
| Average | | | | 37.6885 |

4.2.4 Thermal Properties of Manganin

Thermal Conductivity

Thermal conductivity is the property concerned with a material's ability to conduct heat. Theoretically, it is the magnitude of a quantity of heat that is transferred per unit time between two media at different temperatures when the two media are separated by a wall [113]. In the steady state of time, an amount of heat flows through the cross-section of a solid body. It appears primarily in Fourier's Law for heat conduction.

As opposed to electrical conduction, heat conduction is the flow of internal energy from a region of higher temperature to one of lower temperature by the interaction of the adjacent particles (atoms, molecules, ions, electrons, etc.) in the intervening space. Heat conduction, H , can be defined as:

$$H = \frac{\Delta Q}{\Delta t} = kA \frac{\Delta T}{x} \quad (4.7)$$

where $\frac{\Delta Q}{\Delta t}$ is the rate of heat flow, k is the thermal conductivity, A is the total cross sectional area of the specimen, ΔT is temperature difference, and x is the thickness of conducting surface separating the 2 temperatures. Rearranging the equation gives thermal conductivity:

$$k = \frac{\Delta Q}{\Delta t} \frac{1}{A} \frac{x}{\Delta T} \quad (4.8)$$

It is defined as the quantity of heat, ΔQ , transmitted during time Δt through a thickness x , in a direction normal to a surface of area A , per unit area of A , due to a temperature difference ΔT , under steady state conditions and when the heat transfer is dependent only on the temperature gradient. Alternatively, it can be thought of as a flux of heat (energy per unit area per unit time) divided by a temperature difference per unit length [113].

An experiment was conducted in order to get the thermal conductivity of the Manganin. The experiment set up by is shown in Figure 4.7. A heater is connected to an aluminium block with two thermocouples (T1 and T2) attached with 50mm apart. This aluminium block is connected to the Manganin rod with the other two thermocouples (T3 and T4) at a distance of 30mm. The heat was then ramped to the aluminium block and the readings were taken from the attached thermocouples. The readings were taken at a steady state at the heater set point of 50°C up to 200°C.

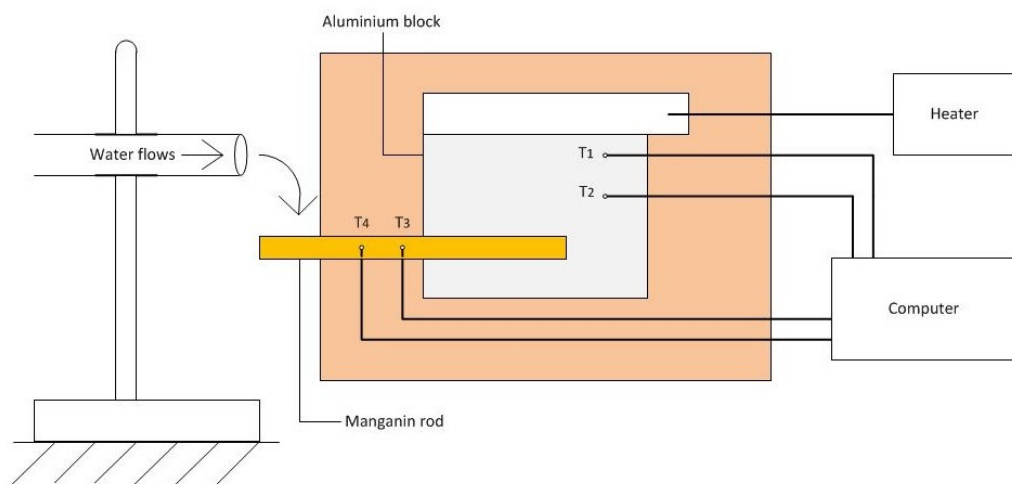


Figure 4.7: Block diagram for thermal conductivity experiment setup.

Area of aluminium block are 10mm thick and 70mm length while Manganin rod has a diameter of 7mm. Both the aluminium blocks and Manganin rod were insulated with fiberglass. Fiberglass performed as an insulator where it slows the spread of heat and cold throughout the aluminium block and Manganin rod. By trapping pockets of air, it retains the heat and allowed the measurements to be conducted precisely.

The end of the Manganin rod is left outside of the insulation in order to be cooled by the water flowing at a constant rate through constant head device. The flowing water will carry off the heat reaching the cold end of Manganin rod. In this way, a balance between the heat input on one end, and the heat carried away at the other end will be acquired. As a result, the temperature at T3 and T4 becomes constant in time and reached what is called a dynamic equilibrium. The adjective “dynamic” is used since heating and cooling goes on continuously, and there is equilibrium because their net effect is to produce no change. When the water carries off heat from the cold end of the rod, its temperature increases; by measuring this temperature increase, the heat output can be calculated.

Assuming no loss of heat, the amount of heat flowing through the aluminium block can be calculated using:

$$Q = -kA \frac{\Delta t}{\Delta x} \quad (4.9)$$

where, Q is the heat supplied to the aluminium block in time t , A is the cross sectional area of the block, Δt is the difference in temperature between two points in the specimen which are distance Δx apart and k is the coefficient of thermal conductivity of the aluminium.

The temperature difference can be determined after all the readings were taken. From there, the thermal conductivity, k , for Manganin can be calculated. However, since the amount of heat, Q , for Manganin is unknown, therefore it is assumed that it has the same Q as aluminium. As the k for aluminium is known to be at 166 W/mK [114], Δx is known and area for the aluminium block can be calculated, the Q for aluminium and calculated value of k is then presented in Table 4.5. Results obtained for average thermal conductivity of Manganin is 157.8 W/mK.

Table 4.5: Calculated results for thermal conductivity of Manganin at different temperature.

| Heater Set Point | Aluminium | | Manganin | | Q Aluminium | k Manganin |
|------------------|-----------|--------|----------|-------|-------------|------------|
| | T1 | T2 | T3 | T4 | | |
| 50 | 48.24 | 47.7 | 30.12 | 24.57 | 1.61 | 226.74 |
| 60 | 62.02 | 61.3 | 34.96 | 25.18 | 2.15 | 171.57 |
| 80 | 82.34 | 81.32 | 43.25 | 28.58 | 3.05 | 162.03 |
| 100 | 103.17 | 101.88 | 51.25 | 31.47 | 3.85 | 151.98 |
| 140 | 145.04 | 143.24 | 69.86 | 43.15 | 5.38 | 157.05 |
| 160 | 164.21 | 162.13 | 77.85 | 46.87 | 6.22 | 156.47 |
| 180 | 177.34 | 175.45 | 86.94 | 51.55 | 5.65 | 124.46 |
| 200 | 193.27 | 191.35 | 94.66 | 54.75 | 5.74 | 112.11 |
| Average | | | | | | 157.80 |

Specific Heat Capacity

The final experiment was conducted to get the specific heat capacity of the Manganin. The setup of the experiment can be referred in Figure 4.8. This experiment set up was modified based from the calorimeter system which detects the change of temperature in an insulated environment. A beaker was filled with water and placed inside an insulation box. The top of the insulation box was connected to a thermocouple rod in order to get the temperature reading of the water inside the beaker. Initially, the temperature reading of the water was taken. The Manganin sample was then heated at 60°C in an oven for one hour. The sample was then put inside the beaker and the new temperature of the water was taken afterwards until it reaches steady state.

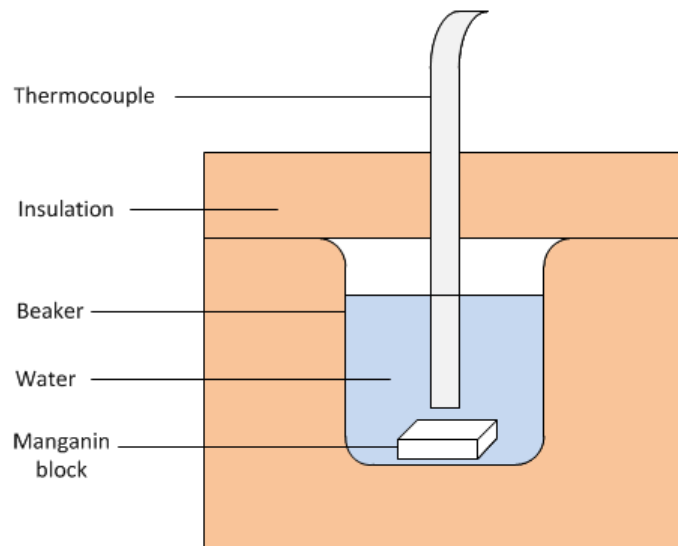


Figure 4.8: Heat capacity experiment setup.

Knowing specific heat capacity of water is $4190 \text{ Jkg}^{-1}\text{K}^{-1}$, the specific heat capacity for the Manganin can be calculated using Equation (4.10), where m is the unit mass, C_p is the specific heat capacity and ΔT is the difference in the initial temperature and when it reach steady state (T_2-T_1).

$$Q = mC_p\Delta T \quad (4.10)$$

Since the mass of water and the mass of Manganin is known, we can calculate the specific heat capacity of Manganin by comparing both materials using a balance of Q . Specific heat capacity for Manganin is calculated at $0.345 \text{ J/g}^{-1}\text{K}^{-1}$. The result is really close to the published value from different manufacture which is $0.4 \text{ J/g}^{-1}\text{K}^{-1}$ [68, 69].

4.3 Summary

In this chapter, the properties of Manganin were investigated and samples were examined in order to know the actual properties for the Manganin material used for this research. These properties, reported in Table 4.6, will be primarily used within the thermos-electric simulation study in the next chapter to focus on the development of the trimming geometry.

Table 4.6: Summary of the measured properties values.

| Sources / Properties | Manufacturer Datasheet | Manganin sample |
|-------------------------------|-------------------------------|------------------------|
| Density (g/cm ³) | 8.4 | 8.42 |
| Hardness (HV) | 110 | 144 |
| Resistivity (Ω m) | 43 | 38 |
| Thermal Conductivity (W/mK) | 22 | 157.8 |
| Specific Heat Capacity (J/gK) | 0.41 | 0.345 |

The results in Table 4.6 show that the density of Manganin samples were found to be similar to the published value. However, the measured hardness value of the Manganin samples is higher than the published value, and it was suggested that this was due to the increased thickness of the test pieces. Resistivity was found to be lower than the published results due the lower resistance values in the shunt resistors. The thermal conductivity property that was calculated from the Manganin sample is significantly higher than the data sheet value and since there is no reasonable explanation for this unexpected increase, the simulation in Chapter 5 will use the published value of 22 W/mK. Finally, the specific heat capacity calculated is lower than the published value and this was related to heat losses while transferring the samples from the oven into the insulation box.

Chapter 5

Development of Trimming Process

Since the characteristics of the material have been identified and explained in the previous chapter, the next stage is to develop a trimming process that will reduce the resistance tolerance of the shunt resistor. A number of trimming designs will also be considered by discussing all of the possible advantages and disadvantages and undertaken a series of tests using ANSYS software. The finite element method (FEM) is the dominant tool for numerical analysis in engineering and is used to assign proper failure criteria [115]. Amendments and modification are crucial throughout this step to get the best design.

5.1 Trimming Geometry

A resistor can be modified to suit its requirement by altering its resistance. Two ways of altering the resistance are by changing the geometry or the resistivity of the material used and the other one is by changing the resistor's nature with external phenomena such as insulation loss and mechanical stress. By studying this resistor technology, the potential of a product can be optimized by matching the right elements to the system needs.

The elements that will be used and manipulated in this project are the geometry of the resistive Manganin material and the selection of process used to alter it.

5.1.1 Theoretical Analysis

In theory, by removing some controlled amount of resistive material into a tolerable and symmetrical shape, the standard tolerance of the shunt resistors can be reduced. The maximum amount of material that needs to be removed can be determined from the expression for the initial electrical resistance of the shunt, R_1 [8]:

$$R_1 = \frac{\rho L}{A} = \frac{\rho L}{W t_1} \quad (5.1)$$

where ρ is the resistivity value of Manganin, L is the length of the Manganin strip, and A is the cross sectional area of the Manganin strip which is the width, W multiplied by the initial thickness, t_1 .

In order to get the value of ρ from the above equation, the value of resistance R_1 should be known and this value is obtained from the digital micro-ohmmeter readings. Once the value of ρ is calculated, Equation (5.2) can be rearranged to find the new thickness, t_2 , required to increase the resistance of the shunt to its targeted value, R_2 , of 100 $\mu\Omega$:

$$R_2 = \frac{\rho L}{W t_2} \therefore t_2 = \frac{\rho L}{W R_2} \quad (5.2)$$

Considering the targeted resistance, R_2 is $100 \mu\Omega$ and the value of L and W are kept constant, the thickness to be removed, $t = t_1 - t_2$ can be removed from the original thickness of the Manganin strip, t_1 . Correspondingly, the volume of the material to be removed from the Manganin strip can be obtained using the following equation:

$$V = W \times L \times t \quad (5.3)$$

5.2 Trimming Techniques

There exist a number of techniques which can be used to trim the required volume of material, V , from the shunt resistor but not all of them are appropriate for the purpose of this project. There are a number of well-established methods of improving the resistance accuracy of thin and thick film discrete resistors by removing resistive material and adjusting the geometry of the element to increase its resistance in a controlled manner towards a target value. The most popular of these techniques are laser trimming, abrasive trimming with a wheel or abrasive particles and machining [32, 116-119]. In the majority of cases the material is removed in single or multiple lines cut perpendicular to the flow of current, to give high rates of resistance change, or in parallel with the current flow to give slower rates of change [28, 120]. Although these methods have yielded some excellent results when adjusting the resistance tolerance of thin and thick film resistors [29, 121, 122], there has been limited application in the area of bulk metal shunts. This section will hence be dedicated towards the study of those techniques which are the most suitable and viable.

5.2.1 Anodization

The trim-anodizing technique is typically used to trim tantalum film resistors. The thickness of the conductive metal is uniformly reduced by the growing layer of insulating tantalum oxide, at the expense of the parent Ta film. Hence a reduction is brought about in the effective thickness of the film. The

minimum anodization voltage for Ta resistors is 30 V. Tantalum oxide grows at the rate of 17Å/V while consuming 6.3 A of Ta per volt. The anodization is conducted at a constant current until the correct resistance value is measured. The resistor is anodized at one value of current until the resistance is close to the final value. Then the current is reduced to a lower value to reduce the anodization rate. This process is repeated until the desired tolerance is achieved. Successive anodizing and measurement of the resistor value are achieved. The resistance of the film must alternate with the anodization. Resistive films are made at least 5% lower in value than specified and low tolerances of 0.01% can be obtained. Anodization is the preferred method for trimming Ta-film resistors because it has the advantage of providing a protective oxide layer on top of the resistor. The interference colour of the film changes as the anodization progresses. Thus, the formed oxide layer shows an even colour. Large resistance values may cause anodization to form a thicker oxide layer near the termination connected to the power supply. Lower current density and slower rates of anodization usually overcome this problem [123].

5.2.2 Laser Trimming

One of the important functions in manufacturing hybrid circuits of ceramic based substrates is the use of laser trimming to the thick film resistors. This laser is small in size where it is measured to be only a few μm in diameter and kerf. Furthermore, this method uses a light beam in order to remove the unwanted material in a short amount of time, usually under 1 ms [32]. The reason for this is because the beam has a very high intensity coherent light pulse that will affect the targeted material, hence leading the material to vaporize after absorbing the light energy. However, the intensity of the power level or laser pulse used can be determined beforehand in order to get the desired result. This also applies to the focus of the laser and the material composition used in the process. The resistance value of the material (resistor) will change as the trimming process is carried out. Therefore, careful analysis must be done to prevent the laser trimming process from exceeding the desired resistance value of the resistor. The most important part to achieve this is by ensuring that the measurement system of the precision laser trimmer is fast

enough to halt the process which stops the laser beam between pulses when the specified value of the resistor is acquired [124].

In this trimming method, the work piece properties are unchanged, but the geometry varies. As seen in Figure 5.1, work piece will melt under the heat obtained from a laser beam and feed through a narrow nozzle. Laser trimming is one of the most accurate and precise trimming methods known but has its drawbacks in the form of expensive equipment and its subsequent maintenance.

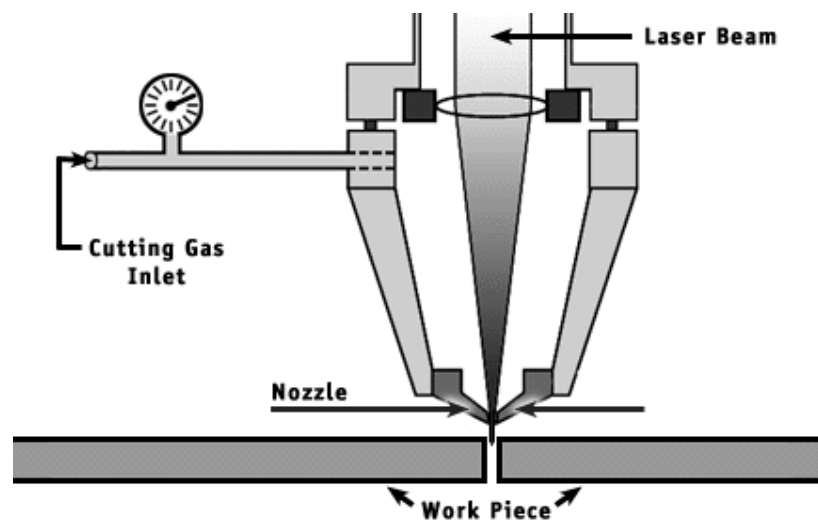


Figure 5.1: Block diagram of laser trimming process [119].

5.2.3 Sand Blast Trimming

Sand-blasting trimming or as it is sometimes called abrasive machining, uses a nozzle to discharge an abrasive powder with a high-pressure gas. The thick-film resistor layer is ground with the abrasive so as to trim its shape. The abrasive jet machining uses steamed abrasive particles which vary in sizes from 10 to 40 μm . These particles are carried with high pressure gas or air at high velocity, which usually measures at 150 to 300 m/sec. The nozzle of this machine releases these high velocity particles onto the work piece and the material on the work piece is removed by erosion. Typically, the inside diameter of the nozzle used in this method is about 0.18 to 0.80 mm and the distance between the nozzle and the work piece is best kept at 0.3 to 20.0 mm. The material removal rate can be controlled by using different sizes of abrasive

particles and flow rates. This method is best used for machining super alloys and refractory type of materials. It can also be used to make detailed hard holes, and machine thin sections of hard materials. The heat generated in this process is low as the gas released through the nozzle serves as the coolant [125].

Typical abrasives used in sand blasting are Al_2O_3 or SiC. These particles have sharp edges and when released from the nozzle to the work piece, will make dents to the surface of the material and remove a small particle from it by a tiny brittle fracture. These small particles that are removed will then be swept away by the air or gas. The process and setup of the process are shown in Figure 5.2.

The diameter, shape, and size of the erosion on the work piece can be influenced by the distance between the nozzle tip and the work surface. Standoff distance (SOD) will determine the spread of the abrasive particles which will increase or decrease the diameter of the cut. The increment of SOD will make the abrasive particle cover a wider area and vice versa. Sand-blasting trimming is advantageous as it is a non-thermal process. However, it leads to exposure of the resistor edge and powder contamination and fails to achieve high-precision trimming [126].

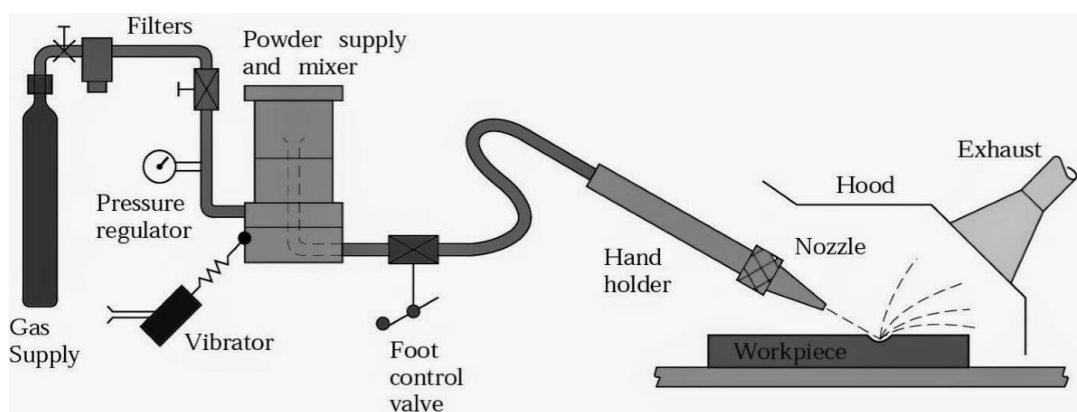


Figure 5.2: Schematic illustration of sand-blast trimming [127].

5.2.4 Milling

The milling process is very commonly used for fine removal of material from a work piece. Extreme tolerances for a work piece can be achieved with this process down to $\pm 0.1 \mu\text{m}$. For parts that needed a fine and precise measurement such as aircraft parts, space stations, and metrology equipment, milling is the way to do it. Milling machines are commonly large in size and typically floor mounted. However, there are smaller milling machines that can be bench mounted. Nowadays, milling machines are equipped with a processor and can be automated. This makes the machine more consistent and precise in manufacturing and components that are identical can be produce quickly and cheaply. Figure 5.3 shows how the end milling process is carried out. An end mill makes either slot cuts or peripheral which to be determined by the step-over distance, across the specific work piece. The depth of the work piece can be machined in a single feed or reached by machining at a smaller axial depth of cut [128].

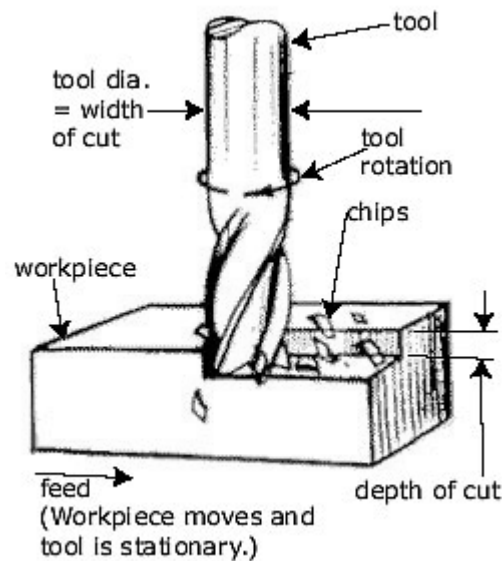


Figure 5.3: Schematic illustration of end milling process [129].

5.2.5 Precision Grinding

Precision grinding is a manufacturing process used in the fabrication and finishing of metal parts with very tight tolerances. The precision grinding process can be used for tiny parts such as those in electronics, as well as very large ones. It involves the use of various tools to size, shape, and texture the surface as needed. Precision grinding techniques as seen in Figure 5.4 include cylindrical grinding and surface grinding (also known as Blanchard or Mattison grinding). Grinding consists of using a spinning wheel made of bonded abrasive particles to remove material from the work piece, making a face of it flat or smooth [130].

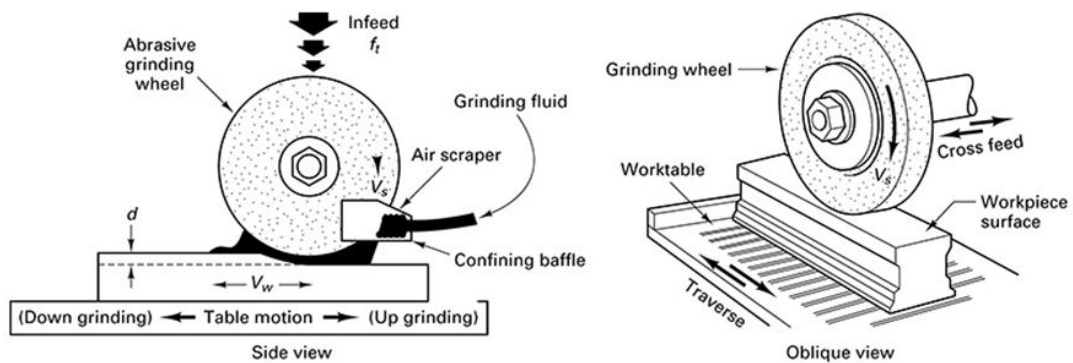


Figure 5.4: Schematic of surface grinding [131].

There are a number of advantages of precision grinding. Firstly, the material removal rate is changeable, depending on the process requirements. Secondly, it costs less and the instrument is easier to maintain compared to other precise techniques such as laser trimming. Lastly, the skill requirement for this process is not high.

Grinding is known to be the most suitable direct contact machining process because the resistance of the work piece can be continuously measured during the process [132]. Furthermore, the cutting disc of the grinder is typically electrically insulated which will give a better result from other machining process such as milling. Therefore, this is the most impressive feature as this will indicate the reading of the resistance while grinding, hence finalising on how much the material needs to be removed. Even though the

amount of the material that needs to be removed can be calculated theoretically, the measurement of the resistance during the trimming process is desirable in order to prevent its value to exceeding $100\mu\Omega$.

5.3 Trimming Techniques Selection

For the purposes of this project, elimination of certain methods of trimming, which do not concur with the aims, is necessary. Manganin resistors are used due to the high level of precision attainable and they should be manufactured accordingly. This requires an accurate and precise feedback mechanism wherein instantaneous values of resistance are recorded throughout the trimming process, which is essential to regulate the various parameters involved thereby hastening or slowing or even completely stopping the process.

Anodization, although precise, is a slow process. Given the material removal rate for anodization, a sufficiently large portion of time would be lost during oxidation. This would lead to losses of time and money, which is not acceptable. Anodization, due to its uneconomic nature, will not be used. Laser trimming though highly precise, is not very cost effective and hence is not entirely economical. Also, in the case of laser trimming, an equally fast and complex system of measurement would be required so as to stop the laser beam between pulses when the desired value has been attained. As this turns out to be a very expensive process, laser trimming on the whole is rejected for this particular project. It is also difficult to cut through thick materials such as shunt resistor.

The design of the feedback in the case of sandblasting is far too complex when compared to most of other trimming techniques. This is because the regulation of the blast, although possible, cannot be done accurately. As a result, sandblasting is not going to be used. Precision grinding on the other hand is economic and efficient in nature. It conforms admirably with the requirements of this project in particular. It is arguably accurate with very little in

the way of inherent errors. Those that do find their way into the process can be negated. Therefore, because of its effectiveness, efficiency, and economic advantages, precision grinding is one of the most suitable choices of process for this research.

For a trimming technique to be successful in removing the correct amount of material, a method has to be chosen where it is simple to test the work piece during the trimming procedure. Therefore, the best process to choose would be the grinding or milling method as the value of the resistance could be shown while the removal of the material is occurring. This is a big advantage as it would be clear to see how much material needs to be removed.

Theoretically, the amount of material to be removed can be calculated, hence making it possible to ensure that the resistance of the work piece will not exceed the target of $100\mu\Omega$. This calculation will also be supported by the combination of trimming and measuring, where, small amounts of the material can be removed simultaneously with the resistance measuring until the required $100\mu\Omega$ value of resistance is achieved. This simultaneous way of trimming and measuring will be discussed in section 5.5.2.

5.4 Modelling of Potential Trim Patterns

A number of different trim designs were modelled using SolidWorks 2015 software to be tested during the initial trimming phase. These designs were created so that a specific volume of resistive material could be removed from the Manganin strip based on the theoretical results from Equation (5.3). In this experiment, 5 initial trim designs were created (Figure 5.5) to allow easy removal of resistive material from the Manganin strip using the milling machining technique.

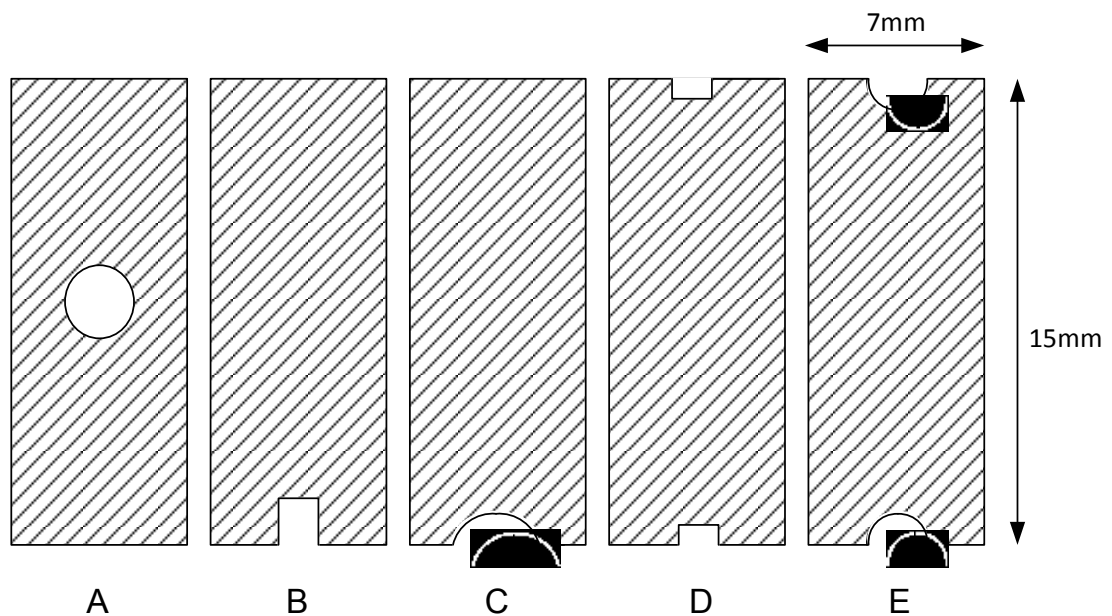


Figure 5.5: Various initial trimming designs and patterns.

All suggested designs were then investigated in the Thermal Electric module using ANSYS 14.5 software to determine the effect of varying trimming geometry on the current flow within the resistor element and the subsequent temperature rise of the shunt. Convection was set at 22°C ambient temperature with 5 W/m²K coefficient and the high voltage potential was set to 0.02 V, giving an equivalent current of 200A through the 100 μΩ shunt. The material properties for Manganin, as determined in Chapter 4, were kept constant throughout (i.e., thermal conductivity of 22 Wm⁻¹K⁻¹, Seeback Coefficient of 0.6 μVK⁻¹ and resistivity of 38 Ωm). A Manganin strip without any trimming was used as a control sample for the analysis. Results for this control strip indicated

that the current flow is stable and uniform having an equal current density of $6.35 \times 10^6 \text{ A/m}^2$ across the cross section of the strip, see Figure 5.6(a).

The average volume of resistive material to be removed from the Manganin strip for all samples of the shunt resistors was calculated using Equation (5.3) to be 6.74 mm^3 . The five designs were modelled by removing this volume of resistive material. All 5 designs were then compared with the untrimmed Manganin strip design to see the difference in total current density and to choose the best design geometry based on the lowest effect. However, the flow of current was found to be unstable at all the cut outs on the Manganin strip with values in the range 1.35×10^7 to $1.55 \times 10^7 \text{ A/m}^2$. These values are significantly higher than that for the untrimmed part of $6.35 \times 10^6 \text{ A/m}^2$.

The result shown in Figure 5.6(b) consists of a drilled hole cut through the centre of the Manganin. The current flow around the edge of the hole is severely constricted and results in the highest current density of all five designs of $1.55 \times 10^7 \text{ A/m}^2$. Furthermore, Design A relies on a number of important factors such as the resistance measurement and volume calculation. The initial measurements would have to be very accurate so the correct diameter cutter could be used. If the calculations are incorrect, when the hole is drilled through the material, the shunts resistance value could be outside of the required tolerance limits.

Results for Design B, in Figure 5.6(c), show that the sharp corners of the square cut severely impede and distort the flow of current. A maximum current density of $1.49 \times 10^7 \text{ A/m}^2$ was recorded at both sharp corners of the cut area. As a result, this will create unwanted heat energy in the region of the shunt. On the other hand, it is observed from Figure 5.6(d), that Design C has a more uniform current density around the edge of the semi-circular cut, thereby allowing an improved flow through the shunt resistor. The overall disturbance to the current flow is minimal when compared to the untrimmed control sample and remains relatively linear around the cut out section, with a maximum current density of $1.47 \times 10^7 \text{ A/m}^2$ being recorded.

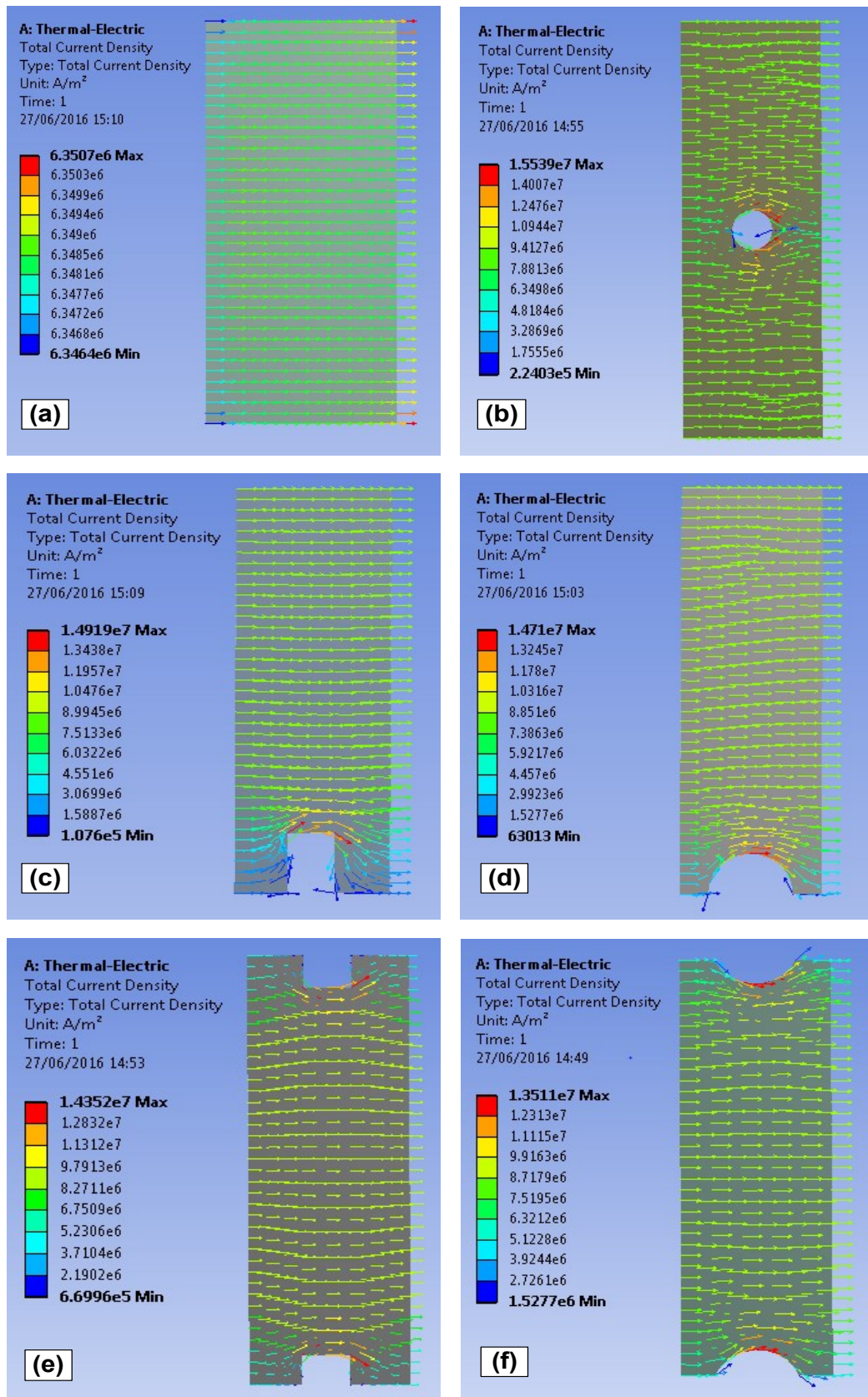


Figure 5.6: Total current density results using ANSYS 14.5 for Manganin strip with different trimming patterns, using: (a) untrimmed, (b) Design A – hole cut, (c) Design B – square cut, (d) Design C – semi-circular cut, (e) Design D – double semi-circular ended cut and (f) Design E – double square ended cut.

Design D and Design E, illustrated in Figure 5.6(e) and Figure 5.6(f) respectively; consist of double entry square and semi-circular cuts from opposing sides of the Manganin strip. These designs produce similar patterns of relatively smooth current flow through the central area of the Manganin and have the desired effect of further reducing the maximum current density to $1.44 \times 10^7 \text{ A/m}^2$ for Design D and $1.35 \times 10^7 \text{ A/m}^2$ for Design E. However, it was considered that the double entry cut approach would be more difficult to control in practice as the designs consist of material removal from both sides of the Manganin strip and the two voltage terminals could also interfere physically with the machining at one side of the strip.

The best current flow pattern is one that travels through the part linearly with as little disruption as possible. It was observed the semi-circular cut allowed a much more uniform current flow than the square cut and further investigation revealed that as the diameter of semi-circular cut was increased, the rate of change of resistance was reduced but the control of resistance accuracy was improved. Through these observations, it is concluded that Design C presents a better approach to trimming the Manganin shunt resistor in terms of minimizing current density and temperature rise and improving resistance accuracy, whilst Design B may have the potential to give higher rates of resistance change and thus reduce trimming time. Moreover, both designs consist of single entry cuts which will simplify the machining operation and also allow easy measurement of the resistance during the trimming process. Therefore, two designs which are Design B and Design C were selected for initial trimming trials to make a comparison with the theoretical analysis.

5.5 Experimental

A suitably small diameter cutting tool needed to be attached to the milling machine because the Manganin strip has a width of only 5mm. Incorrect use of the cutting tool may wreck the work piece and the experiment might fail. The decision to use a 3 mm diameter end mill cutting tool was made in order to remove the resistive material and it was supported by the computer simulation, which shows the most suitable shape or geometry with minimised disturbance for the current to flow in the shunt resistor. One side of the shunt element was fed to the rotating end mill as shown in Figure 5.7.

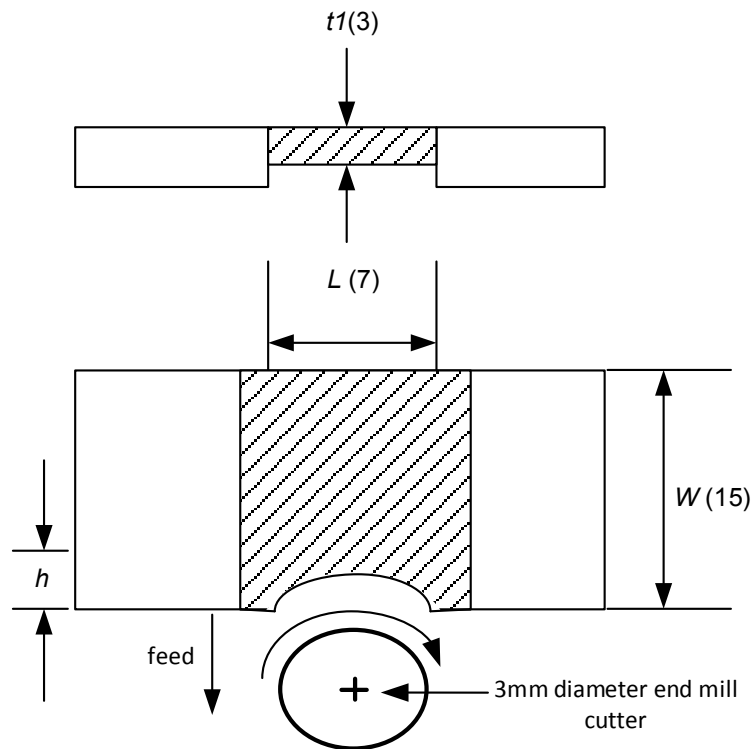
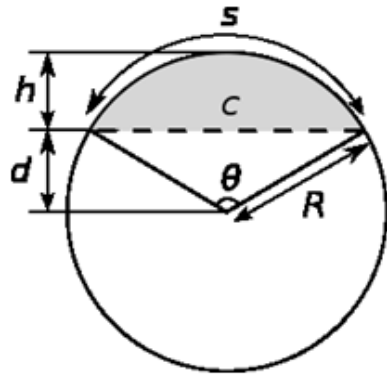


Figure 5.7: Shunt resistor element dimensions and trim geometry.

The depth of cut, h , required to remove the calculated volume of material was determined as follows:



$$h = 2R \sin \frac{\theta}{2} \quad (5.4)$$

where the central angle of the circle, θ , was determined by solving iterations of the following equation for angles of 0 to 360°:

$$\frac{2A}{R^2} - \frac{\theta\pi}{180} + \sin \theta = 0 \quad (5.5)$$

5.5.1 Initial Trials

The machine that was used to removing the resistive material was a Bridgeport BR2J milling machine, which was armed with a 3 mm diameter HSS end mill cutting tool that rotates at 1500 rpm. The machine vice held the shunt while it was fed to the rotating cutting tool until it reached the required pre-calculated, h , depth of cut. Once the criteria had been met, the shunt was retracted from the rotating cutting tool and the final resistance measurement was taken.

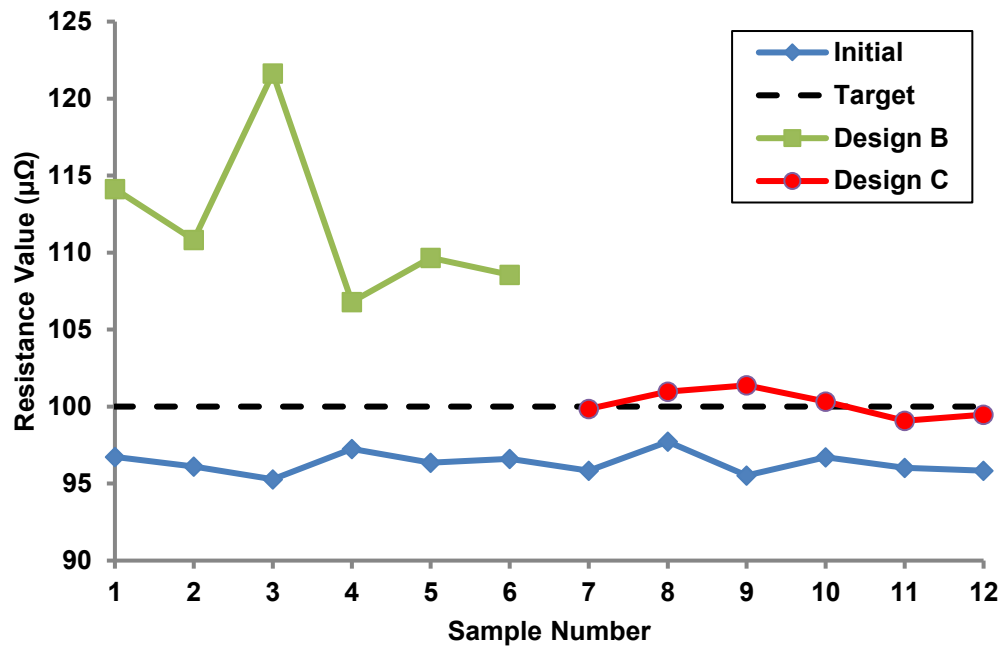


Figure 5.8: Graph for initial trimming process on different design.

Figure 5.8 shows results for resistance before and after the trimming process for Designs B and C obtained from the digital micro-ohmmeter; where the required target is to achieve a resistance of 100 $\mu\Omega$. The initial resistance values before trimming have minimum and the maximum values of 95.28 $\mu\Omega$ and 97.72 $\mu\Omega$ respectively and the corresponding mean value is 96.33 $\mu\Omega$. The dashed line indicates the target resistance value of 100 $\mu\Omega$ to be achieved.

It is noted that there are significant variations in the generated resistance values after the trimming process for Design B and C. Samples 1-6 are trimmed using Design B while samples 7-12 are trimmed using Design C. Fig. 6 is divided into two sections, where trimmed samples for Design B have higher resistance values than targeted as compared to Design C with much lower resistance values close to the targeted resistance of 100 $\mu\Omega$. The minimum and maximum resistance values for Design B are 106.8 $\mu\Omega$ and 121.64 $\mu\Omega$ whereas for Design C are 99.08 $\mu\Omega$ and 101.38 $\mu\Omega$ respectively.

It was observed that the rate of change of resistance was much higher for samples trimmed using Design B compared to Design C. Moreover, the final resistance values obtained for Design B were much higher than the target value of $100\ \mu\Omega$ and were difficult to control within any reasonable tolerance limits. Design C shows more controllable final resistance values after the trimming that are much closer to the target value of $100\ \mu\Omega$. The mean and standard deviation for Design B are calculated at $111.94\ \mu\Omega$ and $4.89\ \mu\Omega$ while for Design C they are $100.18\ \mu\Omega$ and $0.8\ \mu\Omega$ respectively.

5.5.2 Concurrent Trimming

Concurrent engineering or simultaneous engineering is a method of developing or designing products simultaneously. The different stages of development can be carried out at the same time rather than doing them consecutively. From the relevant research studies [133-136], concurrent engineering proves to be cost effective, reduces development time, time to market, and it also improves productivity. Even though the initial implementation is challenging, the benefit of this method and competitive advantage is highly desirable. The method could eliminate the urge of repetition in any stages of development by removing the multiple design reworks, and/or repeated trimming process.

In the previous section, a trial and error approach in trimming the shunt was used in order to get the desired effect. Firstly, the initial resistance value R_1 has to be measured beforehand. After that, one has to calculate the volume of material, V , that should be removed before the trimming is finally carried out. The final measurement of R_2 will then be taken after the trimming is complete. These steps are repeated until the desired effect on the work piece is achieved and by practicing this step-by-step process, an excessively long time is needed in order to complete the study. This repetition of these stages will cost dearly in time, effort, and raw materials. However, by implementing the concurrent engineering method, time could be significantly saved in this product development, especially if it will be produced on a large scale manufacturing line in the future.

However, there were some stages that needed to be carried out carefully in order to get the best result in using the concurrent engineering methods. The failure to comply with these requirements will result in time and cost wasting. This is because the concurrent engineering anticipates the amount of material that has to be removed as early as in its testing stages. The main purpose of concurrent engineering was to simultaneously trim and measure the resistive material without having to retest the trimmed part in the next stage. Therefore, precision is very crucial in implementing this method. If there were any mistakes, the process may have to be repeated with a new shunt resistor and this will result in an increase in the usage of time and raw materials.

There are two ways of implementing concurrent engineering which are automatically and manually. The automated approach is not the best choice in the initial research phase as it will need a larger amount of investment than the manual approach. While the manual approach is more suitable in the initial research in order to test the theory and to make sure that concurrent engineering for trimming shunt resistors for a better tolerance is worthwhile. Once the parameters and result of the manual approach are finalised, perhaps the data can be used in developing an automated approach, especially for use in large manufacturing facilities.

Figure 5.9 shows the concurrent trimming experiment setup for the proposed research. Since concurrent engineering is implemented, the three main building blocks that will simultaneously work during the experiment are setup to the work piece, these are; the Agilent B2902A Power Source, the Agilent 34420A 7.5 Digit Nano-Volt/Micro-Ohm Meter, and the Bridgeport milling machine.

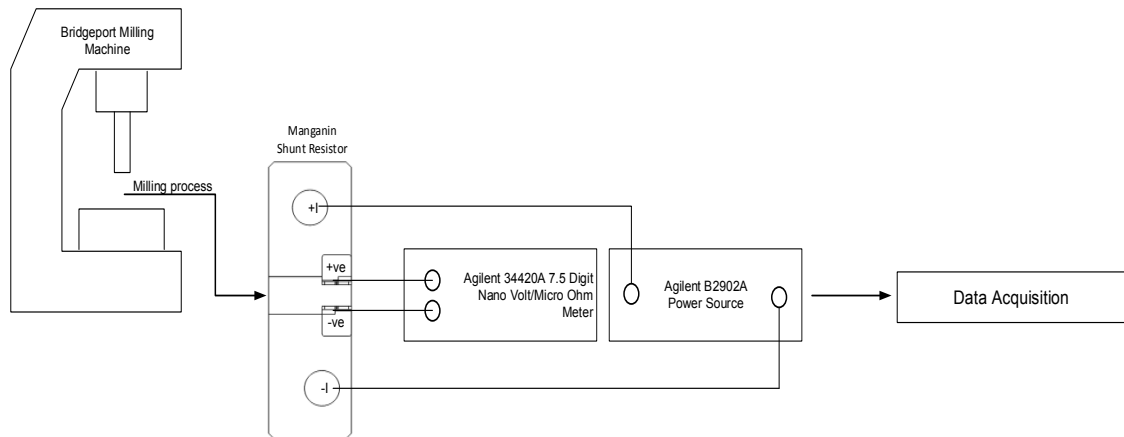


Figure 5.9: Block diagram of concurrent trimming test using a milling machine.

A 3 mm diameter end-mill cutting tool was equipped to the Bridgeport milling machine with a polytetrafluoroethylene (PTFE) jig used to electrically insulate the shank of the cutting tool from the machine spindle. The jig which holds the work piece was also made from PTFE to insulate the shunt from the machine vice. After securely clamping the shunt resistor to the jig, it was connected with cables for current delivery and voltage value measurements. Two 6 mm diameter bolts and nuts were used to fix the current cables securely to the shunt and insulated jig, while the voltage sense cables were soldered using silver solder to the two pre-welded tin plated termination pins of the shunt. The current output for the Agilent B2902A Power Source was set to 1A with a voltage limit of 0.5V.

Initial trials of the experiment focussed on using a modified method of machining described in Section 0, in which the shunt was electrically insulated from the cutting tool and machine vice to reduce noise in the resistance measurements. Shunt was trimmed from the initial resistance to reduce noise in the resistance measurements. Upon feeding 1A of current to the Manganin shunt resistors from the Agilent B2900A Power Source the initial values of resistance were taken before the trimming process started. Resistance measurements were taken every 15 seconds for 1 minute, to allow the voltage readings from the Nano-volt meter to stabilize.

Following this, the end mill cutter position was zeroed against the surface of the Manganin area to be trimmed. Then, the value of depth of cut was set using a dial test indicator (DTI), before the milling procedure took place. For this experiment, the shunt resistor was cut dry with the constant feed rate of 50m/min. During trimming process, the Nano-volt meter digital readout displayed the resistance slowly increase until it reached the target value of $100\mu\Omega$. The milling action was then stopped and the trimmed shunt resistor continuously measured for 1 minute before the final resistance measurement was recorded.

5.5.3 Results

The results of this experiment are shown in Figure 5.10, where the initial resistance and the reading during the trimming process of the concurrent approach are plotted. The main target is to achieve a resistance of $100\mu\Omega \pm 1\%$. From that, Sample 3 shows the highest value of resistance during the experiment with $100.335\mu\Omega$ and Sample 5 shows the lowest resistance with $100.023\mu\Omega$. On the other hand, Sample 1, 2 and 4 gave readings of $100.081\mu\Omega$, $100.094\mu\Omega$ and $100.243\mu\Omega$, respectively. Therefore, the average value for all five samples is calculated at $100.1552\mu\Omega$ which stands at 0.15% of the tolerance resistance and all 5 samples are well within a tolerance of $\pm 1\%$.

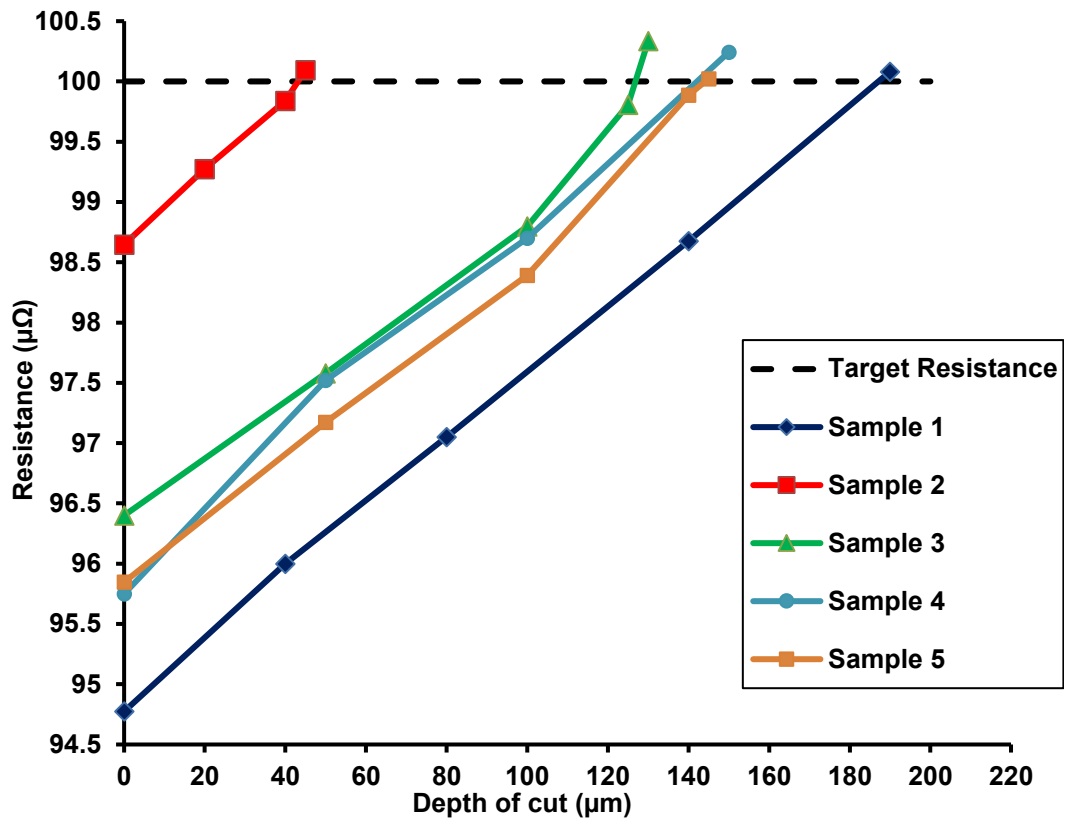


Figure 5.10: Results of resistance versus depth of cut for 5 samples using the initial concurrent trimming process.

These findings suggest that the concurrent trimming approach is a feasible method to monitor the rate of change for the resistance of Manganin shunt resistor and to determine the desirable depth and amount of material removal from Manganin strip. However, it still proved difficult to achieve stable measurements due to the electrical conductivity across the cutting tool during machining.

5.6 Summary

In this chapter, the theory, design geometry and techniques for trimming shunt resistors in metering applications have been examined. Results from ANSYS software on different geometries have shown that Design C presents a better approach in terms of minimizing current density and temperature rise and improving resistance accuracy, whilst Design B may have the potential to give higher rates of resistance change and thus reduce trimming time.

Results from experiments have shown that the concurrent trimming process is a viable method of trimming the resistance value of Manganin shunt resistors. It offers improved trimming accuracy and reductions, both in terms of time and cost of the process, compared to the initial consecutive process. This procedure has the potential for application in large scale manufacturing practice, after the best set up and specifications can be the reference in order to be implemented to the trimming process for the shunt resistors. It will give a lot of benefit to the manufacturer in terms of quality assurance, time and cost. Furthermore, by using concurrent trimming in this experiment, the tolerance of the Manganin shunt resistors is reduced from $\pm 5\%$ of tolerance to less than $\pm 0.5\%$ in a shorter time compared to the consecutive trimming process.

Eventhough the results seem promising, due to the difficulty of measuring the resistance measurements across the milling cutter and the need to insulate the spindle of the milling machine, it was therefore decided to focus on a grinding process which has a lower material removal rate and an electrically insulated cutting disc. The main consideration is to be able to do in-process measurements which can only be done using grinding. Since the results show relatively small differences, the advantage to be able to do in-process measurements for the practical product is chosen eventhough it is not the theoretical best. Furthermore, grinding gave more accurate control of the feed rate which is more practical while at the same time giving a smoother surface and better quality finish.

The following Chapter 6 will focus on developing the concurrent trimming method further to include a precision grinding process with lower material removal rate and automatic resistance measurement feedback loop to try and further reduce the resistance tolerance of the shunts.

Chapter 6

Development of Automated Trimming System

It has been shown in the preceding chapters that trimming the shunt resistors to a tolerance of $<\pm 1\%$ is possible. Therefore, an experimental prototype of an electro-mechanical trimming process to further improve the accuracy and performance of $100\mu\Omega$ Manganin shunt resistors needs to be designed, built and tested in order to prove its operational capability. The main goals of this prototype are to perform the trimming process and obtain shunt resistors with $<\pm 1\%$ tolerance using the electro-mechanical trimming system and determine its feasibility. Additionally, reliability of the theoretical model of material removal will be estimated.

This chapter describes the experimental setup of the prototype for the precision trimming process, which will include the discussion of all sensors and data acquisition systems, which were used to record the performance of the system. The following sections will briefly explain the details of the work piece materials, tooling and equipment used in the trials, together with a comprehensive description of the experimental procedure in the development of the prototype trimming process.

6.1 Experimental Setup

The experimental setup used to trim the shunt resistors is illustrated in Figure 6.1. It consists of five main components including a precision saw, variable power supply, Agilent meters, data acquisition system and LabVIEW software. The prototype is used to trim the entire shunt resistor as the previous technique described in previous chapter using milling machine gave unstable results due to uninsulated cutter and trouble to combine both trimming and measuring system.

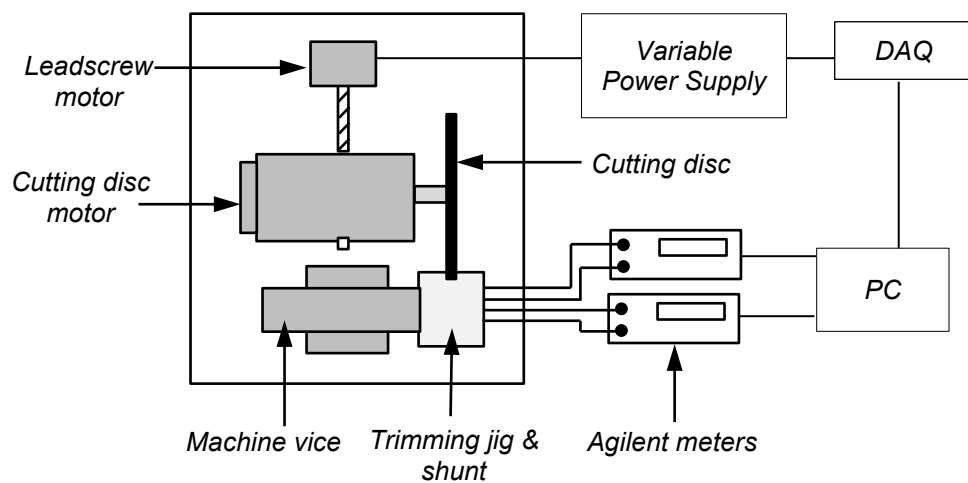


Figure 6.1: Schematic of concurrent trimming system using linear a precision saw.

The trimming process of the shunts will be using a Buehler Isomet 5000 linear precision saw fitted with a 178 mm diameter, 0.8 mm thick rubber bonded silicon carbide (R/SiC) AcuThin cutting disc. The samples were mounted in an insulated trimming jig which was secured in the machine vice and the cutting disc was rotated at a various different speeds and fed into the side of the shunt as seen in Figure 6.2. The concurrent trimming system is planned where the resistance value of the shunt was continuously measured during trimming using the combination of Agilent B2900A power supply and 34420A Nano-volt meter described in Chapter 5.

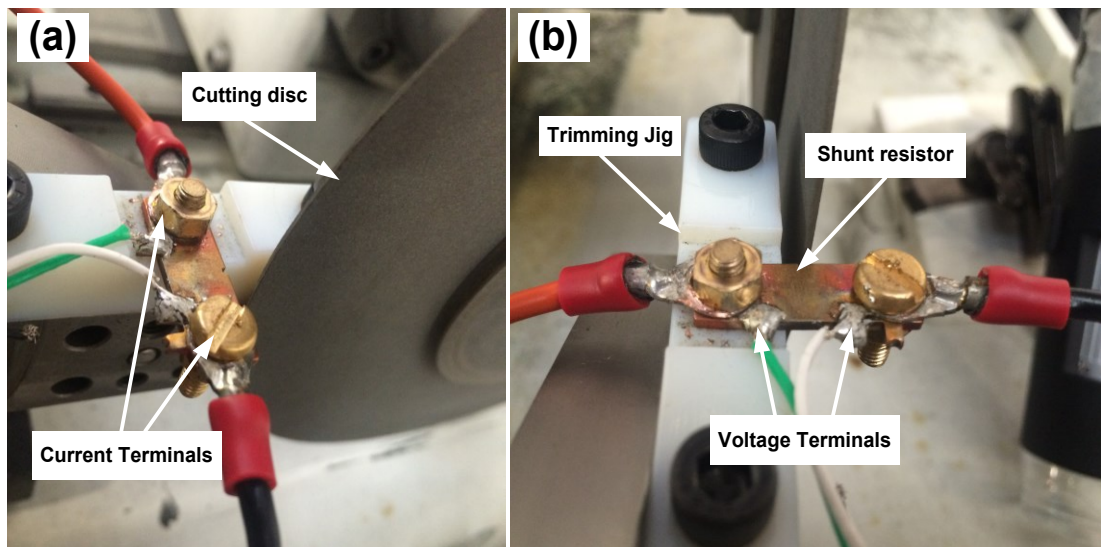


Figure 6.2: Different views of concurrent trimming system.

All resistance measurements were performed using the 4-wire Kelvin method; a fixed current of 1 A was supplied to the shunt via the current (I) terminals from the Agilent B2900A source meter, whilst the voltage drop across the pre-soldered voltage (V) terminals was continuously monitored using the Agilent 34420A Nano-volt meter. A small modification was made to the precision saw where the leadscrew motor of the precision saw is now can be controlled via the variable power supply. This was done in order to be able to control the feed rate of the machine at any desirable rate compared to the default feed of 1.2 mm/min. This will also help the investigation to wider range of feed rates and achieving optimum parameters for the trimming process.

The system is controlled using a National Instruments (NI) USB-6000 data acquisition (DAQ) device and the program is organized via Laboratory Virtual Instrument Engineering Workbench (LabVIEW) 2015 software. The DAQ device can act as a D/A converter and A/D converter, and it has both digital output/input channels and an analogue input channel. In order to record, display, manage and control the data measured by the Agilent B2900A, a NI-DAQmax software works within the environment of LabVIEW software, which is used to conduct the experimental investigations. This software has a comprehensive system design environment of graphical programming language. The system is provided by build-in engineering specific libraries of software functions and hardware interfaces, and it is designed for data analysis and visualisation of results.

The flow of the program in LabVIEW can be seen in Figure 6.3. For each LabVIEW file, there are two display windows: the front panel which represents the user interface for the virtual instruments (VI) and the block diagram panel where the graphical source code is created to control the front panel. The system is designed to calibrate the resistance measurement at the beginning of the trimming process and continuously measure the resistance until the stop button is pressed.

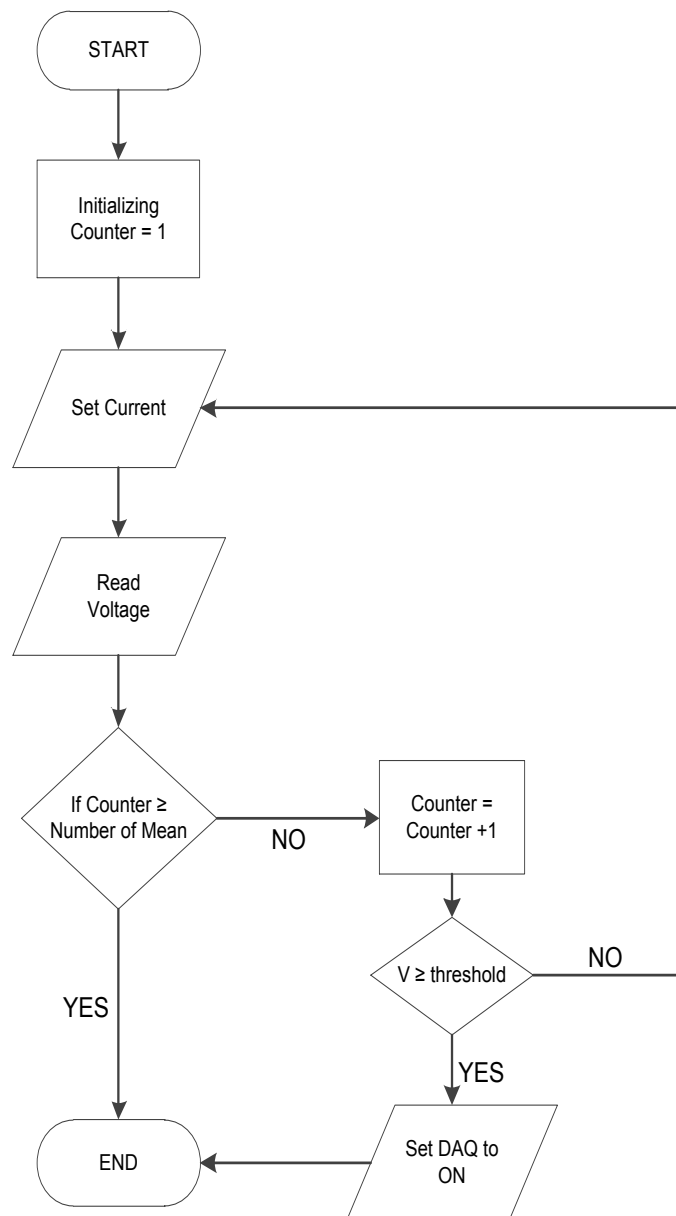


Figure 6.3: Flow diagram of the proposed trimming control.

The software is designed to make sure that the current is set at 1A with a 0.5V limit upon start-up and measures the voltage drop once every second, which is then converted into a resistance value. The whole system is design to only work if the current is set at 1A and the targeted resistance value is higher than the initial resistance value. Figure 6.4 shows the front panel used to control the experiment. Target resistance is inputted before the experiment starts, and is typically set at 1% from the initial value. Once the measured resistance value monitored in LabVIEW software reaches the target value, the DAQ will be activated and will send a signal to the cutting disc to retract it from the shunt via the leadscrew and motor.

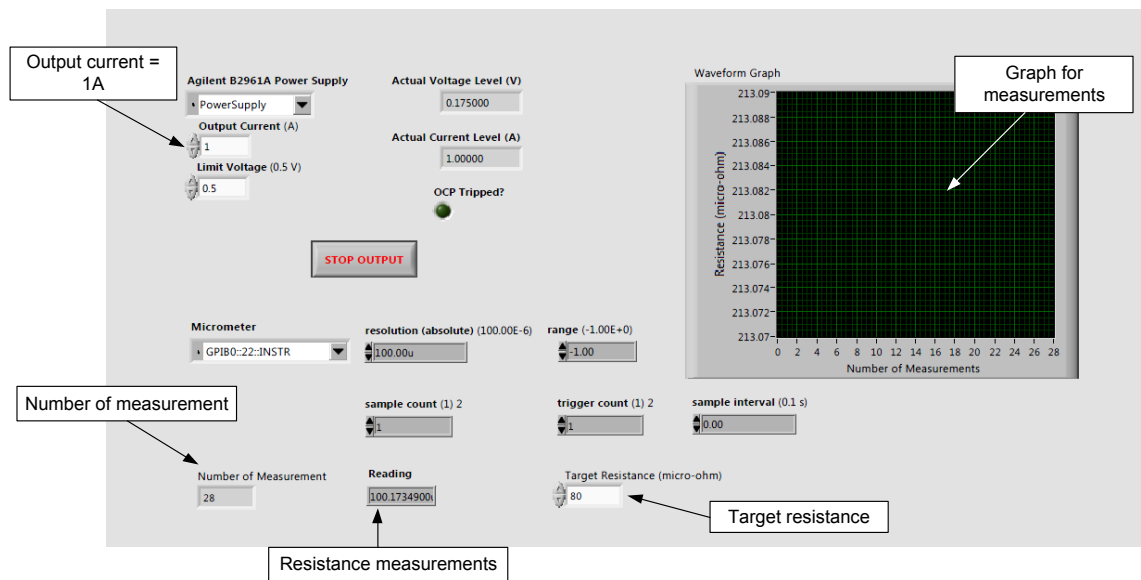


Figure 6.4: Front panel of the LabVIEW system.

Each step to design the prototype electro-mechanical trimming process is discussed in the next section where the block diagram window for each main component is explained in detail.

6.1.1 Power Supply

In order to make sure the power supply can be used in LabVIEW software, the Agilent B2900A power supply needs to be initialised first. The meter is connected to the software using a USB 2.0, A to B cable. Since the power supply coding is not readily available, a coding from the Agilent B29216A with some modifications was made. The output for the power supply needs to be configured where the voltage range and output current need to be written within the VI to work with the software. The power supply is configured with the output current set at 1A and a 0.5V limit voltage. Then, the output will be enabled to switch it on as shown in Figure 6.5.

Figure 6.6 shows the block diagram for setting the current and output protection status for the Agilent B2900A power supply. The software will check if the output and protecting circuits are working properly. The front panel of the VI will show if the power supply is safe to use or not. Then, the output is enabled to measure the actual output supplied by the meter. The input will tell the device that the measurement will be conducted and the output will then check if it is working and conduct the actual measurement in the conditional manner.

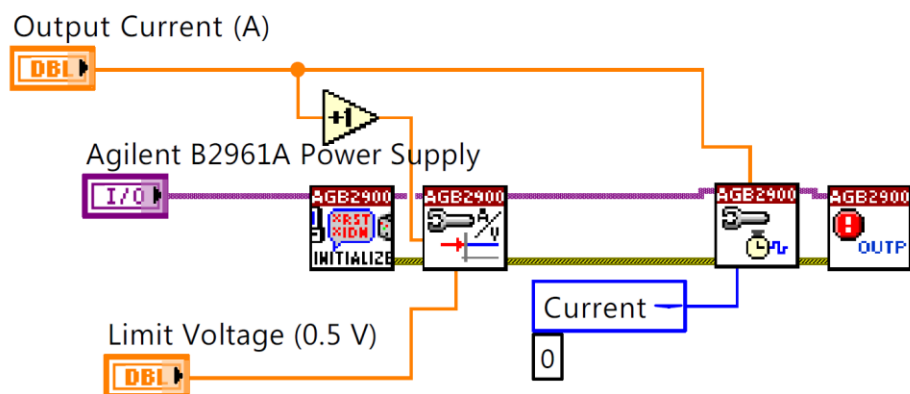


Figure 6.5: Block diagram for initializing the current source.

All blocks to set the current and the output protection status are put inside a 'while' loop which will continue running until one of the conditions is true. On the other hand, the case structure is used to combine both codes to

read the output current and the voltage value that are measured by the device, including the open circuit protection (OCP) status operation, which can also be seen in the front panel of the system. There are 4 conditions to stop the measurement loop which are:

1. If the required number of measurements are done
2. If the stop button is pressed
3. If during the measurement the power supply output is not working
4. If any OCP error happens in the device

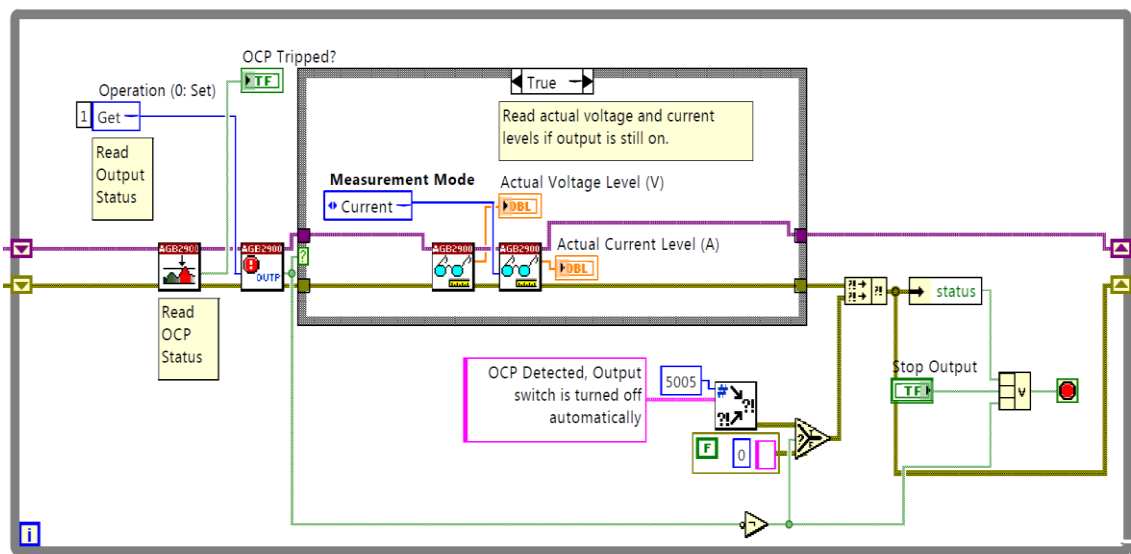


Figure 6.6: Block diagram to set current and output protection status.

6.1.2 Measurement System

Similar to the power supply application, the measurement system is conducted by initializing the multimeter itself by setting the input code to the Agilent 34420A multimeter as shown in Figure 6.7. The meter is connected to LabVIEW software using a Keysight 82357B USB/GPIB Interface High-Speed USB 2.0 cable. The configuration of the meter required an open string to reset the flag which is true. The meter comes with 2 channels and the code to select a specific channel is set to Channel 1 where the 4-wire Kelvin connection will be used.

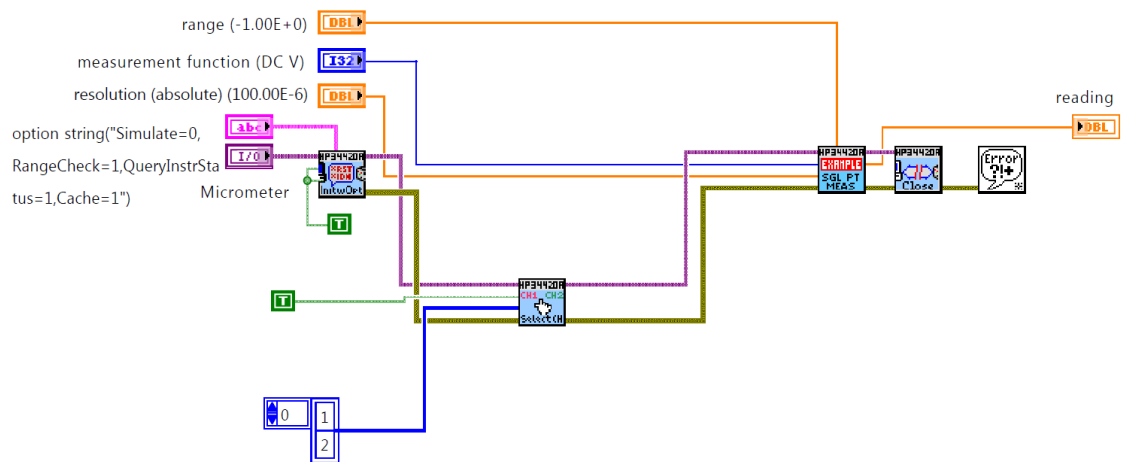


Figure 6.7: Block diagram for the measurement system.

The system is set to use single point measurement where one measurement is collected every second. The type of measurement is selected to DC Voltage and inputted to the software together with the measurement accuracy and the range of the measured voltage. The output for the system is the measured voltage which is then converted as a resistance value of the shunt under test.

6.1.3 System Combination

After both the power supply and multimeter are initialised, the system is combined to be able to supply current to the shunt and read the voltage value at the same time.

Figure 6.8 shows the combination of both systems. The VI can be divided into four main parts; initializing the device, setting up the current, measuring the DC voltage and closing the device. The initializing processes for the devices are the same as those explained in Sections 6.1.1 and 6.1.2.

Both tasks of setting up the current for the power supply and measuring the DC voltage are put inside a 'while' loop structure. Since the Agilent 34420A measures the DC Voltage in volts, the code is written to multiply the measured voltage by 10^6 to change the calculated units of resistance from Ω into $\mu\Omega$. All the measurement values are then added into an array, which is initialized with the first element of '0' to be deleted once all measurements are conducted and all measurement values will then be plotted into a graph which can be seen on the front panel. The input code for target resistance is also made and can be inserted from the front panel of the VI. Both the measurement data and graph can be imported to Microsoft Excel to be saved and processed further.

Closing the devices is basically done to switch off the current output and then close all the communication between the power supply and multimeter with the LabVIEW software. The software then summarizes the occurred errors related to the power supply and multimeter.

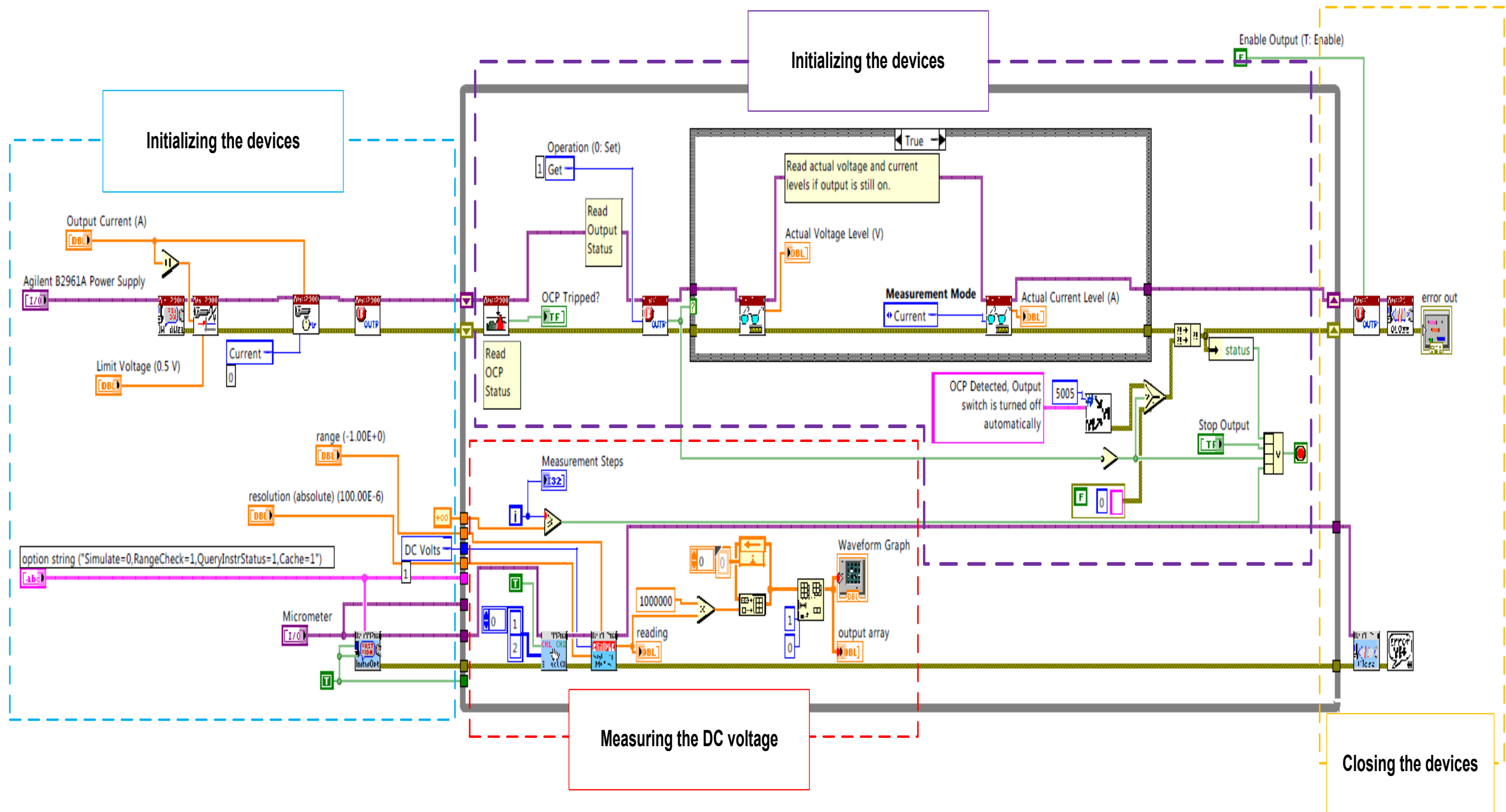


Figure 6.8: Block diagram of concurrent trimming system and divided into different sections.

6.2 Automated System

The next step is to enable the concurrent system to automatically stop the trimming process, once the target resistance is reached. It was decided to use a DAQ which is connected to the cutting saw and LabVIEW software. Data from the resistance measurement using the Agilent meters is sent to the DAQ and the device sends the output to the cutting saw. On further investigation, the saw could not be switched off automatically and it was decided instead to reverse the feed of the saw once the target resistance is achieved.

The experiment used the digital output channel from the NI USB-6000 and it was added to the previous VI using a similar step, as discussed previously, to initialise the device at the beginning of the process and close it at the end. The DAQ is connected to the LabVIEW software using a USB 2.0 cable with the selected output pin of 0 and has an output voltage of 3.4V. In order to reverse the polarity of the cutting saw, a Double Pole Double Throw (DPDT) relay was used in the circuit to change the direction of the cutting saw once the resistance value reached the targeted value.

The DPDT relay was connected to the DAQ device within an external circuit as shown in Figure 6.9 and sends a control signal to the cutting saw. A transistor was used to boost the power of the relay using a voltage power supply at 5V as the DAQ output voltage is not enough to energise the relay coil. Without voltage applied to the coil, the voltage power supply, T1, +ve point will be connected to contact 1, while the T2 -ve point will be connected to contact 3. As a result of that, the precision saw will advance forward and cut the shunt. When voltage was applied to the coil, the relay switches on, causing T1 +ve point to connect to contact 2, and T2 -ve point to connect to contact 4. These changes will cause the precision saw feed to change direction and retract backwards away from the shunt.

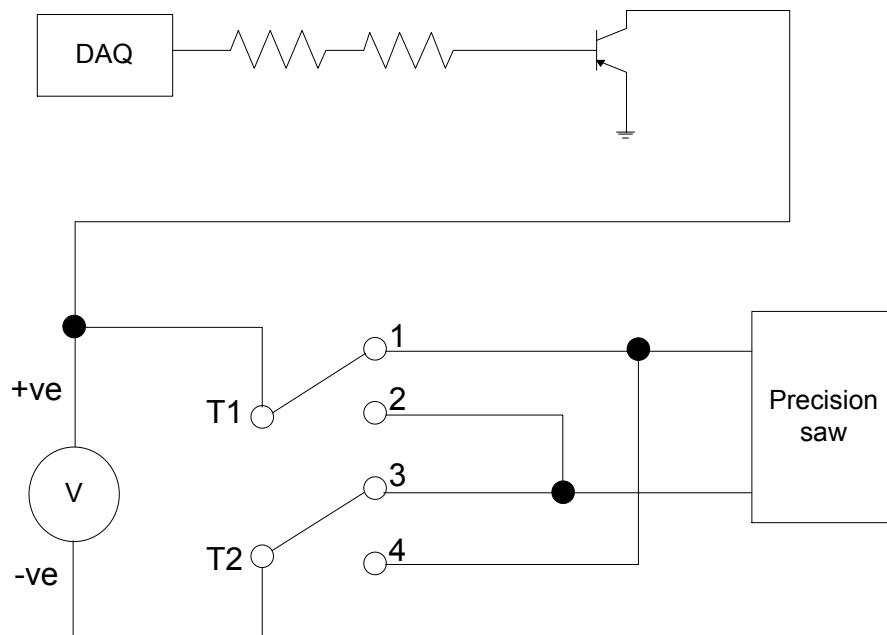


Figure 6.9: External circuit used to control a relay.

Initial tests were conducted with the system and it was confirmed to run as expected. However, after few trials were performed using the system and the data was analysed, it was realised that one measurement per second was not that accurate due to the high speed of the process. More measurements were needed to get accurate results for the process.

To overcome this, the VI for the concurrent trimming process was changed within the measurement system where the single point measurement was replaced with a multipoint measurement as seen in Figure 6.10. By using the multipoint measurement VI, a 'Sample Interval' and 'Sample Count' could be specified, which were used to achieve far higher acquisition rates. For example, to achieve 10 measurements per second, the interval time is set to 0.1s and number of samples to 10; this returns 10 points of data every second. Immediate trigger was used within the VI which puts the multi-meter into a mode where it automatically triggers for measurements without any need to have an external or internal trigger.

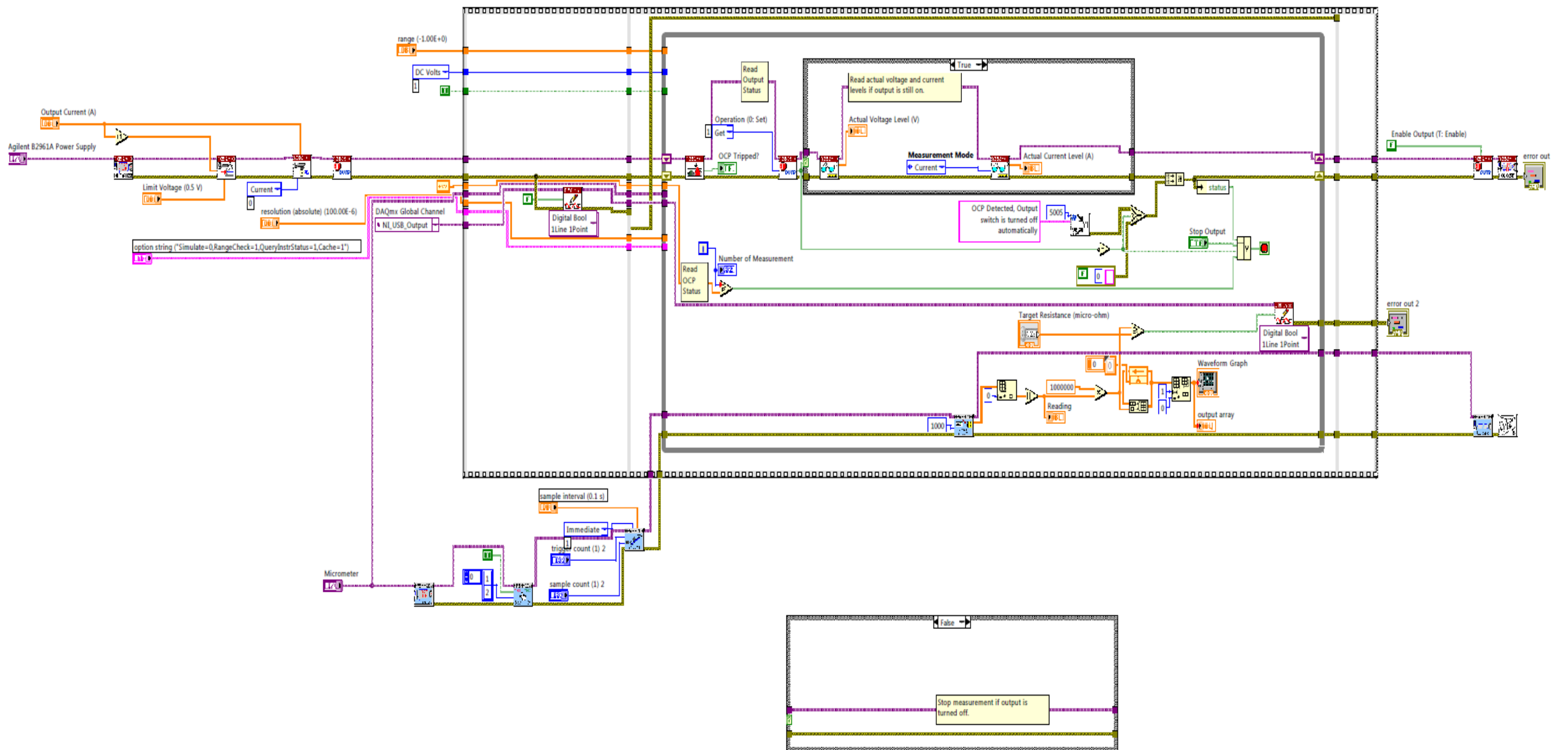


Figure 6.10: Block diagram of concurrent trimming process using multipoint measurement.

The full system was put in the flat sequence structure that will allow all tasks to be performed in the sequence shown in the flow diagram in Figure 6.10. Therefore, when the software runs, the device will receive an immediate trigger, collect the specified number of samples, output them, and then finally wait for another trigger, depending on the amount set in trigger count. However, further investigation revealed that according to the data sheet of the Agilent 34420A, for DC Voltage measurement, it can only measure 0.15 readings/s [137]. The 34420A reading speeds listed in the data sheet have been confirmed to 200 plc integration time with 7 ½ digit setting at 50 Hz which is quite slow as shown in Table 6.1.

Table 6.1: Operating characteristics for Agilent 34420A [137].

| Function | Digits | Integration Time | Readings/s |
|--------------------------------------------------------------------------------------------------------------------------------------------------------------------------------------------------------------------------------------------------------------------------------------------------------------------|--------------|------------------|-------------|
| DCV | 7 1/2 | 200 plc | .15 (.125) |
| Resistance | 7 1/2 | 200 plc | .075 (.062) |
| DCV1 / DCV2 | 7 1/2 | 100 plc | .15 (.125) |
| DCV 1-2 | 6 1/2 | 20 plc | .75 (.625) |
| System Speeds | | | |
| Configuration Rates | 26/s to 50/s | | |
| Auto range Rate (DC Volts) | >30/s | | |
| ASCII reading to RS-232 | 55/s | | |
| ASCII reading to GPIB | 250/s | | |
| Max. Internal Trigger Rate | 250/s | | |
| Max. Ext. Trig. Rate to Memory | 250/s | | |
| <ol style="list-style-type: none"> 1. Speeds are for delay 0, Display OFF, Filter OFF, OCOMP OFF 2. Reading speeds for 60 Hz or (50 Hz), 100 mV through 100 V ranges. 1 mV range 30/s MAX, 10 mV range 170/s MAX 3. Speeds are for NPLC 0.02, Delay 0, Display OFF, Chart Out OFF | | | |

During the time in trying to get the best setup for more measurements per second, the accuracy of the readings reduced to 4 ½ digits. For the 100V range, the least significant digit (LSD) is 100mV and for the 1 mV range, the LSD is 1 µV. Further investigation found that the LabVIEW software can be bypassed by using Keysight Connection Expert or NI Max software to send individual Standard Commands for Programmable Instruments (SCPI) to the Agilent 34420A to give more than 20 measurements per second. The following command sequence was used and then the VISA Read.vi was used to retrieve the data from the instrument:

```
"-> *CLS  
-> *RST  
-> CONF:VOLT:DC  
-> VOLT:NPLC 1  
-> VOLT:RANG 1 mV  
-> TRIG:COUN 10  
-> INIT  
-> FETCH?"
```

The command gave more measurements per second but the readings appeared to be repetitive. It could be seen from the results that the device was overloading, causing the measurements to be repeated. This could be due to the DUT not being connected or the measured voltage being over the range of 1 mV. The device also started experiencing an error occur when the FETCH? Command was received by the device but the internal reading memory was empty. It was therefore decided to use single point measurement for the experiment in order to prevent errors in the measurements. Block diagram for the final configuration can be seen in Figure 6.11.

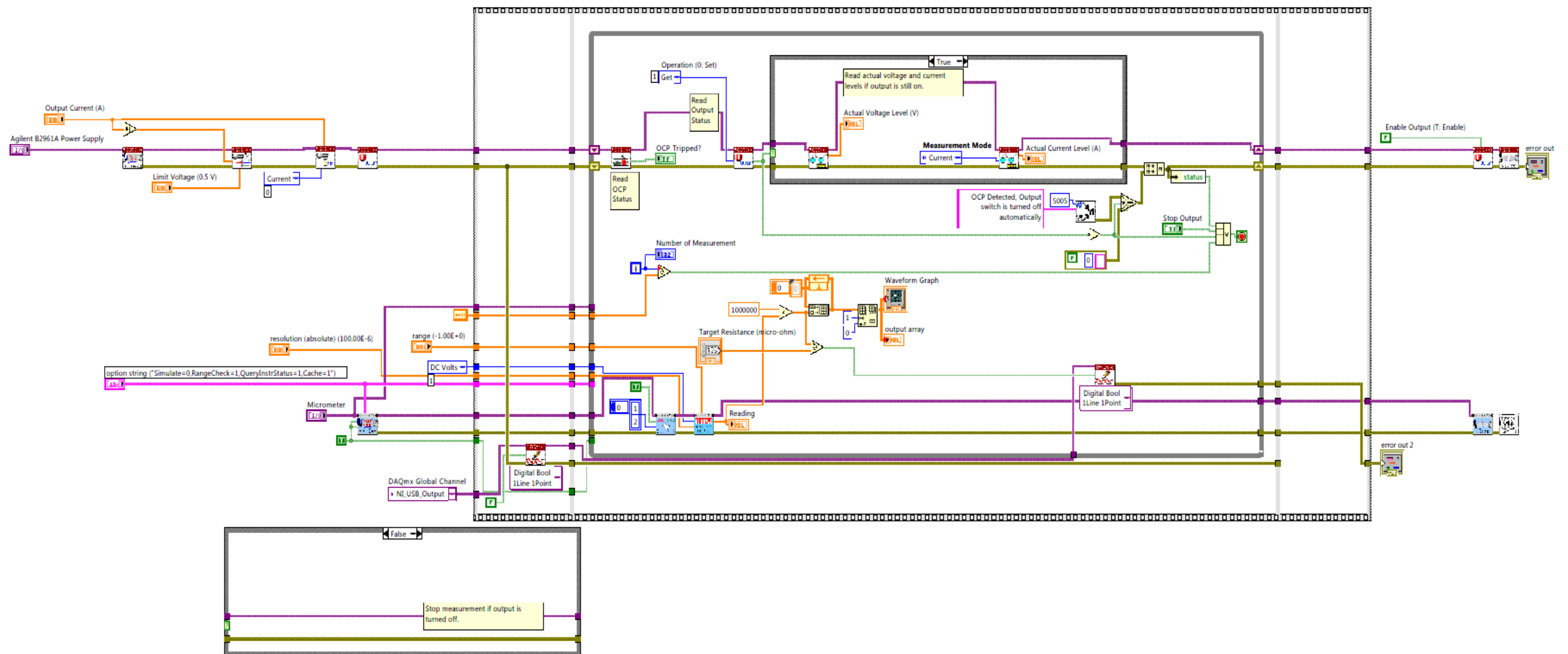


Figure 6.11: Block diagram for final configurations for trimming system.

6.3 System Optimisation

Figure 6.12 depicts the block diagram of the experimental setup for the proposed study. According to the theoretical experiments in the former chapters, the precision trimming process using a precision cutting saw is considered in the system under study. A final setup using LabVIEW software is done where all the code is checked and finalised.

Final modification was made to the VI, where the feed of a cutting saw will only trim the shunt resistor once and then retract straight from the sample. It can be seen from previous results, some of the resistance values overshoot the target value due to the feed continuously trim the shunt whenever the resistance falls below the target. The resistance values will need some time to settle and when the machine keeps on trimming the sample before the resistance has time to reach steady state, it causes higher deviation especially for faster feed rates up to 15 mm/min.

Minor modification was made to the previous system in which for the new system, the target resistance was input at the front panel, and the system will only trim the sample one step at a time before it retracts from the work piece between each trimming processes, while the system will continuously measure the resistance until it reaches steady state. This prevented the system from removing too much material from the shunt causing the tolerance to exceed the target value. The improved trimming system can also be used to predict the resistance value and at the same time reduce the trim time.

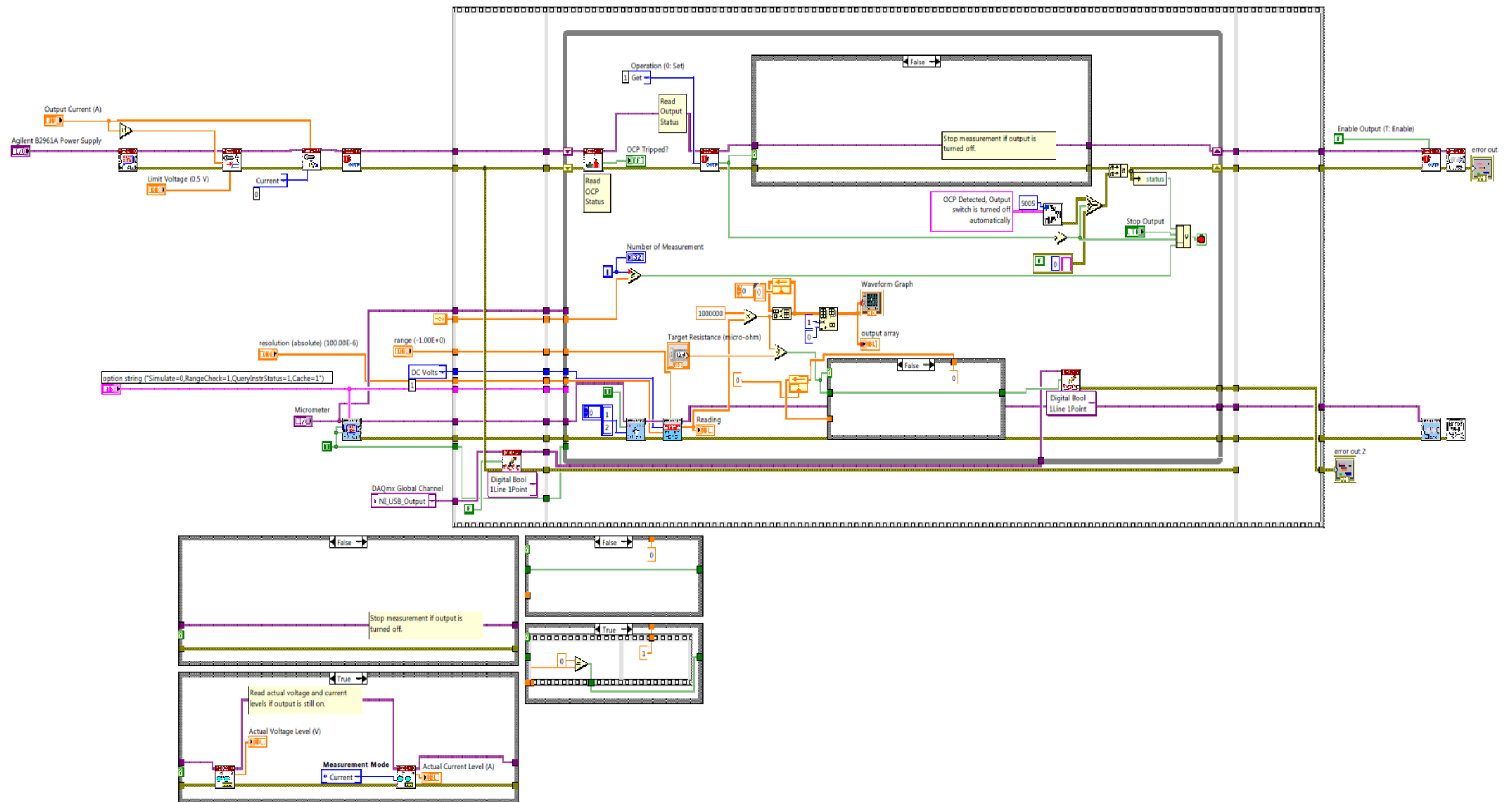


Figure 6.12: Block diagram for precision trimming process.

6.4 Summary

This chapter focuses on the development of automated trimming process with depth explanations on each component used within the system. The system consists of three main components, which are power supply, measurement system and DAQ. Each component was connected to one another through a circuit and can be controlled via LabVIEW software.

Although optimisation of the system produced appropriate results for trimming process, there was still an unacceptable level of measurement within the recorded data. The rate of recorded data of 1 measurement per second can still be argued but further investigations can be suggested using a better device to capture more measurements per second.

Work conducted in this chapter will be used as a working prototype of the electro-mechanical trimming process in the next chapter to properly test the system in order to reduce the tolerance of the shunts.

Chapter 7

Optimisation of the Trimming Process

In this chapter, the focus now is to further, develop and optimise the automated trimming process for use in the manufacture of precision shunt resistors. The developed process has to be practical and cost effective as it would probably be used widely on the mass production scale, as the UK government has already announced that all mechanical meters in each household and industry will be changed to smart energy meters by 2020. The demand for total production of smart energy meters is estimated to be around 30 million units [8, 12, 13, 18].

The current chapter presents the results of work undertaken to observe the effect of various cutting speeds and feed rates of the precision saw developed in Chapter 6 on the trimmed properties of the shunt components. A full factorial of Design of Experiments (DoE) was undertaken to find the optimum process settings under which to trim the Manganin shunt resistors. The research involved two main phases of experimental testing. Phase 1 investigate the cutting speed and feed rate to reduce the resistance tolerance to $\leq \pm 1\%$ in responses to the resistance deviation and reducing trimming time. Phase 2 then looks at a much smaller range of cutting speed in order to get the optimum parameter while trimming the shunt resistors.

7.1 Design of Experiments (DoE)

The definition of an experiment is a test or series of tests which are carried out with different input variables in order to identify and discuss the reasons for the differences that may occur in the resulting output response [138]. The process of planning the experiment is known as the statistical experimental design. This process of planning is to ensure that appropriate data can be obtained and statistically analysed for a better and focused conclusion. A number of factors or variables can be investigated simultaneously in the planning stage in order to know the effects of these variables in the results of the experiment. This stage is very good economically and it will help to make the decision for the best or preferred combinations of variables under the specific experimental conditions. Generally, the experimental design can be split into two categories; fractional and full factorial.

A full factorial design is one where the levels of one factor are evaluated against each level of every other factor, and the arrangement provides all possible effects and interactions, however the scale of testing can be prohibitive [139, 140]. A full factorial DoE measures the response of every possible combination of factors and factor levels. These responses are analysed to provide information about every main factor and each relations effect. Full factorial design is useful when fewer than five factors are being considered. It will become time-consuming and too expensive to test all combinations of factor levels with five or more factors.

For example, the assessment of 4 factors will require 246 experiments at 4 levels in a full factorial design, excluding any replications. A fractional factorial design, on the other hand, would be a more realistic approach, specifically in the initial screening phase, as they require fewer tests. The 246 experiments of a full factorial design can be reduced using a small orthogonal array (OA), such as the L16, in order to investigate the main factor effects whilst still providing satisfactory confidence in the results. The Taguchi method is one such technique, which considers main effects and interaction plots together with analysis of variance (ANOVA) to calculate the relative influence of individual

experiment factors and the corresponding sensitivity of the associated levels in relation to the selected response measures [141].

The Taguchi method proposes that an expert background in statistics is not necessary as the method practices a simple step-by-step approach in the experimental design [142]. This results in a set of procedures that initially involves selecting a suitable OA from a set of standard designs. For example, for two and four levels factors, it is suggest to use L4, L8, L16, L32 designs; for two and three levels combinations use L12, L18 designs and for three level factors use L9, L27 designs. The design selection is followed by assignment of factors into the OA using linear graphs or assignment tables and finally analysis of the experimental data. The best factor combination is extracted from a one-shot experiment followed by a confirmation run in order to validate the results [143]. The main limitation of the technique is that it underestimates the importance of factor interaction effects; although Taguchi implies that their effects can be eliminated by correctly specifying the response variable and carefully selecting corresponding design factors and levels [144].

Taguchi's approach to DoE is easy to adopt and apply for users with limited knowledge of statistics, hence it has gained wide popularity in the engineering and scientific community [145]. There have been plenty of recent applications of Taguchi techniques to materials processing for process optimization; in particular, it is recommended for analysing metal cutting problems for finding the optimal combination of parameters [135, 146-148].

7.1.1 Factor Parameters

Various factors were taken into consideration to decide the optimum parameter to trim shunt resistors. The goal of this experimental work was to investigate the effects of cutting parameters on trimming time, resistance deviation and surface roughness, and to establish a correlation between them. In order to accomplish this, cutting speed and feed rate were chosen as factor parameters. Since only these two factors were taken into consideration, a full factorial design was used, as this type of DoE can evaluated each factor and is able investigate interactions between each factor.

Phase 1 of the experiments involved the variation of cutting speed (V_c) and feed rate (f), each at four levels as seen in Table 7.1. The effect of these two factors (cutting speed and feed rate), on the trimming time (s) and resistance deviation (%) of the shunt resistor sample were evaluated. The experiment was therefore designed as a full factorial design with $4^2 = 16$ treatment combination which was repeated 3 times, giving a total of 48 runs to observe the effect of each factor level on the process outputs of trimming time and resistance deviation.

Table 7.1: Factor parameters and their corresponding levels for the experiment.

| Factor | Level 1 | Level 2 | Level 3 | Level 4 |
|---------------------------------|----------------|----------------|----------------|----------------|
| Cutting speed, V_c (m/min) | 250 | 1000 | 1750 | 2500 |
| Feed rate, f (mm/min) | 1 | 5 | 10 | 15 |

7.2 Results and Discussion

The experimental results were analysed using the ANOVA technique where it was used to interpret experimental data and make necessary decisions. ANOVA is a statistically based, objective decision making tool for detecting differences in the average performance of a group of factors studied [141]. As its name suggests, the procedure involves partitioning the total variability of a response into its individual components. In essence, the technique compares the variability in the mean of an individual factor with the inherent experimental error. A confirmation experiment, especially when a fractional factorial design has been applied, is used in order to validate the conclusions drawn from the analysis [149].

The experimental data presented in Table 7.2 was analysed using Minitab 17 statistical software package to evaluate the average effect of each factor level on the trimming time and the resistance deviation of the shunts. The Percentage Contribution Ratio (PCR) from ANOVA is also calculated. The statistical tools are important indicators in order to show which parameters have the most significant effect on the product quality or process performance. Therefore, the obtained data were subjected to an ANOVA test which is an important method used for interpreting experimental data and making essential decisions. This analysis was carried out for a significance level of $\alpha = 0.05$, i.e. for a confidence level of 95% following statement by Zar [150], that confidence intervals are typically stated at the 95% confidence level with applied practice.

The PCR in a variance analysis reflects the total variance attributed to all factors in an experiment [141]. *PCR* for each variable is calculated using Equation (7.1):

$$PCR = Exp\ SS / Total\ SS \quad (7.1)$$

where; *Exp SS* is the expected sum of squares for each of the factors and *Total SS* is the sum of squares. *Exp SS* is calculated using Equation (7.2):

$$Exp\ SS = SS - Error\ MS \quad (7.2)$$

and the model error of the experiment can be calculated by Equation (7.3):

$$Model\ error = 100\% - (Total\ PCR\ for\ all\ factors) \quad (7.3)$$

Table 7.2: Experimental results for trimming time and resistance deviation.

| Test no. | Factors | | Performance measures | |
|----------|---------------|---------------|----------------------|-----------------------------|
| | Vc (m/min) | F (mm/min) | Time (s) | Resistance Deviation (%) |
| 1 | 15 | 2500 | 5.75 | 1.0085 |
| 2 | 1 | 250 | 35.25 | 0.42 |
| 3 | 15 | 250 | 3.75 | 1.0583 |
| 4 | 1 | 1000 | 27.5 | 0.1009 |
| 5 | 10 | 250 | 5.25 | 0.4404 |
| 6 | 1 | 1750 | 24.25 | 0.0267 |
| 7 | 5 | 250 | 16.75 | 0.2218 |
| 8 | 1 | 2500 | 28.25 | 0.0333 |
| 9 | 10 | 2500 | 4.75 | 0.1044 |
| 10 | 5 | 1000 | 12.5 | 0.3 |
| 11 | 5 | 1750 | 9.25 | 0.0005 |
| 12 | 15 | 1000 | 3.75 | 0.5176 |
| 13 | 10 | 1750 | 4.5 | 0.0314 |
| 14 | 10 | 1000 | 6.75 | 0.2015 |
| 15 | 5 | 2500 | 9.25 | 0.1632 |
| 16 | 15 | 1750 | 2.75 | 0.2125 |
| 17 | 15 | 1000 | 2.5 | 0.2364 |
| 18 | 15 | 250 | 4.5 | 0.4526 |
| 19 | 5 | 2500 | 15.25 | 0.2364 |
| 20 | 15 | 1750 | 3.75 | 0.156 |
| 21 | 5 | 250 | 11.5 | 0.2236 |
| 22 | 1 | 2500 | 21.5 | 0.0929 |
| 23 | 5 | 1000 | 15.25 | 0.0964 |
| 24 | 10 | 250 | 7.75 | 0.2004 |
| 25 | 15 | 2500 | 4.75 | 0.8628 |
| 26 | 10 | 1750 | 5.5 | 0.0147 |
| 27 | 5 | 1750 | 12.25 | 0.0754 |
| 28 | 1 | 250 | 31 | 0.0834 |
| 29 | 1 | 1000 | 28.25 | 0.1032 |
| 30 | 1 | 1750 | 28.25 | 0.0329 |
| 31 | 10 | 1000 | 7.5 | 0.4404 |
| 32 | 10 | 2500 | 7 | 0.5357 |
| 33 | 10 | 1750 | 5.75 | 0.1561 |
| 34 | 5 | 1000 | 13.25 | 0.1165 |
| 35 | 1 | 250 | 35 | 0.0314 |
| 36 | 5 | 2500 | 9.25 | 0.0528 |
| 37 | 10 | 2500 | 8.75 | 0.1386 |
| 38 | 15 | 1750 | 5.5 | 0.101 |
| 39 | 10 | 250 | 10.25 | 0.5885 |
| 40 | 15 | 250 | 7.25 | 1.0856 |
| 41 | 15 | 1000 | 4.5 | 0.7284 |
| 42 | 5 | 250 | 17 | 0.5013 |
| 43 | 10 | 1000 | 8.25 | 0.1632 |
| 44 | 1 | 1750 | 23.5 | 0.0424 |
| 45 | 1 | 2500 | 22.25 | 0.099 |
| 46 | 5 | 1750 | 13.75 | 0.2015 |
| 47 | 15 | 2500 | 3.75 | 0.8912 |
| 48 | 1 | 1000 | 28.25 | 0.1032 |

7.2.1 Trimming Time

The percentage contributions for errors and factors associated with trimming time are given in Table 7.3. Feed rate and cutting speed were both found to be statistically significant factors at the 5% level [151], having P values of 0 and 0.01 respectively. Feed rate had a high PCR value of 91.44% compared to that of cutting speed which was 2.64%. The relatively small error level of 5.92% associated with the trimming time was deemed to be within acceptable levels (up to 15%), suggesting that all important factors had been considered and measurements accurately performed [149].

Table 7.3: ANOVA results for Trimming Time (s).

| | DF | SS | MS | Exp SS | F | P | PCR |
|------------------------------------------------------------------------|-----------|-------------|-------------------------------------------------------------------------|-------------------|------------|------------|-------------|
| Feed Rate | 3 | 4075. 08 | 1358. 36 | 4068 .95 | 221. 66 | 0* | 91.44 |
| Cutting Speed | 3 | 123.5 8 | 41.19 | 117. 45 | 6.72 | 0.00 1* | 2.64 |
| Error | 41 | 251.2 5 | 6.13 | - | - | - | 5.92 |
| Total | 47 | 4449. 92 | * Significant at the 5% level | | | | |
| DF = Degrees of freedom SS = Sum of squares MS = Mean of squares | | | F = F-test value P = Probability PCR = Percent contribution ratio | | | | |

Figure 7.1 shows the main effects plot for the trimming time of the shunt resistors. The time ranged between 2 and 35 seconds, with both factors having a significant effect. The statistical analysis in Table 7.3 shows that the main contributing factor to the trimming time is feed rate and this is supported by the sharpness in the gradient of the slope in Figure 7.1. The trimming time reduces from 27.5 to 3.75 seconds with increase in feed rate from 1 to 15 mm/min and from 15 to 11 seconds with increase in cutting speed from 250 to 1750 m/min. Feed rate is found to be much more significant compared to cutting speed with an 88.88% difference in PCR.

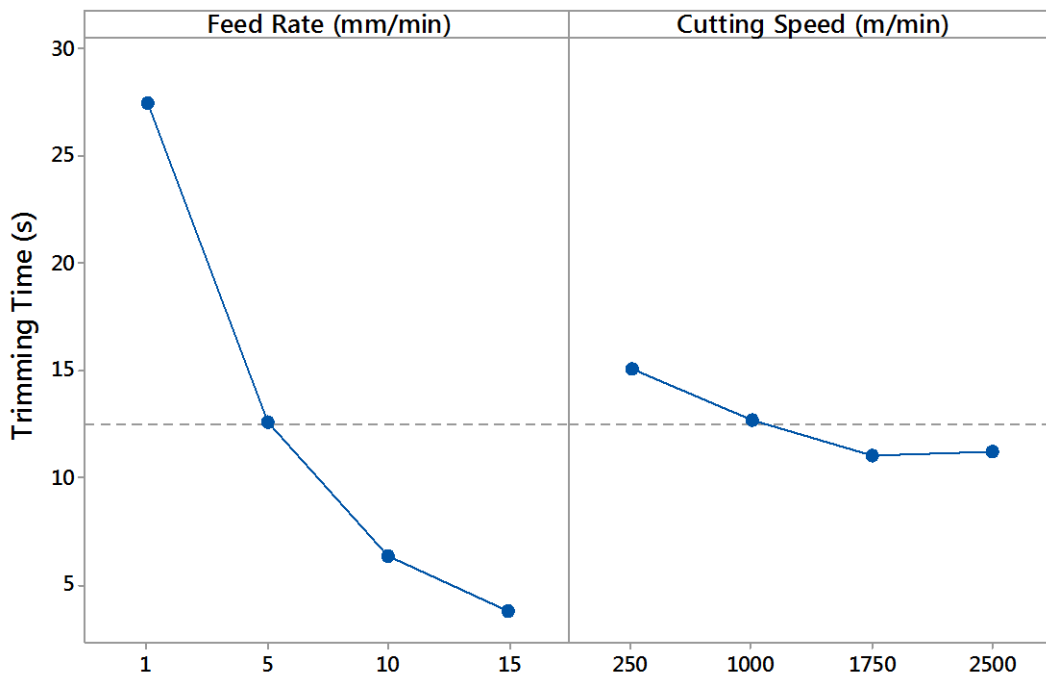


Figure 7.1: Main effects plot for Trimming Time (s).

7.2.2 Resistance Deviation

Table 7.4 shows the ANOVA results for the resistance deviation of the shunts following trimming. P values for both feed rate and cutting speed are 0. Although both factors were found to be statistically significant at the 5% level, the feed rate had the highest PCR of 43.5% followed by cutting speed with 19.23%. The error associated with the resistance deviation (37.27%) was significantly higher than the accepted level of 15% which could be ascribed to possible unconsidered interactions between some of the control factors and the possibility that not all important factors had been considered [152].

Table 7.4: ANOVA results for resistance deviation (%).

| | DF | SS | MS | Exp SS | F | P | PCR |
|------------------------------------------------------------------------|-----------|-------------|-------------------------------------------------------------------------|-------------------|-----------|----------|--------------|
| Feed Rate | 3 | 1.823 62 | 0.60 787 | 1.78 8 | 17.0 6 | 0* | 43.5 |
| Cutting Speed | 3 | 0.825 79 | 0.27 526 | 0.79 017 | 7.73 | 0* | 19.23 |
| Error | 41 | 1.460 48 | 0.03 562 | - | - | - | 37.27 |
| Total | 47 | 4.109 89 | * Significant at the 5% level | | | | |
| DF = Degrees of freedom SS = Sum of squares MS = Mean of squares | | | F = F-test value P = Probability PCR = Percent contribution ratio | | | | |

Figure 7.2 shows the main effects plot for the resistance deviation. Average resistance deviation measured when trimming the shunt resistors at 1750 m/min cutting speed was significantly lower than for other cutting speeds. Lower resistance deviation was obtained when trimming using lower feed rates and medium cutting speeds. Clearly, feed rate was found to have substantial influence on the resistance deviation of the shunts, increasing from 0.09 to 0.64 % with increase in feed rate from 1 to 15 mm/min. Resistance deviation however reduces from 0.48 to 0.08 % with increase in cutting speed from 250 to 1750 m/min and then increase to 0.35 % with increase in cutting speed to 2500 m/min.

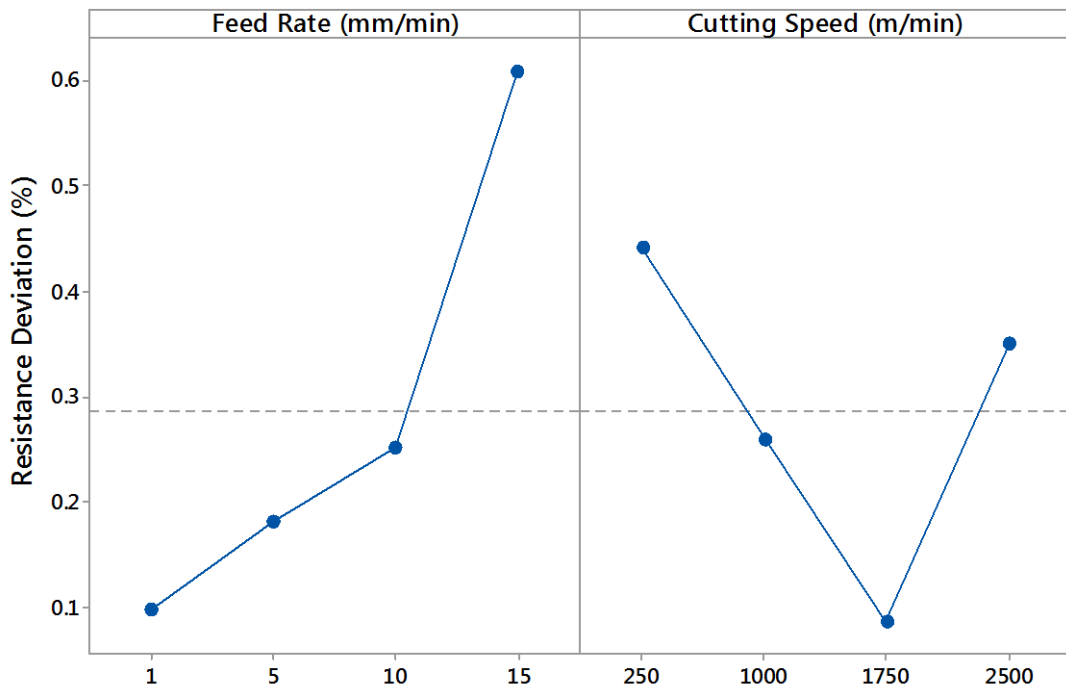


Figure 7.2: Main effects plot for Resistance Deviation (%).

7.2.3 Interaction Plot

Figure 7.3 shows the interaction between the cutting speed and feed rate for resistance deviation. The shunts have a lower resistance deviation when trimmed using 5 mm/min feed rate as opposed to 10 mm/min at 250 and 1000 m/min cutting speeds. However, when the cutting speed is at 1750 m/min, the shunt has a lower resistance deviation when trimmed using 10 mm/min feed rate. Similarly, lower resistance deviation is observed when the shunts were trimmed at 2500 m/min as opposed to 250 m/min cutting speed at 1, 5 and 10 mm/min feed rates. Conversely, when the feed rate is 15 mm/min, the shunts have the highest resistance deviation when trimmed at 2500 m/min cutting speed.

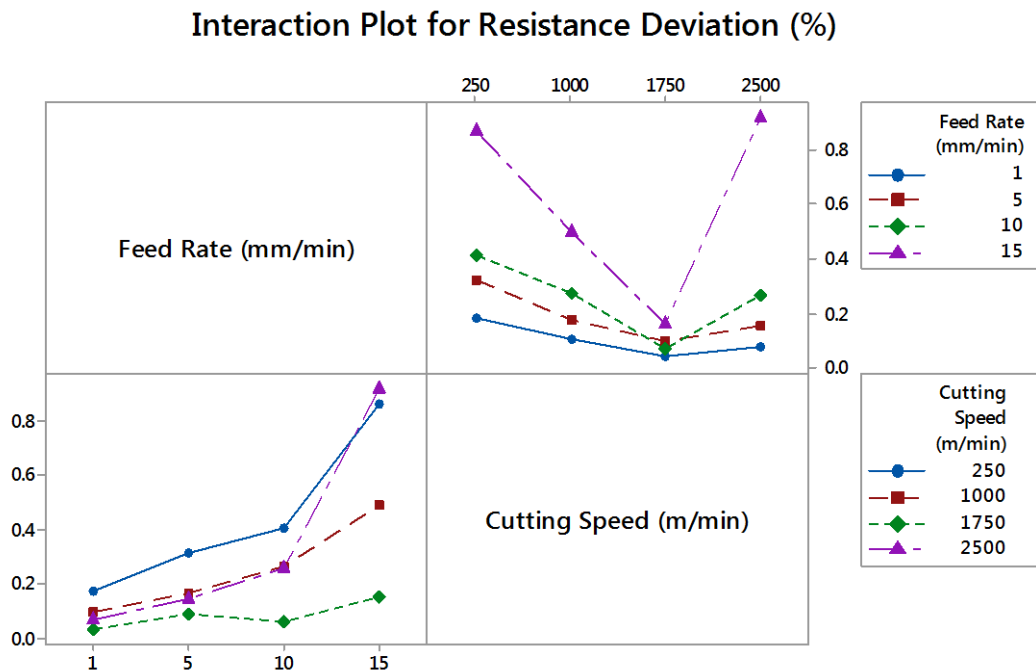


Figure 7.3: Interaction Plot for Resistance Deviation (%).

The interaction between cutting speed and feed rate for trimming time is shown in Figure 7.4. A cutting speed of 2500 m/min trimmed faster than 1750, 1000 and 250 m/min when used at 1 and 5 mm/min feed rates. However, the trimming time for 2500 m/min cutting speed becomes slower when increased to 10 and 15 mm/min feed rates compared to results achieved at 1000 and 1750 m/min cutting speeds. The interaction plot of trimming time versus feed rate shows that the fastest trimming time of 3 seconds is achieved at 1750 mm/min cutting speed and 15mm/min feed rate.

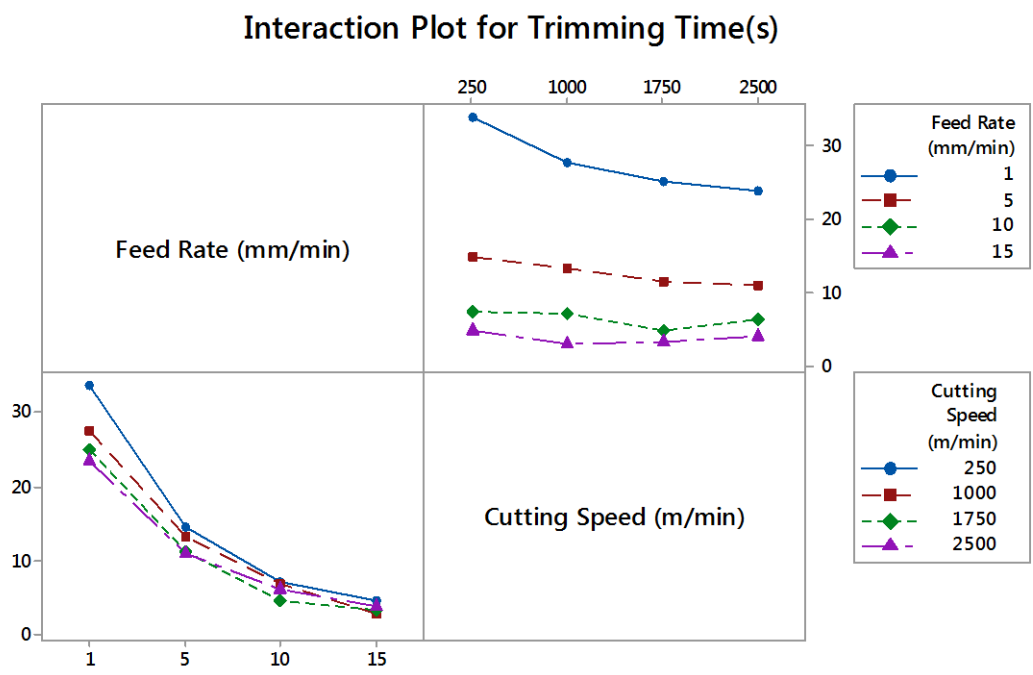


Figure 7.4: Interaction Plot for Trimming Time (s).

Essentially, the analysis suggests that the initial optimal settings for a faster trim time are obtained when employing a 15 mm/min feed rate at 1750 m/min cutting speed. It can also be seen from the results that a lower resistance deviation can be achieved by trimming at a feed rate of 1 mm/min and a cutting speed of 1750 m/min. In order to be able to further reduce the tolerance of the shunt resistors, a slower feed rate is probably needed.

It is also interesting to note that trimming at the highest feed rate of 15 mm/min appears to have the potential to produce shunt resistors with a resistance tolerance less than the initial target value of $\pm 1\%$. Increasing the feed rate also resulted in an increase in material removal rate and thus an increase in the rate of change of resistance.

7.2.4 Surface Roughness

Further investigation was taken to measure the average surface roughness (R_a) of the trimmed shunt resistors to confirm the optimum cutting speed of the trimming process. Surface roughness was measured using an Alicona Infinite Focus G4 optical scanner having a resolution of $0.01\mu\text{m}$. All measurements conformed to ISO 4287-1997 and ISO 4288-1996 [153, 154]. Figure 7.5 shows scans of surface roughness for different speeds of cutting. It can be seen that the average surface roughness is reduce and appears to be smoother when the cutting speed is increased from 250 to 1750 m/min but then it becomes rough when it reached 2500 m/min.

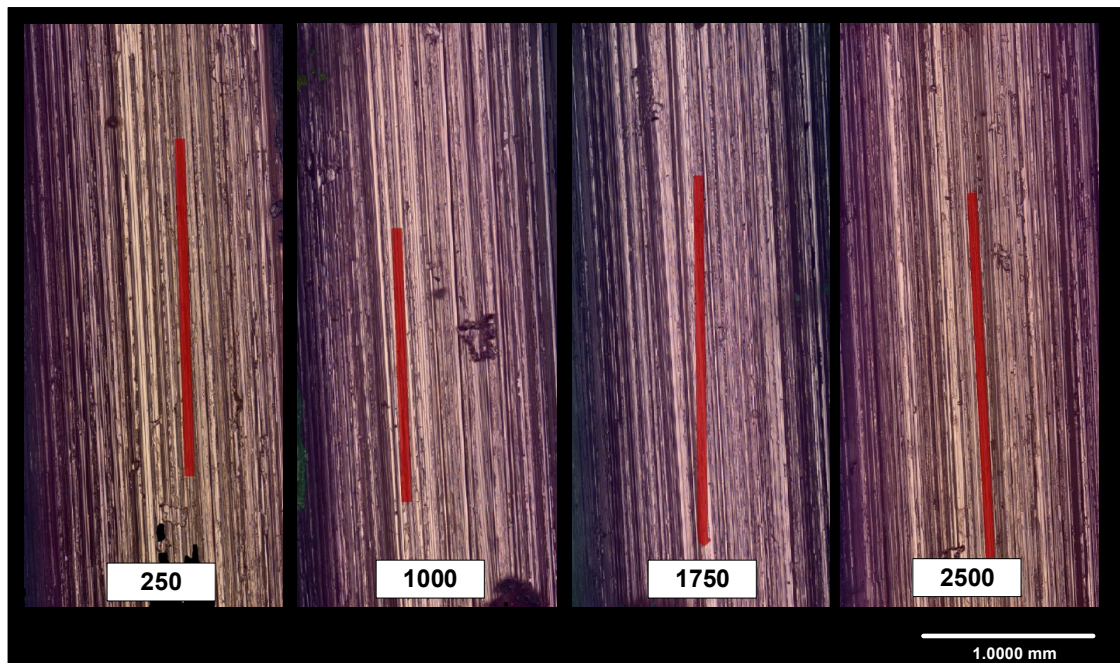


Figure 7.5: Surface images at different cutting speeds.

Figure 7.6 shows the results of Ra as a function of the cutting speed. The tests were conducted at a constant feed rate of 15 mm/min. Instead of specifying optimal levels for all the factors, setting only the feed rate to 15 mm/min was a robust alternative, which would produce reliable (less variable) and low surface roughness values even when the other factors are not controlled [155]. The results show that the surface roughness decreases with increase in cutting speed to 1750 m/min but then increases at 2500 m/min.

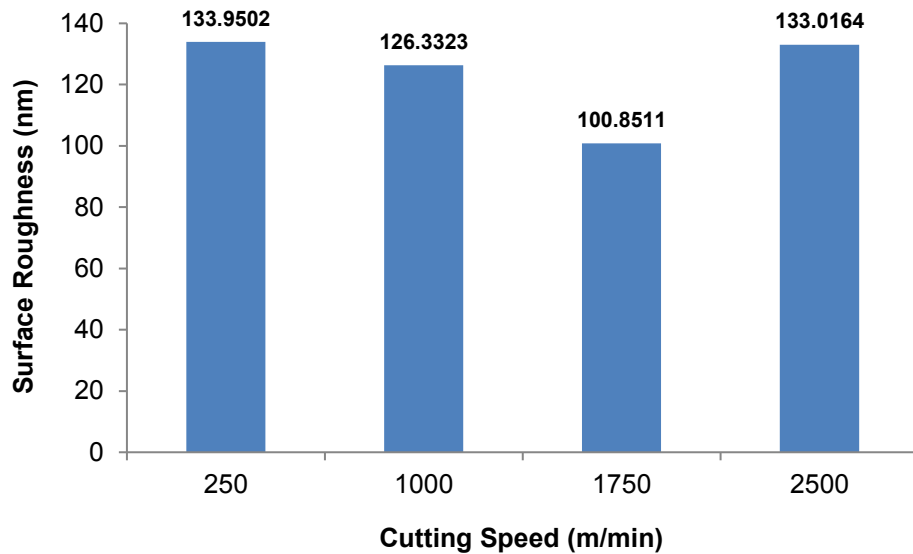


Figure 7.6: Surface roughness (Ra) versus cutting speed.

Previous studies on various metallic based alloys found that surface roughness increases with increased feed rate while it decreases with increased cutting speed and depth of cut [156-158]. While these previous findings cannot be mapped directly to this study, it shows the general trend in both studies are similar where increasing cutting speed reduces Ra . Optimum cutting speed is therefore found to be 1750 m/min and the dynamic balance of the cutting saw appears to become an issue at the higher speed of 2500 m/min. At these higher speeds, minor defects such as a notch shank in the cutting disc have been shown to move cutting tools enough off-centre to induce vibration and hence chatter leading to a deterioration in the surface roughness of the work piece [159].

7.3 Optimisation Process

The trimming time and resistance deviation showed a strong dependency on the feed rate of the cutting disc. The optimum feed rate and cutting speed to reduce the resistance tolerance of the shunt were found to be 1 mm/min and 1750 m/min respectively. Trimming at a low feed rate of 1 mm/min can reduce the tolerance to very low values of around ± 0.1 % but this operation takes around 25 seconds to perform. On the other hand, trimming at a higher feed rate of 15 mm/min can give a faster trimming process time of under 3 seconds whilst maintaining an acceptable tolerance of ± 1 %. Even though cutting speed was found to have a less significant effect on the trimming time, using the optimum cutting speed of 1750 m/min can give a significant reduction in resistance tolerance and improvement in surface roughness of the trimmed shunt when compared to slower and faster speeds.

Phase 2 of the DoE was conducted using a smaller range of cutting speed between 1500 to 2100 m/min in order to further optimise the process. The DoE was performed at different cutting speeds of 1500, 1650, 1800, 1950 and 2100 m/min to find the optimum level. The constant feed rate of 15 mm/min was used and the experiment was repeated 5 times for each cutting speed.

Table 7.5: ANOVA results for resistance deviation (%).

| | DF | SS | MS | F | P |
|------------------------------------------------------------------------|-----------|-----------|--------------------------------------|----------|----------|
| Cutting Speed | 4 | 1.449 | 0.3623 | 2.86 | 0.029* |
| Error | 70 | 8.857 | 0.1265 | - | - |
| Total | 74 | 10.306 | * Significant at the 5% level | | |
| DF = Degrees of freedom SS = Sum of squares MS = Mean of squares | | | F = F-test value P = Probability | | |

A one-way ANOVA was used to analyse the experimental results. Results in Table 7.5 show a significance level of 0.05 which indicates a 5% risk of final difference when the null hypothesis states that the mean resistance deviation percentage of 5 different cutting speeds are equal. The p-value is 0.029, which is less than the significance level of 0.05, thus the null hypothesis is rejected and this concluded that some of the cutting speed variables have different means. From the interval plot in Figure 7.7, 1800 m/min cutting speed has the lowest mean of 0.6% and 1500 m/min cutting speed has the highest of 1% with each interval is within 95% confidence interval.

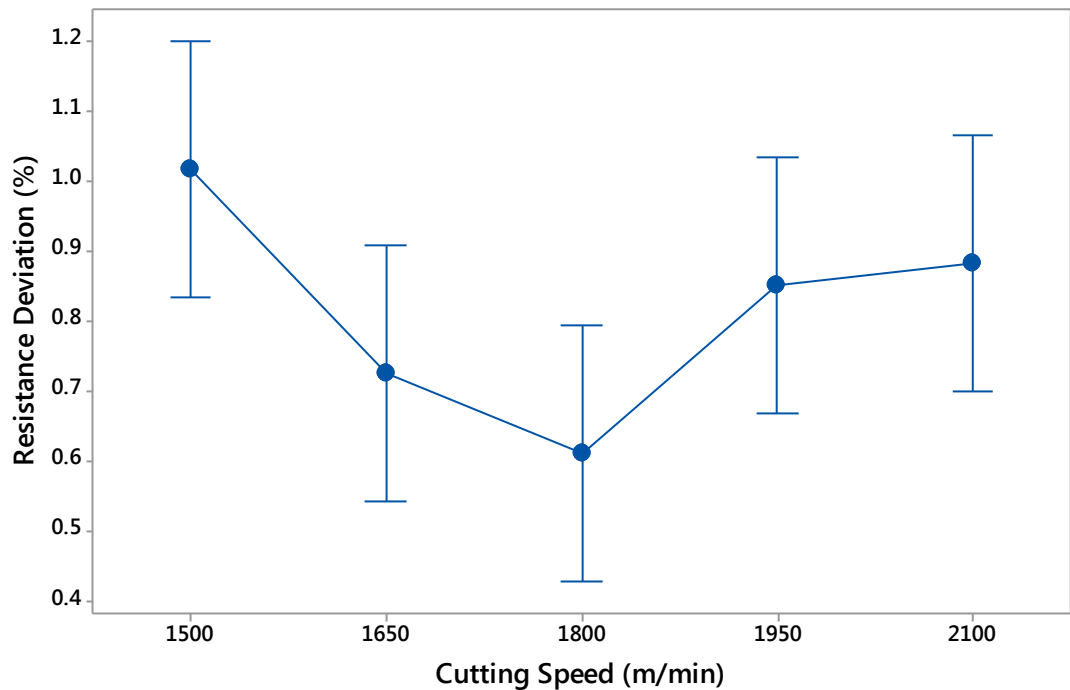


Figure 7.7: Interval plot of resistance deviation vs cutting speeds, error bars for 5 samples at each speed.

The results are supported by the findings in Figure 7.8 which shows the approximate values of the optimum cutting speed using different types of cutting tools. The cutting saw used in the experiment is made from silicon carbide which belongs to the ceramic tools group. A line is drawn on the plot of Figure 7.8 to find the optimum cutting speed for the experiments. Since the hardness of Manganin is known to be 110 HV or 105 Brinnel hardness number and the tensile strength of Manganin is 390 MPa; it can be seen that the cutting speed of 1800 m/min (30 m/s) achieved from the experiments is around the optimum recommended value suggested in Figure 7.8 to prolong the tool life.

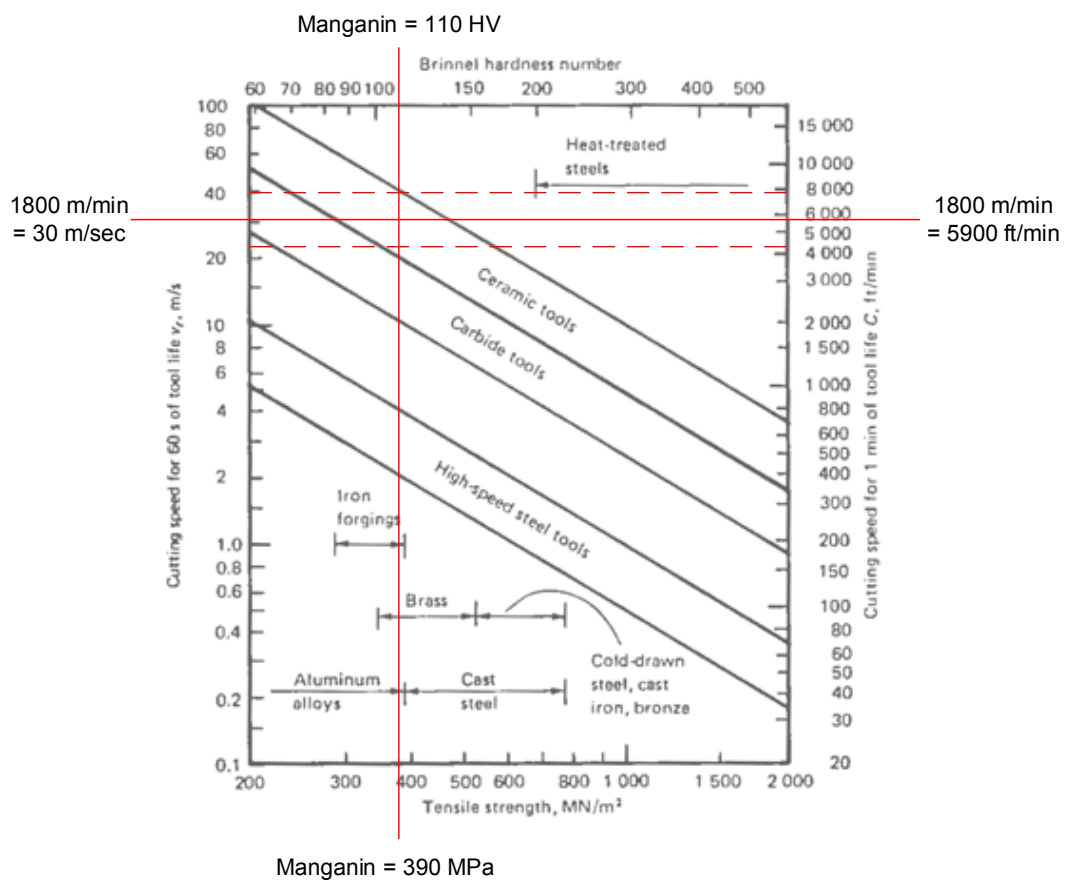


Figure 7.8: Approximate values of the cutting speed. [160]

7.4 Summary

To summarise this chapter, the feed rate and cutting speed for the experiment were selected in conjunction with the trimming time and resistance deviation. These decisions were made by considering the best possible way to balance the need for a reduction in resistance deviation and time taken to trim the shunt resistors. The selected cutting speed is 1800 m/min and feed rate is 15 mm/min.

There is no argument for the selected value of cutting speed as it was proven to be the best way to be implementing in the trimming process as it complies with the two responses of trimming time and resistance deviation. The decision also was supported by the test of surface roughness where the material machined at the specified cutting speed shows a smoother surface roughness compared to the others. This means that the work piece will have a higher quality in surface finishing where minimum defect effects occur.

On the other hand, the feed rate response on the resistance deviation shows that a value of 1 mm/min will give a lower resistance deviation than 15 mm/min. However, this does not mean that the 15 mm/min of feed rate is ruled out from being selected for the trimming process. The fastest feed rate still produces shunts with resistance values in the range of the ± 1 % tolerance and it does this in the least amount of time. This result still fulfils the research objective, hence the 15 mm/min feed rate has been chosen as the optimum parameter to meet the main objective of this research. This machining practice is suitable for a large scale production, where the production time can be reduced with lower tolerance of 1% rather than the existing 5% tolerance.

Chapter 8

Reliability Tests

In the preceding chapters, it has been established that the proposed automated trimming process can reduce the tolerance of shunt resistors to $<\pm 1\%$ but further investigations need to be done in order to confirm that the process conducted on the shunt does not have any effect reflect on the performance of the shunt within the smart energy meter. This chapter will investigate the detrimental effect of trimming conducted on the $100\mu\Omega$ Manganin shunt resistors on their key electrical and structural properties.

8.1 Characterization

Following trimming using the optimum cutting speed and feed rate of 1800m/min and 15mm/min determined in Chapter 7, the resistance accuracy and distribution of the samples were determined before the shunts were subjected to a series of tests in order to establish if the trimming process caused any significant changes to the structural and electrical properties of the components when compared to the untrimmed standard components.

8.1.1 Structural Analysis

The morphology and composition of the Manganin shunt samples were investigated using a FEI Quanta 200 secondary electron microscope at an accelerated voltage of 20 kV. Chemical composition was acquired using an Oxford Instruments INCA X-ray detector at 8000x magnification for 60 seconds. Energy dispersive spectroscopy (EDS) analysis measurements were made using a lithium-drifted silicon detector attached to the scanning electron microscope (SEM).

This SEM instrument is able to provide images of a sample (micrographs) by scanning its surface with a beam of electrons in a raster pattern [161]. The resolution can reach into a few nm and it also can operate in a range of magnification from $\times 10$ to $\times 300K$, hence providing important morphological and topographical information of the scanned surface.

The SEM is combined with appropriate detectors in order to give it the ability to provide information about the elemental composition on the surface of the sample. The principle behind this characterisation is based on the interactions of the electrons with the surface of the sample and the consequent emission of X-rays according to the atomic structure of the specimen. Two different techniques are used to analyse the X-ray emission. The first technique is called Energy Dispersive Spectroscopy (EDS) based on the simultaneous count of the emitted photons at different energies. The other technique is called Wavelength Dispersive Spectroscopy (WDS) and it is based on counting the emitted photons only at a specific wavelength.

Usually EDS is the quicker technique which is able to provide the data in a single scan that will show the quantitative information on the presence of all the elements. On the other hand, WDS is a slower technique that can only provide information about one single element at a time. The only advantage of WDS over EDS is that it possesses a much higher resolution. This advantage will allow it to overcome the typical peak overlapping problem that occurs in EDS because of its lower resolution. The great advantage of a combined

SEM/EDS-WDS system is the capability of performing an elemental analysis for relevant features identified directly by using the microscope [161, 162].

8.1.2 Temperature Coefficient of Resistance (TCR)

Temperature Coefficient of Resistance (TCR) measurement was conducted in order to simulate the temperature the shunt resistors may be subjected to whilst in a smart energy meter. The temperature coefficient of resistance is expressed in parts per million per degree Celsius (ppm). The tests were performed in accordance with MIL STD 202 Method 304 [163] using a Grant oil bath where each shunt was submerged in oil while its resistance values was continuously monitored using the 4-wire Kelvin method described earlier. The temperature of the oil bath was then increased from -10 to +110°C in 10°C increments and allowed to stabilize for 10 minutes at each measurement point before the resistance value of the shunt was recorded. Equation (8.1) was then used to express the rate of change in resistance value per 1°C (TCR) in a prescribed temperature range:

$$TCR = \frac{\Delta R}{R \times \Delta T} 10^{-6} \quad (8.1)$$

Where;

| | |
|------------|------------------------------------------------------------------------------------------------------------------|
| ΔT | is the algebraic difference, in degree, between the specified ambient temperature and the reference temperature; |
| ΔR | is the change in resistance between the two specified ambient temperatures; |
| R | is the resistance value at the reference temperature. |

In general, the TCR in semi-conductors decreases with increasing temperature and may be attributed to the jumping of electrons from the valence band to the conduction band. Due to the higher mobility of electrons in the conduction band, than in the valence band, the electrons are able to move easily, thereby decreasing the TCR. In contrary, the TCR increases in metals and alloys with increasing temperature due to increased vibrations of atoms that hamper the beeline movement of the electrons [164].

8.1.3 High Current

Next, the shunt resistors were connected to a high current supply to determine if trimming the Manganin resistive element has any effect on the temperature rise and potential power rating of the shunt when used in the smart energy meters. Prior to testing, a Type K thermocouple was welded to the rear face of the Manganin element of each shunt to measure its temperature rise. The shunts were then powered up by a Glassman LPC 6-220 model power supply to 4W (200A) and allowed to stabilize until the temperature of the Manganin element reached steady state, see Figure 8.1. Thermal images were then taken using a FLIR T620bx camera. Due to the highly reflective properties of the shunt resistors materials, the samples were all painted with Pyromark 1200 high temperature black coating ($\epsilon=0.97$) prior to thermal imaging.

The datasheet of the Manganin shunt resistor stated that the maximum current that can flow through the resistor is 300A. However, through observations made during the test, 200A is more realistic amount of current that can be governed safely in the wiring used. For the best and optimal performance, the wire that was used as the load lines was chosen based on the gauge size and the total length of the wire in the circuit. The reason behind this is because according to [85], the resistance will decrease with increase in diameter and larger wire will be able to carry more current.

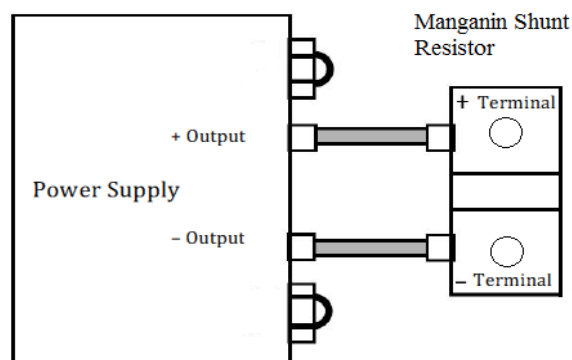


Figure 8.1: Connection of a Manganin shunt resistor to LPC 6-220 models power supply.

8.1.4 High Temperature Stability Test

Resistance stability or reliability is basically a measure of the change in resistance of the film against a certain specification over a period of time. There are a number of conditions under which the reliability of the component can be tested such as direct circuit load, dry heat or humidity.

In this research, a high temperature resistance stability test was conducted in accordance with BS EN 60115-1 standard [165]. The initial resistance value of the shunts was measured before they were stored in an oven in air ambient for 168 hours at an elevated test temperature of 200°C. During testing, the resistance value of the shunts was measured at time intervals of 24, 48, 72 and 168 hours and then compared with the initial resistance to monitor the change in resistance.

Heat treatment of a metal often reduces the number of grain boundaries as the atoms will align more regularly within the crystalline structure. As the purpose of this experiment is to heat the metal shunts to the highest working temperature for a period of 7 days it is predicted that there will be a decrease in the number of grain boundaries. A decline in the number of grain boundaries and therefore a more orderly array of atoms will provide an easier route for the electrons to pass through and therefore it is expected that the resistance of the shunts will decrease [166].

8.1.5 Hardness

Vickers indentation is favoured in hardness test as it does not require any complex machining preparation and does not completely destroyed the sample, allowing it to be used in the future. Therefore, this simplicity in this test makes it popular as a method to quantify toughness [167]. This method typically uses a diamond indenter which is applied to the surface of the work piece. The impression left by the diamond tip is used for the quantification of hardness.

Hardness tests were performed in accordance with ASTM E384 using a Vickers micro-hardness tester model HV-1000A to study fine scale changes in the hardness of the Manganin resistive alloy in 8 different areas surrounding the trim cut. A diamond indenter was applied to the surface of the specimens at a load of 500 gf for 10 seconds. Upon removal of the load, the lengths of the two impression diagonals were measured using an Alicona Infinite Focus G4 optical scanner to $\pm 0.1 \mu\text{m}$, and then averaged. The Vickers hardness value (HV) was then calculated using Equation (8.2) where the load L is in grams-force and the average diagonal d is in μm .

$$HV = \frac{1854.4L}{d^2} \quad (8.2)$$

8.2 Results and Discussion

Top and side views of a typical square cut trim geometry in the Manganin shunt resistor element are shown in Figure 8.2(a) and (b), respectively. The cut depth for all samples was in the range of 0.5 to 1.2 mm depending on the initial resistance value of the part and equates to around 5 to 10% of the initial Manganin element width of 15 mm. The edges of the trimmed grooves were found to be relatively free from burrs and the surface of the grooves was very smooth having roughness average (Ra) values of 100.8511 to 133.9502 nm. Reducing the surface burrs will reduce the chance of current crowding.

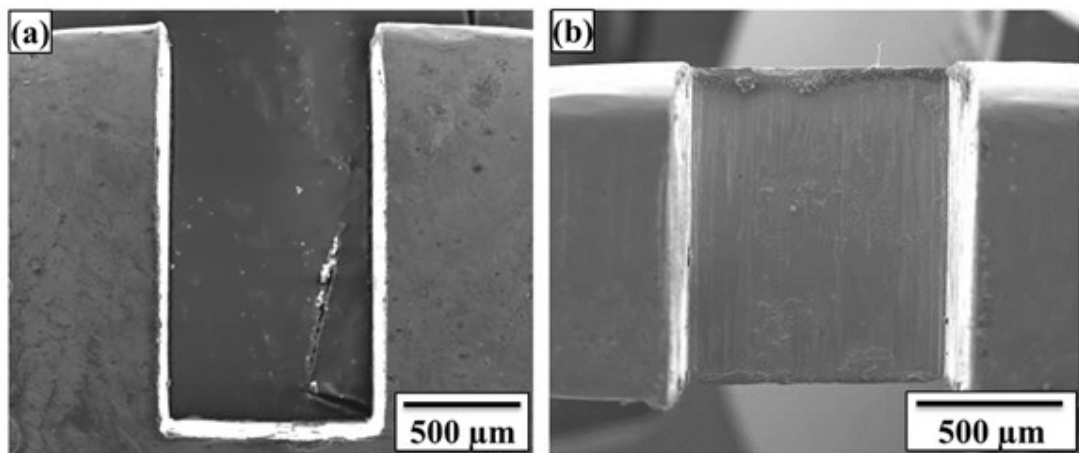


Figure 8.2: (a) Top and (b) side views of a shunt resistor trimmed with a square cut.

Figure 8.3 shows the measured resistance value of the 20 samples before (untrimmed) and after trimming with a square cut to a target resistance value of 100 $\mu\Omega$. It can be clearly seen that the resistance distribution of the sample of shunts after trimming is much smaller than that in the untrimmed condition with values of 95.28 to 98.82 $\mu\Omega$ and 99.96 to 100.56 $\mu\Omega$ respectively. The resistance values of the trimmed parts are all also well within $\pm 1\%$ of the target resistance value of 100 $\mu\Omega$, thus highlighting the systems capability to accurately trim the shunt resistors.

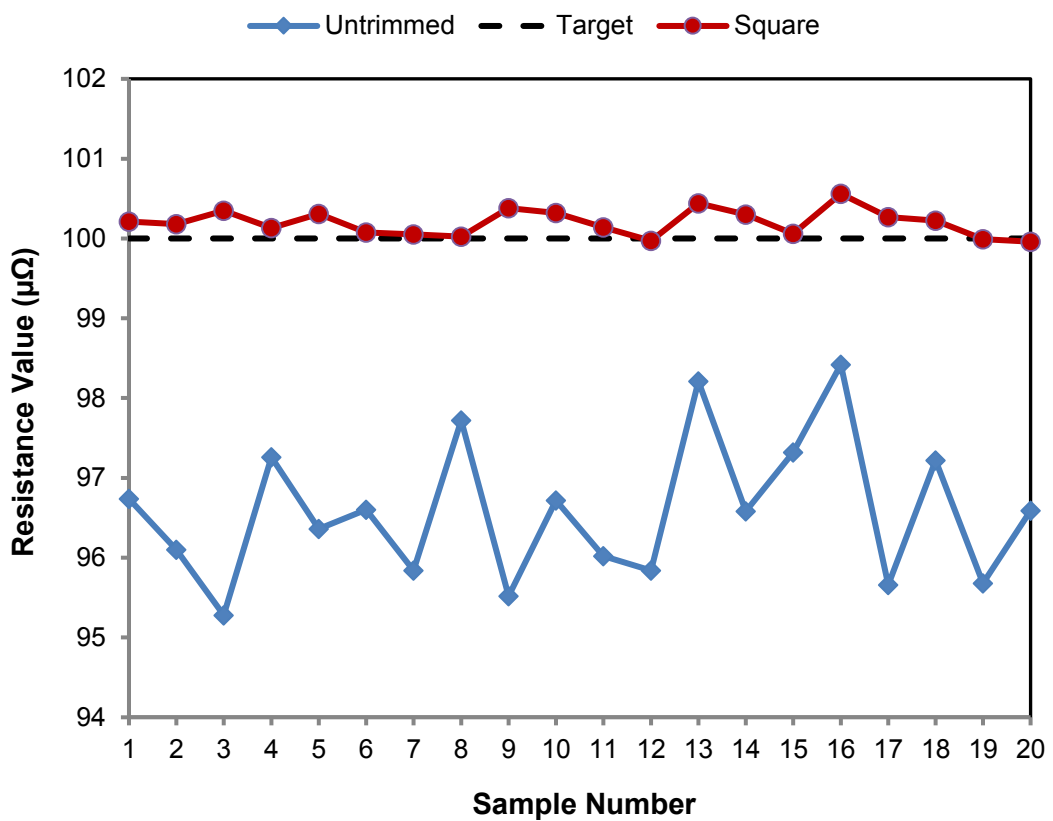


Figure 8.3: Resistance values of the shunt resistors before (untrimmed) and after trimming with the square cut.

8.2.1 Temperature Coefficient of Resistance (TCR)

The graph of resistance against temperature in Figure 8.4 shows a positive correlation for both untrimmed and square cut trimmed shunt resistors in the temperature range of -10°C to $+110^{\circ}\text{C}$. This positive TCR, or decrease in conductivity with increase in temperature, is typical in metals and alloys and can be related to an increase in energy with temperature which causes the ions to vibrate more frequently and subsequently impede the conduction of electrons [168, 169].

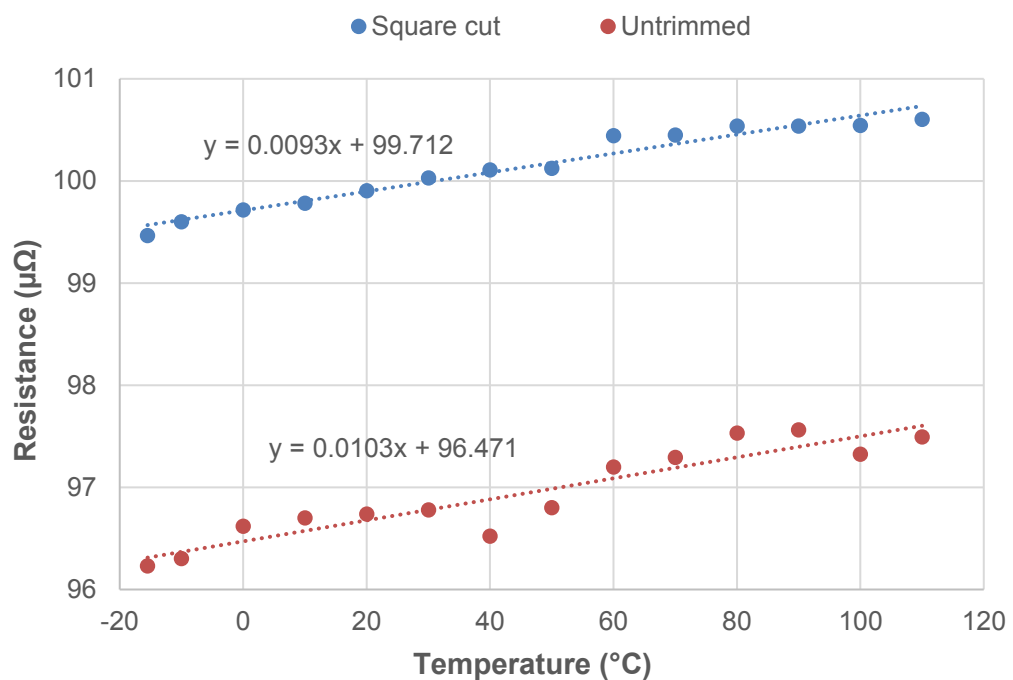


Figure 8.4: Resistance versus temperature for untrimmed and square cut shunt resistor samples.

A similar case was observed in the current study where TCR increased with increasing temperature. It can be further observed that the change in TCR is relatively small in broad temperature range of -10°C to $+110^{\circ}\text{C}$ which is a propitious property to make resistors. The higher TCR value after trimming process does not only make the trimmed sample a potential candidate to construct a resistor, but also the low variation in TCR over a broad temperature range (-10°C to $+110^{\circ}\text{C}$) provides it stability.

However, it can be further observed that the magnitude of this positive TCR is relatively small across this broad temperature range of $-10\text{ }^{\circ}\text{C}$ to $+110\text{ }^{\circ}\text{C}$ which is a propitious property to make precision shunt resistors. The calculated TCR values are consistent across the full temperature range for both the untrimmed and square cut trimmed parts, having values of $+106.48\text{ ppm}/^{\circ}\text{C}$ and $+93.05\text{ ppm}/^{\circ}\text{C}$ respectively. These TCR values are higher than those previously reported for pure Manganin of $15\text{ ppm}/^{\circ}\text{C}$ [170, 171] and this increase can be related to the series resistance and highly positive TCR ($+3930\text{ ppm}/^{\circ}\text{C}$) contribution of the two small areas of copper termination on either side of the Manganin resistive element [172]. However, the difference in TCR between the untrimmed and trimmed parts, which is the main purpose of this test, is relatively small at around $13.4\text{ ppm}/^{\circ}\text{C}$ across the full test temperature range of $-10\text{ }^{\circ}\text{C}$ to $+110\text{ }^{\circ}\text{C}$, thus suggesting that trimming has a negligible effect on this key property of the shunts.

8.2.2 Thermal Modelling

Typical plots of temperature rise for untrimmed and square cut trimmed shunt resistors, powered up to 4 W ($\sim 200\text{ A}$), are shown in Figure 8.5 and Figure 8.6 respectively. The results for both types of shunt follow a very similar trend; starting at room temperature ($\sim 23\text{ }^{\circ}\text{C}$), the temperature of both the untrimmed and trimmed resistor elements increase rapidly in the first 150 seconds to values around $181\text{ }^{\circ}\text{C}$ and $190\text{ }^{\circ}\text{C}$ respectively. After which the increases are more gradual before reaching maximum temperatures of $197\text{ }^{\circ}\text{C}$ and $207\text{ }^{\circ}\text{C}$ respectively at around 500 seconds. The temperature of the two shunts then decreases slightly to around $192\text{ }^{\circ}\text{C}$ for the untrimmed and $198\text{ }^{\circ}\text{C}$ for the trimmed parts and fluctuates around this point until the power supply is switched off at a time of 1200 seconds. After which the temperature of both shunts gradually cools back down to room temperature at around 1500 seconds (not shown on plots).

Plots of resistance versus time for the untrimmed and trimmed shunts, powered up to 4 W , are also shown in Figure 8.5 and Figure 8.6 and follow a very similar trend to those described for the temperature rise test. The

resistance value of the untrimmed part starts at $101\mu\Omega$ and rises quickly to $103\mu\Omega$ within approximately 200 seconds of the current being supplied. The resistance value of the trimmed part starts at $119\mu\Omega$ and rises in an almost identical fashion. After this point the resistance of both shunts increases more gradually before reaching maximum values of $103\mu\Omega$ for the untrimmed part and $121.5\mu\Omega$ for the trimmed part at around 500 seconds. After this point the resistance values reduce very slightly to around $102\mu\Omega$ and $120\mu\Omega$ respectively and remain there until the power is removed at a time of 1200 seconds. Finally, the resistance of the both shunts was observed to gradually returns to their original values as they cool back down to room temperature at around 1350 seconds (not shown on plots).

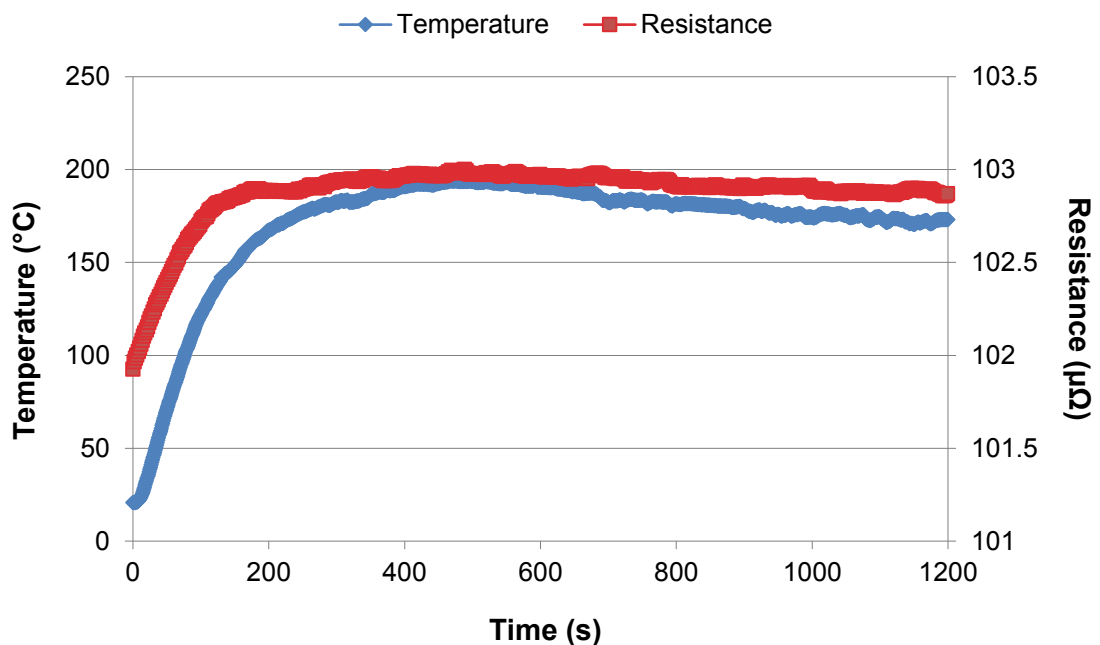


Figure 8.5: Temperature-Resistance graph for untrimmed shunt resistor.

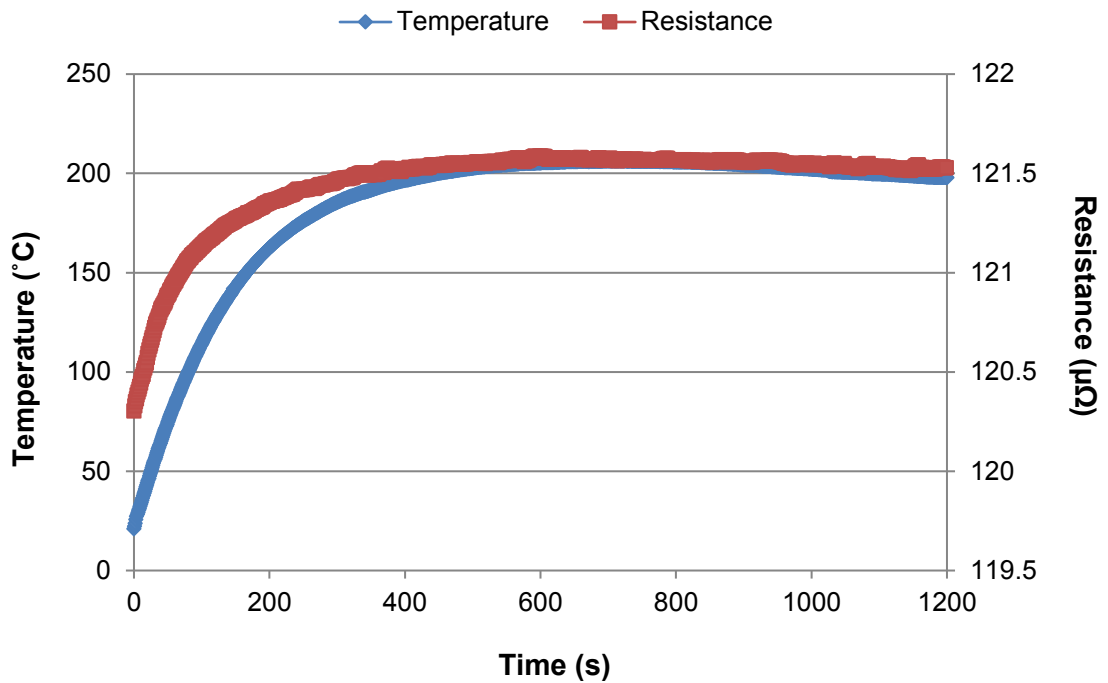


Figure 8.6: Temperature-Resistance graph for shunt resistor trimmed using square cut.

There are several important observations that can be drawn from the results of Figure 8.5. Firstly, the increase in resistance with increase in supplied current is significant for both untrimmed and trimmed parts, having a maximum value of around $1.5 \mu\Omega$ (+1.5%) for both. These increases can be quite clearly related to the inherent TCR of the Manganin material discussed in section 3.1; multiplying the measured TCR of approximately $+80 \text{ ppm}/^\circ\text{C}$ by the maximum temperature rise of 175°C gives an increase in resistance of 1.4%. Although this change can be deemed non-permanent, as the resistance of the shunts return to their original values once the power is removed, this temporary increase in resistance could in turn lead to significant errors when measuring current flow in a smart energy meter. The second observation to be made is that trimming the shunt appears to give a slight increase in the peak temperature rise of the resistor element. This is further supported by the thermal images of the untrimmed and trimmed parts in Figure 8.7, taken after 500 seconds when the shunts had reached their maximum temperature.

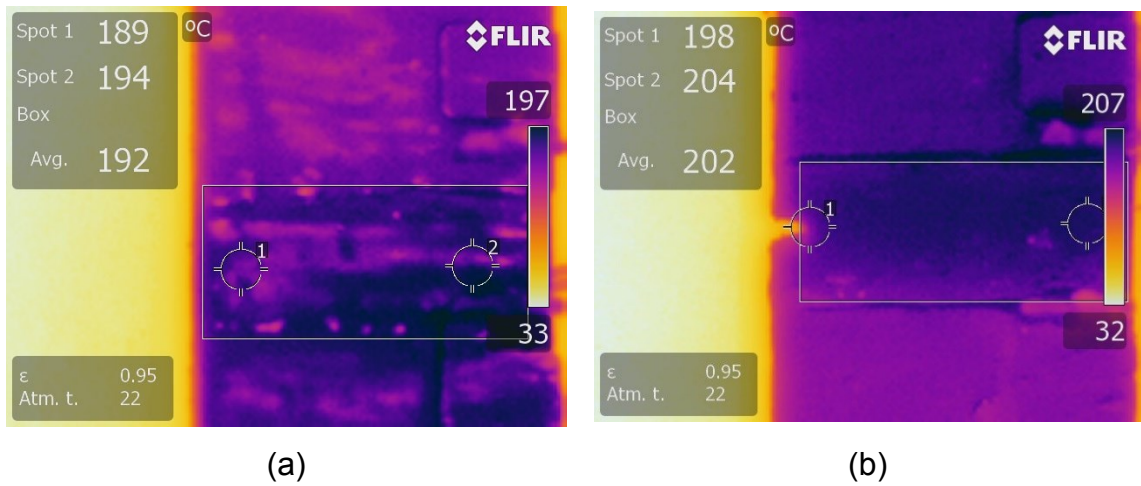


Figure 8.7: Thermal images of $100\mu\Omega$ shunt resistors (a) untrimmed and (b) trimmed with square cut.

The temperature was measured at two spots at either side of the centre of the resistor element for both the untrimmed and square cut trimmed parts. For the untrimmed part in Figure 8.7(a), at spot 1, the temperature was 189°C and at spot 2, it was 194°C . On average, the temperature was 192°C . In contrast to the untrimmed part, for the square trimmed part in Figure 8.7(b), at spot 1, which was located next to the end of the trim plunge, the temperature was 198°C and at spot 2, it was 204°C . On average, the temperature was 202°C , which is 10°C higher than that for the untrimmed shunt. This increase in temperature rise for the trimmed shunt may be attributed to the square shaped plunge cut which impedes the flow of current through the resistive material and causes local current crowding and increased heat dissipation in the central region of the element [173]. This theory is also supported by thermal-electric analysis in Chapter 4. This inferior performance could be a cause for concern as increased operating temperature is known to lead to accelerated ageing and premature failure of resistive devices [174]. This issue is discussed further in the following section.

8.2.3 High Temperature Stability Test

Results for change in resistance of both untrimmed and square cut trimmed shunt samples, following storage for 168 hours at 200°C in air are shown in Figure 8.8, with interim results reported at time intervals of 24, 48, and 72 hours.

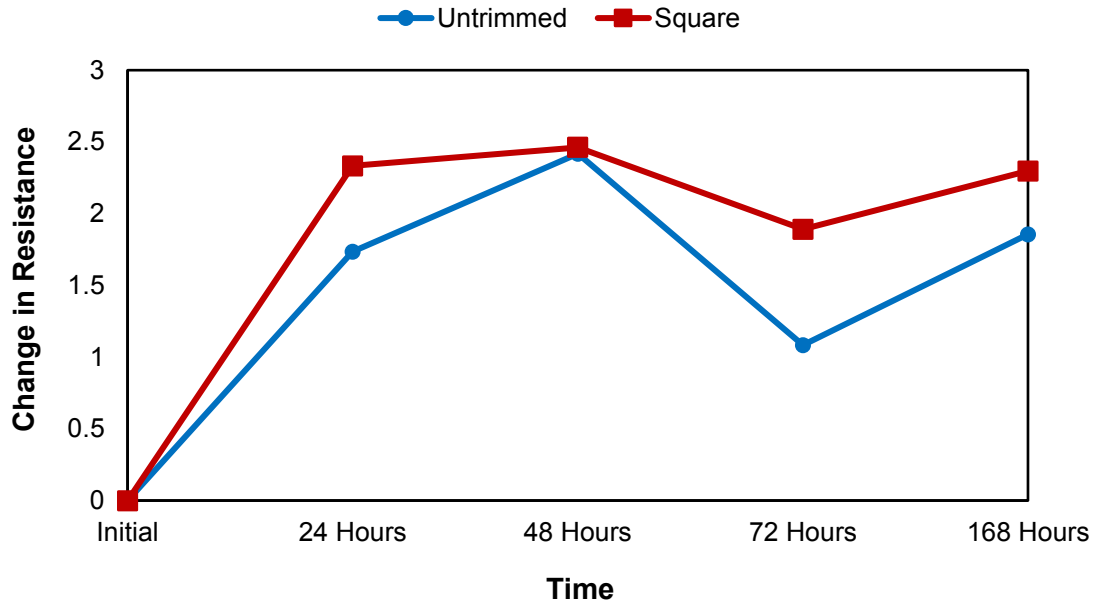


Figure 8.8: Change in Resistance for the shunt resistor over a period of 1 week.

The graph shows that the resistance values of both the untrimmed and square cut trimmed shunt samples increase significantly in the first 24 hours of the test, with changes of 1.7% and 2.3% respectively. This rate of change reduces significantly in the following 24 hours of testing and both samples reach a maximum value of change in resistance of 2.5% after 48 hours storage. After this point the resistance value of both shunts decreases after 72 hours' storage, before increasing again to give final changes in resistance values after 168 hours of 1.9% and 2.4% for the untrimmed and square cut trimmed shunt samples respectively. This initial increase and then subsequent decrease in resistance can be related to two competing mechanisms; initial oxidation of the surface of the Manganin element, resulting in the formation of a high resistance oxide layer, which in turn increases the overall resistance of the material and annealing out of impurities and grain boundary reduction, which both lead to a reduction in resistance of the material [166]. The higher rate of change of resistance in the first 24 hours for the trimmed shunt can be related to an

increased level of surface oxidation of the freshly exposed Manganin surrounding the trim cut. This theory is supported by the XPS chemical spectrums shown in Figure 8.9 for the untrimmed and trimmed shunt resistors before and after high temperature storage.

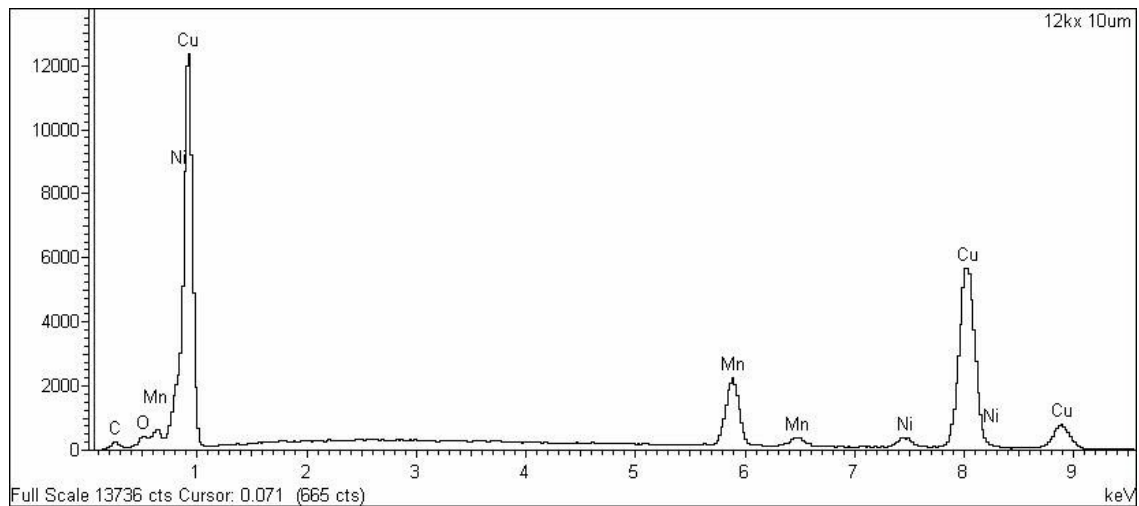


Figure 8.9: Chemical spectrum for Manganin shunt resistor.

The results show that the untrimmed and trimmed samples have similar levels of oxygen concentration prior to testing at 7.5wt.% and 8.2wt.% respectively. However, these levels increase significantly for both samples after storage at 200°C for 168 hrs with values of 16.2wt.% and 18.5wt.% respectively. These results are further supported by the SEM images of the untrimmed and trimmed parts before and after testing shown in Figure 8.10, which clearly show a discoloration and formation of a surface oxide after the high temperature exposure. This increase in surface oxidation of the Manganin element at the elevated test temperature leads to an increase in resistance value of the shunts. Although the resistance changes of the square cut trimmed sample is slightly higher at 2.29%, the stability performance of the untrimmed part is also unacceptable at 1.85% and this is an area that needs to be addressed before focusing on reducing the additional effect of trimming on this key performance characteristic of the shunts.

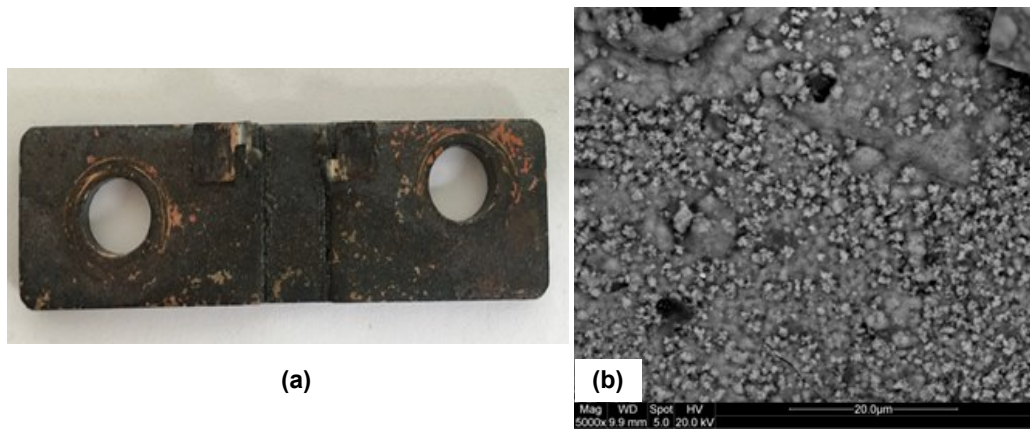


Figure 8.10: (a) Shunt resistor and (b) SEM images of the shunt resistor after stability test.

8.2.4 Hardness

Figure 8.11 shows an image of the square cut shunt resistor with hardness test indentations in 8 different areas on the surface of the Manganin as well as an exploded view of the indentation.



Figure 8.11: Hardness measurement using Alicona microscope.

The hardness values of the shunt resistors before and after trimming are shown in Figure 8.12. The mean hardness slightly increased after trimming from 144HV to 147HV. This may be attributed to the presence of oxygen and carbon impurities introduced during trimming process. An increase in hardness after the trimming process and presence of oxygen indicate that oxygen is not present in

elemental form. As the temperature during trimming process increased due to the frictional forces, it is highly likely that the oxygen has reacted with the substrate form hard oxides at the edge of the cut. As all three elements (Cu, Mn, and Ni) are oxide forming elements, therefore, there is also possibility of the formation of more than one form of oxide. In addition, a very large standard deviation may also be observed that may be attributed to the presence of multi-phase structure in the shunt resistor.

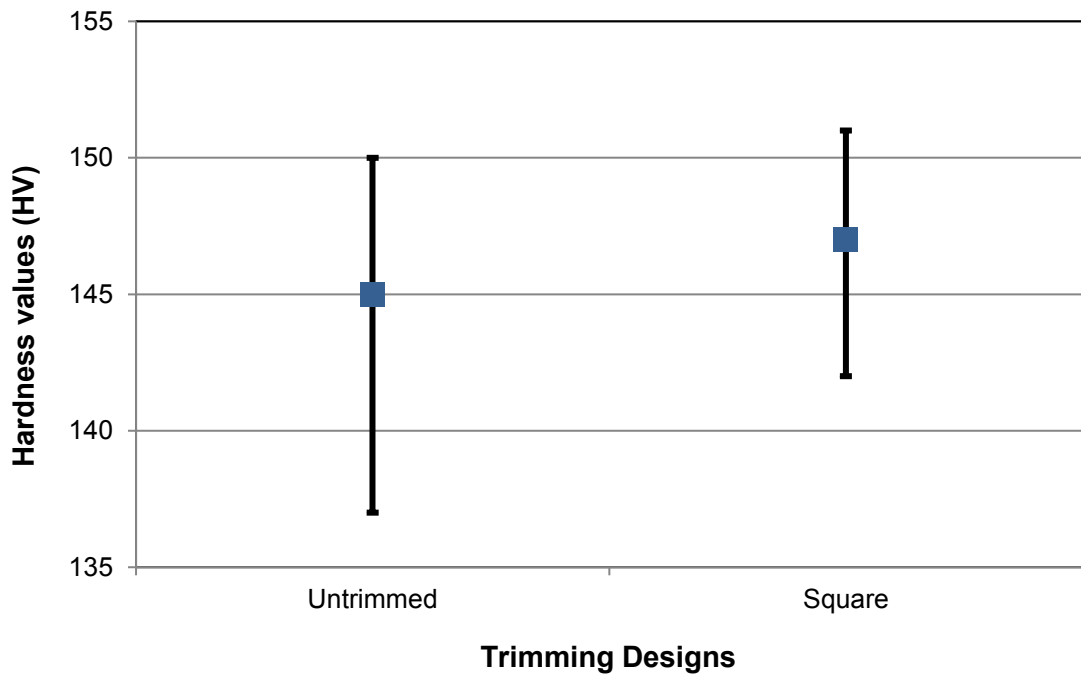


Figure 8.12: Hardness values for the shunt resistor, error bar for 8 different areas on the surface.

The hardness tests showed that there is a suggested trend of the trimmed shunts becoming harder and potentially structurally weaker than the untrimmed shunts with a minimal increase of 2 *HV*.

8.3 Summary

In summary, the results of the work carried out in this chapter shown that the trimming process does affect the chemical composition of the elements within the shunts, hence causing the trimmed shunts to produce a slightly higher percentage of elements such as oxygen and carbon on their surface. The hardness tests showed that there is a suggested trend of the trimmed shunts becoming harder and potentially structurally weaker than the untrimmed shunts but more testing would be needed over a varied number of mechanical and temperature dependent tests in order to verify this.

Both the high current and high temperature stability tests showed no overall permanent damage to the resistance values of the shunts and the trimmed shunts did not display a large difference in behaviour to the untrimmed shunts. The temperature coefficient of resistance tests showed an increase of resistance with an increase of temperature but this test also did not have a permanent effect on the shunts resistance values.

Therefore, it can be concluded that the trimming of shunts in order to create a more accurate resistance of $100 \mu\Omega \pm 1\%$ does not have any significant detrimental effect on their key structural and electrical properties.

Chapter 9

Conclusions and Future Works

The major findings of the research will be highlighted and further improvements, which should be introduced to both theoretical and experimental studies of the precision trimming process for Manganin shunt resistors, are described.

9.1 Conclusions

In this research project, extensive theoretical analysis and experimental studies have been carried out to reduce the tolerance of $100\mu\Omega$ Manganin shunt resistors from $\pm 5\%$ to less than $\pm 1\%$. Through the acquisition of in-depth knowledge pertaining to the characteristics and inherent limitations of the system under study, new development and enhancement techniques of a precision electro-mechanical trimming process have been proposed and presented in this thesis. In addition, experimental demonstration has been performed in a laboratory environment to substantiate the proposed theoretical and simulation studies. The distinctiveness of the project based on the main aims of the research has been achieved and is discussed in the following sections.

The common current sense methods, namely, shunt resistor, induction sensors, and Hall-effect sensors have been compared thoroughly in Chapter 2 in order to select the most favourable current sensor with the desired characteristics. This was shown by the shunt resistor, where the device is stable and repeatable in a wide range of current, temperature, and air humidity, where the value for those characteristics are 0 to 100A, -25 to +55 C, and 30 to 100% relative humidity, respectively [40]. Therefore, the most balanced and suitable current sensing method selected to be used in this research was the shunt resistor.

The other important criteria in this research were choosing the right measurement equipment. This is because when dealing with low resistance, sensitive equipment needed to be deployed as any slight change in the resistance is important and could affect the accuracy, precision, and resolution of the results obtained. After all the measurement techniques, systems and uncertainties had been discussed in Chapter 3, the most suitable measurement system for this research was deemed to be a combination of the Agilent B2900A source meter and 34420A Nano-volt meter and this system had the lowest system error of 0.187%. The development of the measurement system was based on the 4 wire Kelvin connection where the requirement of range for the shunt resistor is 100 $\mu\Omega$. However, in order to future proof the system, it is decided to go down to 50 $\mu\Omega$ to achieve the higher accuracy and repeatability. The research is more interested in getting better repeatability because all measurements are relative and to prove that tight distribution of the measurements is achievable.

The resistive material used in the shunt also plays a role in this research. Properties of Manganin were investigated and samples from different companies were examined in order to get the correct properties of materials to be used in thermal electric module on ANSYS software. Comparison of samples compositions against manufacturer data was investigated amongst density, hardness, resistivity, thermal conductivity and the specific heat capacity. After the investigation, the performance and specifications for the Manganin samples were found to be very similar in terms of their mechanical, thermal, and electrical properties except for the measured thermal conductivity, which was

higher compared to the published data. The experiment was conducted several times and there are still no reasonable explanations for this behaviour, thus analysis in ANSYS was conducted using thermal conductivity data published by the manufacturer.

The trimming technique chosen for this research was grinding. This is because very accurate material removal is possible and the cutting disc of the grinder is typically electrically insulated which gave a more stable and repeatable result than milling. This feature is very much needed in the trimming process, as it does not affect the resistance measurement while grinding, as well as giving the ability to stop the process before the measurement increases beyond the target resistance of $100\mu\Omega$. Five designs were chosen based on tools and equipment available at the time and the geometry is in turn driven by these available removal tools. Results from simulation in ANSYS did not show any significant difference between square cut and semi-circular cut. Since the relative difference was small, the advantage to do in-process measurements for the practical product was preferred over the theoretical best.

A prototype of an automated electro-mechanical trimming system was developed in Chapter 6. The system is controlled using NI USB-6000 DAQ device with written program through LabVIEW software. The system is designed to trim the shunt resistor following the target value, which is over specified by 1% while continuously measuring the resistance value until it reaches steady state.

In Chapter 7, a full factorial experiment was carried out in order to get the optimum input parameter values for the trimming system. This was to optimise the result that will be obtained when the final experiment occurs and to reduce the waste in time, cost, and raw materials. The identified parameters to be investigated were the feed rate and cutting speed that responded to the minimum time of trimming and resistance deviation. Since there is only 2 factors, a thorough investigation was conducted and analysis looked at several different levels. Analysis was conducted using Minitab software and selected cutting speed was 1800 m/min and the feed rate was 15mm/min.

A series of tests were conducted to find out if trimming the shunt resistors would cause any significant effects to the structural and electrical properties of the components compared to the standard one. Results showed that trimming does affect the chemical composition and makes the trimmed shunt harder. However, the change in TCR suggest that trimming has a negligible effect and results in a slight improvement for the shunt.

Correspondingly, the outcome of this practical work justifies the importance of the optimization of relevant system parameters that were proposed and discussed in Chapters 7 and 8. Results from this research have shown that the concurrent trimming process is effective for adjustment of the resistance value of Manganin shunt resistors. It offers improved trimming accuracy and reductions in time and process costs when compared to the normal consecutive process, hence increasing its potential for application in large scale manufacturing environments. By using concurrent trimming in this research, the tolerance of the Manganin shunt resistors has been reduced from $\pm 5\%$ to less than $\pm 1\%$ within 5 seconds. Moreover, it has also been shown that even more accurate tolerance of 0.15% can be achieved by reducing feed rate to 1 mm/min. The decision depends on manufacturers themselves to trade-off between reduced tolerance and time.

9.2 Recommendations for Future Work

From the work discussed in this thesis, it has been highlighted that there are a number of areas that can be investigated further in order to improve the tolerance of the existing shunt resistor for a better tolerance. Perhaps, this will be the early step in achieving the dreams of having precise current sensing components that will be used worldwide and help the world to manage their energy usage by minimising waste. This thesis has contributed to the design, analysis and optimization of a precision trimming process based upon a material removal technique, which has progressively uncovered more research opportunities and areas of improvement pertaining to the area under study.

There are also a number of criteria in the research that may be carried out differently and may worthy of future research. These criteria can be listed as follows:

1. Shunt Construction and Trimming Geometry

Different geometry for the trimmed shunt can be prepared for the research. Since there is still no standard shape or thickness for this research, a new design for the shunt can still be improved and the result of that might be able to lower the existing $\pm 5\%$ resistance tolerance even further. However, consideration for the design must be practiced as complex designs might make the material removal process difficult, especially if it is to be implemented on a mass production scale.

2. Design of Experiments (DoE) parameters

The DoE for this research is still flexible in terms of choosing the parameters. For example, the material properties and size of the cutting disc might be changed and this will probably change the results that were obtained from this research. Other parameters such as the temperature rise during trimming can also be analysed to improve the process further.

3. Predictive Trimming

Lastly, using the current findings in this research, a more comprehensive study can be conducted to predict the removal of material from the shunt resistors. The trimming process could be conducted quicker when the amount of material can be predicted before the process as the resistance does not need to be continuously measured and it could be the best option in larger production. Variation in the shunt assembly and welding process will be compensated for by measuring the initial resistance prior to trimming.

References

- [1] L. E. Doman, (2013). "International energy outlook 2013: US energy information administration: Washington."
- [2] F. Birol, (2008). "World energy outlook," *Paris: International Energy Agency*.
- [3] M. Ashby, A. Miller, F. Rutter, C. Seymour, and U. Wegst, (2009). "The CES EduPack Eco Selector—Background Reading," ed: Granta Design, Cambridge, UK, 2009.
- [4] International Energy Agency (IEA), (2015). World Energy Outlook 2015 (WEO-2015). Available: <http://www.worldenergyoutlook.org/weo2015/> [Accessed 1 January 2016].
- [5] International Energy Agency Technical Staff, (2008). "Key world energy statistics," Technical report, International energy agency.
- [6] E. O'Driscoll and G. E. O'Donnell, (2013). "Industrial power and energy metering—a state-of-the-art review," *Journal of Cleaner Production*, vol. 41, pp. 53-64.
- [7] P. Dutta, M. Feldmeier, J. Paradiso, and D. Culler, (2008). "Energy metering for free: Augmenting switching regulators for real-time monitoring," in *Information Processing in Sensor Networks, 2008. IPSN'08. International Conference on*, pp. 283-294.
- [8] A. Vaughan, (2009). Smart energy meters in every UK home by 2020. Available: <http://www.theguardian.com/environment/2009/may/11/smart-meters-energy-efficiency> [Accessed 21 November 2016].
- [9] T. Harbert. (2008). Chip companies all charged up over smart meters. *EDN Network*. 1-2. Available: <http://www.edn.com/electronics-blogs/other/4325425/Chip-companies-all-charged-up-over-smart-meters>.
- [10] L. Thompson, (2011). Energy rip off: Avoid the smart meter sales trick. Available: <http://www.thisismoney.co.uk/money/bills/article-2019077/Energy-rip-Avoid-smart-meter-sales-trick.html> [Accessed 21 November 2016].
- [11] B. Verma. (2009). Announcement: Key milestone for smart meters rollout [Online]. Department of Energy & Climate Change (DECC). Available: <https://www.gov.uk/government/news/key-milestone-for-smart-meters-rollout> [Accessed 23 January 2017].
- [12] A. MacFaul, (2010). "Smart meter Implementation Strategy Prospectus," Department of Energy and Climate Change (DECC) and Ofgem 27 July 2010. Available: <http://www.ofgem.gov.uk/e-serve/sm/Documentation/Documents1/Smart%20metering%20-%20Prospectus.pdf>
- [13] M. Coaster, (2010). "Smart Metering Implementation Programme: Implementation Strategy," DECC and Ofgem 94f/10, 27 July 2010. Available: <http://www.ofgem.gov.uk/e-serve/sm/Documentation/Documents1/Smart%20metering%20-%20Implementation%20Strategy.pdf>
- [14] A. Donoghue, (2009). Smart meters will benefit UK Jobs. Available: <http://www.techweekeurope.co.uk/news/news-it-infrastructure/smart-meters-will-benefit-uk-jobs-869> [Accessed 15 May 2013].
- [15] Technology.am (2009). Every UK Household May Get Smart Meter for Gas, Electricity. Available: <http://www.technology.am/every-uk-household-may-get-smart-meter-for-gas-electricity-052043.html> [Accessed 25 January 2013].
- [16] C. L. Wadhwa, (2005). *Electrical power systems*, 4th edition ed. New Delhi: New Age International.
- [17] electronicdesign.com (2011). "A block diagram of the key components internal to the smart meter," vol. 80 KB, 62070-fig-2.jpg, Ed., ed: Electronic Design, 2011.
- [18] A. Molina-Markham, P. Shenoy, K. Fu, E. Cecchet, and D. Irwin, (2010). "Private memoirs of a smart meter," in *Proceedings of the 2nd ACM workshop on embedded sensing systems for energy-efficiency in building*, pp. 61-66.

- [19] USwitch UK (2009). Smart meters explained. Available: <http://www.uswitch.com/gas-electricity/guides/smart-meters-explained/> [Accessed 25 January 2013].
- [20] M. Conner, (2009). "Tamper-resistant smart power meters rely on isolated sensors," in *Sensors and Machine Vision / A Supplement to Design News*, ed, 2009, p. 5.
- [21] TT Electronics, (2009). Resistors For Energy Metering - Application Note. (2). Available: http://www.ttelectronics.com/z_downloads/tt_electronics_metering_brochure.pdf.
- [22] D. W. Braudaway, (1999). "Behavior of resistors and shunts: with today's high-precision measurement capability and a century of materials experience, what can go wrong?," *Instrumentation and Measurement, IEEE Transactions on*, vol. 48, pp. 889-893.
- [23] T. O. C. Sloane, (1909). *Elementary Electrical Calculations*: D. Van Nostrand Company.
- [24] J. W. Nilsson and S. A. Riedel, (2008). *Electric Circuits*: Pearson/Prentice Hall.
- [25] R. C. Dorf, (1997). *The Electrical Engineering Handbook, Second Edition*: Taylor & Francis.
- [26] C. M. Creveling, (1997). *Tolerance Design: A Handbook for Developing Optimal Specifications*: Addison-Wesley Reading, MA.
- [27] S. Byrom, (2015). Gas & Electricity Tariff Prices per Unit. Available: https://www.ukpower.co.uk/home_energy/tariffs-per-unit-kwh [Accessed 15 October 2015].
- [28] P. Mach and P. Svasta, (2004). "Influence of trimming of resistive thick films on nonlinearity of their current vs. voltage characteristics," in *Electronics Technology: Meeting the Challenges of Electronics Technology Progress, 2004. 27th International Spring Seminar on*, pp. 309-312 vol.2.
- [29] T. Tobita and H. Takasago, (1991). "New trimming technology of a thick film resistor by the pulse voltage method," *Components, Hybrids, and Manufacturing Technology, IEEE Transactions on*, vol. 14, pp. 613-617.
- [30] F. Y. Wu, (2004). "Theory of resistor networks: the two-point resistance," *J. Phys. A: Math. Gen.*, vol. 37, pp. 6653-6673.
- [31] L. M. Landsberger, (2007). Simplifying Circuit Calibration With Electrically-Adjustable Resistors. 10. Available: http://www.mbridgetech.com/pdfs/microbridge_032307.pdf [Accessed 22 November 2013].
- [32] D. W. Elshabini-Riad and F. D. Barlow, (1998). *Thin Film Technology Handbook*. New York: Mc Graw-Hill Companies Inc.
- [33] Y. Hernik and T. Troianello, (2012). "Foil current sense resistors and their applications," *Instrumentation & Measurement Magazine, IEEE*, vol. 15, pp. 28-30.
- [34] L. B. Cronin and C. J. Kemp, (1992). "Current shunts and resistors in use in NAMAS accredited laboratories," *Science, Measurement and Technology, IEE Proceedings A*, vol. 139, pp. 179-181.
- [35] J. Hewes. (2003). Resistors [Online]. Available: <http://www.kpsec.freeuk.com/components/resist.htm> [Accessed 10 January 2013].
- [36] F. Zandman, P.-R. Simon, and J. Szwarc, (2001). *Resistor Theory and Technology*. Malvern, PA: Vishay Intertechnology Inc.
- [37] S. Ziegler, R. C. Woodward, H.-C. Lu, and L. J. Borle, (2009). "Current sensing techniques: A review," *IEEE Sensors Journal*, vol. 4, pp. 354-376.
- [38] P. Ripka, (2010). "Electric current sensors: a review," *Measurement Science and Technology*, vol. 21, p. 112001.
- [39] P. Ripka, (2004). "Current sensors using magnetic materials," *Journal of optoelectronics and advanced materials*, pp. 587-592.
- [40] K. Casey, (2011). The Need for Current Sense, Circuit Protection and Communications in Smart Meters. Available: <http://electronicdesign.com/energy/need-current-sense-circuit-protection-and-communications-smart-meters> [Accessed 26 January 2013].

- [41] S. Kara, G. Bogdanski, and W. Li, (2011). "Electricity metering and monitoring in manufacturing systems," in *Glocalized solutions for sustainability in manufacturing*, ed: Springer, pp. 1-10.
- [42] K. Iwansson, G. Sinapius, W. Hoornaert, and S. Middelhoek, (1999). *Measuring current, voltage and power* vol. 7: Elsevier.
- [43] W. Koon, (2002). "Current sensing for energy metering," in *Conference Proceedings IIC-China/ESC-China*, pp. 321-324.
- [44] P. Jain, (2012). Current Sensors. Available: <http://www.engineersgarage.com/articles/current-sensor> [Accessed 11 November 2014].
- [45] B. Yarborough, (2015). Components and Methods for Current Measurement. Available: <http://www.vishay.com/docs/30304/currentmeasurement.pdf> [Accessed 1 October 2015].
- [46] B. Fotouhi, (2001). "Indirect output current sensing," ed: Google Patents, 2001.
- [47] P. Semig and C. Wells, (2008). A Current Sensing Tutorial--Part 1: Fundamentals. Available: http://www.eetimes.com/document.asp?doc_id=1279404& [Accessed 10 August 2015].
- [48] J. Froehlich, E. Larson, S. Gupta, G. Cohn, M. Reynolds, and S. Patel, (2011). "Disaggregated end-use energy sensing for the smart grid," *IEEE Pervasive Computing*, vol. 10, pp. 28-39.
- [49] N. Mrmak, P. V. Oorschot, and J. W. Pustjens, (2012). Shunt resistor. Available: <http://www.resistorguide.com/shunt-resistor/> [Accessed 10 November 2014].
- [50] C. Honsberg and S. Bowden. (2014). Shunt Resistance [Online]. Available: <http://www.pveducation.org/pvcdrom/solar-cell-operation/shunt-resistance> [Accessed 12 August 2015].
- [51] R. Elliott, (2006). Meters, Multipliers & Shunts. Available: <http://sound.westhost.com/articles/meters.htm> [Accessed 20 August 2014].
- [52] C. W. McLyman, (2007). "Reviewing current transformers and current transducers," in *2007 Electrical Insulation Conference and Electrical Manufacturing Expo*.
- [53] S. Ziegler, R. C. Woodward, H.-C. Lu, and L. J. Borle, (2009). "Current sensing techniques: A review," *Sensors Journal, IEEE*, vol. 9, pp. 354-376.
- [54] S. Tumanski, (2007). "Induction coil sensors—A review," *Measurement Science and Technology*, vol. 18, p. R31.
- [55] D. A. Ward and J. L. T. Exon, (1993). "Using Rogowski coils for transient current measurements," *ENGINEERING SCIENCE AND EDUCATION JOURNAL*, pp. 105-113, June 1993.
- [56] Electrotechnik, (2014). "Rogowski Coil," ed, 2014.
- [57] L. A. Kojovic and R. Beresh, (2010). "Practical Aspects of Rogowski Coil Applications to Relaying," IEEE Power Engineering Society. Available: http://www.pes-psrc.org/Reports/Practical%20Aspects%20of%20Rogowski%20Coil%20Applications%20to%20Relaying_Final.pdf
- [58] R. S. Popovic, (2003). *Hall effect devices*: CRC Press.
- [59] X. Jiang, S. Dawson-Haggerty, P. Dutta, and D. Culler, (2009). "Design and implementation of a high-fidelity ac metering network," in *Information Processing in Sensor Networks, 2009. IPSN 2009. International Conference on*, pp. 253-264.
- [60] B. Klaiber and P. Turpin, (2012). Sensing currents for maximum efficiency. Available: <http://powerelectronics.com/alternative-energy/sensing-currents-maximum-efficiency> [Accessed 07 September 2014].
- [61] T. R. Kuphaldt, "Chapter 8-DC Metering Circuits," in *Ammeter Impact on Measured Circuit*, ed: Design Science License.
- [62] O. Darrigol, (2000). *Electrodynamics from Ampère to Einstein*: Clarendon Press.
- [63] Brown & Sharpe Manufacturing Company, (1914). *Practical Treatise on Milling and Milling Machines*: Brown & Sharpe Manufacturing Company.

- [64] P. G. Huray, (2011). *Maxwell's Equations*: Wiley.
- [65] allspectrum.com, (2011). "Ohms Law Formula Wheel," vol. 102 KB, ed: All Spectrum, 2011.
- [66] D. O. Woodbury, (1949). *A measure for greatness: a short biography of Edward Weston*: McGraw-Hill.
- [67] M. B. Stout, (1960). *Basic electrical measurements*: Prentice Hall.
- [68] Sandvik, (2015). Manganin 43 Resistance Wire. Available: <http://www.matweb.com/search/datasheet.aspx?matguid=d855d1a0b73a47b5851f765e8d7f95c4&ckck=1> [Accessed 21 January 2015].
- [69] Kanthal, (2015). Manganina 43. Available: <http://kanthal.com/en/products/material-datasheets/wire/resistance-heating-wire-and-resistance-wire/manganin-43/> [Accessed 21 January 2015].
- [70] Isabellenhütte, (2014). Manganin. Available: http://www.isabellenhuette.de/pdf/WIDER_LEG/MANGANIN-ISABELLENHUETTE-R.pdf [Accessed 20 January 2015].
- [71] GoodFellow, (2014). Manganin - Resistance Alloy. Available: <http://www.goodfellow.com/E/Manganin-Resistance-Alloy-Alloy.html> [Accessed 20 January 2015].
- [72] Vishay Intertechnology Inc. , (2012). Shunts, Current Shunts, and Current-Sensing Resistors. Available: http://www.vishay.com/docs/49159/power-metal-strip-shunts-current-shunts_vmn-pl0005-1409.pdf [Accessed 22 June 2015].
- [73] P. E. Langan, J. R. Jowett, S. G. Thomson, and D. O. Jones. (2004). *A GUIDE TO LOW RESISTANCE TESTING*. Available: <http://www.testequipmentdepot.com/megger/pdf/low-resistance-testing.pdf> [Accessed 10 March 2013].
- [74] J. R. Davis and ASM International Handbook Committee, (2001). *Copper and Copper Alloys*. Materials Park, Ohio: ASM International.
- [75] S. J. Rosenberg, (1968). "Nickel and its alloys," DTIC Document.
- [76] D. A. Nickel and F. Sadeghi, (1999). "In-Situ Rolling Element Bearing Temperature and/or Pressure Measurement," DTIC Document.
- [77] S. B. Field and C. Franconi, (2012). *Physics and Technology of Hyperthermia*: Springer Netherlands.
- [78] C. EduPack, (2007). "The Cambridge Engineering Selector," ed: Granta Design, Rustat House, 2007.
- [79] Z. Sun and R. Karppi, (1996). "The application of electron beam welding for the joining of dissimilar metals: an overview," *Journal of Materials Processing Technology*, vol. 59, pp. 257-267.
- [80] D. Kopeliovich, (2012). "Electron Beam Welding (EBW)," vol. 20KB, electron_beam_welding.png, Ed., ed, 2012.
- [81] A. C. Fischer-Cripps, (2004). *The Electronics Companion*: Taylor & Francis.
- [82] E. Coates, (2015). Resistors & Circuits Module 1. Available: http://www.learnabout-electronics.org/Resistors/resistors_01a.php [Accessed 12 August 2015].
- [83] K. A. Kuhn. (2011). Measuring the Temperature Coefficient of a Resistor [Online]. Available: <http://www.kennethkuhn.com/students/ee431/text/ee431lab3.pdf>
- [84] Isabellenhütte Heusler GmbH & co. KG, (2015). Ultimate Performance Where It's Least Expected – In Every Detail. Available: http://www.isabellenhuette.de/uploads/media/IHH_Bauelementebroschuere_engl_02.pdf [Accessed 10 August 2015].
- [85] D. M. Cook, (1975). *The Theory of the Electromagnetic Field*: Dover Publications.
- [86] H. Kanematsu and D. M. Barry, (2016). *Corrosion Control and Surface Finishing: Environmentally Friendly Approaches*: Springer Japan.
- [87] Isabellenhütte Company, (2012). Low-Ohmic Precision And Power Resistors. 14. Available:

- http://www.isabellenhuetten.de/uploads/media/IHH_Bauelementebroschuere_engl_01.pdf.
- [88] Vishay Intertechnology, (2008). "Application Note: Resistive Products," ed, 2008.
- [89] The National Institute of Standards and Technology (NIST). (2008). NIST General Information [Online]. Available: http://www.nist.gov/public_affairs/general_information.cfm [Accessed 21 August 2013].
- [90] O. H. Chesterland, (2014). Basic Techniques for Accurate Resistance Measurement. *Reduce Measurement Errors in your Application* [Online]. Available: http://www.dataloggerinc.com/content/resources/white_papers/654/basic_techniques_for_accurate_resistance_measurement/ [Accessed 20 October 2014].
- [91] Cropico, (2007). A Guide to: Low Resistance Measurement. 39. Available: <http://www.seaward.co.uk/downloads/Guide%20to%20Low%20Resistance%20Booklet.pdf>.
- [92] Seaward Electronic Ltd, (2014). Kelvin Bridges. Available: <http://www.seaward.co.uk/kelvin-bridge>.
- [93] R. H. Dieck and S. Instrumentation, (1992). *Measurement uncertainty: methods and applications*: Instrument Society of America Research Triangle Park, NC.
- [94] I. Lira, (2002). "Evaluating the measurement uncertainty: fundamentals and practical guidance," ed: IOP Publishing, 2002.
- [95] B. Voljc, M. Lindic, and R. Lapuh, (2009). "Direct Measurement of AC Current by Measuring the Voltage Drop on the Coaxial Current Shunt," *Instrumentation and Measurement, IEEE Transactions on*, vol. 58, pp. 863-867.
- [96] H. W. Coleman and W. G. Steele, (2009). *Experimentation, validation, and uncertainty analysis for engineers*: John Wiley & Sons.
- [97] F. Alferink, (2013). Accuracy, precision & resolution. Available: <http://meettechnik.info/measurement/accuracy.html> [Accessed 20 May 2015].
- [98] B. N. Taylor, (2009). *Guidelines for Evaluating and Expressing the Uncertainty of NIST Measurement Results (rev: DIANE Publishing)*.
- [99] S. Xie, (2015). Practical Filter Design Challenges and Considerations for Precision ADCs. Available: <http://www.analog.com/library/analogdialogue/archives/50-04/practical-filter.pdf>.
- [100] R. J. Van de Plassche, (2013). *CMOS integrated analog-to-digital and digital-to-analog converters* vol. 742: Springer Science & Business Media.
- [101] Keithley, (2015). Technical Information: Low Current/High Resistance Measurements. Available: http://www.tek.com/sites/tek.com/files/media/document/resources/TechInfo_LoL-HiR.pdf.
- [102] Keithley, (2004). *Low Level Measurements Handbook : Precision DC Current, Voltage and Resistance Measurements*, 6 ed. Cleveland, Ohio: Keithley Instruments, Inc.
- [103] T. Wilczyńska, R. Wiśniewski, and V. Semina, (2009). "Thermal properties of manganin dynamic high-pressure sensor after complex Ti–Kr high fluence implantation, modelling and interpretation," *Vacuum*, vol. 83, pp. S268-S270.
- [104] A. E. N. Greenwood, (1997). *Chemistry of the Elements.*, Second ed. Oxford, Amsterdam, Boston, London, New York, Paris, San Diego, San Francisco, Singapore, Sydney, Tokyo.: Butterworth – Heinemann.
- [105] B. K. Tanner, (2013). *X-Ray Diffraction Topography: International Series in the Science of the Solid State* vol. 10: Elsevier.
- [106] J. Goldstein, (2012). *Practical scanning electron microscopy: electron and ion microprobe analysis*: Springer Science & Business Media.
- [107] E.Y.Tsymba, (2015). Section 1: Crystal Structure. Available: http://unlcms.unl.edu/cas/physics/tsymbal/teaching/SSP-927/Section%2001_Crystal%20Structure.pdf.

- [108] P. J. Schields, (2004). Bragg's Law and Diffraction: How waves reveal the atomic structure of crystals. Available: <http://skuld.bmsc.washington.edu/~merritt/bc530/bragg/>.
- [109] T. Lin, Y. B. Chao, and Z. H. Ren, (2005). "Piezoresistance response of thin film manganin sensors," *Sensors and Actuators A: Physical*, vol. 118, pp. 222-225.
- [110] A. R. Franco Jr, G. Pintaúde, A. Sinatora, C. E. Pinedo, and A. P. Tschiptschin, (2004). "The use of a Vickers indenter in depth sensing indentation for measuring elastic modulus and Vickers hardness," *Materials Research*, vol. 7, pp. 483-491.
- [111] D. Hetzner, (2003). "Microindentation Hardness Testing of Materials Using ASTM E384," *Microscopy and Microanalysis*, vol. 9, pp. 708-709.
- [112] C. Mariani, (2015). "Testing Materials (Hardness)," ed: Antonio Nascimento, 2015.
- [113] J. H. Lienhard, (2013). *A heat transfer textbook*: Courier Corporation.
- [114] Aalco Metals Limited, (2015). "Aluminium Alloy - Commercial Alloy - 6061 - T6 Extrusions," ed, 2015.
- [115] M. R. Gosz, (2006). *Finite Element Method – Application in Solids, Structures and Heat Transfer*. USA: Taylor & Francis Group, LLC.
- [116] M. Wroński, S. Kamiński, E. Miś, and A. Dziedzic, (2005). "New trim configurations for laser trimmed thick-film resistors—theoretical analysis, numerical simulation and experimental verification," *Microelectronics Reliability*, vol. 45, pp. 1941-1948.
- [117] S. KAMINSKI, E. MIS, M. SZYMENDERA, and A. DZIEDZIC, (2005). "New trim configurations for laser trimmed thick-film resistors: Experimental verification," *Journal of microelectronics and electronic packaging*, vol. 2, pp. 19-24.
- [118] Y. N. Antonov, (2006). "Use of laser trimming for the development of a project for accuracy-normalization of the resistance of resistors in hybrid integrated circuits," *Journal of Communications Technology and Electronics*, vol. 51, pp. 1351-1355.
- [119] J. Meijer, (2004). "Laser beam machining (LBM), state of the art and new opportunities," *Journal of Materials Processing Technology*, vol. 149, pp. 2-17.
- [120] S. Privitera, O. Le Neel, C. Leung, P. Dumont-Girard, B. Cialdella, C. Bongiorno, and R. Modica, (2012). "Morphological and Electrical Characterization of Electrically Trimmable Thin-Film Resistors," *Electron Devices, IEEE Transactions on*, vol. 59, pp. 3549-3554.
- [121] P. Sandborn and P. A. Sandborn, (2008). "A Random Trimming Approach for Obtaining High-Precision Embedded Resistors," *Advanced Packaging, IEEE Transactions on*, vol. 31, pp. 76-81.
- [122] J. Babcock, P. Francis, R. Bashir, A. Kabir, D. Schroder, M. Lee, T. Dhayagude, W. Yindepol, S. Prasad, and A. Kalnitsky, (2000). "Precision electrical trimming of very low TCR poly-SiGe resistors," *Electron Device Letters, IEEE*, vol. 21, pp. 283-285.
- [123] S. Wernick, R. Pinner, and P. G. Sheasby, (1992). "The surface treatment and finishing of aluminum and its alloys," *S. Wernick, R. Pinner, and P. G. Sheasby, 1320 pages, 5th edition, 2 volumes, 492 illustrations, 230 tables and 2534 references. Price. 170(US\$ 340. 00). Book*.
- [124] A. Elshabini-Riad and I. Bhutta, (1993). "Lightly trimming the hybrids," *Circuits and Devices Magazine, IEEE*, vol. 9, pp. 30-34.
- [125] G. Boothroyd, (1988). *Fundamentals of Metal Machining and Machine Tools, Third Edition*: Taylor & Francis.
- [126] T. Jagadeesha. *Abrasive Jet Machining* Available: http://www.nitc.ac.in/dept/me/jagadeesha/mev303/Chapter2_%20AJM.pdf.
- [127] M. K. Mathew, (2014). "Abrasive Jet Machining," ed, 2014.
- [128] CustomPartNet, (2009). Milling. Available: <http://www.custompartnet.com/wu/milling>.
- [129] Sinotech Inc., (2014). "Milling," ed, 2014.
- [130] D. A. Stephenson and J. S. Agapiou, (2016). *Metal cutting theory and practice*: CRC press.

- [131] M. Cockerham, (2014). "Ch. 26 – Abrasive Machining and Finishing Operations," ed, 2014.
- [132] M. Elbestawi, (1998). "METAL CUTTING THEORY AND PRACTICE," *MACHINING SCIENCE AND TECHNOLOGY*, vol. 2, pp. 383-384.
- [133] Y.-S. Ma, G. Chen, and G. Thimm, (2008). "Paradigm shift: unified and associative feature-based concurrent and collaborative engineering," *Journal of Intelligent Manufacturing*, vol. 19, pp. 625-641.
- [134] E. A. Fielding, J. R. McCardle, B. Eynard, N. Hartman, and A. Fraser, (2014). "Product lifecycle management in design and engineering education: International perspectives," *Concurrent Engineering*, vol. 22, pp. 123-134.
- [135] D. Yang and M. Dong, (2012). "A hybrid approach for modeling and solving product configuration problems," *Concurrent Engineering*, vol. 20, pp. 31-42.
- [136] H.-C. Chang and H.-Y. Chen, (2014). "Optimizing product form attractiveness using Taguchi method and TOPSIS algorithm: A case study involving a passenger car," *Concurrent Engineering*, p. 1063293X13520317.
- [137] Agilent Technologies. (2003). Agilent 34420A Nano Volt / Micro Ohm Meter [Online]. Available: http://instructor.physics.lsa.umich.edu/adv-labs/Tools_Resources/HP%2034420A%20User's%20guide.pdf
- [138] D. C. Montgomery, (2008). *Design and analysis of experiments*: John Wiley & Sons.
- [139] R. Woll and C. Burkhard, (2005). "Full Factorial Design, Taguchi Design or Genetic Algorithms—Teaching Different Approaches to Design of Experiments," in *Innovations in Classification, Data Science, and Information Systems*, ed: Springer, pp. 567-574.
- [140] R. J. Eggert, (2005). *Engineering Design*. New Jersey: Pearson Education, Inc.
- [141] P. J. Ross, (1996). "Taguchi techniques for quality engineering," *Mcgraw-hil International editions*.
- [142] J. J. PIGNATIELLO JR and J. S. RAMBERG, (1991). "Top ten triumphs and tragedies of Genichi Taguchi," *Quality Engineering*, vol. 4, pp. 211-225.
- [143] G. Taguchi, S. Chowdhury, and Y. Wu, (2005). *Taguchi's quality engineering handbook*: Wiley.
- [144] M. S. Phadke, (1995). *Quality engineering using robust design*: Prentice Hall PTR.
- [145] G. Taguchi, S. Chowdhury, and S. Taguchi, (2000). *Robust engineering*: McGraw-Hill Professional.
- [146] W. Yang and Y. Tarng, (1998). "Design optimization of cutting parameters for turning operations based on the Taguchi method," *Journal of Materials Processing Technology*, vol. 84, pp. 122-129.
- [147] J. Ghani, I. Choudhury, and H. Hassan, (2004). "Application of Taguchi method in the optimization of end milling parameters," *Journal of Materials Processing Technology*, vol. 145, pp. 84-92.
- [148] C. Nian, W. Yang, and Y. Tarng, (1999). "Optimization of turning operations with multiple performance characteristics," *Journal of Materials Processing Technology*, vol. 95, pp. 90-96.
- [149] P. J. Ross, (1988). "Taguchi techniques for quality engineering: loss function, orthogonal experiments, parameter and tolerance design."
- [150] J. H. Zar, (1984). "Comparing simple linear regression equations," *Biostatistical analysis*, vol. 2, pp. 292-305.
- [151] K. A. Pituch, T. A. Whittaker, and J. P. Stevens, (2015). *Intermediate statistics: A modern approach*: Routledge.
- [152] Y. Dodge, (2006). *The Oxford dictionary of statistical terms*: Oxford University Press on Demand.
- [153] ISO EN, "4287: 2009," *Geometrical Product Specifications (GPS)-Surface texture: Profile method—Terms, definitions and surface texture parameters (ISO 4287: 1997+ Cor 1: 1998+ Cor 2: 2005+ Amd 1: 2009)(includes Corrigendum AC: 2008 and Amendment A1: 2009)*.

- [154] Geometrical Product Specifications, (1997). "Surface texture: Profile method-Rules and procedures for the assessment of surface texture (ISO 4288: 1996)," *German version EN ISO*, vol. 4288, p. 1997.
- [155] S. Khamel, N. Ouelaa, and K. Bouacha, (2012). "Analysis and prediction of tool wear, surface roughness and cutting forces in hard turning with CBN tool," *Journal of mechanical science and technology*, vol. 26, pp. 3605-3616.
- [156] J. Sun and Y. Guo, (2009). "A comprehensive experimental study on surface integrity by end milling Ti-6Al-4V," *Journal of Materials Processing Technology*, vol. 209, pp. 4036-4042.
- [157] M. Nouari, G. List, F. Girot, and D. Coupard, (2003). "Experimental analysis and optimisation of tool wear in dry machining of aluminium alloys," *Wear*, vol. 255, pp. 1359-1368.
- [158] Z.-C. Lin, W.-L. Lai, H. Lin, and C. Liu, (2000). "The study of ultra-precision machining and residual stress for NiP alloy with different cutting speeds and depth of cut," *Journal of materials processing technology*, vol. 97, pp. 200-210.
- [159] A. Shih, L. Wang, K. K. Singh, R. Singh, and V. Kartik, (2015). "43rd North American Manufacturing Research Conference, NAMRC 43, 8-12 June 2015, UNC Charlotte, North Carolina, United States Comparative Study of Chatter Detection Methods for High-Speed Micromilling of Ti6Al4V," *Procedia Manufacturing*, vol. 1, pp. 593-606, 2015/01/01.
- [160] G. Boothroyd, (1975). *Fundamentals of metal machining and machine tools*: Scripta Book Co.
- [161] D. McMullan, (1995). "Scanning electron microscopy 1928-1965," *Scanning*, vol. 17, pp. 175-185.
- [162] L. Corbari, M.-A. Cambon-Bonavita, G. J. Long, F. Grandjean, M. Zbinden, F. Gaill, and P. Compère, (2008). "Iron oxide deposits associated with the ectosymbiotic bacteria in the hydrothermal vent shrimp *Rimicaris exoculata*," *Biogeosciences Discussions*, vol. 5, pp. 1825-1865.
- [163] Department of Defense, (2002). "MIL STD 202 Method 304 " in *Test Method Standard Electronic and Electrical Component Parts* ed, 2002.
- [164] Learning and Teaching Scotland, (2011). *Physics: Semiconductors and Band Theory Support Material*, HIGHER ed. Scotland: National Qualifications Curriculum Support.
- [165] British Standards Institution, (2012). "BS EN 60115-1:2011+A11:2015," in *Fixed resistors for use in electronic equipment. Generic specification*, ed: BSI, 2012, p. 83.
- [166] R. E. Reed-Hill and R. Abbaschian, (1973). "Physical metallurgy principles."
- [167] G. D. Quinn and R. C. Bradt, (2007). "On the Vickers indentation fracture toughness test," *Journal of the American Ceramic Society*, vol. 90, pp. 673-680.
- [168] G. T. Meaden, (2013). *Electrical resistance of metals*: Springer.
- [169] E. Barsoukov and J. R. Macdonald, (2005). *Impedance spectroscopy: theory, experiment, and applications*: John Wiley & Sons.
- [170] W. M. Haynes, (2014). *CRC handbook of chemistry and physics*: CRC press.
- [171] C. G. Douglas, (1995). "Physics: Principles with applications," ed: Prentice Hall New Jersey, 1995.
- [172] G. Dyos, (2012). *The Handbook of Electrical Resistivity: New materials and pressure effects*. London, UK: The Institution of Engineering and Technology.
- [173] X. Zhu, H. Kotadia, S. Xu, H. Lu, S. Mannan, C. Bailey, and Y. Chan, (2013). "Modeling Electromigration for Microelectronics Design," *Journal of Computational Science and Technology*, vol. 7, pp. 251-264.
- [174] M. Ohring, (1998). *Reliability and failure of electronic materials and devices*: Academic Press.

Appendices

A New Trimming Approach for Shunt Resistors Used in Metering Applications

Siti Nabilah Misti*, Martin Birkett, David Bell and Roger Penlington

Faculty of Engineering and Environment
Northumbria University
Newcastle upon Tyne, United Kingdom
*siti.misti@northumbria.ac.uk

Abstract— A growing number of smart energy meters and electric charging stations have sparked a demand for a high precision, low value shunt resistors to measure the flow of electrical current. This paper investigates the possibility of trimming 100 micro ohms Manganin shunt resistors with tolerance of 5 percent to improve their accuracy and performance for use in smart energy meters. In theory, reducing the standard 5 percent tolerance of the shunt resistors can be achieved by removing controlled amounts of the resistive material. In this experiment, theoretical analysis is carried out to determine the maximum amount of resistive material that can be removed from Manganin shunt resistor to reduce its standard tolerance of 5 percent. Two alternative designs are then used to trim the material from the Manganin strip using machining techniques. Implications of the experimental results to the flow of electrical current and temperature rise in the shunt resistors are discussed. Results from the initial trimming trials show that the standard tolerance of 5 percent can be reduced to less than 1 percent.

Keywords— Shunt resistors; Manganin; smart energy meter; trimming; tolerance

I. INTRODUCTION

The electricity meter has been used to measure electrical energy supplied to consumers since the beginning of the 20th century. The electricity meter records the amount of electrical energy consumed in kilowatt hours (KWh) on a mechanical numeric readout. Every country in the world wants electrical energy to thrive economically but the risks associated with generating electricity can only be reduced by cutting down on electrical energy usage. One way to achieve this is to use smart energy meters where the consumer can measure their own energy consumption and armed with the relevant data, they can now use that information to make smarter decisions to manage their energy usage.

A smart meter is a device that enables consumer to monitor their own power usage and can also automatically send electronic readings to energy suppliers. Utility companies nowadays are pushing to replace old mechanical meters with smart energy meters with up to 500 million units being produced worldwide over the next 7 years [1, 2]. In the United Kingdom, the Department of Energy and Climate Change (DECC) have announced their intentions to equip all UK

houses with a smart energy meter by 2020. It is estimated that this installation will save in the region of £14 billion, reducing the average household energy bill £65 per annum [3].

Fig. 1 shows a system block diagram for a single-phase smart energy meter where the shunt resistor is used as a transducer for phase current sensing. The shunt measures the flow of electrical current which is then used together with a voltage measurement to calculate the instantaneous power consumption. The more accurately the current can be measured, the more accurate the calculated power consumption will be.

Shunt resistors offer advantages of low power loss, high stability and precision of electric resistance across a wide temperature range, when compared to other current sensing methods [1]. They are typically manufactured using a Manganin alloy element which is electron beam welded to two copper terminations, see Fig. 3 Manganin consists of 86% copper, 12% manganese and 2% nickel (Cu86/Mn12/Ni2 wt.%) and is the standard resistive alloy used for precision shunt resistors due to its moderate resistivity of $48.2 \times 10^{-8} \Omega m$ and low temperature coefficient of resistance (TCR) of $\pm 15 \text{ ppm}/^\circ\text{C}$ [4, 5]. Manganin also has desirable working properties such as extremely low thermal electromotive force (EMF) at

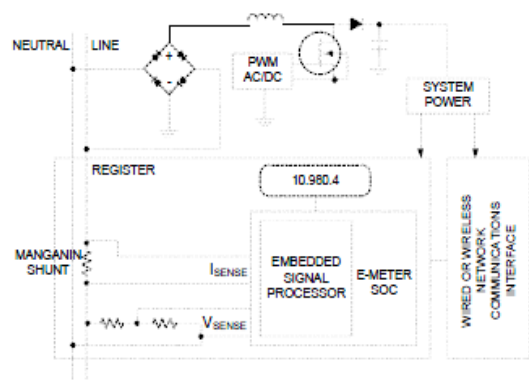


Fig. 1. Connection of a Manganin shunt in Smart Energy Meter [6].

20°C of 0.1 $\mu\text{V/K}$ and excellent long-term stability of electrical resistance [5].

Although Manganin has these excellent properties, it is still difficult to produce shunt resistors to tight dimensional and thus resistive tolerances due to limitations in the current manufacturing techniques. The most accurate shunts available on the market to-date have standard manufacturing tolerances of $\pm 5\%$.

The aim of this paper is therefore to investigate the possibility of reducing the standard tolerance of 100 $\mu\Omega$ shunt resistors to $\pm 1\%$ or better using a new trimming approach. This will lead to more precise current sensing thus improves the accuracy and reliability of smart energy meters.

II. METHODOLOGY

The experimental procedure is shown in Fig. 2 and was carried out using different combinations of measurement system and varying trimming processes. The experiment employed a sample of 20, 100 $\mu\Omega$, 3 W power rated shunt resistors with $\pm 5\%$ tolerance. The 20 samples were randomly selected for testing from a production batch of 150 parts in order to generate more reliable test data.

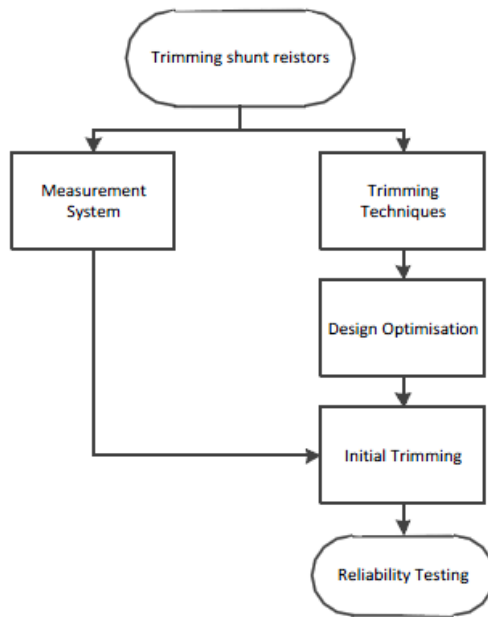


Fig. 2. Block diagram depicting the procedures involved in the experiment.

III. MEASUREMENT SYSTEM

In order to achieve the objective of reducing the tolerance of the shunt resistors, a system to accurately measure the resistance value is required. Measuring the value of a 100 $\mu\Omega$ resistor is not trivial and a system accuracy of $\pm 0.1\%$ (i.e., 10% of the initial 1% tolerance target) should be strived for. In this experiment a digital micro-ohmmeter, type Cropico D07, was

used to measure the resistance value of the shunts. The four-wire (Kelvin) method of measurement was used as it is preferred for resistance values below 100 Ω as it reduces the effect of test lead resistance giving more accurate and consistent results.

As shown in Fig. 3 the four-wire (Kelvin) method involves feeding a constant known current (I) through the shunt resistor whilst accurately measuring the voltage potential (ve) dropped across the Manganin strip. Although some small current will flow in the potential leads, it is insignificant and can be disregarded. In order to produce a realistically measurable voltage drop, a source current of 10 A is used. This produces a voltage of nominally 1 mV across the 100 $\mu\Omega$ Manganin strip. However, since this substantially large current of 10 A can cause unwanted heating effects within the resistor element, a pulsed current of 10ms was used to enable more accurate resistance measurements to be taken.

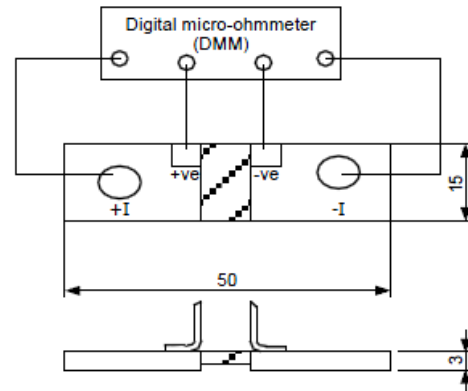


Fig. 3. Connection of the shunt resistor to digital micro-ohmmeter using four wires Kelvin method to measure the resistance.

In this experiment, the resistance value of each the 20 shunt resistors was measured 5 times to observe if the digital micro-ohmmeter could give accurate and repeatable readings. Measurements were taken at a 15 second intervals to ensure consistency in the experiment and reduce fluctuation of the readings. The results collected from the micro-ohmmeter readings indicated that each resistor used in the experiment was within a 100 $\mu\Omega \pm 5\%$ tolerance. These readings were then used to calculate the amount of material to be removed in the trimming process.

IV. TRIMMING PROCESS

Standard shunts with resistance values of 100 $\mu\Omega \pm 5\%$ must be within the range 95 $\mu\Omega$ to 105 $\mu\Omega$. In order to improve the tolerance of the shunt resistors to $\pm 1\%$, the resistance values must be below 101 $\mu\Omega$. Shunt resistors between 99 $\mu\Omega$ and 101 $\mu\Omega$ are already within $\pm 1\%$, and are acceptable without being trimmed. Only those between 95 $\mu\Omega$ and 99 $\mu\Omega$ require trimming. This is achieved by removing a small portion of Manganin from the resistive element to increase its resistance value to within the target range of 99 $\mu\Omega$ to 101 $\mu\Omega$.

For this experiment, 12 out of the initial 20 shunt resistor samples were within the range 95-99 $\mu\Omega$ required for initial trimming. Each one of the samples was measured using a digital microscope, type Keyence VHX-2000, in order to obtain a precise dimension of the length, width and thickness of the Manganin strip.

A. Theoretical Analysis

In theory, by removing some controlled amount of resistive material into tolerable and symmetrical shape, the standard tolerance of the shunt resistors can be reduced. The maximum amount of material that needs to be removed can be determined from the expression for the initial electrical resistance of the shunt, R_1 [8]:

$$R_1 = \rho L / A \quad (1)$$

where ρ is the resistivity value of Manganin, L is the length of the Manganin strip, and A is the cross sectional area of the Manganin strip which is the width, W multiplied by the initial thickness, T_1 .

In order to get the value of ρ from the above equation, the value of resistance R_1 should be known and this value is obtained from the digital micro-ohmmeter readings. Once the value of ρ is calculated, equation (1) can be rearranged to find the new thickness, T_2 required to increase the resistance of the shunt to its targeted value, R_2 , of 100 $\mu\Omega$:

$$T_2 = \rho L / WR_2 \quad (2)$$

Considering the targeted resistance, R_2 is 100 $\mu\Omega$ and the value of L and W are kept constant, the thickness to be removed, $t = T_1 - T_2$ can be removed from the original thickness of the Manganin strip, T_1 . Correspondingly, the volume of the material to be removed from the Manganin strip can be obtained using the following equation:

$$V = W \times L \times t \quad (3)$$

The average volume of resistive material to be removed from the Manganin strip for all 12 samples of the shunt resistors was calculated to be 6.74 mm^3 .

B. Trimming Techniques

There are number of possible techniques that could be used to trim the Manganin strip, of which the most suitable technique will be selected. Trimming can be carried out by several techniques include sand blasting, laser cutting, machining and grinding [9].

Since a relatively large volume of material needed to be removed from the Manganin strip, laser cutting and sand blasting were deemed unsuitable. Of the remaining techniques, trimming using a milling or grinding machine are by far the most effective and economic methods when compared to other precise techniques such as laser cutting. Both methods conform admirably with the requirements of the experiment in particular since material removal rate can be changed in accordance with the process and material.

However, since Manganin alloy comprises 86 wt.% copper and is categorized as a soft material, it has a high potential to cause the grit of an abrasive grinding wheel to clog up and significantly reduce the material removal rate [10]. Therefore in this experiment, machining was chosen to be the best technique, as it particularly suitable for applications requiring fine removal of material from the work piece [11]. As most of the milling machines available are computer controlled, producing precision trimmed parts in large quantities could be realistically projected. Furthermore, the shunt resistors could be easily connected to the digital micro-ohmmeter to monitor changes in the value of resistance while the removal of the material is taking place.

C. Design Optimization

A number of different trim designs were modelled using SolidWorks 2013 software to be tested during the initial trimming phase. These designs were created so that a specific volume of resistive material can be removed from the Manganin strip based on the theoretical results from equation (3). In this experiment, 5 initial trim designs were created (Fig. 4) to allow easy removal of resistive material from the Manganin strip using the machining technique.

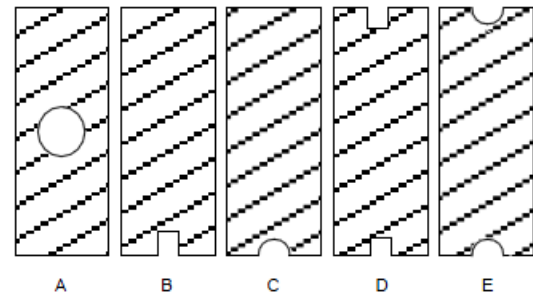


Fig. 4. Various trimming design and patterns suggestion modelled in Solidwork 2013 software.

All suggested designs were then investigated in the Thermal Electric module using ANSYS 14.5 software to determine the effect of varying trimming geometry on the current flow within the resistor element and the subsequent temperature rise of the shunt. Convection was set at 22°C ambient temperature with 5 $\text{W/m}^2\text{K}$ coefficient and the high voltage potential was set to 0.02 V, giving an equivalent current of 200 A through the shunt. The material properties for Manganin were kept constant throughout (i.e., thermal conductivity of 22 $\text{Wm}^{-1}\text{K}^{-1}$, Seebeck Coefficient of 0.6 μVK^{-1} and resistivity of 45 $\mu\Omega\text{cm}$). A Manganin strip without any trimming was used as a control sample for the analysis. Results for this control strip indicated that the current flow is stable and uniform (i.e., equal current density of $6.35 \times 10^8 \text{ A/m}^2$) across the cross section of the strip.

All 5 designs were modelled by removing 6.74 mm^3 of material from the Manganin strip. The flow of current was found to be unstable at all the cut outs on the Manganin strip. The result shown in Fig. 5(a) consists of a drilled hole cut through the centre of the Manganin. The current flow around

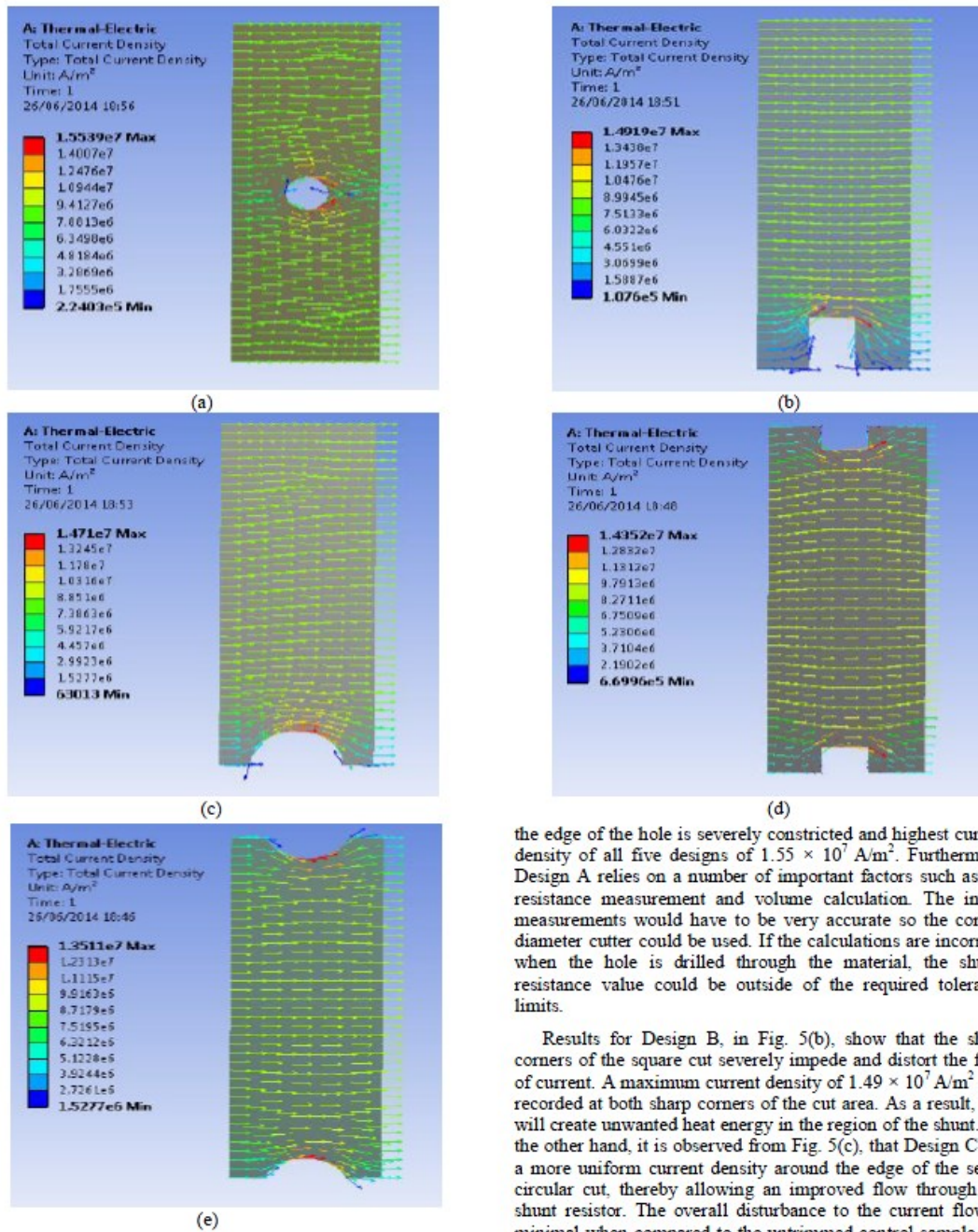


Fig. 5. Total current density results using ANSYS 14.5 for Manganin strip with different trimming patterns, using: (a) Design A – hole cut, (b) Design B – square cut, (c) Design C – semi circular cut, (d) Design D – double semi circular ended cut and (e) Design E – double square ended cut.

the edge of the hole is severely constricted and highest current density of all five designs of $1.55 \times 10^7 \text{ A/m}^2$. Furthermore, Design A relies on a number of important factors such as the resistance measurement and volume calculation. The initial measurements would have to be very accurate so the correct diameter cutter could be used. If the calculations are incorrect, when the hole is drilled through the material, the shunt's resistance value could be outside of the required tolerance limits.

Results for Design B, in Fig. 5(b), show that the sharp corners of the square cut severely impede and distort the flow of current. A maximum current density of $1.49 \times 10^7 \text{ A/m}^2$ was recorded at both sharp corners of the cut area. As a result, this will create unwanted heat energy in the region of the shunt. On the other hand, it is observed from Fig. 5(c), that Design C has a more uniform current density around the edge of the semi-circular cut, thereby allowing an improved flow through the shunt resistor. The overall disturbance to the current flow is minimal when compared to the untrimmed control sample and remains relatively linear around the cut section, with a maximum current density of $1.47 \times 10^7 \text{ A/m}^2$ being recorded.

Design D and Design E, illustrated in Figs. 5(d) and (e) respectively, consist of double entry square and semi-circular cuts from opposing sides of the Manganin strip. These designs produce similar patterns of relatively smooth current flow through the central area of the Manganin and have the desired effect of further reducing the maximum current density to $1.44 \times 10^7 \text{ A/m}^2$ for Design D and $1.35 \times 10^7 \text{ A/m}^2$ for Design E. However it was considered that the double entry cut approach would be more difficult to control in practice as the designs consist of material removal from both sides of the Manganin strip and the two voltage terminals could also interfere with the machining at one side of the strip, see Fig. 3.

The best current flow pattern is one that travels through the part linearly with as little disruption as possible. It was observed the semi-circular cut allowed a much more uniform current flow than the square cut and further analysis revealed that as the diameter of semi-circular cut was increased, the rate of change of resistance was reduced but the control of resistance accuracy was improved. Through these observations, it is concluded that Design C presents a better approach to trimming the Manganin shunt resistor in terms of minimising current density and temperature rise and improving resistance accuracy, whilst Design B may have the potential to give higher rates of resistance change and thus reduce trimming time. Moreover both designs consist of single entry cuts which will simplify the machining operation and also allow the easy measurement of the resistance during the trimming process. Therefore two designs which are Design B and Design C were selected for trimming trials to make a comparison with the theoretical analysis.

D. Initial Trimming

Both designs B and C were trimmed using Bridgeport milling machine with different types of cutter. In particular, a slitting saw capable of producing perfectly square corners was used to create 6 samples for Design B by using different blade thickness of 1.5 mm, 1.75 mm and 2 mm (i.e., 2 samples for each cutter size). For Design C, an end mill cutter is used to create the semi-circular cut by using 3 mm, 3.5 mm and 4 mm diameter tools for 6 samples (i.e., 2 samples for each cutter size).

After trimming, the resistance of all 12 samples of shunt resistor were measured again using the digital micro-ohmmeter to obtain the final resistance value. Each reading was taken 5 times to make sure the accuracy and repeatable of the results were consistent with the initial resistance measurements. All readings were recorded and the average value was compared with the initial readings to see if the resistance tolerance was reducing after trimming.

V. RESULTS AND DISCUSSIONS

Fig. 6 shows results for resistance before and after the trimming process for Designs B and C obtained from the digital micro-ohmmeter, where the required target is to achieve a resistance of $100 \mu\Omega$. The initial resistance values before trimming have minimum and the maximum values as $95.28 \mu\Omega$ and $97.72 \mu\Omega$ respectively. The corresponding mean value is $96.33 \mu\Omega$. The dashed line indicates the target resistance value of $100 \mu\Omega$ to be achieved.

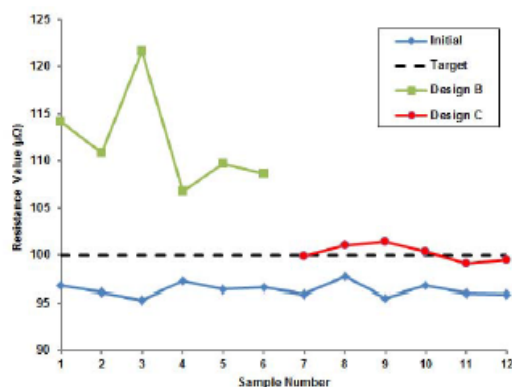


Fig. 6. Resistance value for 12 sample of shunt resistors during the initial trimming trials.

It is noted that there are significant variations in the generated resistance values after the trimming process for Design B and C. Samples 1-6 are trimmed using Design B while samples 7-12 are trimmed using Design C. Fig. 6 is divided into two sections, where trimmed samples for Design B have higher resistance values than targeted as compared to Design C with much lower resistance values close to the targeted resistance. The minimum and maximum resistance values for Design B are $106.8 \mu\Omega$ and $121.64 \mu\Omega$ whereas for Design C are $99.08 \mu\Omega$ and $101.38 \mu\Omega$ respectively.

It was observed that the rate of change of resistance was much higher for samples trimmed using Design B compared to Design C. Moreover, the final resistance values obtained for Design B were much higher than the target value of $100 \mu\Omega$ and were difficult to control within any reasonable tolerance limits. Design C shows more controllable final resistance values after the trimming that are much closer to the target value of $100 \mu\Omega$. The mean and standard deviation for Design B are calculated at $111.94 \mu\Omega$ and $4.89 \mu\Omega$ while for Design C they are $100.18 \mu\Omega$ and $0.8 \mu\Omega$ respectively.

VI. CONCLUSION

In this paper, the theory, designs and techniques for trimming shunt resistors in metering applications have been examined. Based on these investigations, a method using a milling machine has been proposed to demonstrate whether the standard tolerance of $\pm 5\%$ for $100 \mu\Omega$ shunt resistors could be reduced. The outcomes from the initial trimming were very promising with the tolerance being reduced to approximately $\pm 1\%$. This meant that the process of trimming the shunt resistors was very much possible if it could be done on a larger scale. This will help to develop and optimize a novel trimming process to adjust the tolerance and improve the performance of Manganin shunt resistors in the production of energy metering devices. It will also deliver the high linearity required for accurate power measurement and the isolation necessary to meet industry standards in regulating power and communications for smart energy meters. The experimental results presented in this paper will serve as a guide for further

study in conducting the trimming process using concurrent and predictive trimming methods to improve tolerance accuracy and reduce the trim time.

ACKNOWLEDGMENT

This work is funded and supported by Majlis Amanah Rakyat, Malaysia (MARA) and special thanks to TT Electronics PLC for providing the shunt resistor samples for this research.

REFERENCES

- [1] M. Conner, Tamper-resistant smart power meters rely on isolated sensors, in *Sensors and Machine Vision / A Supplement to Design News*, ed, 2009, p. 5.
- [2] T. Harbert. (2008) Chip companies all charged up over smart meters. EDN Network. 1-2. Available: <http://www.edn.com/electronics-blogs/other/4325425/Chip-companies-all-charged-up-over-smart-meters>.
- [3] B. Verma. (2009, 23 January 2013). Announcement: Key milestone for smart meters rollout. Available: <https://www.gov.uk/government/news/key-milestone-for-smart-meters-rollout>.
- [4] C. R. Cosens, Electro-plating copper on manganin, *Journal of Scientific Instruments*, vol. 10, pp. 256-258, 1933.
- [5] Isabellenhütte Company. (2 December 2012). Manganin. Available: http://www.isotekcorp.com/sites/default/files/sites/default/files/pdfs/Manganin_0.pdf.
- [6] Texas Instruments, Smart Metering, ed: Texas Instruments Incorporated, 2009.
- [7] Cropico. (2007, A Guide to: Low Resistance Measurement. 39. Available: <http://www.seaward.co.uk/downloads/Guide%20to%20Low%20Resistance%20Booklet.pdf>
- [8] F. Y. Wu, Theory of resistor networks: the two-point resistance, *J. Phys. A: Math. Gen.*, vol. 37, pp. 6653-6673, 2004.
- [9] P. Sandborn and P. A. Sandborn, A Random Trimming Approach for Obtaining High-Precision Embedded Resistors, *Advanced Packaging, IEEE Transactions on*, vol. 31, pp. 76-81, 2008.
- [10] I. Peroni, E. Gottardi, A. Peruzzi, G. Ponti, and G. Ventura, Thermal conductivity of manganin below 1 K, *Nuclear Physics B - Proceedings Supplements*, vol. 78, pp. 573-575, 1999.
- [11] Brown & Sharpe Manufacturing Company, *Practical Treatise on Milling and Milling Machines*. Brown & Sharpe Manufacturing Company, 1914.

Practical Implementation of a Concurrent Trimming Approach for Manganin Shunt Resistors

Siti Nabilah Misti, Martin Birkett, David Bell, Roger Penlington

Abstract— As electrical energy prices continue to rise each year, accurate energy consumption monitoring becomes increasingly important. Therefore, there is a growing demand for high precision, low value shunt resistors in order to measure the flow of electrical current in applications such as smart energy meters and electric vehicle charging stations. This paper will discuss the concurrent trimming approach using machining to reduce the standard $\pm 5\%$ tolerance of $100\mu\Omega$ Manganin shunt resistors which is used in metering applications. The experimental results reveal that the concurrent trimming approach can reduce the standard trimming time by more than 50% more than half the normal trimming time. The resistance value of shunt is obtained approximately at $100\mu\Omega$ and is in the range of targeted value of $100\mu\Omega$ with tolerance of less than $\pm 5\%$.

Keywords—Concurrent trimming, Manganin shunt resistor, machining, tolerance.

I. INTRODUCTION

Manganin shunt resistors are used in smart energy meters to determine the amount of energy consumed by the household. These shunt resistors are typically manufactured by using a Manganin alloy element that is electron beam welded to two copper terminations. Due to the current manufacturing techniques used in the production of the Manganin shunt, it is difficult to produce resistors to an accurate dimensions and hence precise resistive tolerances. Currently, this configuration can achieve resistance values down to $100\mu\Omega$ with tolerances of $\pm 5\%$ [1-3]. Consequently, manufacturers of the shunt resistors are still looking at ways to reduce the tolerance, hence improving the accuracy and precision of the device.

Precise resistance of the shunt can be calibrated through a process known as trimming, where material is partially removed or "trimmed" from the shunt until the resistance reaches its targeted value [4, 5]. This, only works if the shunt resistors are intentionally manufactured with a lower resistance than the targeted value. Theoretically, by trimming the resistive material into a tolerable and symmetrical shape, it can lower the standard tolerance of the shunt resistors [6, 7]. By removing controlled amounts of Manganin from the shunt, the tolerance of the Manganin shunt resistors can be lowered to less than $\pm 5\%$.

The normal approach in trimming the shunt resistors requires a trial and error approach (i.e. measure the resistance value, calculate how much material to remove, trim the shunt resistor based on the amount of material to be removed and finally measure the resistance after the shunt has been trimmed). As the normal approach of testing and modifying the test subject is a step by step process, it can take an excessively long time to complete. Therefore by adopting the concurrent engineering method, in the product development and for a large scale manufacture the production time can be significantly reduced.

Concurrent engineering, also known as simultaneous engineering is a method of designing and developing products, in which the different stages run simultaneously, rather than consecutively. Recent relevant research studies [8-11] have discovered that the concurrent method decreases product development time and also the time to market, leading to improved productivity and reduced costs. Though initial implementation can be challenging, the competitive advantage means it is beneficial in the long term. It removes the need to have multiple design reworks, by creating an environment for designing a product right the first time round.

Similarly, with the trimming approach for the shunt, there are a number of stages that needed to be considered in order to reduce the tolerance of the resistor. The concurrent trimming approach is different from the normal process because it anticipates the amount of material that needs to be removed from the shunt resistors in its testing stages. The main purpose of concurrent trimming is to simultaneously trim and measure the resistive material without the need to retest the trimmed part afterwards. Whereby applying the concurrent technique, the result will be obtained faster and the design of the newly trimmed shunt resistor can be finalized. However, the concurrent trimming approach needs to be done carefully because if there is a mistake in removing the resistive material, the process might have to be repeated with a new shunt resistor. Therefore, precision in this stage is crucial.

The concurrent approach can be used in two different ways which are by automated and manual approach. The automated system will need a much large amount of investment than the manual process. Thus, the manual approach will be a more suitable process to test the theory and determine if the concurrent trimming approach is worthwhile.

Siti Nabilah Misti*, Martin Birkett, David Bell and Roger Penlington, are with Northumbria University Newcastle, United Kingdom
*Emailid: siti.misti@northumbria.ac.uk

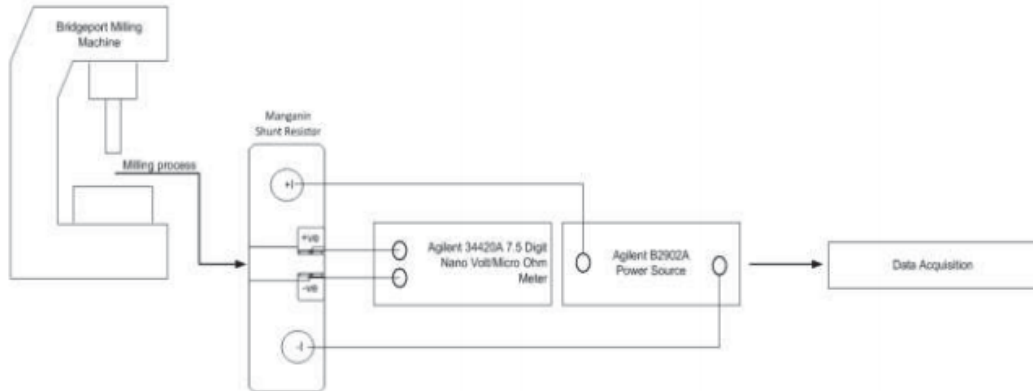


Fig. 1: Block diagram of the experimental setup.

II. THE EXPERIMENT SETUP

Fig. 1 depicts the block diagram of the experimental setup for the proposed research, with the relevant parameters summarized in Table I. The concurrent trimming approach encompasses three main building blocks, which include: Bridgeport milling machine, Agilent B2902A Power Source and Agilent 34420A 7.5 Digit Nano-Volt/Micro-Ohm Meter.

TABLE I
PARAMETERS OF THE EXPERIMENTAL SETUP

| Agilent B2900A Power Source | |
|------------------------------------------|-----------------|
| Parameter | Value |
| Data Source | |
| Modulation format | Amps (I) |
| Source rate | 1 A |
| Source ranging | 1 μ A |
| Limit | 0.5 V |
| Force | \pm 250 V max |
| Pulse | |
| Peak | 0 nA |
| Delay | 5 ms |
| | 50 μ s |
| Trigger (Auto) | |
| Source | 1 |
| Measure | 1 |
| Agilent 34420A Nano-Volt/Micro-Ohm Meter | |
| Parameter | Value |
| Function | DCV/Temp |
| Range/Digits | 7 |
| Max Measurement level | 12 V |
| Sense | Ω 4W |

For the Bridgeport milling machine, a 3mm diameter end-mill cutting tool was chosen for the experiment as the milling area will be on Manganin strip which has a width of 5mm. The shank of the cutting tool was electrically insulated from the milling machine using a nylon sleeve. The shunt resistor was

also clamped in a nylon jig to insulate it from the machine vice. The shunt was connected to two electrically conductive cables to deliver the current and another cable to measure the voltage values. The current cable was fixed to the shunt and jig by using 6mm diameter nut and bolt while the voltage sense cable was directly soldered to two pre-welded tin plated termination pins on the shunt using silver solder.

For the Agilent B2902A Power Source, the current was set to be an output of 1A with the voltage limit set to 0.5V. Table II shows that the combined measurement accuracy for the Agilent 34420A 7.5 Digit Nano-Volt/Micro-Ohm Meter with the Agilent B2900A Power Source gives a total system error of 0.186%. This must be taken into account when analyzing results from this work.

TABLE II
MEASUREMENT SYSTEMS ACCURACY

| Parameter | Value | |
|----------------------|-----------------------------|------------------------------------------|
| | Agilent B2900A Power Source | Agilent 34420A Nano-Volt/Micro-Ohm Meter |
| % Reading | 0.03 | |
| Offset | 0.0015 | |
| % Range | | 0.0002 |
| Total error | 0.0018 | 0.00000012 |
| Total % Error | 0.18 | 0.006 |
| Total System % Error | 0.186 | |

The concurrent trimming approach for this experiment involved an operative to carry out every action needed in the normal process. However, instead of measuring resistance and then trimming small amounts of Manganin from the shunt resistor consecutively, it is possible to continuously measure the resistance value using the combination of Agilent B2902A Power Source and Agilent 34420A 7.5 Digit Nano-Volt/Micro-Ohm Meter, whilst simultaneously removing the Manganin from the shunt resistor. By carrying out the

measuring and milling actions simultaneously or concurrently, it will be quicker than doing the actions separately or consecutively as with the normal trimming process.

III. METHODOLOGY AND POST-ANALYSIS

A. Data Acquisition

Upon feeding 1A of current to the Manganin shunt resistors from the Agilent B2900A Power Source the initial values of resistance were taken before the trimming process started. Resistance values were taken every 15 seconds for 1 minute, to allow the voltage readings from the nano-volt meter to stabilize. Following this, the end mill cutter position was zeroed against the surface of the Manganin area to be trimmed. Then, the value of depth of cut was set using a dial test indicator (DTI), before the milling procedure took place. For initial testing, the Manganin was cut dry at two different cutting speeds of 500m/min and 1000m/min and the feed rate was kept constant at 50m/min.

During cutting process, the nano-volt meter digital readout displayed the voltage slowly increasing until it reached the target value of 100μΩ. The milling action was then stopped and the trimmed shunt resistor was removed from the jig.

B. Computation of Material Removal

Resistance values recorded from the initial testing in Table III and Table IV were compared and it can be clearly seen that the faster speed of the spindle; the more accurate values are recorded.

TABLE III
INITIAL TRIALS BY USING FAST SPINDLE SPEED

| Sample Number | Average Initial Resistance (μΩ) | Depth of cut (mm) | Average Resistance After (μΩ) |
|---------------|---------------------------------|-------------------|-------------------------------|
| 1 | 101.795 | 0.04 | 102.597 |
| 2 | 102.463 | 0.04 | 103.574 |
| 3 | 103.451 | 0.04 | 104.675 |

TABLE IV
INITIAL TRIALS BY USING SLOW SPINDLE SPEED

| Sample Number | Average Initial Resistance (μΩ) | Depth of cut (mm) | Average Resistance After (μΩ) |
|---------------|---------------------------------|-------------------|-------------------------------|
| 1 | 104.473 | 0.04 | 106.502 |
| 2 | 106.115 | 0.04 | 108.524 |
| 3 | 108.139 | 0.04 | 110.574 |

Over 20 initial trials were carried out and on average; the faster speed gives smaller rate of change which is 25.25μΩ/mm while slower speed gives higher rate of change of resistance which is 25.54μΩ/mm. This can be related to an increase in the amount of heat being transferred into the shunt at the slower machining speed. Based on the initial trials, the speed and the depth of the cut were used as a reference to predict the amount of material to be removed from the Manganin shunt resistors. The mean change of resistance of 1.1μΩ over 40μm depth gives an estimated rate of change of 0.028μΩ/μm.

Estimation of the change in resistance at the higher machining speed can be made by using 0.028μΩ/μm (i.e., the value calculated from Table III). This estimation will help in achieving the main objective which is to lower the tolerance of ±5% for the Manganin shunt resistor. After the initial resistance readings are recorded, the value will be deducted from the target value of the shunt resistor (i.e., resistance value of 100μΩ) and then divided by 0.028μΩ/μm to predict the depth of cut for the milling process for any Manganin shunt resistor.

IV. RESULTS AND DISCUSSIONS

Result generated from MATLAB in Fig. 2 show that the resistance change can be predicted before the milling process by using the change of resistance acquired and calculated in the trial runs. Comparing the calculated value and the actual result, the prediction or estimation is proven to be reliable.

These findings suggest that the concurrent trimming approach is a feasible method to monitor the rate of change for the resistance of Manganin shunt resistor and to determine the desirable depth and amount of material removal from Manganin strip. The depth of the end mill cutter must be concurrently examined with the micro-ohm meter readings to identify if the trimming process needs to be stopped before the depth of cut reaches the calculated amount.

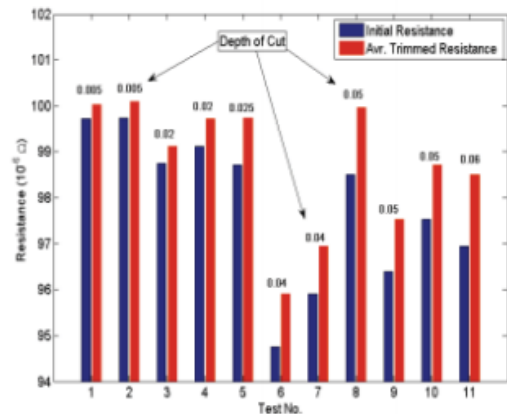


Fig. 2: The corresponding resistance values of the Manganin shunt resistors using different depth of cut to predict the rate of change for the resistance.

The calculated depth of cut can be used in order to find the amount of material to be removed and also to predict how much the resistance value will increase in accordance to the trials of concurrent trimming approach.

Furthermore, Fig. 3 shows results for initial resistance and after the trimming process for concurrent trimming approach; where the required target is to achieve a resistance of 100μΩ. Only 3 samples are used for the experiment due to the limited number of sample received for this project. Sample 3 gives the highest value of resistances after the concurrent trimming approach is conducted which is 100.335μΩ whereas for Samples 1 and 2 are 100.081μΩ and 100.094μΩ respectively.

The average value for all 3 samples is 100.17 $\mu\Omega$ which is 0.17% of the tolerance resistance.

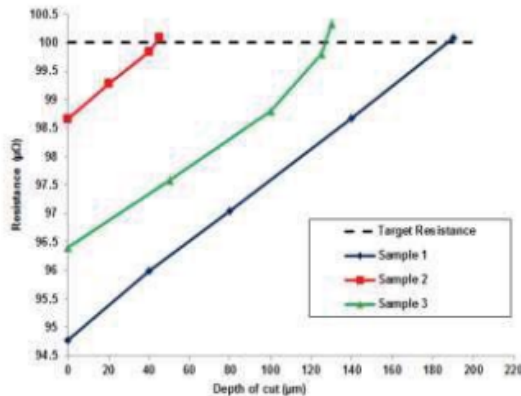


Fig. 3: Graph of resistance vs. depth of cut for the concurrent trimming of Manganin shunt resistors.

V. CONCLUSION

Results from this paper have shown that the concurrent trimming process is a viable method of trimming the resistance value of Manganin shunt resistors. It offers improved trimming accuracy and reductions in time and process costs when compared to the normal consecutive process. This procedure has the potential for application in large scale manufacture when the best point of reference of the trimming process for the shunt resistors is discovered and it will give a lot of benefit to the manufacturer in terms of quality assurance, time and cost. By using concurrent trimming in this experiment, the tolerance of the Manganin shunt resistors is reduced from $\pm 5\%$ of tolerance to less than $\pm 0.5\%$ in a shorter time compared to the normal consecutive trimming process.

ACKNOWLEDGMENT

This work is funded and supported by Majlis Amanah Rakyat, Malaysia (MARA).

REFERENCES

- [1] TT Electronics. (2009, Resistors For Energy Metering - Application Note. (2). Available: http://www.ttelectronics.com/z_downloads/tt_electronics_metering_brochure.pdf
- [2] Vishay Intertechnology, "Application Note: Resistive Products," ed, 2008.
- [3] Isabellenhütte Company. (2012, Low-Ohmic Precision And Power Resistors. 14. Available: http://www.isabellenhuetten.de/uploads/media/IHH_Bauelementebroschuere_engl_01.pdf
- [4] P. Mach and P. Svasta, "Influence of trimming of resistive thick films on nonlinearity of their current vs. voltage characteristics," in Electronics Technology: Meeting the Challenges of Electronics Technology Progress, 2004. 27th International Spring Seminar on, 2004, pp. 309-312 vol.2.
- [5] T. Tobita and H. Takasago, "New trimming technology of a thick film resistor by the pulse voltage method," Components, Hybrids, and

- Manufacturing Technology, IEEE Transactions on, vol. 14, pp. 613-617, 1991.
<http://dx.doi.org/10.1109/33.83952>
- [6] F. Y. Wu, "Theory of resistor networks: the two-point resistance," J. Phys. A: Math. Gen., vol. 37, pp. 6653-6673, 2004.
<http://dx.doi.org/10.1088/0305-4470/37/26/004>
- [7] L. M. Landsberger. (2007, 22 November 2013). Simplifying Circuit Calibration With Electrically-Adjustable Resistors. [Microbridge Technical White Paper]. 10. Available: http://www.mbridge.com/pdfs/microbridge_032307.pdf
- [8] Y.-S. Ma, G. Chen, and G. Thimm, "Paradigm shift: unified and associative feature-based concurrent and collaborative engineering," Journal of Intelligent Manufacturing, vol. 19, pp. 625-641, 2008.
<http://dx.doi.org/10.1007/s10845-008-0128-y>
- [9] E. A. Fielding, J. R. McCardle, B. Eynard, N. Hartman, and A. Fraser, "Product lifecycle management in design and engineering education: International perspectives," Concurrent Engineering, vol. 22, pp. 123-134, 2014.
<http://dx.doi.org/10.1177/1063293X13520316>
- [10] D. Yang and M. Dong, "A hybrid approach for modeling and solving product configuration problems," Concurrent Engineering, vol. 20, pp. 31-42, 2012.
<http://dx.doi.org/10.1177/1063293X11436219>
- [11] H.-C. Chang and H.-Y. Chen, "Optimizing product form attractiveness using Taguchi method and TOPSIS algorithm: A case study involving a passenger car," Concurrent Engineering, p. 1063293X13520317, 2014. S. P. Bingulac, "On the compatibility of adaptive controllers (Published Conference Proceedings style)," in Proc. 4th Annu. Allerton Conf. Circuits and Systems Theory, New York, 1994, pp. 8-16.
<http://dx.doi.org/10.1177/1063293X13520317>

About Author (s):



Siti Nabilah Misti is currently a PhD researcher at the Department of Mechanical Engineering, Northumbria University Newcastle, United Kingdom. She received her MSc degree in Engineering from the Northumbria University in 2012 and BSc degree in Production & Operation (Manufacturing) from Universiti Tun Hussein Onn Malaysia (UTHM), Malaysia in 2008. She worked as Operation Manager for 3 years back in Malaysia before furthering her studies for master degree. Her research interests include product and process development and optimization, Total Productive Management (TPM) and manufacturing.



Martin Birkett is a Senior Lecturer within the Mechanical Engineering Department at Northumbria University, UK. He worked in the manufacturing industry for sixteen years and also did some part time lecturing. During the time in the industry, he completed a Craft Apprenticeship in Engineering Maintenance before moving on to work as a Production Engineer and then Senior Research and Development Engineer. During this period, he also continued to study on a part-time basis for ONC/HNC and then my BEng (Hons) and PhD degrees, both of which are completed at Northumbria University. His research interests include development and optimization of materials and manufacturing processes.



David Bell was awarded a BSc in Industrial Technology from Newcastle upon Tyne Polytechnic in 1985 and an MSc in Industrial Technology from Teesside Polytechnic in 1986. He is a Fellow of the Higher Education Academy and prior to that a Member of the ILT since 2002. He is currently employed as Associate Dean International within the Faculty of Engineering and Environment at Northumbria University. He has worked at Northumbria University in various roles since 1982 including the role of Acting Dean for 16 months. Prior to academia he worked in industry for companies such as Thorn, Electrolux and

Moore International as a Manufacturing Engineer, Engineering Manager and Business Manager. Current research interests include Manufacturing improvement tools. He became a member of the IET and Chartered Engineer in 1986.



Roger penlington is Research Fellow in the Department of Mechanical and Construction, Northumbria University, UK. He did his first degree at Sheffield City Polytechnic and his PhD was in glass manufacture at Sheffield Hallam University (SHU). He joined Northumbria in 1994 to undertake research into glass manufacture specifically aspects related to heat transfer, fluid flow and forming processes. He took up a lecturing role in 1998 and have been awarded a Teaching Fellowship in recognition of research into engineering education. His research interests are in the areas of manufacturing technology with particular reference to fluid dynamics and heat transfer in glass manufacture and electronic components. He also active in engineering education research serving on the steering committee of the UK Engineering Education Special Interest Group. In his research, he seek to retain links between industry and academia through project sponsorship and also currently serve as President of the Society of Glass Technology.

EXPERIMENTAL INVESTIGATION INTO ABRASIVE CONCURRENT TRIMMING FOR MANGANIN SHUNT RESISTOR

*Siti Nabilah Misti
Northumbria University
Newcastle upon Tyne, United Kingdom

Martin Birkett
Northumbria University
Newcastle upon Tyne, United Kingdom

David Bell
Teesside University
Middleborough, United Kingdom

Roger Penlington
Northumbria University
Newcastle upon Tyne, United Kingdom

Keywords: Design of Experiment (DoE); trimming; shunt resistor
** Corresponding author Phone: 01912274301, Fax: 01912273167*
E-mail address: siti.misti@northumbria.ac.uk

ABSTRACT

This paper presents a novel electro-mechanical trimming process to improve the accuracy and performance of 100 $\mu\Omega$ Manganin shunt resistors for use in current sensing applications such as smart energy meters. More specifically, the work focuses on the development of a precision trimming process to improve the resistance tolerance of the shunt resistors. A novel laboratory prototype of an automated concurrent trimming system is developed which combines the mechanical cutting process and electrical measurement system to remove controlled amounts of material from the Manganin shunt. Designs of experiments are conducted in order to find the optimum feed rate and cutting speed for the trimming process. The impact of cutting speed between 250 to 2500 m/min and feed rate between 1 to 15 mm/min was investigated. The optimum speed is measured at 1750 m/min with the feed rate at 1 mm/min. The results obtained can be used to inform production processes for large scale manufacture of precision shunt resistors.

INTRODUCTION

As electrical energy prices continue to rise, accurate energy consumption monitoring is becoming increasingly important and the introduction of smart energy meters is well-known in this capacity [1, 2]. The smart energy meters primary role is to provide the user with accurate real-time data to aid them in making informed decisions regarding their energy usage. However, to do this efficiently and accuracy of the meter itself must also be minimized [3].

One of the key components in the smart energy meter is the current sensing shunt resistor and its resistance must be as low as possible, typically in the range 100 $\mu\Omega$ to 10 m Ω , to minimize energy usage. Although this low resistance requirement reduces power consumption it is inherently difficult to manufacture shunt resistors in this micro-ohm range to the required precision and at reasonable cost. Typical resistance accuracy of commercially available shunts suitable in this application is 100 $\mu\Omega$ \pm 5%, which can in turn lead 5% errors in power measurement within the smart meter.

In this work, a novel laboratory prototype of an electro-mechanical trimming process is developed to trim the shunt resistor in order to reduce their tolerance from \pm 5% to \pm 1%. Different types of machining process and suitable geometry have already been analysed by the authors [4]. The focus now is to select, develop and optimise a trimming process that can be used in manufacturing stage. The developed process has to be practical and cost effective as it would probably be used widely on the production floor as the government already announced that all mechanical meter in each household and industry will be changed to smart energy meter by 2020. The demand for total production of smart energy meter is estimated to be around 30 million units [2, 5-7].

This paper presents the results of work undertaken to observe the effect of various cutting speeds and feed rates on the trimmed properties of components. A full factorial of

Designs of Experiment (DoE) was undertaken to find the optimum process settings under which to trim the Manganin shunt resistors.

The experiments involved the variation of cutting speed and feed rate each at four levels as seen in Table 1. The effect of two factors (cutting speed and feed rate), on the trimming time (s) and resistance deviation (%) of the shunt resistor sample was evaluated. The experiment was designed as a full factorial design with $4^2 = 16$ treatment combination which were repeated 3 times giving a total of 48 runs (Refer Annex A) to observe the effect of each factor level on the process outputs.

Table 1: Process factors and their corresponding levels for the experiment.

| Factor | Level 1 | Level 2 | Level 3 | Level 4 |
|-----------------------|---------|---------|---------|---------|
| Cutting speed (m/min) | 250 | 1000 | 1750 | 2500 |
| Feed rate (mm/min) | 1 | 5 | 10 | 15 |

EXPERIMENTAL SETUP

The shunt samples (Figure 1) were trimmed using a Buehler Isomet 5000 linear precision saw, fitted with a 178 mm diameter, 0.8 mm thick rubber bonded silicon carbide (R/SiC) AcuThin cutting disc. The samples were mounted in an insulated trimming jig which was secured in the machine vice and the cutting disc was rotated at a 250 to 2500 m/min and fed into the side of the shunt at feed rates of 1 to 15 mm/min.

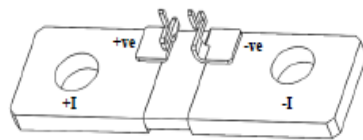


Figure 1: Manganin shunt resistor sample.

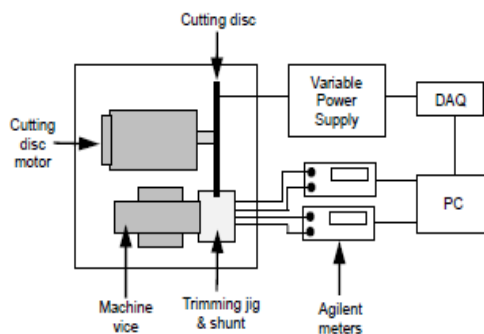


Figure 2: Schematic of the concurrent trimming system using linear precision saw.

Figure 2 shows a schematic of the concurrent trimming system where the resistance value of the shunt was continuously measured during trimming using the combination of Agilent B2900A power supply and 34420A nanovolt meter. All resistance measurements were performed using the 4-wire Kelvin method. A fixed current of 1 A was supplied to the shunt via its current (I) terminals from an Agilent B2900A source meter, whilst the voltage drop across its pre-soldered voltage (V) terminals was continuously monitored using an Agilent 34420A nanovolt meter.

The concurrent trimming system is controlled using a National Instruments USB-6000 data acquisition (DAQ) device and the program is organized via LabVIEW 2015 software. The DAQ device can act as a D/A converter and A/D converter, and it has both a digital output/input channels and an analogue input channel. The experiment used the digital output channel, which is connected to a relay in an external circuit and sends a control signal to the precision saw. The flow of the program in LabVIEW can be seen as shown in Figure 3.

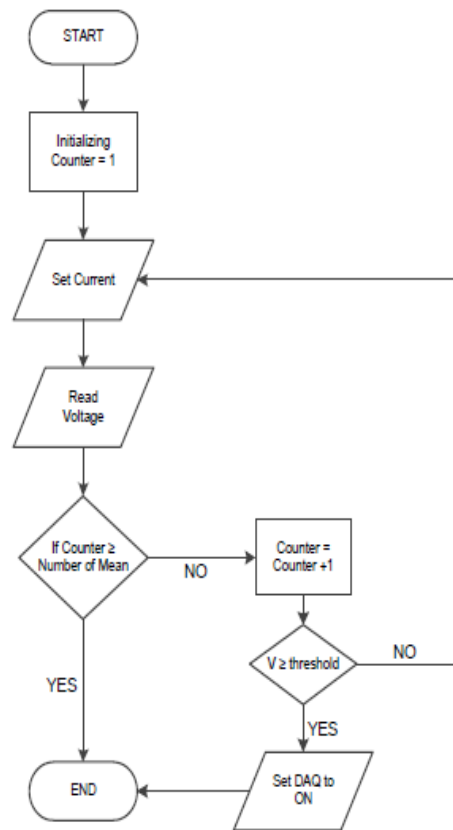


Figure 3: Flow diagram of the proposed trimming control.

The software is designed to make sure that the current is set at 1A with a 0.5V limit upon start-up and measures the voltage drop at the rate of 2 measurements per second which is converted to resistance value. Figure 4 shows the front panel used to control the experiment. Target resistance is inputted before the experiment starts, and is typically set at 1% from initial value. Once the measured resistance value monitored in the LabVIEW software reaches the target value, the DAQ will be activated and will send a signal to the cutting disc to retract from the shunt. The full LabVIEW automated system can be seen in Annex B.

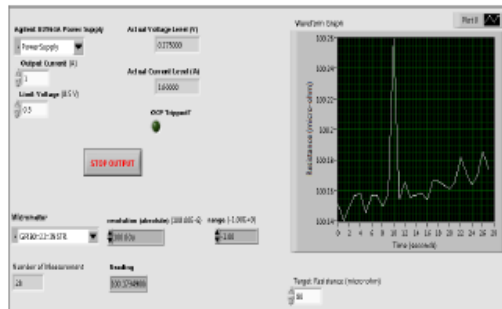


Figure 4: Front panel of the LabVIEW system.

Surface roughness was measured using Alicona Infinite Focus G4 optical scanner having a resolution of 0.01µm. All measurements conformed to ISO4287 and ISO4288.

RESULTS AND DISCUSSION

The experimental data was analysed using Minitab 17 statistical software package to evaluate the average effect of each factor level on the trimming time and the resistance deviation of the shunts. The Percentage Contribution Ratio (PCR) from an analysis of variance (ANOVA) is also calculated. The statistical tools are important indicators in order to show which parameters have the most significant effect on the product quality or process performance. Therefore, the obtained data were subjected to an ANOVA test which is an important method used for interpreting experimental data and making essential decisions.

Percent contribution in a variance analysis reflects total variance attributed to all factors in an experiment [8]. PCR for each variable is calculated using equation 1 below:

$$PCR = \frac{Exp\ SS}{Total\ SS} \tag{1}$$

where; *Exp SS* is the expected sum of squares for each of the factors and *Total SS* (sum of squares). *Exp SS* is calculated using equation 2:

$$Exp\ SS = SS - Error\ MS \tag{2}$$

and the model error of the experiment can be calculated by:

$$Model\ error = 100\% - (Total\ PCR\ for\ all\ factors) \tag{3}$$

The percent contributions of error and factors associated with trimming time are given in Table 2. Feed rate and cutting speed were both found to be statistically significant factors at the 5% level [9], having P values of 0 and 0.01 respectively. Feed rate had a high PCR value of 91.44% compared to that of cutting speed which was 2.64%. The relatively small error level (5.92%) associated with the trimming time was within the acceptable levels (up to 15%), suggesting that all important factors had been considered and measurements accurately performed [10].

Table 2: ANOVA results for Time (s).

| | DF | SS | MS | Exp SS | F | P | PCR |
|---------------|----|-------------|-------------------------------|-------------|------------|------------|-------|
| Feed Rate | 3 | 407 5.08 | 135 8.36 | 4068. 95 | 221. 66 | 0* | 91.44 |
| Cutting Speed | 3 | 123. 58 | 41.1 9 | 117.4 5 | 6.72 | 0.0 01* | 2.64 |
| Error | 41 | 251. 25 | 6.13 | - | - | - | 5.92 |
| Total | 47 | 444 9.92 | * Significant at the 5% level | | | | |

DF = Degrees of freedom
 SS = Sum of squares
 MS = Mean of squares
 F = F-test value
 P = Probability
 PCR = Percent contribution ratio

Figure 5 shows the main effects plot for the time that took to trim the shunt resistors. In general, time ranged between 2 and 35 seconds with both factors have a significant effect on the trimming time. The statistical analysis showing that the main contributing factor to trimming time is feed rate with the indication of sharpness in the gradient of the slope. Trimming time reduces from 27.5 to 3.75 seconds with the change of feed rate from 1 to 15 mm/min and from 15 to 11 seconds with the change of cutting speed from 250 to 1750 m/min. Feed rate is found to be much more significant compared to cutting speed with 88.88 % different in PCR.

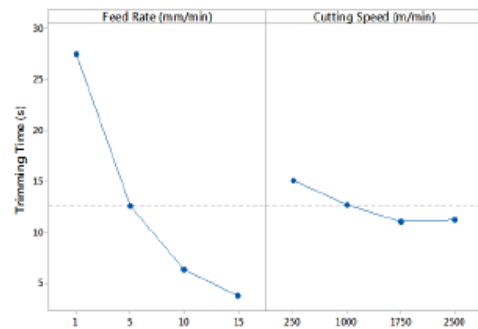


Figure 5: Main effects plot for Trimming Time (s).

Table 3 shows the ANOVA results for the resistance deviation. P values for both feed rate and cutting speed are 0. Although both factors were found statistically significant at the 5% level but the feed rate had the highest PCR for 43.5% followed by cutting speed with 19.23% PCR. The error associated with the resistance deviation (37.27%) was significantly higher than the accepted level (15%) which could be ascribed to possible unconsidered interactions between some of the control factors and that the possibility of not all important factors had been considered.

Table 3: ANOVA results for resistance deviation (%).

| | DF | SS | MS | Exp SS | F | P | PCR | |
|---------------|----|-------------|-------------------------------|-------------|-----------|----|-------|--|
| Feed Rate | 3 | 1.82 362 | 0.60 787 | 1.788 | 17. 06 | 0* | 43.5 | |
| Cutting Speed | 3 | 0.82 579 | 0.27 526 | 0.790 17 | 7.7 3 | 0* | 19.23 | |
| Error | 41 | 1.46 048 | 0.03 562 | - | - | - | 37.27 | |
| Total | 47 | 4.10 989 | * Significant at the 5% level | | | | | |

DF = Degrees of freedom
 SS = Sum of squares
 Exp SS = Expected sum of squares
 F = F-test value
 P = Probability
 PCR = Percent contribution ratio

Figure 6 shows the main effects plot for the resistance deviation. Average resistance deviation measured when trimming the shunt resistors had 1750 m/min cutting speed differed significantly from others cutting speed. Lower resistance deviation was obtained when trimming using lower feed rate and medium cutting speed. Clearly, feed rate was found to have substantial influence on the resistance deviation.

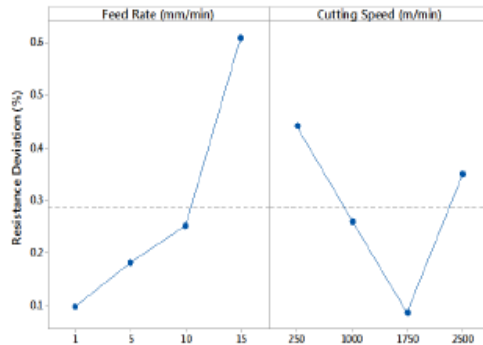


Figure 6: Main effects plot for Resistance Deviation (%).

Essentially the results showed that faster trim time could be obtained when employing a 15 mm/min feed rate with 1750 m/min cutting speed. It can also be seen from the results that a lower resistance deviation can be achieved by trimming at a feed rate of 1 mm/min and a cutting speed of 1750 m/min. In order to be able to further reduce the tolerance of the shunt

resistors, a slower feed rate is needed. However, even trimming at the highest feed rate of 15 mm/min appears to have the potential to produce shunt resistors with a resistance tolerance less than the initial target value of $\pm 1\%$. As feed rate was increased, contact time between the cutting tool and the shunt resistor increased, resulting in an increase in material removal rate.

Further investigation was undertaken on the surface roughness (Ra) of the trimmed shunt resistor to confirm the optimum cutting speed of the trimming process. Figure 7 shows the results of average surface roughness (Ra) as a function of the cutting speed. The tests were conducted at a constant feed rate of 1 mm/min. The results show that the surface roughness decreases with the increased in cutting speed but then increased at 2500 m/min.

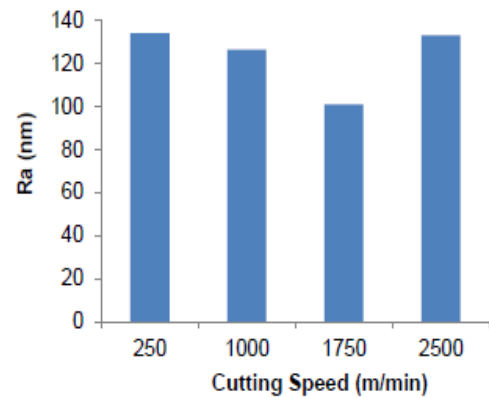


Figure 7: Surface roughness (Ra) versus cutting speed.

Previous studies on different based alloy found that surface roughness increases with increased fibre orientation and feed rate while it decreases with increased cutting speed and depth of cut [11-13]. While their findings cannot be mapped directly to this study, it shows the general trend in both studies are similar where cutting speed had lower effects on Ra. Optimum cutting speed is found to be 1750 m/min and the dynamic balance of the cutting saw becomes an issue at the higher speed of 2500 m/min. At these higher speeds, minor defects such as a notch shank in the cutting disc has been shown to move the tool enough off-centre to induce vibration and hence chatter leading to a deterioration in the surface roughness.

CONCLUSION

This paper has summarized the results of experimental work on the concurrent trimming of 100 $\mu\Omega$ Manganin shunt resistors. The trimming time and resistance deviation showed a strong dependency on the feed rate. The optimum feed rate and cutting speed to reduce the resistance tolerance of the shunt were found to be 1 mm/min and 1750 m/min respectively. Trimming at a low feed rate of 1 mm/min can reduce the

tolerance to very low values of around $\pm 0.1\%$ but this operation takes around 25 seconds to perform. On the other hand, trimming at a higher feed rate of 15 mm/min can give a faster trimming process time of under 3 seconds whilst still maintaining a suitable tolerance of $\pm 1\%$. Even though cutting speed was found to have a less significant effect on the trimming time, using the optimum cutting speed of 1750 m/min can give a significant reduction in resistance tolerance and improvement in surface roughness of the trimmed shunt when compared to slower and faster speeds.

The next stages of this work will involve using these current findings to undertake a more comprehensive study of predicting the removal of material from the shunt resistor associated to smart energy meter. Phase 2 of DoE will be done using smaller range of speed rate between 1500 to 2000 m/min in order to get more accurate results. Moreover, these original results will be extended to be able to use in trimming various type of resistor in the future.

ACKNOWLEDGMENTS

This work is funded and supported by Majlis Amanah Rakyat, Malaysia (MARA).

NOMENCLATURE

| | |
|-------------|-----------------------------------------------------------------------------------|
| $\mu\Omega$ | micro-ohm |
| m Ω | milli-ohm |
| DoE | Design of Experiment |
| \pm | plus-minus, indicating the tolerance or statistical margin of error of a quantity |
| I | electric current |
| % | Percentage |
| A | amplitude |
| mm | millimetres |
| min | minutes |
| nm | nano-meters |
| V | voltage |
| DAQ | Data acquisition |
| LabVIEW | Laboratory Virtual Instrument Engineering Workbench |
| ANOVA | Analysis of Variance |
| PCR | Percentage Contribution Ratio |
| Ra | Surface roughness |

REFERENCES

- [1] K. Casey. (2011, 26 January 2013). The Need for Current Sense, Circuit Protection and Communications in Smart Meters. Available: <http://electronicdesign.com/energy/need-current-sense-circuit-protection-and-communications-smart-meters>
- [2] M. Coaster, "Smart Metering Implementation Programme: Implementation Strategy," DECC and Ofgem 94/10, 27 July 2010 2010.
- [3] K. S. K. Weranga, D. P. Chandima, and S. P. Kumarawadu, "Smart metering for next generation energy efficiency & conservation," in Innovative Smart Grid Technologies - Asia (ISGT Asia), 2012 IEEE, 2012, pp. 1-8.
- [4] S. N. Misti, M. Birkett, D. Bell, and R. Penlington, "A new trimming approach for shunt resistors used in metering applications," in Electronic Design (ICED), 2014 2nd International Conference on, 2014, pp. 94-99.
- [5] A. Molina-Markham, P. Shenoy, K. Fu, E. Cecchet, and D. Irwin, "Private memoirs of a smart meter," in Proceedings of the 2nd ACM workshop on embedded sensing systems for energy-efficiency in building, 2010, pp. 61-66.
- [6] A. Vaughan. (2009, 21 January 2013). Smart energy meters in every UK home by 2020. Available: <http://www.theguardian.com/environment/2009/may/11/smart-meters-energy-efficiency>
- [7] A. MacFaul, "Smart meter Implementation Strategy Prospectus," Department of Energy and Climate Change(DECC) and Ofgem 27 July 2010 2010.
- [8] P. J. Ross, "Taguchi techniques for quality engineering," McGraw-hill International editions, 1996.
- [9] K. A. Pituch, T. A. Whittaker, and J. P. Stevens, Intermediate statistics: A modern approach: Routledge, 2015.
- [10] P. J. Ross, "Taguchi techniques for quality engineering: loss function, orthogonal experiments, parameter and tolerance design," 1988.
- [11] J. Sun and Y. Guo, "A comprehensive experimental study on surface integrity by end milling Ti-6Al-4V," Journal of Materials Processing Technology, vol. 209, pp. 4036-4042, 2009.
- [12] M. Nouari, G. List, F. Girot, and D. Coupard, "Experimental analysis and optimisation of tool wear in dry machining of aluminium alloys," Wear, vol. 255, pp. 1359-1368, 2003.
- [13] Z.-C. Lin, W.-L. Lai, H. Lin, and C. Liu, "The study of ultra-precision machining and residual stress for NiP alloy with different cutting speeds and depth of cut," Journal of materials processing technology, vol. 97, pp. 200-210, 2000.

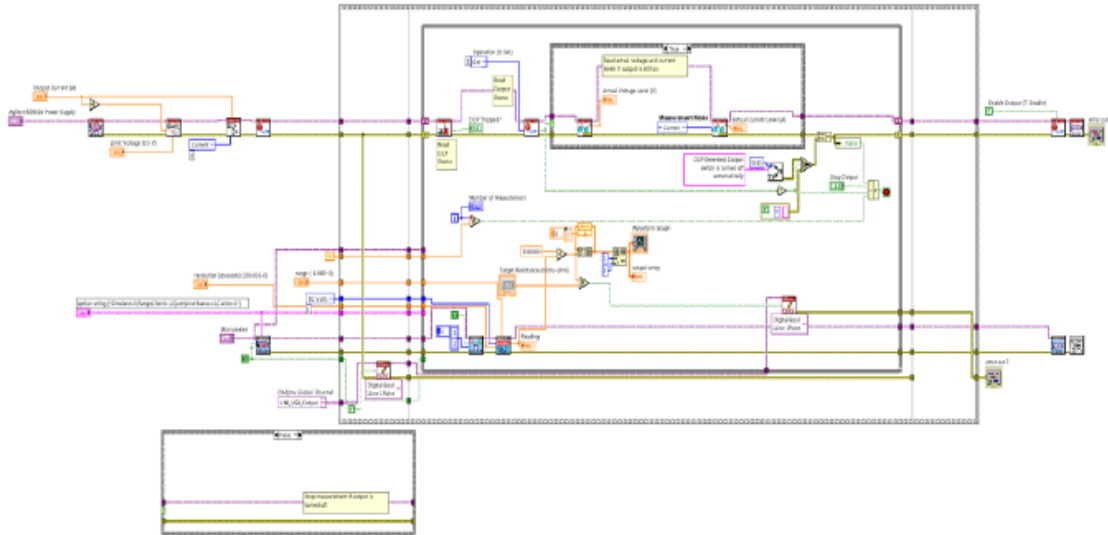
ANNEX A


















FULL FACTORIAL DESIGN MATRIX FOR THE TWO FACTORS (FEED RATE AND CUTTING SPEED)
WITH 4 LEVELS EACH

| StdOrder | RunOrder | PtType | Blocks | Feed Rate (mm/min) | Cutting Speed (m/min) |
|----------|----------|--------|--------|-----------------------|--------------------------|
| 48 | 1 | 1 | 3 | 15 | 2500 |
| 33 | 2 | 1 | 3 | 1 | 250 |
| 45 | 3 | 1 | 3 | 15 | 250 |
| 34 | 4 | 1 | 3 | 1 | 1000 |
| 41 | 5 | 1 | 3 | 10 | 250 |
| 35 | 6 | 1 | 3 | 1 | 1750 |
| 37 | 7 | 1 | 3 | 5 | 250 |
| 36 | 8 | 1 | 3 | 1 | 2500 |
| 44 | 9 | 1 | 3 | 10 | 2500 |
| 38 | 10 | 1 | 3 | 5 | 1000 |
| 39 | 11 | 1 | 3 | 5 | 1750 |
| 46 | 12 | 1 | 3 | 15 | 1000 |
| 43 | 13 | 1 | 3 | 10 | 1750 |
| 42 | 14 | 1 | 3 | 10 | 1000 |
| 40 | 15 | 1 | 3 | 5 | 2500 |
| 47 | 16 | 1 | 3 | 15 | 1750 |
| 14 | 17 | 1 | 1 | 15 | 1000 |
| 13 | 18 | 1 | 1 | 15 | 250 |
| 8 | 19 | 1 | 1 | 5 | 2500 |
| 15 | 20 | 1 | 1 | 15 | 1750 |
| 5 | 21 | 1 | 1 | 5 | 250 |
| 4 | 22 | 1 | 1 | 1 | 2500 |
| 6 | 23 | 1 | 1 | 5 | 1000 |
| 9 | 24 | 1 | 1 | 10 | 250 |
| 16 | 25 | 1 | 1 | 15 | 2500 |
| 11 | 26 | 1 | 1 | 10 | 1750 |
| 7 | 27 | 1 | 1 | 5 | 1750 |
| 1 | 28 | 1 | 1 | 1 | 250 |
| 2 | 29 | 1 | 1 | 1 | 1000 |
| 3 | 30 | 1 | 1 | 1 | 1750 |
| 10 | 31 | 1 | 1 | 10 | 1000 |
| 12 | 32 | 1 | 1 | 10 | 2500 |
| 27 | 33 | 1 | 2 | 10 | 1750 |
| 22 | 34 | 1 | 2 | 5 | 1000 |
| 17 | 35 | 1 | 2 | 1 | 250 |
| 24 | 36 | 1 | 2 | 5 | 2500 |
| 28 | 37 | 1 | 2 | 10 | 2500 |
| 31 | 38 | 1 | 2 | 15 | 1750 |
| 25 | 39 | 1 | 2 | 10 | 250 |
| 29 | 40 | 1 | 2 | 15 | 250 |
| 30 | 41 | 1 | 2 | 15 | 1000 |
| 21 | 42 | 1 | 2 | 5 | 250 |
| 26 | 43 | 1 | 2 | 10 | 1000 |
| 19 | 44 | 1 | 2 | 1 | 1750 |
| 20 | 45 | 1 | 2 | 1 | 2500 |
| 23 | 46 | 1 | 2 | 5 | 1750 |
| 32 | 47 | 1 | 2 | 15 | 2500 |
| 18 | 48 | 1 | 2 | 1 | 1000 |

ANNEX B

BLOCK DIAGRAM FOR PROGRAM VI



| | | | |
|-------------------------------------------------------------------------------------|-------------------------------------------|-------------------------------------------------------------------------------------|----------------------------------------------|
|  | Agilent B2900 Series.Ivlb:Close.vi |  | hp34420a Initialize With Options.vi |
|  | Error Cluster From Error Code.vi |  | Agilent B2900 Enable Output.vi |
|  | General Error Handler.vi |  | Agilent B2900 Configure Source.vi |
|  | hp34420a Close.vi |  | Agilent B2900 Configure Output Protection.vi |
|  | hp34420a Single Point Measurement.vi |  | Agilent B2900 Initialize.vi |
|  | hp34420a Select Channel.vi |  | DAQmx Write (Digital Bool 1Line 1Point).vi |
|  | Agilent B2900 Read Spot Measurement.vi |  | DAQmx Write.vi |
|  | Agilent B2900 Output Protection Status.vi |  | Control_MicroMeter.ctf |
|  | DAQmx Fill In Error Info.vi | | |